Model Based Control of Single-Phase Marine Cooling Systems

Hansen, Michael

Publication date:
2014

Document Version
Accepted author manuscript, peer reviewed version

Model Based Control of Single-Phase Marine Cooling Systems

Ph.D. Dissertation

Michael Hansen

Aalborg University
Department of Electronic Systems
Fredrik Bajers Vej 7C
DK-9220 Aalborg Ø

Hansen, Michael
Model Based Control of Single-Phase Marine Cooling Systems
ISBN 978-87-7152-008-8
First Edition, October, 2013

A.P. Møller - Mœrsk A/S
Maersk Maritime Technology - Strategic R&D
Esplanaden 50
DK-1098 Copenhagen
Denmark

Department of Electronic Systems
Aalborg University
Fredrik Bajers Vej 7C
DK-9220 Aalborg Ø
Denmark

This thesis has been printed with Computer Modern 10pt and been typeset using LaTeX 2_ε. Figures are mainly created using Microsoft® Office Visio® 2007 while data plots are created with Matlab®.

Title:
Model Based Control of Single-Phase Marine Cooling Systems

Author:
Michael Hansen

Supervisors:
Prof. Jakob Stoustrup
Assoc. Prof. Jan Dimon Bendtsen

List of published papers:

[A] Michael Hansen, Jakob Stoustrup, Jan Dimon Bendtsen, "Modeling of Nonlinear Marine Cooling Systems with Closed Circuit Flow," *Proceedings of the 18th IFAC World Congress*, pp. 5537–5542, 2011.

[B] Michael Hansen, Jakob Stoustrup, Jan Dimon Bendtsen, "Control of Non-linear Marine Cooling System," *Proceedings of the IEEE International Conference on Control Applications*, pp. 88–93, 2011.

[C] Michael Hansen, Jakob Stoustrup, Jan Dimon Bendtsen, "An LPV Model for a Marine Cooling System with Transport Delays," *Proceedings of the 14th International Conference on Harbor, Maritime & Multimodal Logistics Modelling and Simulation*, pp. 119–124, 2011.

[D] Michael Hansen, Jakob Stoustrup, Jan Dimon Bendtsen, "Robust Nonlinear Control Design with Application to a Marine Cooling System," *Proceedings of the 7th IFAC Symposium on Robust Control Design*, pp. 381–386, 2012.

[E] Michael Hansen, Jakob Stoustrup, Jan Dimon Bendtsen, "Modeling and Control of a Single-Phase Marine Cooling System," *Accepted for publication, Control Engineering Practice*, 2013.

[F] Michael Hansen, Jakob Stoustrup, Jan Dimon Bendtsen, "Experimental Validation of Model for a Single-Phase Marine Cooling System," *Submitted for publication*, 2013.

This thesis has been submitted for assessment in partial fulfillment of the PhD degree. The thesis is based on the submitted or published scientific papers which are listed above. Parts of the papers are used directly or indirectly in the extended summary of the thesis. As part of the assessment, co-author statements have been made available to the assessment committee and are also available at the Faculty. The thesis is not in its

Abstract

This thesis is concerned with the problem of designing model-based control for a class of single-phase marine cooling systems. While this type of cooling system has been in existence for several decades, it is only recently that energy efficiency has become a focus point in the design and operation these systems. Traditionally, control for this type of cooling system has been limited to open-loop control of pumps combined with a couple of local PID controllers for bypass valves to keep critical temperatures within design limits. This research considers improvements in a retrofit framework to the control strategy and design for this particular class of marine cooling systems. The project has been carried out under the Danish Industrial PhD programme and has been financed by Maersk Maritime Technology together with the Danish Ministry of Science, Technology and Innovation. The main contributions in this thesis are on the subjects of modeling and control of a single-phase marine cooling system and experimental model validation.

A great deal of attention is on the derivation and experimental validation of a model covering the relationships between pressure, flow and temperature in the cooling system. The proposed model is derived with the intention of being scalable and of low complexity, while capturing important dynamics to make it suitable for model-based control design and simulation. Based on experimental data compiled from a retrofitted test installation on board the container vessel "Maersk Senang", it is shown that the part of the proposed model relating to the thermodynamics is dynamically accurate and with relatively small steady state deviations. The same is shown for a linear version of the part of the model governing the hydraulics of the cooling system.

On the subject of control, the main focus in this work is on the development of a nonlinear robust control design. The design is based on principles from feedback linearization to compensate for nonlinearities as well as transport delays by including a delay estimate in the feedback law. To deal with the uncertainties that emerged from the feedback linearization, an H_∞-control design is applied to the resulting linear system. Disturbance rejection capabilities and robustness of performance for this control design methodology is compared to a baseline design derived from classical control theory. This shows promising results for the nonlinear robust design as disturbance rejection overall is improved, while robustness of performance is similar to the baseline design,

even when considering significant model uncertainties. This improvement to the control is expected to result in a significant reduction of the annual energy consumption of the single-phase marine cooling system. For the specific configuration and control used for the test installation on board "Maersk Senang", it is estimated that energy savings above 53% are achievable.

Resumé

Denne afhandling omhandler problemstillingerne omkring design af model-baseret regulering for en klasse af enkeltfase maritime kølesystemer. Selvom denne type af kølesystemer har eksisteret i adskillige årtier, så er det kun for nyligt at energiforbruget af disse systemer har fået opmærksomhed i forbindelse med design og drift. Reguleringen der traditionelt har været anvendt til denne type af kølesystemer har været begrænset til åben-sløjfe regulering af pumper, kombineret med enkelte lokale PID regulatorer til bypass-ventiler, med det formål at holde kritiske temperaturer inden for fastsatte grænseværdier. Dette projekt beskæftiger sig med forbedringer af reguleringstrategien for denne type af kølesystemer indenfor rammerne af et retrofit scenarie. Projektet er blevet gennemført under det danske Erhvervs-PhD program og er blevet financeret af Maersk Maritime Technology sammen med Ministeriet for Forskning, Innovation og Videregående Uddannelse. Hovedbidragene i denne afhandling er fordelt på tre emner, nemlig modellering og reguleringsdesign for enkeltfase maritime kølesystemer, samt eksperimentel modelvalidering.

Et særligt fokus er rettet mod udledning og eksperimentel validering af en model der beskriver sammenhængene mellem tryk, flow og temperatur i kølesystemet. Den fremsatte model er udledt med henblik på skalerbarhed og lav kompleksitet, mens samtidig at indeholde en tilstrækkelig beskrivelse af relevant systemdynamik for at gøre den anvendelig i sammenhæng med modelbaseret reguleringsdesign og simulering. Baseret på data opsamlet fra en testinstallation på containerskibet "Maersk Senang", er det vist, at den del af modellen der beskriver systemets termodynamik, er nøjagtig hvad angår dynamik, og kun har relativt små steady-state afvigelser. Det samme er vist for en lineær udgave af den del af modellen der beskriver sammenhængen mellem tryk og flow i kølesystemet.

I sammenhæng med regulering er fokus på udvikling af et ulineært robust reguleringsdesign. Dette design er baseret på principperne fra feedback linearisering for at kompensere for ulinearitеter, men også transportrelaterede tidsforsinkelser ved at inkludere et estimat af denne forsinkelse i tilbagekoblingen. For at håndtere de usikkerheder der opstår som følge af feedback lineariseringen, er et H_∞-reguleringsdesign anvendt til det resulterende lineære system. Egenskaben til at undertrykke forstyrrelser og robustheden

af det fremsatte reguleringsdesign er sammenholdt med et baseline design baseret på klassisk reguleringsteori. Resultaterne heraf er lovende, idet egenskaben til at undertrykke forstyrrelser generelt er forbedret, mens robustheden tilsvarer den for baseline reguleringen, selv med betydelige modelusikkerheder. Denne forbedring af reguleringen forventes at resultere i en betydelig reduktion af det årlige energiforbrug for denne type af maritime kølesystemer. For den specifikke konfiguration og regulering anvendt i forbindelse med test installationen på "Maersk Senang" estimeres det, at der kan opnås energibesparelser på over 53 %.

Contents

Abstract v

Resumé vii

Preface xvii

I Introduction and Summary 1

Introduction 3

1 Background and motivation . . . 3
2 Brief introduction to the marine cooling system . . . 9
3 State of the art and related work . . . 16
4 Objectives . . . 21
5 Contributions . . . 22
6 Outline of thesis . . . 24

Summary of work 27

7 Summary of contributions . . . 27
7.1 Model and control structure . . . 27
7.2 Marine cooling system hydraulics . . . 28
7.3 Marine cooling system thermodynamics . . . 36
8 Potential savings through improved instrumentation and control . . . 48
9 Conclusion and recommendations . . . 51
9.1 Conclusion . . . 51
9.2 Recommendations and future outlook . . . 52
References . . . 54

II Papers **61**

A Modeling of Nonlinear Marine Cooling Systems with Closed Circuit Flow **63**
1 Introduction . . . 65
2 System Description . . . 67
3 Modeling . . . 69
3.1 Hydraulic model . . . 69
3.2 Thermodynamic model . . . 71
4 Model Verification . . . 75
5 Conclusions . . . 76
References . . . 77

B Control of Non-linear Marine Cooling System **81**
1 Introduction . . . 83
2 Model . . . 84
2.1 Hydraulics . . . 85
2.2 Thermodynamics . . . 87
3 Control Design . . . 88
3.1 Design of Flow Controllers . . . 88
3.2 Design of Temperature Controllers . . . 90
4 Simulation Results . . . 92
5 Conclusions and Future Works . . . 96
References . . . 96

C An LPV Model for a Marine Cooling System with Transport Delays **99**
1 Introduction . . . 101
2 Nonlinear Model . . . 102
3 Construction of LPV Model . . . 105
4 Simulation Studies . . . 108
5 Concluding Remarks . . . 111
References . . . 112

D Robust Nonlinear Control Design with Application to a Marine Cooling System **115**
1 Introduction . . . 117
2 Marine Cooling System Model . . . 118
3 Feedback Linearization Design . . . 120
4 Robust Control Design . . . 122
5 Simulation Example . . . 125
6 Concluding Remarks . . . 127
References . . . 130

E Modeling and Control of a Single-Phase Marine Cooling System 131
1 Introduction . . . 133
2 Modeling . . . 134
3 Control Structure and Design . . . 141
3.1 Flow Control . . . 142
3.2 Baseline Temperature Control Design . . . 143
3.3 Nonlinear Robust Temperature Control Design . . . 144
4 Simulation Example . . . 149
5 Conclusion . . . 154
References . . . 155

F Experimental Validation of a Single-phase Marine Cooling System Model 157
1 Introduction . . . 159
2 Marine Cooling System Model . . . 161
3 Experimental Setup . . . 163
4 Parameter Estimation . . . 165
5 Experimental Validation . . . 168
6 Application of control . . . 171
6.1 Inner loop control design . . . 173
6.2 Outer loop control design . . . 173
6.3 Simulation . . . 178
7 Conclusion . . . 178
References . . . 180

G Technical report on instrumentation of a full scale test platform 183
1 Introduction . . . 184
2 Current instrumentation and operation . . . 185
3 Estimated power reduction . . . 186
4 Revised instrumentation . . . 189
5 Implemented control . . . 198
6 Achieved power reduction . . . 202
7 Concluding remarks . . . 205
References . . . 206

List of Notations

Abbreviations

AMS	Alarm and monitoring system
CFWC	Central fresh water coolers
FW	Fresh water
HMI	Human machine interface
HT	High temperature
LMTD	Log mean temperature difference
LO	Lube oil
LOC	Lube oil cooler
LPV	Linear parameter varying
LQR	Linear-quadratic regulator
LT	Low temperature
MCR	Maximum continuous rating
ME	Main engine
MIMO	Multiple-input multiple output
MPC	Model predictive control
PLC	Programmable logic controller
PM	Phase margin

SFOC	Specific fuel oil consumption
SISO	Single-input single output
SW	Seawater
TC	Turbocharger
TEU	Twenty-foot equivalent unit
VFD	Variable-frequency drive

Mathematical symbols

$\mathbb{C}^{n\times m}$	Space of $n \times m$ complex matrices.
$\mathbb{R}$	Set of real numbers.
$\mathbb{R}^{n\times m}$	Space of $n \times m$ real matrices.
$\mathbb{R}_+$	Set of real non-negative numbers.
$\mathcal{C}^k(\mathbb{M}, \mathbb{N})$	Set of continuous functions mapping from $\mathbb{M}$ to $\mathbb{N}$ with continuous derivatives up to order k.

Physical quantities

$\dot{m}$	Mass flow rate.
ρ_{FW}	Density of fresh water.
ρ_{SW}	Density of sea water.
$c_{p,FW}$	Specific heat capacity of fresh water.
$c_{p,SW}$	Specific heat capacity of sea water.
H	Pump head.
h	Specific enthalpy.
P	Power.
p	Pressure.
q	Volumetric flow rate.

T	Temperature.
T_i	Coolant temperature at outlet of consumer i.
$T_{LT,in}$	Coolant temperature at low temperature circuit inlet.
$T_{LT,out}$	Coolant temperature at low temperature circuit outlet.
$T_{SW,in}$	Sea water temperature at sea water circuit inlet.
$T_{SW,out}$	Sea water temperature at sea water circuit outlet.

Preface

This thesis is submitted as a collection of papers in partial fulfillment of the requirements for a Doctor of Philosophy at the Section of Automation and Control, Department of Electronic Systems, Aalborg University, Denmark. The work presented in this thesis has been supported by the Danish Ministry of Science, Technology and Innovation under the Industrial PhD programme. The work was carried out in the period spanning from March 2010 to March 2013 at Maersk Maritime Technology - Strategic R&D and at the Section of Automation and Control, Aalborg University.

I would like to thank my supervisors Prof. Jakob Stoustrup and Assoc. Prof. Jan Dimon Bendtsen for their support and for the numerous of interesting discussions. I could not have wished for better guidance and inspiration than what they have provided me with for the past 3 years. I would also like to thank all of my colleagues in MMT, among those my company supervisors Peter Ring and Jasper Boessenkool, as well as the source to all practical knowledge on maritime related machinery, Per Hother Rasmussen. A special thanks to Steffen Hartvig Nielsen for many insightful discussions and without whom the test installation on the container vessel "Maersk Senang" would never have materialized. In that connection I would like to thank the crew on "Maersk Senang" for their patience, help and useful inputs. Also a thank you to Senior Specialist, Carsten Skovmose Kallesøe at Grundfos Holding A/S, Bjerringbro for being willing to provide help and share his extensive knowledge on pump systems.

During the course of this project I had the privilege of visiting the Department of Mechanical and Aerospace Engineering at the University of California, San Diego. I would like to express my gratitude to Prof. Miroslav Krstić for giving me this opportunity, and for some very insightful discussions during my stay. Also, I would like to thank the PhD students at the Department of Mechanical and Aerospace Engineering, UCSD who helped making it an enjoyable and memorable stay. Finally, I would like to thank my family and friends for their love and support.

Michael Hansen
Aalborg University, October 27, 2013

Part I

Introduction and Summary

Introduction

1 Background and motivation

This project was initiated by Maersk Maritime Technology which is a part of the A.P. Moller - Maersk Group. The A.P. Moller - Maersk Group is a global company, employing approximately 108,000 people in around 130 countries and is involved in a range of activities within transport, energy, offshore, and retail industries, among others. The role of Maersk Maritime Technology is to provide sustainable and cost effective solutions within the field of maritime technology to the business units comprising the A.P. Moller - Maersk Group.

In recent years, Maersk Maritime Technology has initiated a variety of retrofit projects aimed at energy optimization of mainly container vessels and oil tankers. A number of these retrofit projects are concerned with the introduction of feedback control to different types of subsystems that currently employs only limited control or no control at all. The work in this thesis relates to such an initiative and is focused on the main engine cooling system for ocean-going container vessels.

From a control point of view there are two main issues to be addressed for this type of cooling system: Reduction of power consumption and optimization of operating conditions for the machinery connected to the cooling system. This type of main engine cooling system is designed such that they can provide sufficient cooling under worst case conditions, i.e., when the main engine is running at full speed and the seawater temperature is high. As a result, the capacity of the cooling system under most operating conditions is several times larger than what is necessary. However, a limited number of actuators combined with only a few simple controllers means that the power consumption of the cooling system for a large number of vessels remains the same, even when the required cooling is only a fraction of designed capacity. On some vessels the power consumption of the cooling system is stepwise reduced based on the load of the main engine and the seawater temperature using a simple open-loop control strategy. Still, this reduction is rather conservative due to the lack of feedback control. Only in a recent retrofit framework have feedback control been introduced to adjust the amount of generated cooling to match what is actually necessary under the given operating conditions.

However, a significant potential for reducing power consumption still remains. This potential is strengthened by the recent introduction of "Slow-Steaming" in container shipping. When slow-steaming, the speed of the vessel is reduced, which significantly lowers both power output and fuel consumption of the main engine as illustrated by Table 1 [1].

Table 1: Relationship between speed, engine power relative to maximum continuous rating (MCR), and fuel consumption [1].

Speed (% of design speed)	Engine power (% of MCR)	Fuel consumption
100 %	75 %	100 %
90 %	55 %	73 %
80 %	38 %	52 %
70 %	26 %	35 %

Since heat dissipated by the main engine and much of the auxiliary machinery is correlated with the main engine power output, the reduction of vessel speed also decreases the cooling required from the main engine cooling system. This means that the potential for lowering the power consumption of the main engine cooling system increases as the speed of the vessel decreases. In 2010 Maersk Line, currently the largest container ship operator in the world, had 73 % of their fleet slow steaming at main engine loads below 40 % of maximum continuous rating (MCR) [2].

Fig. 1 shows an example of an average operational profile from 2011 for a series of 6500 twenty-foot equivalent units (TEU) container vessels. For this series, the capacity of the cooling system is designed for 100 % of MCR and 32 °C seawater, but in 2011 the vessels in this series never operated under such conditions.

Besides the main engine of the vessel, the cooling system is also responsible for cooling auxiliary equipment such as auxiliary engines, air conditions units, main engine scavenge air coolers, among other things. These may however, have different optimal operating conditions i.e., temperatures which reduces the energy consumption or wear of the individual consumers of the marine cooling system. The current instrumentation and control of the marine cooling system does not allow for the temperature of individual consumers to be controlled to different set-points. Changing the control to enable set-point control is not guaranteed to reduce the power consumption of the cooling system in itself, but can induce savings through the consumers of the cooling system.

The focus in this thesis is mainly on the latter issue, that is, set-point control of consumer temperature, but with some attention to capacity adjustment for reducing the cooling system power consumption.

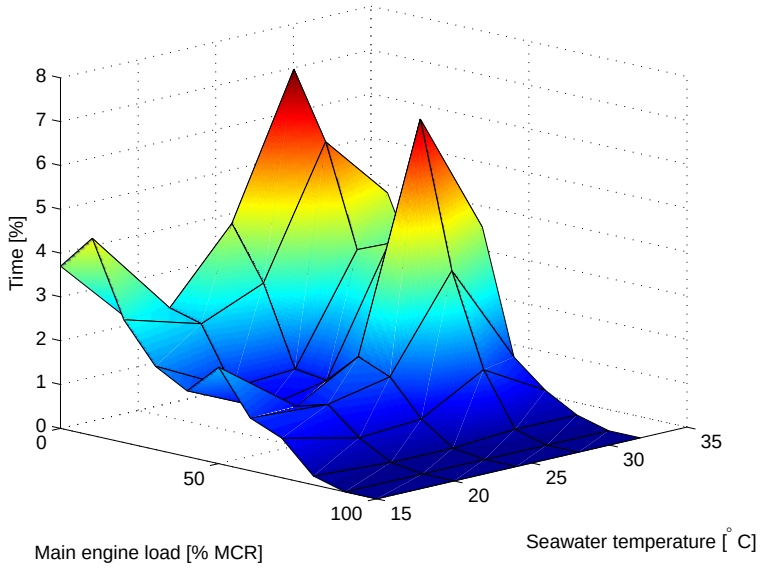

Fig. 1: Average operational profile from 01-01-2011 to 01-01-2012 of a 6500 TEU class container vessel series.

Economic Aspects

Power consumed on board a container vessel is typically generated from either auxiliary engines, a shaft generator or in some cases a waste heat recovery (WHR) system. The latter uses exhaust gas from the main engine to produce steam that drives a steam turbine-generator system. While power produced from a WHR system is a relatively cheap byproduct of the main engine waste heat, it cannot always be utilized as a minimum load on the main engine is necessary to sustain a sufficient steam production. Also, excess power generated by the WHR system can often be used to drive an electric shaft motor that can help reduce the fuel oil consumption of the main engine.

This means that the power generated onboard a container vessel on most cases can be tied to a cost in fuel, which is often Heavy Fuel Oil (HFO). In this sense, the price of HFO has a significant impact on the price of energy produced onboard the vessel. Especially in recent years the price of HFO has seen some significant fluctuations and the trend has generally been increasing, as illustrated by Fig. 2 [3].

This means that the economic aspects of reducing power consumption of subsystems such as the main engine cooling system, is highly dependent on the future development of fuel prices.

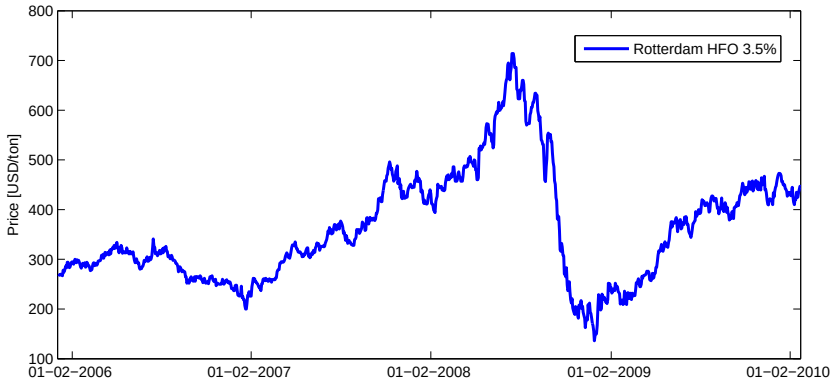

Fig. 2: Development of HFO (IFO380) prices in Rotterdam from 03-01-2006 to 22-02-2010 [3]. The 3.5% refers to the maximum sulfur content of the fuel oil.

Example of potential savings: Part 1

Appendix G investigates the saving potential for a 6500 TEU container vessel by introducing speed control for the pumps in the cooling system. The estimate is based on assumptions of operational profile and structure of the revised main engine cooling system. Using manual operation of pumps as a reference, the power reduction is estimated to be around 1.470.000 kWh/year.

Depending on how power for the main engine cooling system is produced, the resulting savings in fuel oil will vary. For the main engine, the specific fuel oil consumption (SFOC) will typically be around 175 g/kWh while an auxiliary engine will be close to 220 g/kWh [4]. As a result, the average SFOC for the power production will vary from vessel to vessel depending on the exact utilization of shaft generator, auxiliary engines and possible WHR system. Combining different SFOC values for the power production with various HFO price scenarios gives an indication of the possible savings in USD as shown in Table 2.

Table 2 shows that the economic aspect is very sensitive to the price of HFO. With the price of HFO currently (13-03-2013) being in the vicinity of 640 USD/ton, the potential yearly saving is around 225.000 USD for a vessel in this series as all power is produced by auxiliary engines with a SFOC of approximately 240 g/kWh.

Environmental Aspects

In recent years focus on CO_2, NO_x, and SO_x emissions from the shipping industry has increased significantly. Though ships in general are becoming more energy efficient,

Table 2: Relationship between SFOC [g/kWh], HFO prices [USD/ton], and resulting yearly savings in thousands USD per vessel.

		HFO price			
		200	400	600	800
SFOC	160	46.9	93.9	140.8	187.8
	180	52.8	105.6	158.4	211.2
	200	58.7	117.4	176.0	234.7
	220	64.5	129.1	193.6	258.2
	240	70.4	140.8	211.2	281.7

emissions from shipping are projected to rise, largely driven by a growing demand for maritime transportation [4]. When considering green house gases, CO_2 is usually of great concern due to its quantity and global warming potential. In 2007, shipping was estimated to be responsible for emitting 1,046 million ton CO_2, which is equivalent to 3.3 % of the global CO_2 emission [5].

Several abatement measures have been identified and it has been estimated that CO_2 emissions potentially can be reduced by 27-47 % by 2030 compared to a frozen technology scenario [6]. One of these measures is speed control of pumps and fans, which is what the focus in this PhD project relates to. This area is estimated to hold an abatement potential of 0.2 - 1 % and while this constitutes a relatively small part of the total potential, it is applicable to all types of ships, and the necessary technology in terms of equipment is already available on the market [1] [5].

This area also relates to the Energy Efficiency Design Index (EEDI) which is a mandatory measure of energy efficiency for new build ships which entered into force on January 1, 2013. [7] [8]. The EEDI sets requirements for the minimum energy efficiency level per capacity mile (measured in grams of CO_2 per tonnes miles) for ships of different types and sizes. The requirements level tightens over time to increase the energy efficiency of ships to be built in the future, and reductions factors are currently set until 2025 [9]. Experience from retrofit initiatives like the one considered in this thesis can be transferred to newly built vessels and help reach future EEDI levels.

Example of potential savings: Part 2

Continuing the example from Section 1 the attention is turned to the estimation of CO_2 and SO_x emission reductions as a result of introducing speed control to the pumps in the marine cooling system. Both CO_2 and SO_x emissions depends on the type of fuel being used, which in this case is assumed to be either HFO with a 2.7 % sulfur content or marine diesel oil (MDO) with a 0.5 % sulfur content. The corresponding emissions factors are shown in Table 3 while emission reductions for different SFOC values are illustrated in Fig. 3 and Fig. 4.

Table 3: CO_2 and SO_x emissions factors [kg/kg fuel] for HFO (2.8% S) and MDO (0.5% S) [5].

	CO_2	SO_x
HFO	3.13	0.053
MDO	3.19	0.01

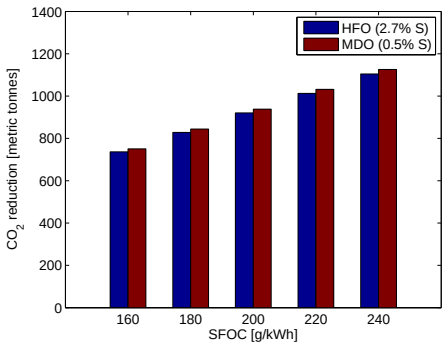

Fig. 3: Relationship between SFOC [g/kWh] and yearly reduction in tonnes CO_2 emissions for HFO and MDO, respectively.

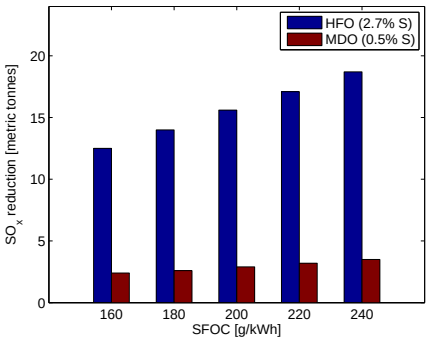

Fig. 4: Relationship between SFOC [g/kWh] and yearly reduction in tonnes SO_x emissions for HFO and MDO, respectively.

From Fig. 3 and Fig. 4 it is evident that the reduction of CO_2 emissions is only slightly influenced by the type of fuel, while reductions in SO_x emissions are significantly larger for HFO, due to the low content of sulfur in MDO. Relating this to the average CO_2 emission per capita in Denmark, the potential reduction in CO_2 for each vessel in this example is equivalent to the total CO_2 emission of between 88 and 124 Danish residents in 2009 [10]. More significantly, the yearly SO_x reduction per vessel in this example corresponds to the amount of SO_x emitted by between 920 and 6840 Danish residents in 2010 [11], with the spread mainly being a result of the difference in sulfur content between HFO and MDO.

2 Brief introduction to the marine cooling system

This chapter is intended to provide a brief introduction to the single-phase marine cooling system and the components herein. It also gives a short description of the test installation on board the container vessel "Maersk Senang", which has been retrofitted as a part of this PhD project.

A simplified layout of a typical main engine cooling system for a container vessel is illustrated in Fig. 5. The system is composed by:

- Seawater (SW) circuit
- Low temperature, fresh water (LT FW) circuit
- High temperature, fresh water (HT FW) circuit

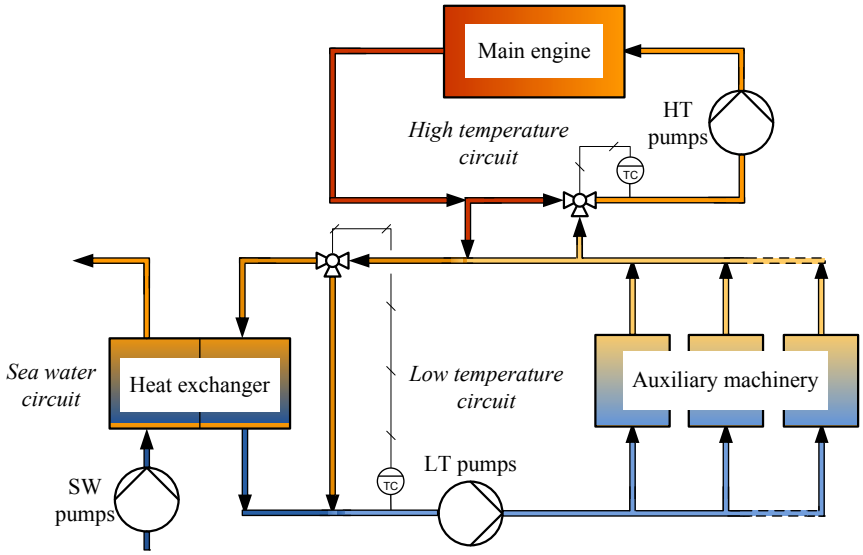

Fig. 5: Simplified layout of a general type main engine cooling system.

Heat from the main engine jacket is dissipated in the HT FW circuit, while heat from all the auxiliary machinery, that is, auxiliary engines, lube oil coolers, air conditions units, etc., is dissipated in the LT FW circuit. Heat from both the LT FW and HT FW circuit is removed through a heat exchanger by means of the SW circuit. The cooling system operates as a single-phase system, i.e., there is no phase change of coolant in any of the three circuits.

Components and configuration

The main engine cooling system consists of four main components: Piping, control valves, heat exchangers and pumps. As the number and size of consumers can vary from container vessel to container vessel, so can the extensiveness of the piping as well as the number and size of pumps and valves. However, in most cases the general structure of the main engine cooling system conforms to that of Fig. 5, and operation of the system varies little between different vessels.

Piping
The piping distributes coolant in the system and accounts for a significant part of the pressure loss in the system. The size of the main engine and relative spacing of auxiliary machinery requires an extensive network of pipes in the cooling system. As a results, transport delays occurs in some of the system temperatures, as it takes time to pump coolant from one end of the system to the other.

Control valves
The main engine cooling system is equipped with two feedback controlled 3-way valves to ensure that temperatures in the LT FW and HT FW circuits stays within design limits. The valve in the LT FW circuit controls the amount of coolant that bypasses the heat exchanger such that the temperature of the coolant to the auxiliary machinery stays close to some constant set point. Similar, the valve in the HT FW circuit controls the ratio of recirculated coolant and coolant taken from the LT FW circuit to ensure a constant temperature of the coolant flowing to the main engine.

Heat exchangers
Heat exchangers are used for transferring heat from one medium to another without mixing the two, and are usually configured as two heat exchangers in parallel for redundancy. In this context heat exchangers are used in several places, for instance to separate the SW circuit from the LT FW circuit, but some of consumers are in fact also heat exchangers, such as the Main Engine Lube Oil Coolers (ME LOCs). To avoid confusion, the term ”Central Fresh Water Coolers” (CFWC) is used when referring to the heat exchangers that separate the SW circuit from the LT FW circuit, while specific names are used for individual consumers.

Pumps
Pumps in the LT FW, HT FW and SW circuits are usually grouped as two or three centrifugal pumps in parallel with one pump working as stand-by. Pumps play an essential role in the main engine cooling system as they generate the flow that transfers heat from consumers to the seawater. They are also the main power consumers in the main engine cooling system, and at least one pump in each circuit is always running, even when the vessel is in port and the main engine is stopped.

On some vessels, the SW and LT FW pumps have two speed settings where the speed is determined from the seawater temperature and main engine load at the given time. On many vessels however, the pumps are single-speed, and the only way to reduce the power consumption of the main engine cooling system is to manually turn pumps off that are considered not to be necessary.

The capacity of the main engine cooling system depends on the amount of heat that can be transferred to the seawater through the heat exchanger. In steady state this can be expressed as [12]:

$$\dot{Q}_{SW} = \dot{m}_{SW} c_{p,SW} (T_{SW,out} - T_{SW,in}) \ , \tag{1}$$

where $\dot{Q}_{SW}$ is heat transferred to the seawater, $\dot{m}_{SW}$ is the mass flow rate through the SW circuit, $c_{p,SW}$ is specific heat of seawater while $T_{SW,in}$ and $T_{SW,out}$ are temperature of the seawater in and out of the SW circuit, respectively.

Fig. 6 illustrates a simplified example of how variations in seawater temperature and heat dissipation in terms of main engine load percentage influences the required SW circuit flow rate. In the example from Fig. 6 it is assumed that the temperature of the heated seawater overboard is at a constant 49 °C to avoid precipitation fouling of the heat exchanger [13].

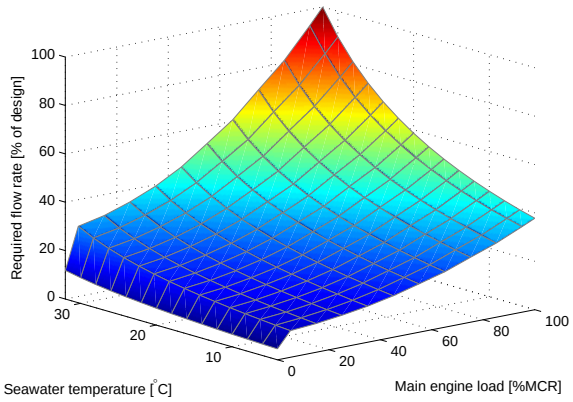

Fig. 6: Simplified relationship between seawater temperature, heat load expressed through the ME load percentage, and required flow rate.

The cooling system is designed to provide sufficient cooling when the seawater temperature, $T_{SW,in}$, is high, and heat dissipation in the HT FW and LT FW circuits is at its maximum. This means that the mass flow rate can be reduced whenever the heat load on the system or the seawater temperature is below design values, which, in particular for slow steaming vessels, is a significant part of the time.

Pump characteristics

Controlling the speed of the pumps is the key to effectively reduce the power consumption of the cooling system, but also plays an important role in set-point control of temperatures in the cooling system. For centrifugal pumps the Affinity Laws can be used for predicting changes in power consumption, flow rate and pump head as a result of changing the impeller speed [14]:

$$\frac{H_2}{H_1} = \left(\frac{N_2}{N_1}\right)^2 \qquad \frac{q_2}{q_1} = \frac{N_2}{N_1} \qquad \frac{P_2}{P_1} = \left(\frac{N_2}{N_1}\right)^3 , \tag{2}$$

where N is the rotational shaft speed, q is volumetric flow rate, H is pump head, and P is power consumption. The cubic relationship between a change in rotational shaft speed and power consumption means that a flow reduction of e.g. 10 % results in a reduction of power consumption by about 27 %.

The relationship between flow rate and pump head is described by a pump performance curve which can be approximated by a second order polynomial [15]:

$$H(q) = a_{h0}\omega_{ns}^2 + a_{h1}q\omega_{ns} + a_{h2}q^2 , \tag{3}$$

where ω_{ns} is the normalized rotational shaft speed while a_{h0}, a_{h1} and a_{h2} are pump specific coefficients that can be estimated from a pump performance curve usually supplied by the pump manufacturer. For pumps in parallel the resulting pump performance curve is obtained by adding the flow rate of each individual pump at the same pump head.

Similar to the pump performance curve, the power characteristics of a centrifugal pump can be approximated by the polynomial [16]:

$$P(q) = a_{p0}\omega_{ns}^3 + a_{p1}q\omega_{ns}^2 + a_{p2}q^2\omega_{ns} , \tag{4}$$

where a_{p0}, a_{p1} and a_{p2} are pump specific coefficients.

A traditional way of controlling flow rate is by use of control valves to throttle the flow by changing the system characteristic curve. This reduces the flow rate, and consequently the pump power consumption depending on the pump performance and power curves as illustrated by Fig. 7. If using pump speed control the same flow reduction can be achieved by lowering the pump speed from N_1 to N_2 which changes the pump power and performance curves, usually resulting in an significant power reduction compared to valve throttling.

Instrumentation of Maersk Senang

A significant part of this PhD project has been concerned with the instrumentation of a new test platform on board the container vessel, "Maersk Senang". The purpose of this

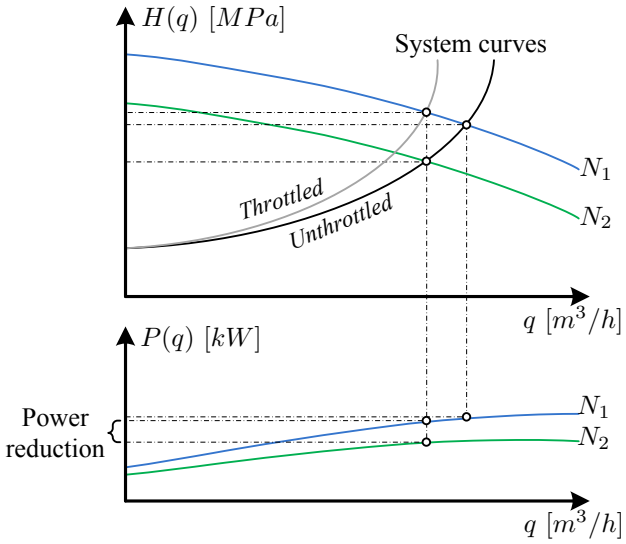

Fig. 7: Relationship between system characteristic curve, pump performance curve and pump power consumption when reducing flow rate by throttling and changing pump speed.

Fig. 8: The 6500 TEU container vessel, "Maersk Senang", subject for retrofit of the test platform.

test platform has been to obtain experimental data in order to validate models, control designs, and estimated savings.

The vessel measures 319 × 40 m and has a capacity of 6500 twenty-foot equivalent units (TEU). It is powered by an 85.000 bhp two-stroke diesel engine with a cooling system designed for a heat load of approximately 45.000 kW. It also features four auxiliary engines for power production, each rated to a power output of approximately 2.1 MW. The vessel does not have a WHR system or a shaft generator, so all power is produced by auxiliary engines. This chapter briefly outlines the revised instrumentation, and presents some of the key numbers in this context. The interested reader is referred

to Appendix G for a detailed description of the test platform and the considerations in relation to this.

Instrumentation

The existing and unmodified cooling system on this series of vessels follows the overall structure and layout presented in Fig. 5. To facilitate implementation of the control strategy and design considered in this PhD project, as well as to validate models and estimated potential savings, the cooling system is retrofitted with a number of sensors and actuators. This includes installation of temperature transmitters, pressure transmitters, VFDs and controllable butterfly valves. The extend of the instrumentation is chosen partly by what is practically feasible given the physical layout of the cooling system, and partly by considering the cost/benefit relationship for different levels of instrumentation. This is covered in more details in Appendix G.

The revised cooling system instrumentation is shown in Fig. 9-11 where new components are colored in red. An important note is that while the valves for the ME LO Coolers are controllable, the valve for the ME Air Cooler 2 is a shut-off valve operated externally. This means that the coolant supply for this consumer is shut off when it is not in operation, which generally can be assumed to be at ME loads below 50 %. For details on annotation and description of measurements in the revised cooling system, see Table 4.

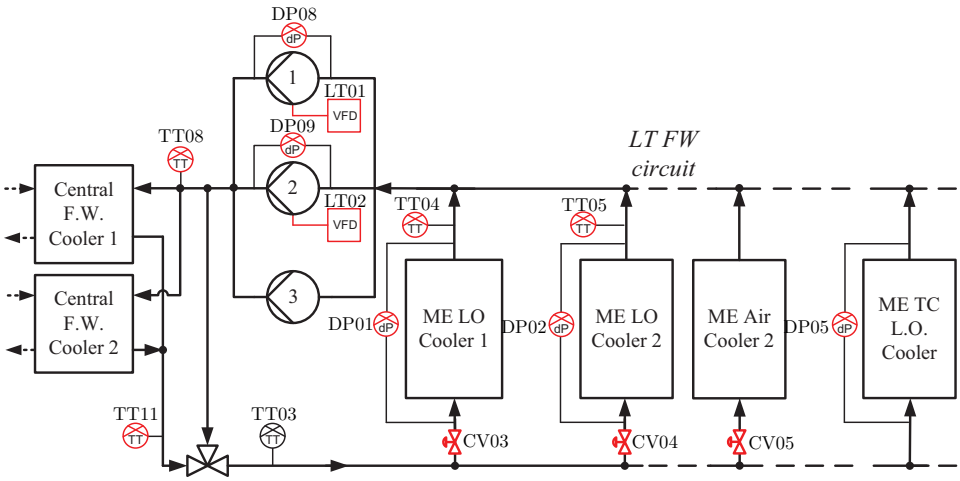

Fig. 9: Revised instrumentation of LT FW circuit. New components are colored in red.

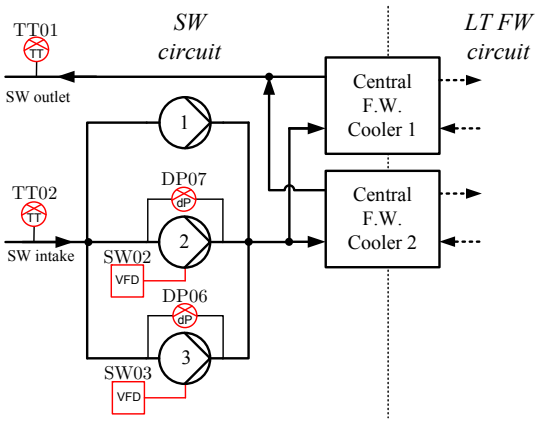

Fig. 10: Revised instrumentation of SW circuit. New components are colored in red.

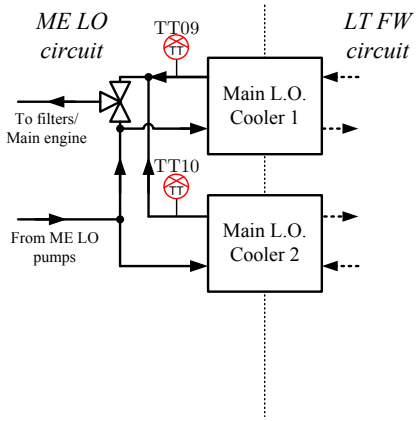

Fig. 11: Revised instrumentation of ME LO circuit. New components are colored in red.

Table 4: New components for the modified main engine cooling system.

Tag no.	Measurement	Range	Reference	Description
TT01	$T_{SW,out}$	-10–60°C	KP RT-B	SW outlet temperature
TT02	$T_{SW,in}$	-10–60°C	KP RT-B	SW inlet temperature
DP07	$\Delta H_{p,SW2}$	0–4 bar	Rosemount 2051	SW pump 2 diff. pressure
DP06	$\Delta H_{p,SW3}$	0–4 bar	Rosemount 2051	SW pump 3 diff. pressure
SW02	-	42–100 %	ABB ACS800	SW pump 2 VFD
SW03	-	42–100 %	ABB ACS800	SW pump 3 VFD
TT03	$T_{LT,3WV}$	0–60°C	KP RT-B	LT FW 3-way valve temperature
TT04	T_1	0–80°C	KP RT-B	ME LOC 1 FW temperature
TT05	T_2	0–80°C	KP RT-B	ME LOC 2 FW temperature
TT08	$T_{CC,in}$	0–80°C	KP RT-B	CFWC FW inlet temperature
TT011	$T_{CC,out}$	0–60°C	KP RT-B	CFWC FW outlet temperature
DP01	Δp_1	0–1 bar	Rosemount 2051	ME LOC 1 FW diff. pressure
DP02	Δp_2	0–1 bar	Rosemount 2051	ME LOC 2 FW diff. pressure
DP05	Δp_{TC}	0–1 bar	Rosemount 2051	ME TC LOC FW diff. pressure
DP08	$\Delta H_{p,LT1}$	0–4 bar	Rosemount 2051	LT FW pump 1 diff. pressure
DP09	$\Delta H_{p,LT2}$	0–4 bar	Rosemount 2051	LT FW pump 2 diff. pressure
CV03	-	0–100 %	ARI-ZESA	ME LOC 1 FW valve
CV04	-	0–100 %	ARI-ZESA	ME LOC 2 FW valve
CV05	-	Open/cl.	ARI-ZESA	ME air cooler 2 FW valve
LT01	-	42–100 %	ABB ACS800	LT FW pump 1 speed
LT02	-	42–100 %	ABB ACS800	LT FW pump 2 speed
TT09	$T_{LO,1}$	0–80°C	KP RT-B	ME LOC 1 LO temperature
TT10	$T_{LO,2}$	0–80°C	KP RT-B	ME LOC 2 LO temperature

3 State of the art and related work

The focus in this project is model based control design and experimental validation for a marine type cooling system. To provide an overview of current practices within the maritime industry, as well as related work within the control engineering community, this chapter is divided into three parts. These cover newly suggested solutions from suppliers to the maritime industry, results on modeling of this and similar types of systems, and control methods relevant in this context.

Industrial solutions

Not until recently have energy efficiency been of concern in the design of marine cooling systems. Focus has been on cheap system design and reliability through simplicity, while temperature control has mainly been achieved using by-pass loops. The use of feedback control has been based on single-input single-output (SISO) theory, primarily limited to PID controllers that are tuned during commissioning of the vessel. Apart from a few retrofitted vessels, the speed of the pumps in the SW and LT FW circuits has been controlled either manually by switching off pumps, or by feedforward control based on seawater temperature and main engine load. In the latter case, a two-speed pump is used in parallel with two single speed pumps to create three different pump speed settings [17].

A few suppliers for the maritime industry have in the past few years announced solutions for speed control of pumps in the main engine cooling system, but focus have mainly been on the SW circuit side [18] [19]. The common approach is to control the temperature of the coolant in the LT FW circuit by fitting the SW pumps with variable speed drives (VSD) and adjusting the seawater flow rate, such that the heat exchanger bypass is effectively closed. A single supplier have suggested to also include speed control for the LT FW pumps and include control valves for the largest consumers in the LT circuit [20]. In this setup, the differential pressure over the LT circuit consumers is controlled to a constant set point by adjusting the speed of the LT FW pumps. Furthermore, the flow rates through the largest consumers are controlled using valves to adjust the supplied cooling. This approach is very similar to what is investigated in this PhD thesis, but to the best of the author's knowledge, there are currently no implementation of this control setup on a full scale main engine cooling system.

Modeling and system analysis

Relatively few examples of using mathematical models for analyzing and simulating dynamic behavior of this type of marine cooling system can be found in the literature. In [21], a dynamical model for the same type of marine cooling system is derived and experimentally validated. The focus is on analysis of temperature transient behavior in

the design phase of the cooling system, and flow rate analysis is based on the Hardy Cross method of balancing flows [22]. The Hardy Cross method is an iterative approach to calculate steady state flows in a hydraulic network with known inputs, outputs and network parameters. While this is a simple and widely used method for analysis and design of hydraulic networks, it suffers from convergence problems [23] and is not suitable for model based control design.

The first and so far only preceding example of both mathematical modeling and subsequent control design for this type of marine cooling system is found in [17]. The work considers two different approaches for control design: PID control with cross- and disturbance-decoupling, and model predictive control (MPC). Though [17] utilizes a static flow model and verification of control designs is accomplished entirely through simulation studies, the results indicates that significant power savings can be obtained through introduction of either control scheme.

The marine cooling system belongs to a class of closed circuit flow systems, such as district heating systems and mine ventilation networks. Research into nonlinear model based control design for mine ventilation networks have received considerable attention in the literature, see e.g. [24] [25] [26]. Mine ventilation networks share both structural and nonlinear flow properties with the marine cooling system. The objective for the mine ventilation network is to maintain a low concentration of noxious and explosive gases by ensuring a sufficient air flow through the individual branches of the mine [24]. This problem is related to that of ensuring a sufficient flow of coolant through the consumers in the LT FW circuit, but does not cover the thermodynamic aspects of the marine cooling system.

The district heating system is also similar to the marine cooling system in terms of structure and flow dynamics, but is somewhat closer related due to its thermodynamic properties. However, the control objective for the district heating system is to achieve constant end-user pressure, preferably through a set of decentralized linear control actions [27]. Results on this problem can be found in [28] [29] [30] [31]. While the modeling approach from [28] is adopted for the work in this thesis, decentralized control is not necessarily a desired aspect for the marine cooling system. Furthermore, since temperature control in the case of the district heating system is left to the end-user, heat transfer and transport delays are not considered in the control strategy. Some examples can be found in the literature on modeling of heat transfer and transport delays in district heating system [32] [33] [34], but these are based on quasi-dynamic modeling i.e., they use static flow models, and are generally not intended for control design.

Control methods

The marine cooling system constitutes a multiple-input multiple-output (MIMO) system, and applicable control methods for this type of system ranges from decentralized SISO controllers based on classical control theory, to model-based MIMO controllers

that accounts for nonlinearities and time delays. A common example under the framework of classical control theory is the PID controller, which in virtue of its versatility is found in 95 % of controller implementations in process industries [35]. For design and tuning of PID controllers, see e.g. [36] [35] [37]. In spite of its wide applicability, the use of PID control for nonlinear processes such as the marine cooling system does have its drawbacks. The linear nature of PID control means that it is often only possible to guarantee local asymptotic stability at the operating point when applied to nonlinear systems [38].

Gain scheduling

A method to extend the region of validity for the linearization approach is gain-scheduling, which has found frequent use in industrial applications. In the gain-scheduling framework, the nonlinear system is linearized at several operating points and a local linear controller is designed for each operating point. A global control solution is then obtained by shifting between local controllers depending on the current operating condition of the system [39] [40].

Closely related to the traditional gain-scheduling technique is linear parameter varying (LPV) control. A large class of nonlinear systems can be represented as a linear parameter varying system, that is, a linear system whose dynamics depend on one or more exogenous time-varying parameters [41]. A practical example is found in [42] which considers the conversion of a third order nonlinear model for the air path of a turbocharged diesel engine to an LPV model. In the LPV control framework, the time-varying parameters are measured on-line and used for scheduling control laws according to changes in the system dynamics. The only a priori knowledge of the time-varying parameters is typically the range of variations and in some cases upper bounds for the rate of variations. For results on LPV control, see e.g. [43] [44] [45]. Practical application of LPV control theory can be found in [46] [47] which considers design of autopilot systems for missiles.

LPV control theory has also been extended to systems with parameter-varying time delays. The marine cooling system is an example of such, as the transport of coolant depends on the flow rates in the system, which causes transport delays in various temperatures. Analysis of LPV systems with parameter-varying delays is considered in [48] while [49] [50] [51] also considers the state-feedback synthesis problem for this type of system. A practical application example of LPV control to a system with parameter-dependent delays can be found in [52], which considers the problem of controlling the air-fuel ratio in a spark ignition engine.

Delay compensation

Due to the flow dependent delays, the marine cooling system falls in the category of nonlinear systems with parameter-varying state delays.

The problem of delays in control applications has received considerable attention in the control literature, see [53] for an extensive overview. One of the first and most well-known results on this subject is the Smith predictor for compensation of constant input-delays for stable, linear systems [54]. A modification of the Smith predictor to deal with unstable systems is known as finite spectrum assignment (FSA) or predictor feedback, and was developed around 1980 [55] [56] [57]. The basic idea behind predictor feedback is to use future values of the state in the feedback law. This "prediction" of the state is based on the variations of constants formula using the current state as initial value. This means that the feedback law includes a term which integrates over the control history and as a consequence becomes infinite dimensional. Issues related to implementation of the integral term in the predictor feedback law are dealt with in [58].

The concept of predictor feedback has later been extended to nonlinear systems with constant input delays, which is the subject of [59] [60] and is also treated in a chapter of [61]. For nonlinear systems with constant state delays, results can be found in [62] [63] [64]. A comparatively small number of results exists on the subject of compensation of systems with *time-varying* delays. This subject is dealt with in [65] [66] [67], but only for linear systems with delays in the input. A recent result considered the application of predictor feedback to nonlinear systems with time-varying input and state delays [68], but this is still a very open research subject.

Feedback linearization

An intuitive approach to deal with nonlinear systems that includes time-varying state delays is to extend control design methods for nonlinear, non-delay systems, such as for example feedback linearization. The objective in feedback linearization is to find a nonlinear change of variables and a nonlinear state feedback law to obtain an equivalent linear model [38]. Two approaches under the framework of feedback linearization have found a great number of applications: Full-state linearization [69] [70] and input-output linearization [71] [72] [73]. In full-state linearization the objective is to completely linearize the state equations while the input-output linearization seeks to linearize the input-output map, which means that the state equations may only be partially linearized.

Some results can be found in the literature on the extension of feedback linearization to nonlinear systems with state delays. One of the first results is found in [74] which considers nonlinear SISO systems with constant state delays. The authors suggest an extension to the Lie derivative by introducing the concept of time into the operator, and subsequently propose two feedback linearizing control schemes: A memoryless controller, and a controller with memory. A related approach can be found in [75] which considers the problem of output control for a nonlinear MIMO system with constant state delays. This is achieved by means of an extended input-output linearization that includes delayed state variables, which is very similar to the controller with memory in [74].

Robust control

Since feedback linearization techniques relies on exact cancellation of nonlinear terms, modeling errors and model uncertainties can significantly degrade the performance of the feedback linearization. Since the problem of inexact cancellation of nonlinear dynamics can be expressed as model uncertainties or uncertain norm bounded disturbances, feedback linearization is sometimes combined with robust controller synthesis to address this issue of robustness.

In robust control the problem of uncertainties in models and disturbances is explicitly addressed in the control design. This framework allows for design of controllers that can provide robustness in relation to system perturbations and additive disturbances [76]. A well-known result within this field emerged in 1988 where a state-space solution involving only two algebraic Riccati equations for a compensator of the same order as the augmented system was announced [77] [78]. An application example is found in [79] [80] which utilizes a bilinear pole transformation to obtain a well-posed H_∞ problem for an undamped spring-mass system. Today, robust control theory is well established for linear systems, and the interested reader is referred to textbooks, such as e.g. [81] [82] [83].

Some examples of combining feedback linearization with robust control theory can be found in the literature. One example builds on the results from [84] which considers input-output feedback linearization of the nonlinear ball and beam problem, but without considering the issue of inexact cancellation of dynamics. This is later addressed in [85] where a μ-synthesis controller was designed for the feedback linearized ball and beam problem to achieve robust stability and robust performance.

Application of mixed sensitivity H_∞-synthesis for an automatic bucket leveling mechanism on an electro-hydraulically actuated wheel loader is presented in [86]. The authors consider two cases of robust control design: Application to a linearized system model, and application to the nonlinear system model through feedback linearization. By means of simulations, the authors showed improved robustness towards parameter uncertainties for the feedback linearized system with H_∞ control, compared to the linear H_∞ control design.

The problem of robust nonlinear control for a boiler-turbine-generator system using an approximate dynamic feedback linearization and H_∞ theory is considered in [87]. Through a simulation example, the authors demonstrated improved robustness and performance of the proposed controller, compared to conventional PID control and a nonlinear control scheme based on exact feedback linearization.

While examples can be found in the literature on the application of nonlinear control design techniques which considers delays or robustness towards uncertainties, there seems to be an open research area for nonlinear system with parameter-varying delays. Application of a control design technique that addresses such issues is the focus in this thesis.

4 Objectives

The overall scope of this project is to clarify potential savings and implications as a consequence of introducing advanced feedback control to the marine cooling system. To this end, four research objectives have been identified to form the basis for the work presented in this thesis.

In this work, a model-based control design approach is chosen to effectively deal with the challenges that the system poses in terms of nonlinear dynamics, delays and disturbances. As a consequence, a dynamic model of the marine cooling system suitable for control design in terms of complexity and accuracy is an important tool. Derivation of such a model is the first research objective. As ships of different types and sizes can have cooling systems that all fall in the category of systems that conforms to the structure considered in this work, a scalable control design methodology is sought for. This is the second research objective.

Part of the work in this project concerns the specification and instrumentation of a full-scale test platform onboard a container vessel in normal operation. This facilitates measurement of process variables for the marine cooling system that up till now have not been available for e.g. model validation. Experimental validation of derived models is therefore the third research objective. The background for this project is founded by the idea and intention of reducing power consumption of the marine cooling system. Verification of actually obtained power reductions by the implementation of new control laws is the fourth and last research objective.

Summarized, the four research objectives are:

Research Objective 1: Modeling
To provide and demonstrate a structured, first-principle approach for obtaining a dynamic model of the marine cooling system that is suitable for control design and simulation.

Research Objective 2: Control design methodology
To demonstrate a scalable control design methodology applicable to the class of marine cooling systems that conforms to the structure considered in this work.

Research Objective 3: Experimental validation of models
To validate the modeling approach under Research Objective 1 via experimental data from a full-scale test setup.

Research Objective 4: Verification of savings
To verify estimated savings via experimental data obtained through the implementation of new control laws.

Together, these research objectives make up the scope of this project, and all the work presented in this thesis can be related to one or more of these objectives.

5 Contributions

The main contributions in this project are divided into three categories which are closely related to the research objectives in Chapter 4.

Modeling

- Proposal of a dynamic model for the marine cooling system that covers both the hydraulic and thermodynamic behavior of the system. Due to structural similarities, the hydraulic part of the model builds on results for district heating systems. This includes use of network theory as well as the analogy between hydraulic and electrical circuits, resulting in a simple and scalable model. The thermodynamic part of the model is derived using a first-principle approach and features low complexity while still including important nonlinearities and flow dependent delays [Paper A].

- Proposal of an LPV model with parameter-varying delays derived from the thermodynamic part of the model presented in [Paper A]. The LPV model closely approximates the dynamics of the full nonlinear model, and facilitates the use of LPV control theory for systems with parameter-varying delays [Paper C].

Control strategy and design

- Proposal of a baseline control strategy for the marine cooling system using classical control theory. PI controllers are used in a cascaded control structure, and design is based on linearized versions of the models from [Paper A]. While the proposed control strategy does not account for delays or nonlinearities, simulations illustrate reasonable performance in terms of set-point control and disturbance rejection [Paper B].

- Proposal of a nonlinear robust control strategy for the marine cooling system based on feedback linearization theory and H_∞-synthesis. The control strategy uses a similar cascaded structure as the baseline design, but applies principles from feedback linearization to the outer thermodynamic control loop to compensate for nonlinearities and delays. The H_∞ controller ensures robustness towards uncertainties arising from inexact cancellation of nonlinear terms in the feedback linearization. While disturbance rejection and robustness of performance is improved compared to the baseline design, complexity of the control design is somewhat increased. Two versions of the nonlinear robust control design have been proposed, namely without [Paper D] and with [Paper E] [Paper F] integral action.

Experimental validation

- Parameter estimation and validation of the models proposed in [Paper A] using experimental data. The parameter estimation and validation covers the full thermodynamic part of the model but only the *linearized* hydraulic part due to the number of available measurements [Paper F].
- Experimental validation of the baseline control strategy through implementation on the full-scale test platform [Appendix G].
- Verification of estimated savings induced by the implementation of the baseline control strategy [Appendix G].

6 Outline of thesis

This thesis is based on a collection of publications written throughout the course of the PhD project. Consequently, the thesis is divided into two parts: The first part provides an introduction, summary of work and conclusions for this PhD project, while the second part contains all the related publications. More specifically, the structure of the remaining thesis is as follows:

Part I

Chapter 7 provides a summary of the work and results on modeling, control design and experimental validation. This chapter is intended to give a coherent overview of the problems and solutions that are considered in this work. Conclusions and recommendations, including suggestions for future work, are presented in Chapter 9.

Part II

This part contains the publications written during the PhD project. These are included in the following order:

[A] Michael Hansen, Jakob Stoustrup, Jan Dimon Bendtsen, "Modeling of Nonlinear Marine Cooling Systems with Closed Circuit Flow," *Proceedings of the 18th IFAC World Congress*, pp. 5537–5542, 2011.

[B] Michael Hansen, Jakob Stoustrup, Jan Dimon Bendtsen, "Control of Non-linear Marine Cooling System," *Proceedings of the IEEE International Conference on Control Applications*, pp. 88–93, 2011.

[C] Michael Hansen, Jakob Stoustrup, Jan Dimon Bendtsen, "An LPV Model for a Marine Cooling System with Transport Delays," *Proceedings of the 14th International Conference on Harbor, Maritime & Multimodal Logistics Modelling and Simulation*, pp. 119–124, 2011.

[D] Michael Hansen, Jakob Stoustrup, Jan Dimon Bendtsen, "Robust Nonlinear Control Design with Application to a Marine Cooling System," *Proceedings of the 7th IFAC Symposium on Robust Control Design*, pp. 381–386, 2012.

[E] Michael Hansen, Jakob Stoustrup, Jan Dimon Bendtsen, "Modeling and Control of a Single-Phase Marine Cooling System," *Accepted for publication, Control Engineering Practice*, 2013.

[F] Michael Hansen, Jakob Stoustrup, Jan Dimon Bendtsen, "Experimental Validation of Model for a Single-Phase Marine Cooling System," *Submitted for publication*, 2013.

The layouts of the above publications have been revised from their original form to fit the layout of this thesis and some errors have been corrected as well. Also, notation has been slightly changed in some of the publications to achieve a uniform notation that conforms to the nomenclature list provided in the beginning of the thesis. In addition to the above publications, an unpublished technical report outlining the work in relation to the test installation onboard "Maersk Senang" has also been prepared as a part of this PhD project:

[G] Michael Hansen, "Technical report on instrumentation of a full scale test platform," *Unpublished technical report*, 2013.

Summary of work

7 Summary of contributions

This chapter summarizes the contributions from this PhD project on the subjects of modeling, control design and experimental validation. The chapter is based on papers A-F but to add to the coherency of the summary, the contributions are presented in a slightly different order than the one used in most of the papers. First, Section 7.1 outlines the structure of both the model and control design approach for the marine cooling system considered in this project. This is followed by sections 7.2 and 7.3, which covers the results on modeling, parameter estimation, model validation and control design for respectively the hydraulic, and thermodynamic part of the marine cooling system. The results presented in this chapter are aimed at being applicable for any type and size of single-phase cooling system that conforms to the general structure considered in this project, and are therefore not limited to the test platform described in [Appendix G].

7.1 Model and control structure

The purpose of the dynamic model considered in this PhD project was twofold: First and foremost it was a necessary foundation for the model-based control design approach that was taken in this work. Secondly, it served as a simulation model for preliminary verification of new control designs. Generally, the model of the cooling system was considered to follow the simple, overall structure illustrated in Fig. 12.

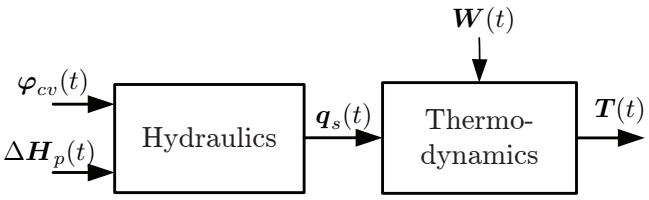

Fig. 12: Structure of the marine cooling system model.

The hydraulic part of the model describes the dynamic of the flow rates, $\boldsymbol{q}_s(t)$, when the cooling system is subjected to inputs from control valves, $\boldsymbol{\varphi}_{cv}(t)$, and pumps, $\Delta\boldsymbol{H}_p(t)$. Flow rates acts as inputs to the thermodynamic part of the model, which describes the dynamic of the system temperatures, $\boldsymbol{T}(t)$, as a function of $\boldsymbol{q}_s(t)$ and disturbances, $\boldsymbol{W}(t)$. Disturbances in this context relates to the heat load of the individual consumers as well as the seawater temperature. Partitioning of the cooling system model into a hydraulic and thermodynamic part was chosen mainly because it eased the derivation of the overall model. The partitioning was further justified by the separation of time scales between the dynamics of the hydraulics and thermodynamics. This made it relevant to consider a cascade control structure for the marine cooling system, as illustrated in Fig. 13.

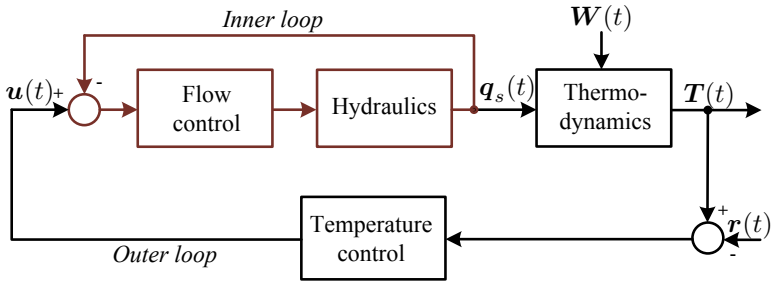

Fig. 13: Block diagram for the cascade control setup.

While different control design techniques have been investigated in this work, in each case, the control structure matches the structure shown in Fig. 13. Therefore, all work relating to the hydraulic part of the cooling system, i.e., the *inner loop* in Fig. 13, is summarized in Section 7.2, while work relating to the thermodynamics, or *outer loop* in Fig. 13, is presented in Section 7.3.

7.2 Marine cooling system hydraulics

The hydraulic model was first presented in [Paper A] and again in [Paper E]. The model was of interest in this work since control of individual flow rates in the different branches of the system is a prerequisite for the temperature set-point control considered in Section 7.3. The modeling approach was based on the general framework presented in [31] and made use of the analogy between electrical and hydraulic circuits where voltage and current corresponds to pressure and flow, respectively.

From a hydraulic point of view, the cooling system is a network made up by three types of components, namely: Pipes, valves and pumps. Each component is characterized by either an algebraic or dynamic relationship between the flow through the component and the pressure across it. In this context, the total number of components

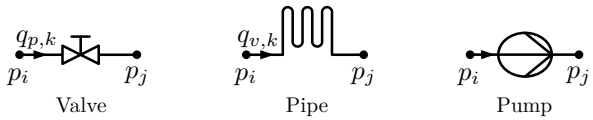

in the hydraulic network was denoted m, while the number of loops in the associated graph, i.e. the number of consumers was denoted p. Combining individual models for pipes, valves and pumps resulted in a generic model, which for component $i = 1, 2, \ldots, m$ is expressed by:

$$\Delta p_i = J_i \dot{q}_{c,i} + \lambda_i(K_{p,i}, q_{c,i}) + \mu_i(K_{v,i}, q_{c,i}) + \mu_{cv,i}(\varphi_{cv,i}, q_{c,i}) - \Delta H_{p,i}, \tag{5}$$

where Δp_i is the pressure across the component, J_i is the inertance of the component, $q_{c,i}$ is the flow through the component, while $K_{p,i}$, $K_{v,i}$, $\varphi_{cv,i}$ are hydraulic resistances. Also, $\Delta H_{p,i}$ is the pump head delivered by the component and $\mu, \mu_{cv}, \lambda \in C^{\infty}(\mathbb{R}_+ \times \mathbb{R}, \mathbb{R})$ are strictly monotonically increasing functions of both their arguments. It applies for (5) that: $J_i = \lambda_i = \mu_i = \mu_{cv,i} = 0$ if the i'th components is a pump, $\mu_i = \mu_{cv,i} = \Delta H_{p,i} = 0$ if the i'th component is a pipe, $J_i = \lambda_i = \Delta H_{p,i} = \mu_{cv,i} = 0$ if the i'th component is a valve, and $J_i = \lambda_i = \Delta H_{p,i} = \mu_i = 0$ if the i'th component is a control valve.

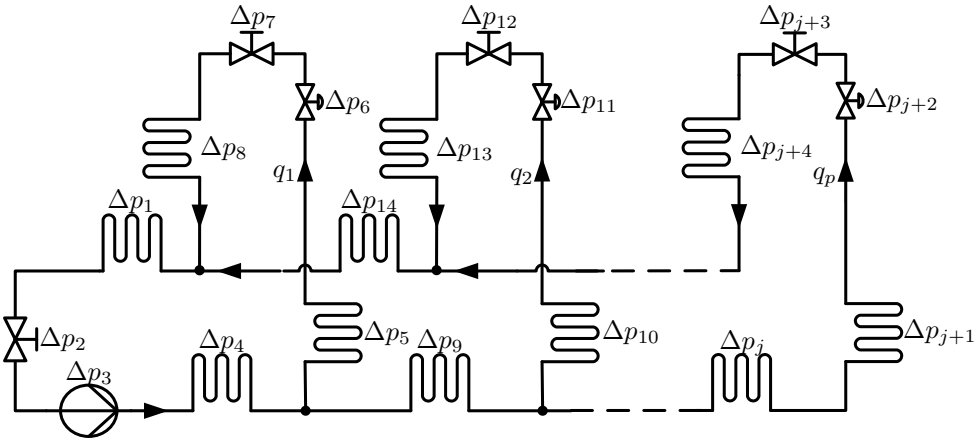

Fig. 14: Generic hydraulic structure of the LT FW side of the single-phase cooling system model.

Equations governing the dynamics of the consumer flow rates are given by the application of Kirchhoff's loop law to each fundamental loop in the hydraulic network. Basically, it means that the sum of pressure drops throughout any closed loop in the LT FW side of the cooling system illustrated in Fig 14, must equal zero. In a compact notation this was formulated as:

$$\boldsymbol{B}\boldsymbol{J}\boldsymbol{B}^T\dot{\boldsymbol{q}} = -\boldsymbol{B}\boldsymbol{\lambda}(\boldsymbol{K}_p, \boldsymbol{B}^T\boldsymbol{q}) - \boldsymbol{B}\boldsymbol{\mu}(\boldsymbol{K}_v, \boldsymbol{B}^T\boldsymbol{q}) - \boldsymbol{B}\boldsymbol{\mu}_{cv}(\boldsymbol{\varphi}_{cv}, \boldsymbol{B}^T\boldsymbol{q}) + \boldsymbol{B}\Delta\boldsymbol{H}_p\ , \tag{6}$$

with:

$$\begin{aligned}\Delta \boldsymbol{H}_p &= [\Delta H_{p,1}, \ldots, \Delta H_{p,m}]^T \ , \\ \boldsymbol{J} &= diag\{J_1, \ldots, J_k\} \ , \\ \boldsymbol{\lambda}(\boldsymbol{K}_p, \boldsymbol{q}_c) &= [\lambda_1(K_{p,1}, q_{c,1}), \ldots, \lambda_m(K_{p,m}, q_{c,m})]^T \ , \\ \boldsymbol{\mu}(\boldsymbol{K}_v, \boldsymbol{q}_c) &= [\mu_1(K_{v,1}, q_{c,1}), \ldots, \mu_m(K_{v,m}, q_{c,m})]^T \ , \\ \boldsymbol{\mu}_c(\boldsymbol{\varphi}_{cv}, \boldsymbol{q}_c) &= [\mu_{c,1}(\varphi_{cv,1}, q_{c,1}), \ldots, \mu_{c,m}(\varphi_{cv,m}, q_{c,m})]^T \ ,\end{aligned} \tag{7}$$

where $\boldsymbol{B} \in \mathbb{R}^{p \times m}$ is the fundamental loop matrix, and $\boldsymbol{q} = [q_1, q_2, \ldots, q_p]^T$ is a vector of consumer flow rates. In the context of this work λ_i, μ_i and $\mu_{c,i}$ has been characterized by:

$$\mu_i(K_{v,i}, q_{c,i}) = K_{v,i} q_{c,i}^2 \tag{8}$$

$$\mu_{c,i}(\varphi_{cv,i}, q_{c,i}) = \varphi_{cv,i} q_{c,i}^2 \tag{9}$$

$$\lambda_i(K_{p,i}, q_{c,i}) = K_{p,i} q_{c,i}^2 \ , \tag{10}$$

which can be related back to the Darcy-Weisbach equation [88]. While (8)-(10) are not strictly monotonically increasing for negative argument values, these expressions are sufficient for this application as it is only relevant to consider unidirectional flow rates, i.e., $q_{c,i} \in \mathbb{R}_+$ for $i = 1, 2, \ldots, m$.

The model in (6) is not limited to a specific number of consumers, and while focus has primarily been on the LT FW circuit part of the cooling system, the same methodology is applicable to the SW circuit. [Paper F] considers application of this model to the test platform presented in [Appendix G]. To simplify the model, it was assumed that consumers in the LT FW circuit could be divided into four groups, resulting in four free flows as illustrated in Fig. 15. Since the valve expressed by ς_{SOV} was an externally controlled shut-off valve it was not considered a controllable input in the context of this work, and was assumed not to change position during normal operation.

Through some calculations, it was possible to convert the expression obtained from (6) into equations for each of the four flows:

$$\begin{aligned}\dot{q}_i =& k_{i,1} q_1^2 + k_{i,2} q_2^2 + k_{i,3} q_3^2 + k_{i,4} q_4^2 + k_{i,5}(q_1 + q_2)^2 + k_{i,6}(q_1 + q_2 + q_3)^2 \\ &+ k_{i,7}(q_1 + q_2 + q_3 + q_4)^2 + k_{i,8} q_1^2 \varphi_1 + k_{i,9} q_2^2 \varphi_2 + k_{i,10} \Delta H_{p,LT} \ ,\end{aligned} \tag{11}$$

where $k_{i,j}$ are circuit specific parameters for $i = 1, \ldots, 4$ and $j = 1, \ldots, 10$. Similar, for the SW circuit the flow dynamics was governed by:

$$J_{SW} \dot{q}_{SW} = k_{SW} q_{SW}^2 - \Delta p_{io} + \Delta H_{p,SW} \ , \tag{12}$$

where J_{SW} is the inertance of the SW circuit piping, k_{SW} is the hydraulic resistance in the Central Fresh Water Coolers and SW circuit piping, and Δp_{io} is a constant pressure term accounting for the difference in height between SW intake and outlet.

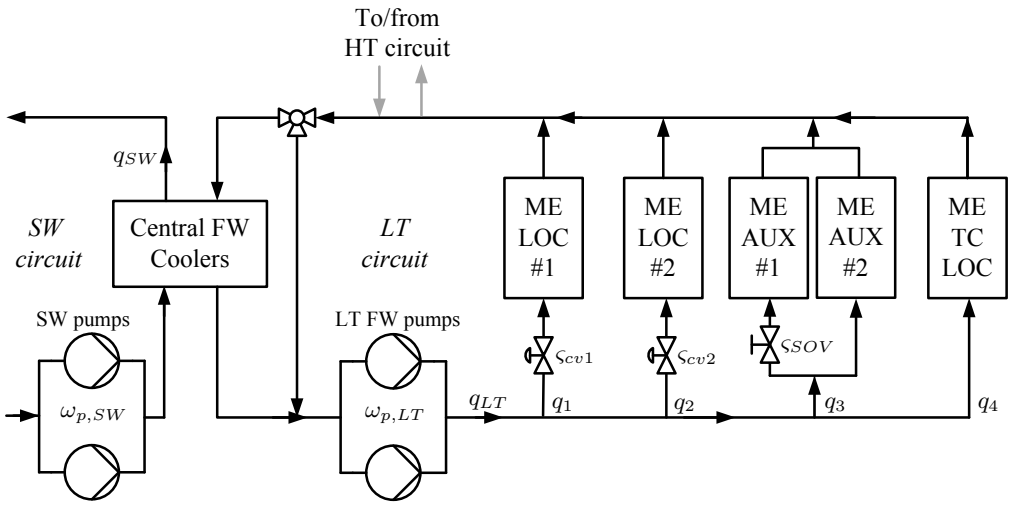

Fig. 15: Simplified overview of the pilot installation layout.

Hydraulic model validation

Validation of the linearized hydraulic model was considered in [Paper F]. This also covered estimation of model parameters from experimental data, as these could not be derived from the cooling system documentation. The linearized model was obtained from a Taylor expansion of (11) and brought to the standard form of:

$$\dot{x}_h = A\boldsymbol{x}_h + B\boldsymbol{u}_h \ , \tag{13}$$

where $A \in \mathbb{R}^{4\times4}$, $B \in \mathbb{R}^{4\times3}$. Since the main application for this linearized model was control design, the model inputs were expressed as the opening percentage of valves, ς_{cv1}, ς_{cv2}, and percentage of maximum pump speed, $\omega_{p,LT}$, rather than hydraulic resistance and pump head. The input and state vectors was therefore defined as:

$$\boldsymbol{x}_h = \begin{bmatrix} \hat{q}_1 \\ \hat{q}_2 \\ \hat{q}_3 \\ \hat{q}_4 \end{bmatrix} \qquad \boldsymbol{u}_h = \begin{bmatrix} \hat{\varsigma}_{cv1} \\ \hat{\varsigma}_{cv2} \\ \hat{\omega}_{p,LT} \end{bmatrix} \ . \tag{14}$$

The same approach was applied to the much simpler SW circuit resulting in a single transfer function:

$$G_{SW}(s) = \frac{\hat{q}_{SW}(s)}{\hat{\omega}_{p,SW}(s)} \ . \tag{15}$$

The operating points used in the parameter estimation for the models given by (13) and (15) are illustrated in Table 5. The plots in Fig. 16 compares the simulated model response with the measured response from the test platform, when both were subjected to the inputs shown in Fig. 17.

Table 5: Operating point for estimation of parameters for the linearized hydraulic model.

$\bar{q}_1$	$\bar{q}_2$	$\bar{q}_3$	$\bar{q}_4$	$\bar{q}_{SW}$
0.0712 m^3/s	0.0707 m^3/s	0.0591 m^3/s	0.0131 m^3/s	0.1681 m^3/s
$\bar{\varsigma}_{cv1}$	$\bar{\varsigma}_{cv2}$	$\bar{\omega}_{p,LT}$	$\bar{\omega}_{p,SW}$	
61.10 %	70.75 %	59.55 %	50 %	

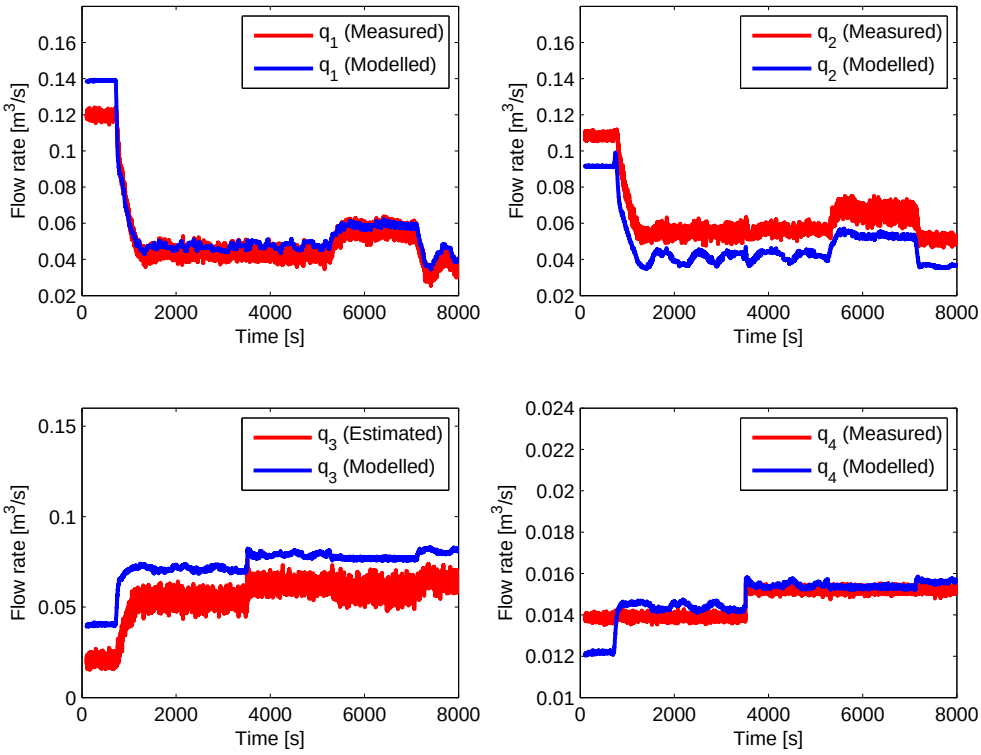

Fig. 16: Comparison of measured and modeled response for the linearized hydraulic model. The deviation for $t < 800$ s is a result of the linearization of the hydraulic model, and the fact that the system at that point is far from the operating used for the linearization.

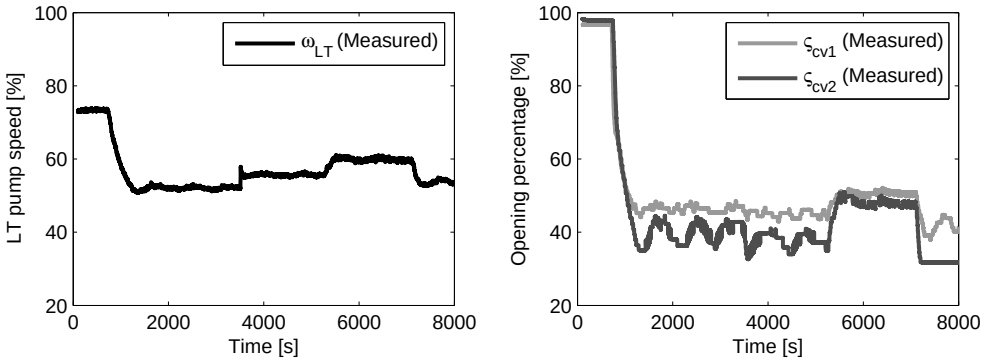

Fig. 17: Associated inputs for the model validation in Fig. 16.

As evident from Fig. 16 the dynamics of the simulated and measured response matched fairly well. The main deviations were in the offsets between the two responses, especially when the system was far from the operating point of the linearized model.

Flow control design

A control design approach for the inner loop based on classical control theory was investigated in [Paper B] and [Paper F], while an LQR approach was considered in [Paper E]. In all three papers, the objective was to control the individual consumer flow rates and the flow rate in the SW circuit to some given reference using control valves and pumps as actuators. The design in [Paper B] and [Paper E] both considered the same fictitious two-consumer system, and assumed that the LT FW pump head was held constant. In this sense, the inner loop plant model was formulated as:

$$\begin{bmatrix} \dot{\hat{q}}_1 \\ \dot{\hat{q}}_2 \\ \dot{\hat{q}}_{SW} \end{bmatrix} = \begin{bmatrix} a_{11} & a_{12} & 0 \\ a_{21} & a_{22} & 0 \\ 0 & 0 & a_{33} \end{bmatrix} \begin{bmatrix} \hat{q}_1 \\ \hat{q}_2 \\ \hat{q}_{SW} \end{bmatrix} + \begin{bmatrix} b_{11} & b_{12} & 0 \\ b_{21} & b_{22} & 0 \\ 0 & 0 & b_{33} \end{bmatrix} \begin{bmatrix} \hat{\varphi}_{cv1} \\ \hat{\varphi}_{cv2} \\ \Delta\hat{H}_{p,SW} \end{bmatrix} , \quad (16)$$

or:

$$\dot{\hat{\boldsymbol{q}}}_s = \boldsymbol{M}\hat{\boldsymbol{q}}_s + \boldsymbol{N}\hat{\boldsymbol{\psi}} , \quad (17)$$

The LQR design in Paper E considered the standard cost-function:

$$J = \int_0^\infty (\hat{\boldsymbol{q}}_s^T \boldsymbol{Q}\hat{\boldsymbol{q}}_s + \hat{\boldsymbol{\psi}}^T \boldsymbol{R}\hat{\boldsymbol{\psi}})dt , \quad (18)$$

where the matrices $\boldsymbol{Q}$ and $\boldsymbol{R}$ were determined using Bryson's rule [89], and the control law $\hat{\boldsymbol{\psi}} = -\boldsymbol{F}\hat{\boldsymbol{q}}_s$ was found by solving the associated algebraic Ricatti equation.

Contrary to the LQR design, the control design presented in [Paper B] ignored the cross-couplings in (16) and was based on standard PI controllers using phase margin, PM, and crossover frequency, ω_c, as design parameters. In other words, it considered feedback control for the three transfer functions from (16):

$$G_{SW}(s) = \frac{\hat{q}_{SW}(s)}{\Delta\hat{H}_{p,SW}(s)} \qquad G_{q1}(s) = \frac{\hat{q}_1(s)}{\hat{\varphi}_{cv1}(s)} \qquad G_{q2}(s) = \frac{\hat{q}_2(s)}{\hat{\varphi}_{cv2}(s)} \ . \tag{19}$$

using controllers of the form:

$$D(s) = K_{PI}\left(1 + \frac{1}{sT_{PI}}\right) \ . \tag{20}$$

This design approach was repeated in [Paper F] but for the validated model from (13). This meant that actuator inputs were expressed as opening percentage of control valves, and speed percentage of pumps, rather than hydraulic resistance and pump head. Also, the LT FW pump head were no longer assumed to be constant, but was indirectly used to ensure a constant flow rate through consumers without temperature control. In this sense, the inner control loop consisted of feedback control of the four transfer functions from (13):

$$G_{q1}(s) = \frac{\hat{q}_1(s)}{\hat{\varsigma}_{cv1}(s)} \tag{21}$$

$$G_{q4}(s) = \frac{\hat{q}_4(s)}{\hat{\omega}_{p,LT}(s)} \tag{22}$$

$$G_{q2}(s) = \frac{\hat{q}_2(s)}{\hat{\varsigma}_{cv2}(s)} \tag{23}$$

$$G_{SW}(s) = \frac{\hat{q}_{SW}(s)}{\hat{\omega}_{p,SW}(s)} \ . \tag{24}$$

Control of the flow q_4 was related to the objective of maintaining a constant flow through the consumers that were not included in the outer temperature control loop. Therefore, the reference for this controller was assumed to be constant by default, but it could potentially be used for trimming the flow rate through consumers without temperature control.

As a results, the structure of the inner control loop in Paper F followed that of Fig. 18. Phase margin and cross-over frequency were used as design parameters and were chosen as: $PM = 70°$, $\omega_c = 0.2$ rad/s. Performance of the inner control loop was evaluated using the linearized model from (13) and the simulation result is shown in Fig. 19 for the LT FW circuit. The choice of design parameters was just one example of how the inner loop control could be designed, and it is likely that there are other design parameters that would yield better results. Also, while it was considered possible to improve performance of the inner control loop by introducing feed-forward to deal with the cross-couplings, it was deemed unnecessary in the context of this work, due to the cascade control structure.

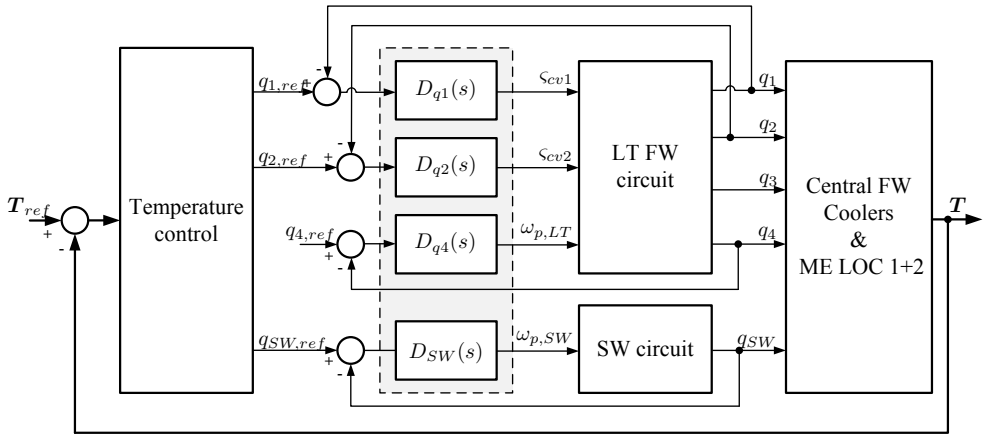

Fig. 18: Control structure considered in Paper F for the inner control loop.

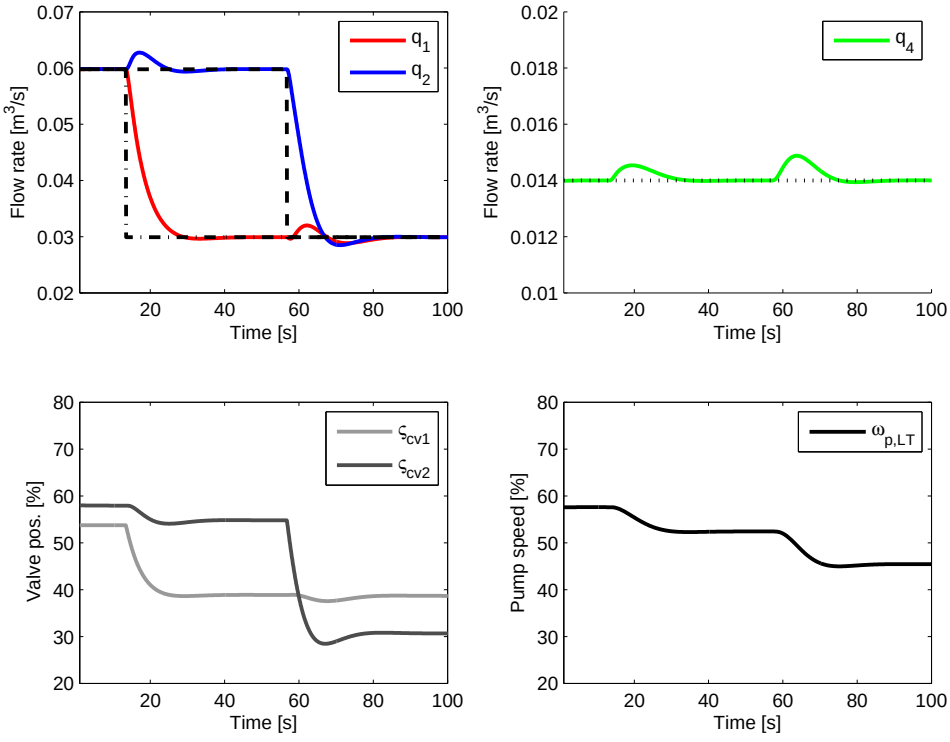

Fig. 19: Closed loop response for q_1, q_2 and q_4 when subjected to reference step.

7.3 Marine cooling system thermodynamics

The thermodynamic part of the model was presented in [Paper A] and [Paper E]. The thermodynamic model describes the change in temperature of the coolant in the cooling system as a function of heat load, flow rates and seawater temperature. The model is based on the assumption that heat transfer only takes place in consumers and the Central FW Coolers. For reasons of simplicity and scalability, all consumers were considered to possess the same model structure, thus only deviating on model parameters. Consequently, the overall thermodynamic model consisted of two parts: One governing the dynamic of the Central FW Coolers and one governing the dynamics of each consumer.

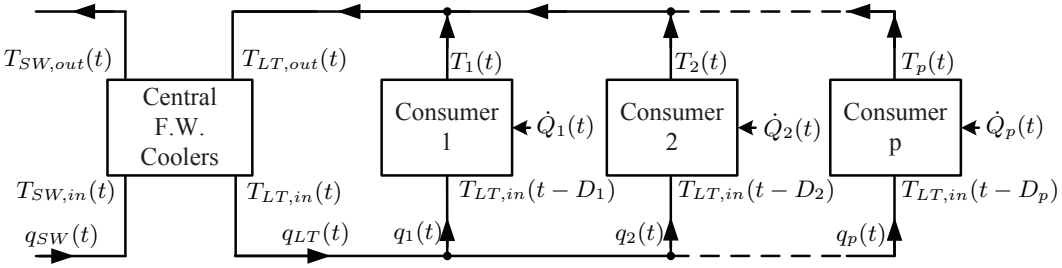

Fig. 20: Structure and notation for model of cooling system thermodynamics.

With the notation and structure as illustrated in Fig. 20 the dynamics of the coolant temperature at the outlet of consumer $i = 1, 2, \ldots, p$ is given by:

$$\dot{T}_i(t) = \frac{1}{\rho c_p V_i}\left[q_i(t)\rho c_p(T_{LT,in}(t - D_i(\boldsymbol{q})) - T_i(t)) + \dot{Q}_i(t)\right] , \tag{25}$$

where V_i is a parameter relating to the inner volume of the consumer, T_i is temperature of the coolant at the outlet of the consumer, $\dot{Q}_i$ is the heat load on the consumer, while ρ and c_p are respectively the density and specific heat of the coolant.

The model for the Central FW Cooler is similar to (25) except that the heat load is stated explicitly:

$$\begin{aligned}\dot{T}_{LT,in}(t) = \frac{1}{V_{CC}}\Big[&q_{LT}(t)(T_{LT,out}(t) - T_{LT,in}(t)) \\ &+ q_{SW}(t)\frac{\rho_{SW}c_{p,SW}}{\rho c_p}(T_{SW,in}(t) - T_{SW,out}(t))\Big] ,\end{aligned} \tag{26}$$

where ρ_{SW} and $c_{p,SW}$ are the density and specific heat of seawater, respectively.

Delay model

Delays $D_1(\boldsymbol{q}), \ldots, D_p(\boldsymbol{q})$ from (25) arise from transport of coolant from the central coolers to the respective consumers in the cooling system. This means that the delays depend on the layout of the system as well as the flow rates to the individual consumers.

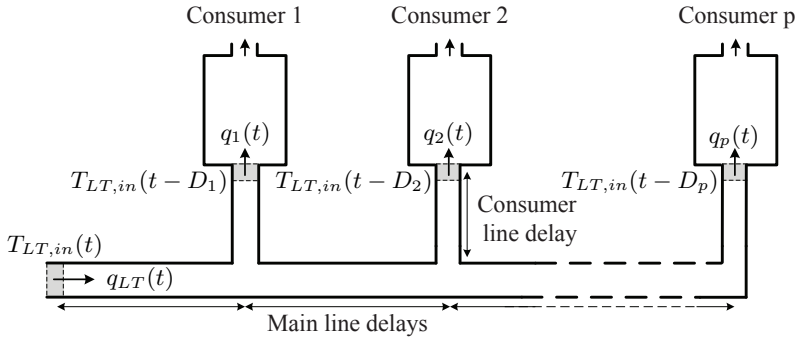

Fig. 21: Structure for cooling system delay model.

Based on the structure in Fig. 21 delays were described by:

$$D_i(\boldsymbol{q}) = \underbrace{\sum_{j=1}^{i} \left(a_{m,j} \sum_{k=j}^{n} q_k^{-1} \right)}_{\text{Main line delays}} + \underbrace{a_{c,i} q_i^{-1}}_{\text{Consumer line delay}}, \tag{27}$$

where $a_{m,j}$ and $a_{c,i}$ correspond to inner volumes of the main line pipe section j, and consumer line pipe section i, respectively. While the delay model in (27) is only valid for constant flow rates, it was used in this work under the assumption that flow rates for normal operating conditions varies slowly, and that the approximation error would therefore be small.

LPV representation of thermodynamic model

The bilinear nature of the thermodynamic model combined with the wide range of operating conditions for the cooling system, made it obvious to consider a gain scheduling approach to the control design. In this context, it was relevant to consider rewriting the thermodynamic model into an LPV form which facilitated a more structured design approach than some of the traditional gain scheduling techniques. Hence, the LPV representation builds on equations (25) and (26) but with the additional assumption

that:

$$\begin{aligned} q_1(t) =& c_1 q_{LT}(t) \\ q_2(t) =& c_2 q_{LT}(t) \\ &\vdots \\ q_p(t) =& c_p q_{LT}(t) \ , \end{aligned} \tag{28}$$

where $\{c_i\}_{i=1}^{p}$ are positive constants, subject to:

$$\sum_{i=1}^{p} c_i = 1 \ .$$

To preserve the inclusion of flow dependent delays in the thermodynamic model, an LPV formulation with parameter dependent delays was sought for:

$$\begin{aligned} \dot{\boldsymbol{x}}(t) =& A(\boldsymbol{p}(t))\boldsymbol{x}(t) + \sum_{i=1}^{k} A_{Di}(p(t))\boldsymbol{x}(t - D_i(\boldsymbol{p}(t))) \\ &+ B_1(\boldsymbol{p}(t))\boldsymbol{w}(t) + B_2(\boldsymbol{p}(t))u(t) \ . \end{aligned} \tag{29}$$

where $\boldsymbol{x}(t) \in \mathbb{R}^{n_x}$ is the state vector, $\boldsymbol{w}(t) \in \mathbb{R}^{n_w}$, is the disturbance vector and $\boldsymbol{u}(t) \in \mathbb{R}^{n_u}$ is the input vector. The scheduling parameters were chosen as:

$$\boldsymbol{p}(t) = \begin{pmatrix} p_1(t) \\ p_2(t) \end{pmatrix} = \begin{pmatrix} \tilde{q}_{LT}(t) \\ (T_{SW,in}(t) - T_{SW,out}(t)) \end{pmatrix} \ , \tag{30}$$

where $\tilde{q}_{LT}(t)$ represents the time varying operating point of the LT FW circuit flow $q_{LT}(t)$. Through some simple approximations the thermodynamic model was rewritten into:

$$\dot{T}_i(t) \approx \frac{1}{V_i}\left[c_i p_1(t)(T_{in}(t - D_i(p_1(t))) - T_i(t)) + c_i \hat{q}_{LT}(t))(\bar{T}_{LT,in} - \bar{T}_i) + \frac{\dot{Q}_i(t)}{\rho c_p}\right] \tag{31}$$

$$\dot{T}_{LT,in}(t) \approx \frac{1}{V_{CC}}\left[p_1(t)(T_{LT,out}(t) - T_{LT,in}(t)) + q_{SW}(t)\frac{\rho_{SW} c_{p,SW}}{\rho c_p} p_2(t)\right] \ . \tag{32}$$

Similar, with the definition of the scheduling parameter in (30) and the assumption in (28) the delay model was written as:

$$D_i(\boldsymbol{p}(t)) = \sum_{j=1}^{i}\left(a_{m,j}\sum_{k=j}^{n}\frac{1}{c_k p_1(t)}\right) + \frac{a_{c,i}}{c_i p_1(t)} \ . \tag{33}$$

Formulated as in (29) resulted in A, A_{Di}, B_1 and B_2 matrices in the form:

$$A(\boldsymbol{p}(t)) = \begin{bmatrix} \frac{-c_1}{V_1}p_1(t) & 0 & \cdots & 0 \\ 0 & \ddots & & \vdots \\ \vdots & & \frac{-c_p}{V_p}p_1(t) & 0 \\ 0 & \cdots & 0 & \frac{-1}{V_{CC}}p_1(t) \end{bmatrix}, \tag{34}$$

$$A_{Di}(\boldsymbol{p}(t)) = \begin{bmatrix} 0 & \cdots & 0 & \delta_{i,1}\frac{c_1}{V_1}p_1(t) \\ \vdots & \ddots & & \vdots \\ 0 & \cdots & 0 & \delta_{i,n}\frac{c_n}{V_p}p_1(t) \\ 0 & \cdots & & 0 \end{bmatrix}, \tag{35}$$

$$B_1(\boldsymbol{p}(t)) = \begin{bmatrix} \frac{1}{V_1 c_p \rho} & 0 & \cdots & 0 \\ 0 & \ddots & & \vdots \\ \vdots & & \frac{1}{V_p c_p \rho} & 0 \\ 0 & \cdots & 0 & \frac{1}{V_{CC}}p_1(t) \end{bmatrix}, \tag{36}$$

$$B_2(\boldsymbol{p}(t)) = \begin{bmatrix} \frac{c_1(\bar{T}_{in}-\bar{T}_1)}{V_1} & 0 \\ \vdots & 0 \\ \frac{c_p(\bar{T}_{in}-\bar{T}_n)}{V_p} & 0 \\ 0 & \frac{\rho_{SW}c_{p,SW}}{\rho c_p}p_2(t) \end{bmatrix}, \tag{37}$$

for $i = 1, \ldots, p$ and where δ is defined as:

$$\delta_{i,j} = \begin{cases} 1 & \text{for } i = j \\ 0 & \text{for } i \neq j \end{cases}$$

Thermodynamic model validation

[Paper F] considered validation of the thermodynamic model when applied to the Central FW Coolers as well as ME LO Cooler 1 and 2 on board the container vessel "Maersk Senang". This also included estimation of unknown model parameters from experimental data. Due to the layout of this particular cooling system, as well as the limited number of measurements, the delays included in (25) were simplified to:

$$D_1 = D_2 = \frac{a_m}{q_{LT}}, \tag{38}$$

i.e., delays for ME LO Cooler 1 and 2 were assumed to be equal, and only included the delay on the main distribution line. With the Central FW Coolers being modeled by (26) and each of the two ME LO Coolers by (25), four parameters were estimated from experimental data for the thermodynamic model, namely: V_1, V_2 V_{CC} and a_m.

Table 6: Estimated parameters for thermodynamic model.

a_m	V_1	V_2	V_{CC}
12.74 m^3	9.11 m^3	9.39 m^3	13.6 m^3

Model parameters, V_1, V_2 and V_{CC} for the thermodynamic model were estimated using the sensitivity approach from [90]. The parameter a_m was estimated using least squares from the cross covariance of measurements $T_{LT,in}(t)$ and $T_1(t)$ when the system was operated in steady state. The resulting estimated parameters are listed in Table 6.

Fig. 22 and Fig. 23 show that the dynamics of the simulated response corresponded well to the measured response of the cooling system. While there are steady state offset errors, these are relatively small, and were partly attributed to the uncertainties in the heat load estimation.

Temperature control design

Two different design approaches for the outer control loop were investigated in the context of this project. Paper B considered a baseline design based on classical control theory while a nonlinear robust design was presented in [Paper D], [Paper E] and [Paper F]. For both design approaches the objective was set-point control of the coolant temperatures for Central FW Coolers and relevant consumers.

The baseline design in [Paper B] employed standard PI controllers by linearizing the thermodynamic model at the operating point $(\bar{T}_i, \bar{q}_i, \bar{q}_{LT}, \bar{T}_{SW,in}, \bar{T}_{SW,out}, \bar{T}_{LT,in})$, i.e., it considered the transfer functions:

$$G_i(s) = \frac{\hat{T}_i(s)}{\hat{q}_i(s)} = \frac{\frac{1}{\bar{q}_i}(\bar{T}_{LT,in} - \bar{T}_i)}{s\frac{V_i}{\bar{q}_i} + 1} \tag{39}$$

$$G_{LT_{in}}(s) = \frac{\hat{T}_{LT,in}(s)}{\hat{q}_{SW}(s)} = \frac{\frac{c_{p,SW}\rho_{SW}}{c_p\rho\bar{q}_{LT}}(\bar{T}_{SW,in} - \bar{T}_{SW,out})}{\left(s\frac{V_{CC}}{\bar{q}_{LT}} + 1\right)}\ , \tag{40}$$

for $i = 1, 2, \ldots, p$. Phase margin and crossover frequency were used as design parameters, and the design was subsequently used for performance comparisons in [Paper D] and [Paper E]. This baseline design was also implemented on board the container vessel

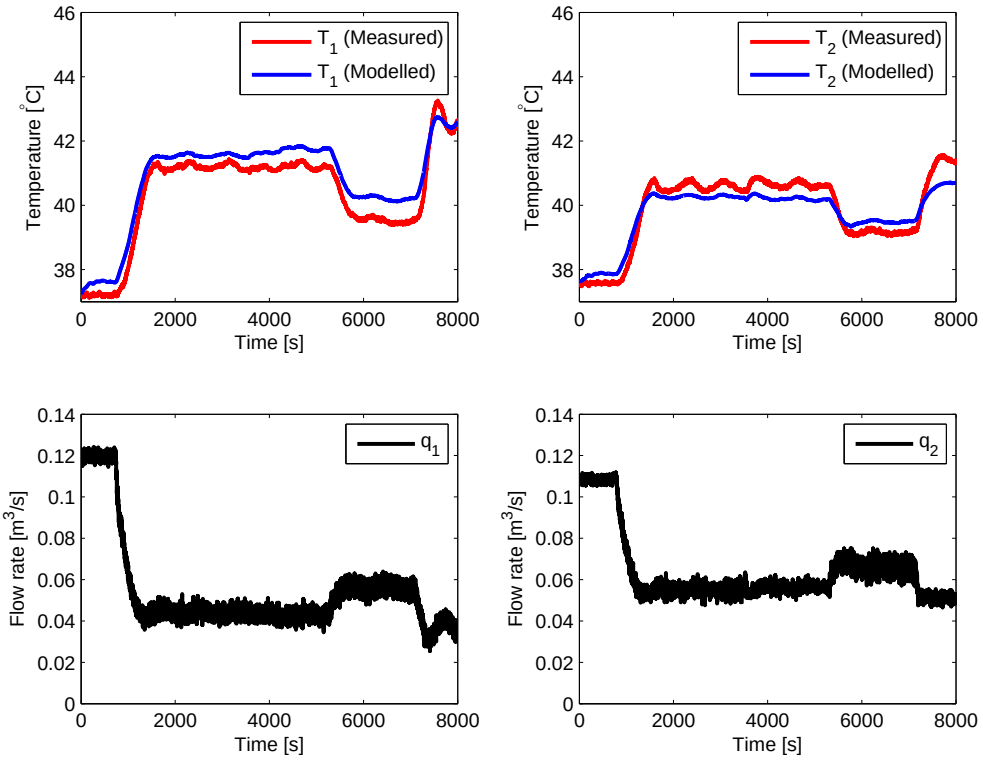

Fig. 22: Comparison of measured and modeled response for the thermodynamic model of ME LO Cooler 1 and 2.

"Maersk Senang" as briefly covered in [Appendix G].

The nonlinear robust control design was first proposed in [Paper D] and was later extended to include integral action in [Paper E] while [Paper F] considered application of the method to the validated model of the cooling system on board "Maersk Senang". The design builds on a combination of feedback linearization and robust control theory to accommodate for nonlinearities, delays and model uncertainties. To structure the control problem for the outer loop, $\boldsymbol{x} \in \mathcal{R}^{n_x}, \boldsymbol{u} \in \mathcal{R}^{n_u}$ and $\boldsymbol{w}_1 \in \mathcal{R}^{n_d}$ were defined as:

$$\boldsymbol{x} = \begin{bmatrix} T_1(t) \\ \vdots \\ T_p(t) \\ T_{LT,in}(t) \end{bmatrix} \quad \boldsymbol{u} = \begin{bmatrix} q_1(t) \\ \vdots \\ q_p(t) \\ q_{SW}(t) \end{bmatrix} \quad \boldsymbol{w}_1 = \begin{bmatrix} \dot{Q}_1(t) \\ \vdots \\ \dot{Q}_p(t) \end{bmatrix}. \tag{41}$$

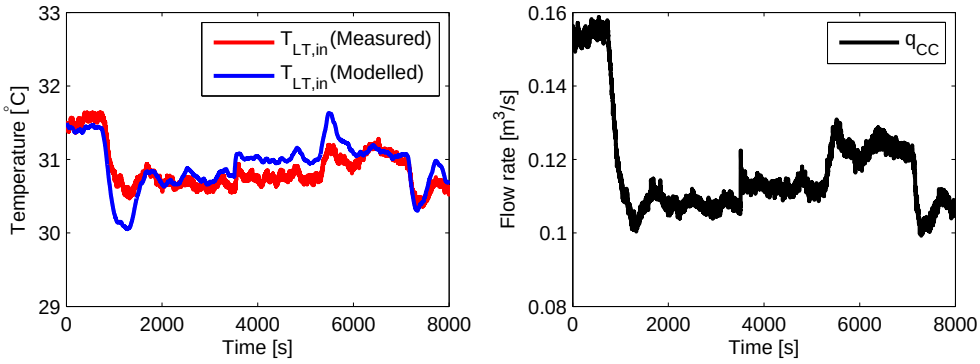

Fig. 23: Comparison of measured and modeled response for the thermodynamic model of the Central FW Coolers.

From the principles of feedback linearization it is known that the nonlinear state equations can be linearized through the state feedback law:

$$\boldsymbol{u} = \alpha(\boldsymbol{x}) + \gamma^{-1}(\boldsymbol{x})\boldsymbol{v} \ ,$$

if the state equations follow the structure:

$$\dot{\boldsymbol{x}} = A\boldsymbol{x} + B\gamma(\boldsymbol{x})[\boldsymbol{u} - \alpha(\boldsymbol{x})] \ , \tag{42}$$

and under the assumption that $\gamma(\boldsymbol{x})$ is non-singular in the domain of interest. To ease the notation, the following definitions were introduced:

$$\Lambda = \frac{\rho_{SW} c_{p,SW}}{\rho c_p} \Delta T_{SW}(t) \ , \tag{43}$$

$$\Phi(\boldsymbol{x}) = T_{LT,out}(t) - T_{LT,in}(t) \ , \tag{44}$$

$$\Psi_i(\boldsymbol{x}) = T_{LT,in}(t - D_i(\boldsymbol{u})) - T_i(t) \ , \tag{45}$$

for $i = 1, 2, \ldots, p$. For the fictitious cooling system considered in [Paper D] and [Paper E] all consumers were assumed to be included in the outer control loop, which meant that the sum of the coolant flows through the consumers equaled the coolant flow through

Central FW Coolers. This meant that the system was represented as:

$$\dot{\boldsymbol{x}} = \begin{bmatrix} \frac{1}{V_1} & 0 & \dots & 0 \\ 0 & \ddots & & \vdots \\ \vdots & & \frac{1}{V_p} & 0 \\ 0 & \dots & 0 & \frac{1}{V_{cc}} \end{bmatrix} \begin{bmatrix} \Psi_1(\cdot) & 0 & \dots & 0 \\ 0 & \ddots & & \vdots \\ \vdots & & \Psi_p(\cdot) & 0 \\ \Phi(\cdot) & \dots & \Phi(\cdot) & \Lambda(\cdot) \end{bmatrix} \boldsymbol{u} \tag{46}$$

$$+ \begin{bmatrix} \frac{1}{\rho c_p V_1} & 0 & \dots & 0 \\ 0 & \ddots & & \vdots \\ \vdots & & & \frac{1}{\rho c_p V_p} \\ 0 & \dots & \dots & 0 \end{bmatrix} \boldsymbol{w}_1 \ . \tag{47}$$

Since the temperature control in [Paper D] and [Paper E] was assumed to include all consumers, the drift term from (42) was zero, i.e., $\alpha(\boldsymbol{x}) = \boldsymbol{0}$. However, for the application of nonlinear robust design presented in [Paper F] the feedback linearization differed slightly, as the cooling system contained consumers for which the temperature was not controlled by the outer loop. This led to a nonzero drift term, $\alpha(\boldsymbol{x})$ and a system representation on the form:

$$\dot{\boldsymbol{x}} = \overbrace{\begin{bmatrix} \frac{1}{V_1} & 0 & 0 \\ 0 & \frac{1}{V_p} & 0 \\ 0 & 0 & \frac{1}{V_{cc}} \end{bmatrix}}^{B} \overbrace{\begin{bmatrix} \Psi_1(\boldsymbol{x}) & 0 & 0 \\ 0 & \Psi_2(\boldsymbol{x}) & 0 \\ 0 & 0 & \Lambda \end{bmatrix}}^{\gamma(\boldsymbol{x})} \overbrace{\begin{bmatrix} q_1 & - & 0 \\ q_2 & - & 0 \\ q_{SW} & - & \left(\frac{-q_{LT}(t)\Phi(\boldsymbol{x})}{\Lambda}\right) \end{bmatrix}}^{[\boldsymbol{u}-\alpha(\boldsymbol{x})]}$$

$$+ \overbrace{\begin{bmatrix} \frac{1}{\rho c_p V_1} & 0 \\ 0 & \frac{1}{\rho c_p V_2} \\ 0 & 0 \end{bmatrix}}^{B_w} \overbrace{\begin{bmatrix} \dot{Q}_1 \\ \dot{Q}_2 \end{bmatrix}}^{\boldsymbol{w}_1} \ . \tag{48}$$

In both cases, the resulting linear system was of the form:

$$\dot{\boldsymbol{x}} = B\boldsymbol{v} + B_w \boldsymbol{w}_1 \ . \tag{49}$$

It was argued that $\gamma(\boldsymbol{x})$ could be considered non-singular in the range of interest due to the positive heat transfer from the consumers to the coolant that persists while the system is in operation. The flow dependent delays are included in the feedback linearization by means of (27) and under the assumption that the delays are bounded, which was reasoned for on a basis of unidirectional and nonzero flow.

Because the feedback linearization relies on exact cancellation of nonlinear terms, any model uncertainties or mismatch between the estimated delay and actual delay will

degrade the performance of the feedback linearization. In [Paper F], this led to the formulation of the control problem:

$$\dot{\boldsymbol{x}} = \boldsymbol{B}(I_3 + \Delta_\gamma)\boldsymbol{v} + \Delta_\alpha + \boldsymbol{B}_w \boldsymbol{w}_1 \tag{50}$$

$$= \boldsymbol{B}\boldsymbol{v} + \boldsymbol{B}\boldsymbol{w}_2 + \tilde{\boldsymbol{B}}_w \tilde{\boldsymbol{w}}_1 \tag{51}$$

$$\boldsymbol{y} = \boldsymbol{x} + \boldsymbol{n} \ , \tag{52}$$

where $\boldsymbol{w}_2 \in \mathbb{R}^3$ is a disturbances term included to account for the uncertainties in the design and $\boldsymbol{n} \in \mathbb{R}^3$ is measurement noise. It was assumed for Δ_γ and Δ_α that:

$$\frac{1}{\rho_\alpha}||\Delta_\alpha||_\infty = \frac{1}{\rho_\alpha} \sup_\omega \sigma_{\max}(\Delta_\alpha(j\omega)) \leq 1 \tag{53}$$

$$\frac{1}{\rho_\gamma}||\Delta_\gamma||_\infty = \frac{1}{\rho_\gamma} \sup_\omega \sigma_{\max}(\Delta_\gamma(j\omega)) \leq 1 \ , \tag{54}$$

where $\rho_\alpha \in \mathbb{R}_+$ and $\rho_\gamma \in \mathbb{R}_+$. In (51), $\tilde{\boldsymbol{B}}_w \in \mathbb{R}^{3\times 3}$ and $\tilde{\boldsymbol{w}}_1 \in \mathbb{R}^3$ were augmented to include Δ_α and subsequently scaled such that $||\tilde{\boldsymbol{w}}_1||_\infty \leq 1$. To accommodate for uncertainties and disturbances in a structured way, the linear control input $\boldsymbol{v}$ was designed using robust control theory. To reject constant disturbances the feedback linearized model was augmented to include integral error states, resulting in an outer control loop as shown in Fig. 24.

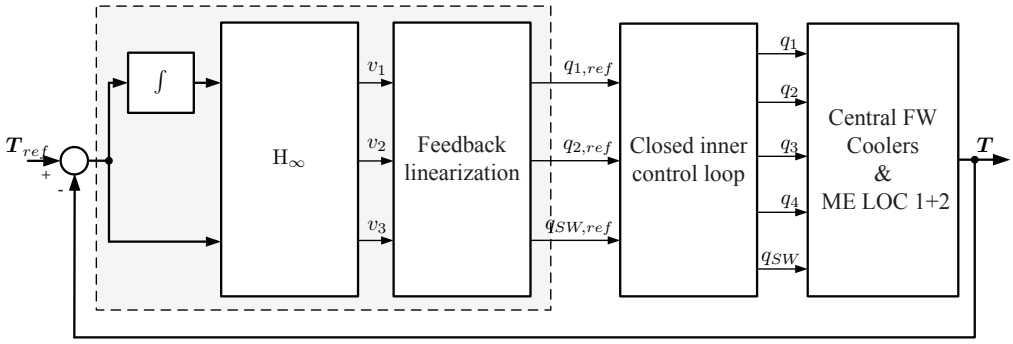

Fig. 24: Control structure considered in Paper F for the outer control loop.

The exogenous inputs, $\tilde{\boldsymbol{w}}_1$, $\boldsymbol{w}_2$ and $\boldsymbol{n}$, were combined into a single vector to formulate a standard H_∞ problem. Also, an error vector, $\boldsymbol{z}$, penalizing states and control inputs were introduced, yielding:

$$\boldsymbol{w} = \begin{bmatrix} \tilde{\boldsymbol{w}}_1 \\ \boldsymbol{w}_2 \\ \boldsymbol{n} \end{bmatrix} \qquad \boldsymbol{z} = \begin{bmatrix} \boldsymbol{x} \\ \rho_\gamma \boldsymbol{v} \end{bmatrix} \ . \tag{55}$$

As a result of the feedback linearization, all the poles for the linear equivalent system were placed on the imaginary axis and the problem was not solvable with standard H_∞ theory directly. This technicality was dealt with by application of the $j\omega$-axis pole shifting transformation to the feedback linearized system [80]:

$$s = \frac{\tilde{s} + p_1}{(\frac{\tilde{s}}{p_2}) + 1} \ , \tag{56}$$

where $p_1, p_2 < 0$ are the endpoints of the diameter of a circle being mapped by (56) from the left s-plane into the $j\tilde{\omega}$-axis of the $\tilde{s}$-plane. An H_∞-controller was designed for the approximate model obtained through (56), and the inverse bilinear transformation was subsequently applied to realize the final H_∞-controller. Since the parameters p_2 and especially p_1 in (56) plays essential roles when placing dominant closed loop poles in the s-plane they were the main design parameters for the H_∞ control design along with the weighting factor, ρ_γ. Parameters used for the H_∞ control design in [Paper F] are shown in Table 7.

Table 7: Design parameters for the nonlinear robust outer loop control design in Paper F.

p_1	p_2	ρ_γ	ρ_α
-0.003	-100	1.9	0.009

The values of ρ_γ and ρ_α were estimated numerically from noise bounds on the measurements included in $\boldsymbol{\gamma}$ and $\boldsymbol{\alpha}$, as well as uncertainty bounds on the parameters in the delay estimation. Delay estimation errors were included in ρ_γ by bounding the derivative of the time delayed variable and evaluating the temperature deviation for the worst case delay estimation error.

Robustness of performance for the nonlinear robust design in [Paper F] was evaluated by considering parameter perturbations of $\pm$ 30% for a_m, V_1, V_2 and V_{CC}, resulting in 16 combinations of extreme values. These combinations were all simulated, and the responses for the system with perturbed parameters were plotted in shades of gray along with the response for the nominal system in colors. The simulation considered step-wise changes in the heat load for the two ME LO Coolers as illustrated in Fig. 25. For comparison, the baseline design from [Paper B] was applied to the validated model as well, and subjected to the same simulation scenario as well. The responses for T_1 and T_2 are shown in Fig. 26 while the response for $T_{LT,in}$ is shown in Fig. 27. Both the nonlinear robust design and baseline design use the inner loop control from Fig. 18.

The robust nonlinear design was superior to the baseline design in terms of disturbance rejection while robustness of performance was very similar, though with a slight advantage to the nonlinear control design.

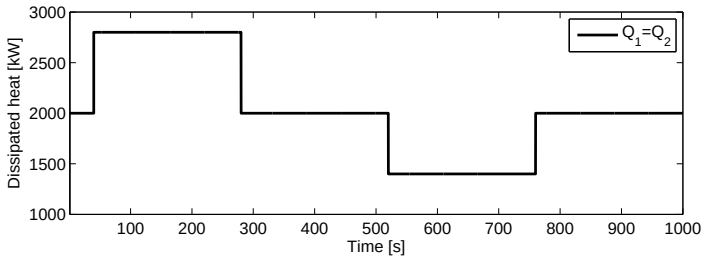

Fig. 25: Step-wise changes in the heat dissipated in the two ME LO coolers.

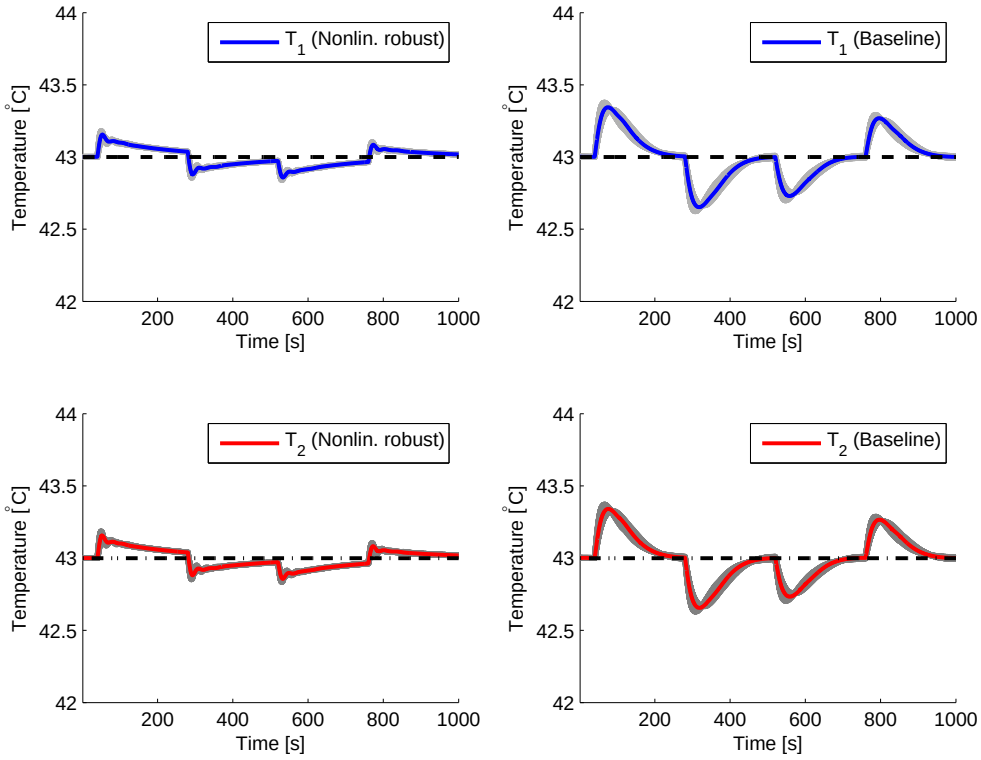

Fig. 26: Comparison of T_1 and T_2 for the nonlinear robust control design from Paper F and the baseline design in Paper B. The baseline controllers were designed for $PM = 70^\circ$ and $\omega_c = 0.03$ rad/s.

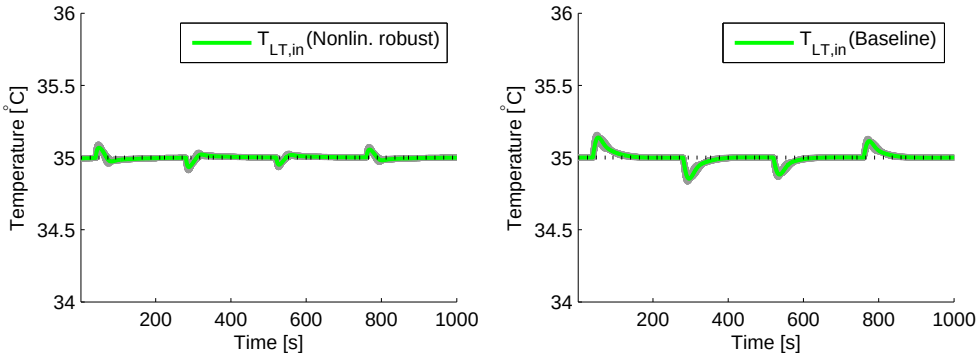

Fig. 27: Comparison of $T_{LT,in}$ for the nonlinear robust control design from Paper F and the baseline design in Paper B. The baseline controller was designed for $PM = 70^\circ$ and $\omega_c = 0.06$ rad/s.

8 Potential savings through improved instrumentation and control

The aim of this chapter is to outline the potential saving obtainable through the new instrumentation and control scheme implemented on the container vessel, "Maersk Senang". The potential saving depends on several parameters such as controller set-points, the operational profile of the vessel and how the current energy consumption is calculated. To give an initial estimate on this, a worst-case power consumption profile is calculated and combined with the average operational profile from 2011 for the 6500 TEU vessel series previously considered in Chapter 1. The power consumption profile determines the total pump power consumption as a function of the ME load percentage and seawater temperature.

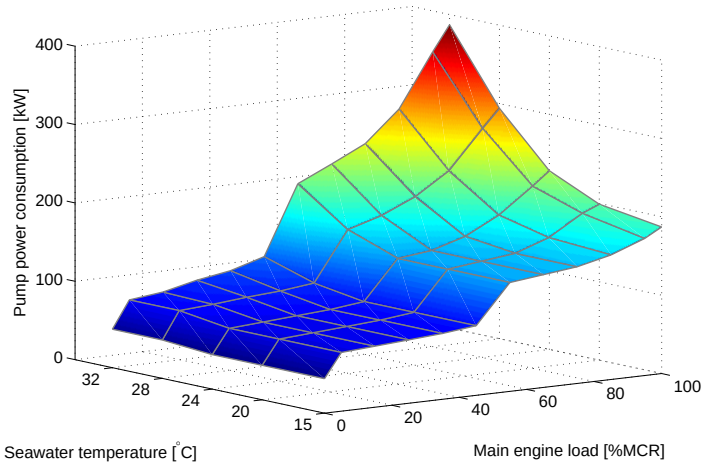

Fig. 28: Power consumption profile for the instrumentation considered in this PhD project.

The worst-case power consumption profile illustrated in Fig. 28 is calculated from the assumptions that:

- There are always 2 auxiliary engines running.
- The efficiency of the VFDs is 91 % under all load conditions.
- The pump power consumption is calculated from the rated pump motor power rather than power at nominal speed (which is lower).
- There is always maximum coolant flow through consumers without temperature control.

While the profile in Fig. 28 considers the power consumption for both the SW and LT FW pumps, it is mainly the LT FW pumps that are of interest in this scope. This is a consequence of the focus in this project primarily being on the LT FW part of the system, but also the fact that this is the only part of the system where control is implemented on the test platform in the context of this PhD project. As a result, there is only experimental data available from the test platform to verify power savings for the LT FW circuit.

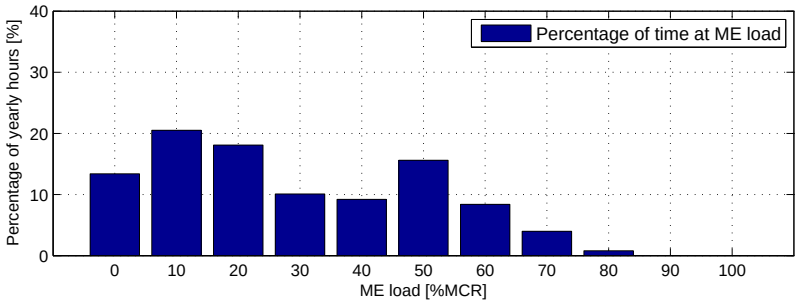

Fig. 29: The percentage of yearly hours the vessels in this series operated at a given ME load in the period from 01-01-2011 to 01-01-2012.

When considering the power consumption of the LT FW pumps alone, it is sufficient to look at the amount of time a vessel spends at a given ME load, as the seawater temperature under normal operating conditions do not influence the use of the LT FW pumps. An initial, worst-case power consumption estimate for the LT FW pumps is calculated based on their contributions in the profile from Fig. 28 and the operational profile from Fig. 29.

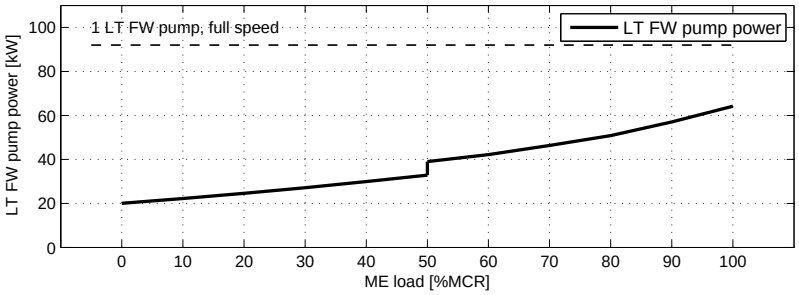

Fig. 30: LT FW pump power consumption as a function of the ME load percentage. See [Appendix G] for an explanation of the derivation of this plot.

In a similar way, a power consumption profile is calculated based on measurements obtained from the test platform during operation. From experimental data and the assumptions listed in [Appendix G] the relationship between the ME load and the LT FW pump power consumption is established as shown in Fig. 30. By combining the power consumption profile from Fig. 30 and the average operational profile from Fig. 29 it is possible to obtain an estimate of the total yearly energy consumption for the LT FW pumps based on experimental data. This is shown in Table 8 along with the initial worst-case calculation.

Table 8: Estimated yearly energy consumption for the revised LT FW cooling system control.

	Energy consumption [kWh/year]	Savings [%]	Payback [months]
Current system	1.406.100	0	-
Revised system, worst-case	656.742	53	15
Revised system, (measured)	246.380	82	10

The payback time in Table 8 is calculated with a 7% discount rate for the payback and only considers the cost of the hardware installation. This means that it does not include expenses relating to development of control software, licenses or man hours for project management.

The span between the worst-case estimate and the estimate based on measurements is explained by two main factors: First is the assumption on how the system is operated with respect to the consumers without temperature control. In case of the estimate based on measurements, the set points are adjusted according to inputs from the crew rather than design specifications, which results in reduced flow rates through consumers without temperature control compared to the worst-case estimate. Secondly, is the assumption on low VFD efficiency and high pump motor power used for the power calculation in the worst-case estimate, which results in a higher estimated energy consumption than what is expected in practice.

While the actual energy consumption ultimately depends on the operational profile from the time of the retrofit, the worst case estimate and estimate based on measurements in Table 8 are considered to be reasonable guidelines for the upper and lower bounds on the actual power consumption for this configuration. However, the stated savings and associated payback times also depends on the estimated consumption for the unmodified system, which means that they are very sensitive to the actual utilization of the cooling system before the retrofit. Consequently, the actual payback time for the same retrofit on two similar vessels may vary as a result of different operating profiles and crew.

9 Conclusion and recommendations

The work presented in this thesis have considered development of a model and new control methods for a class of single-phase marine cooling system in a retrofit framework. The problem originated from a desire to decrease the energy consumption for this type of cooling system, while ensuring sufficient cooling for the consumers connected to the system. The result of this work is presented as a collection of papers enclosed in Part II of this thesis, and has been summarized in the previous chapters. This chapter presents the conclusions drawn on the basis of these results, as well as the author's recommendation for future investigations on the subject of model-based control for this type of cooling system.

9.1 Conclusion

A model based control strategy was employed in this work to deal with the challenges that this class of single-phase marine cooling system posed in terms of non-linear dynamics and transport delays. The main contributions in this project therefore fall under the three categories: Modeling, control structure and design, and experimental validation.

Modeling
A scalable and low complexity model of the single-phase marine cooling system was derived in [Paper A]. The modeling approach for the part of the model relating to the hydraulics of the cooling system was based on results from district heating systems, while the thermodynamics part of the model was derived from first principles. The results on the thermodynamic modeling were extended in [Paper C] to provide a linear parameter-varying model to facilitate gain-scheduling design techniques.

Control structure and design
A baseline control design based on classical control theory was proposed in [Paper B]. A cascade control structure was used to exploit the separation of time scales between the dynamics of the hydraulics and thermodynamics of the cooling system. The purpose of the baseline design was mainly to provide a base of comparison for other design techniques, but this work has also shown that this simple design is fairly robust and exhibits reasonable disturbance rejection capabilities.

A nonlinear robust control design based on principles from feedback linearization and robust control theory was first proposed in [Paper D], and was extended to include integral action in [Paper E] and [Paper F]. The linearizing feedback law was used partly to deal with nonlinearities, but it also included a delay estimate to compensate for flow dependent delays. To account for uncertainties arising from inexact cancellation in the feedback linearization, a H_∞-control design was applied to the equivalent linear system. Results from the comparison of this design to the

baseline design showed improved disturbance rejection for the nonlinear robust design, but with similar robustness of performance even with considerable model uncertainties.

Experimental validation
Experimental data was compiled from the retrofitted test installation on the container vessel "Maersk Senang" and was used in [Paper F] to estimate model parameters as well as to validate the proposed model. Results from the model validation showed that despite the low model complexity, the dynamics of the simulated response was very close to the measured response. In [Appendix G] experimental data was used to evaluate the potential energy saving obtainable through new instrumentation and control of the LT FW circuit. The results showed that a potential annual energy saving of up to 82 % could be achieved if set-points were tweaked according to crew input, and with the given operational profile.

Flow dependent delays have received a considerable amount of attention in this work, both in the derivation of the dynamic model, and in the proposed nonlinear robust control design. Even so, the base-line design implemented in the test-installation on "Maersk Senang" performed well, despite the lack of delay compensation. While this does not rule out the need for delay compensation in all cases, it shows that these delays do not *necessarily* cause stability problems in the control of this type of cooling system. Consequently, in the cases where it is possible to leave out delay compensation in the control design, it would not only reduce the complexity of the feedback laws, but also avoid the non-trivial task of determining parameters in the delay model.

When it comes to the energy consumption of the cooling system, this seems largely determined by the choice of set-points and there is no distinguishable difference in the base-line design and the proposed nonlinear robust design in this context. However, contrary to the base-line design, the performance of the nonlinear robust design is not limited to a small region around an operating point, which makes it possible to use less conservative set-points for this design. This can potentially allow the cooling system to consistently operate closer to an optimal set-point, and indirectly lead to lower energy consumption for the nonlinear robust design.

9.2 Recommendations and future outlook

This section presents some of the author's recommendations for future research directions within the field of single-phase marine cooling systems. It also lists some of the practical challenges that should be taken into consideration if retrofitting a large number of vessels with the proposed control structure and strategy.

Having achieved set-point control for the consumers, focus should be moved to set-point optimization for the various types of consumers in the cooling system.

With the scavenge air coolers being the predominant group of consumers in terms of heat load and flow requirement, it would be relevant to consider optimizing the set-point for these to maximize the SFOC of the main engine while ensuring that the water content of the scavenge air stays below critical limits. This could also remove the current restriction on the temperature of the coolant to the consumers, ($T_{LT,in}$), as this is usually set to 34-36 °C to avoid water carry-over from the scavenge air coolers to the cylinders. This would make the 3-way valve in the LT FW circuit redundant, and the exergy loss in the bypass of the Central FW Coolers could be avoided.

If the restriction on the temperature of the coolant to the consumers where removed, it would be relevant to consider using this to optimize the load distribution between the SW pumps and LT FW pumps given the operating conditions in terms of seawater temperature and ME load.

With the increased number of measurements it would be relevant to investigate how fault detection and isolation algorithms could be used in the context of the single-phase marine cooling system. This could help avoid damage to the cooling system or any of the consumers connected to it, but it could also be of use for the crew when accommodating faults.

With the base-line design implemented on "Maersk Senang" performing well despite its lack of delay compensation, it would be relevant to analyze the conditions for which delays are a concern in terms of stability. While the layout and operation of the cooling system on "Maersk Senang" may not require the control to include delay compensation, this may not hold true for other vessels, and determining if and when delay compensation is necessary for a specific vessel would be a valuable tool. This would especially be important in the case where ($T_{LT,in}$) is used for energy optimization, i.e., where the constant set-point restriction is removed.

In context of implementation of the revised instrumentation and control strategy presented in this work, the following practical issues should be considered carefully:

The control structure and design presented in this work is based on the assumption of a specific layout of the system, and deviations from this layout may limit the scale of the implementation. A thorough investigation of the cooling system layout of the vessel series considered for retrofit is therefore necessary to determine what is practically feasible.

Some of the modifications in relation to this retrofit, such as installation of control valves, are very difficult to do except when the vessel is in dry-dock. For most vessels this only happens once every fourth year, so this should be taken into account if planning a large scale roll-out.

References

[1] J. Faber, H. Wang, D. Nelissen, B. Russell, and D. St-Amand, "Reduction of GHG Emissions from Ships," *International Maritime Organization (IMO)*, vol. 61, 2009.

[2] R. Jorgensen, "Slow steaming - The full story," *Group Relations - A.P. Moller - Maersk Group*, 2011.

[3] L. Bloomberg, "Rotterdam IFO380 prices from 03-01-2006 to 22-02-2010," *Bloomberg database*, 2010.

[4] Ø. Buhaug, J. Corbett, Ø. Endresen, and V. Eyring, "Updated Study on Greenhouse Gas Emissions from Ships: Phase I Report," *International Maritime Organization (IMO)*, no. September, 2008.

[5] O. Buhaug, J. J. Corbett, O. Endresen, and V. Eyring, "Second IMO GHG study 2009," *International Maritime Organization (IMO)*, 2009.

[6] J. Faber, A. Markowska, D. Nelissen, M. Davidson, I. C. Eyring, Veronika, P. Roche, E. Humpries, N. Rose, J. Graichen, and M. Cames, "Technical support for european action to reducing greenhouse gas emissions from international maritime transport," *Commissioned by: European Commission*, 2009.

[7] MEPC, "Guidelines on the Method of Calculation of the Attained Energy Efficiency Design Index (EEDI) for New Ships," *IMO*, vol. 212, no. March 2012, pp. 1–20, 2013.

[8] ——, "Protocol of 1997 to Amend the International Convention for the Prevention of Pollution From Ships, 1973, as Modified by the Protocol of 1978 Relating," *IMO*, vol. 203, no. July 2011, pp. 1–17, 2008.

[9] Z. Bazari and T. Longva, "Assessment of IMO Mandated Energy Efficiency Measures for International Shipping," *International Maritime Organization (IMO)*, no. October, 2011.

[10] United Nations Statistics Division, "Carbon dioxide emissions (CO2), metric tons of CO2 per capita (CDIAC)," *Millennium Development Goals Database*, 2012, last database update: 12 Sep, 2012.

[11] Centre on Emission Inventories and Projections (CEIP), "Emissions per capita, Emissions per GDP, Emissions per GNI/PPP," *Inventory Review 2012*, 2012.

[12] M. Massoud, *Engineering Thermofluids: Thermodynamics, Fluid Mechanics, and Heat Transfer*. Springer, 2005.

[13] S. J. Pugh, G. F. Hewitt, and H. Müller-Steinhagen, "Fouling During the Use of Seawater as Coolant - the Development of a User Guide," *Heat Transfer Engineering*, vol. 26, pp. 35–43, 2005.

[14] T. Ahonen, J. Tamminen, J. Ahola, J. Viholainen, N. Aranto, and J. Kestilä, "Estimation of pump operational state with model-based methods," *Energy Conversion and Management*, vol. 51, no. 6, pp. 1319–1325, 2010.

[15] Z. Wu, M. Tryby, E. Todini, and T. Walski, "Modeling variable-speed pump operations for target hydraulic characteristics," *Journal American Water Works*, 2009.

[16] B. Ulanicki, J. Kahler, and B. Coulbeck, "Modeling the Efficiency and Power Characteristics of a Pump Group," *Journal of Water Resources Planning and Management*, vol. 134, 2008.

[17] T. L. Andersen, D. F. Lauritzen, and J. T. Madsen, "Optimized control for energy optimization of shipboard cooling system," *Master thesis, Aalborg University, Section for Automation and Control*, 2009.

[18] E. W. Schreiber and J.-E. Räsänen, "Using Variable Frequency Drives (VFD) to save energy and reduce emissions in newbuilds and existing ships," *ABB Marine and Cranes*, 2012.

[19] Desmi, "DESMI OptiSave^{TM}- Optimizing Pump Speed to Current Conditions," *www.desmi.com*, 2011.

[20] K. Kirkegaard, "Grundfos Industrial Solutions," in *Green Ship Technology Conference, 2012*, 2012.

[21] T. Mrakovcic, V. Medica, and N. Skific, "Numerical Modelling of an Engine-Cooling System," *Journal of Mechanical Engineering*, no. 50, pp. 104–114, 2004.

[22] H. Cross, "Analysis of flow in networks of conduits or conductors," *University of Illinois Bulletin*, 1936.

[23] R. K. Gupta, *Analysis and control of flows in pressurized hydraulic networks*. A.A. Balkema Publishers, 2006.

[24] Y. Hu, O. I. Koroleva, and M. Krstić, "Control design for mine ventilation network systems," in *Proceedings of Conference On Decision and Control, 2002*, 2002, pp. 543–548.

[25] Y. Hu, O. Koroleva, and M. Krstić, "Nonlinear control of mine ventilation networks," *Systems & Control Letters*, vol. 49, pp. 239–254, 2003.

[26] O. Koroleva and M. Krstić, "Nonlinear and adaptive decentralized controllers for fluid flow networks," in *Proceedings of American Control Conference, 2003.*, vol. 4, 2003, pp. 3178–3183.

[27] T. Jensen, "Plug & Play Control of Hydraulic Networks," Ph.D. dissertation, Aalborg University, 2011.

[28] C. De Persis and C. S. Kallesøe, "Proportional and proportional-integral controllers for a nonlinear hydraulic network," in *Proceedings of the 17th IFAC World Congress*, 2008.

[29] ——, "Pressure regulation in nonlinear hydraulic networks by positive controls," in *European Control Conference*, 2009.

[30] ——, "Quantized controllers distributed over a network: An industrial case study," in *Mediterranean Conference on Control and Automation*, 2009.

[31] ——, "Pressure regulation in nonlinear hydraulic networks by positive and quantized controls," *IEEE Transactions on Control Systems Technology*, vol. 19, pp. 1371–1383, 2011.

[32] P. Jie, Z. Tian, S. Yuan, and N. Zhu, "Modeling the dynamic characteristics of a district heating network," *Energy*, vol. 39, pp. 126–134, 2012.

[33] I. Gabrielaitiene, B. Bøhm, and B. Sunden, "Modelling temperature dynamics of a district heating system in Naestved, Denmark - A case study," *Energy Conversion and Management*, vol. 48, pp. 78–86, 2007.

[34] H. V. Larsen, B. Bøhm, and M. Wigbels, "A comparison of aggregated models for simulation and operational optimisation of district heating networks," *Energy Conversion and Management*, vol. 45, pp. 1119–1139, 2004.

[35] K. J. Åström and T. Hägglund, *PID controllers: theory, design, and tuning.* Research Triangle Park, N.C:ISA, The International Society for Measurement and Control, 1995.

[36] G. F. Franklin, J. D. Powell, and A. Emami-Naeini, *Feedback Control of Dynamical Systems.* Prentice Hall, 2006.

[37] M. Chidambaram and R. Padma Sree, "A simple method of tuning PID controllers for integrator/dead-time processes," *Computers & Chemical Engineering*, vol. 27, pp. 211–215, 2003.

[38] H. K. Khalil, *Nonlinear Systems.* Prentice Hall, 2001.

[39] J. S. Shamma, *Analysis and design of gain scheduled control systems*. Massachusetts Institute of Technology, 1988.

[40] W. J. Rugh, "Analytical framework for gain scheduling," *Control Systems, IEEE*, 1991.

[41] R. Toth, *Modeling and Identification of Linear Parameter-Varying Systems*. Springer, 2010.

[42] M. Jung and K. Glover, "Control-oriented linear parameter-varying modelling of a turbocharged diesel engine," in *Proceedings of 2003 IEEE Conference on Control Applications, 2003.*, 2003, pp. 155–160.

[43] J. S. Shamma and M. Athans, "Gain scheduling: Potential hazards and possible remedies," *IEEE Control Systems Magazine*, no. June, 1992.

[44] P. Apkarian and P. Gahinet, "A convex characterization of gain-scheduled H controllers," *Automatic Control, IEEE Transactions on*, vol. 40, pp. 853–864, 1995.

[45] J. S. Shamma and M. Athans, "Guaranteed properties of gain scheduled control for linear parameter-varying plants?" *Automatica*, vol. 27, pp. 559–564, 1991.

[46] F. Wu, A. Packard, and G. Balas, "LPV control design for pitch-axis missile autopilots," *Proceedings of Conference on Decision & Control, 1995*, no. December, pp. 2–7, 1995.

[47] J. S. Shamma and J. R. Cloutier, "Gain-scheduled missile autopilot design using linear parameter varying transformations," *Journal of Guidance, Control, and Dynamics*, vol. 16, pp. 256–263, 1993.

[48] X. Zhang, P. Tsiotras, and C. Knospe, "Stability analysis of LPV time-delayed systems," *International Journal of Control*, vol. 75, pp. 538–558, 2002.

[49] F. Wu and K. M. Grigoriadis, "LPV Systems with parameter-varying time delays: analysis and control," *Automatica*, vol. 37, pp. 221–229, 2001.

[50] K. Tan, K. M. Grigoriadis, and F. Wu, "H_∞ and L_2 - to - L_∞ gain control of linear parameter-varying systems with parameter-varying delays," in *IEEE Proceedings - Control Theory and Applications*, vol. 150, 2003, p. 509.

[51] C. Briat, O. Sename, and J. Lafay, "Delay-scheduled state-feedback design for time-delay systems with time-varying delays - A LPV approach," *Systems & Control Letters*, vol. 58, pp. 664–671, 2009.

[52] R. Zope, J. Mohammadpour, K. Grigoriadis, and M. Franchek, "Robust fueling strategy for an SI engine modeled as an linear parameter varying time-delayed system," in *American Control Conference (ACC), 2010*. IEEE, 2010, pp. 4634–4639.

[53] J.-P. Richard, "Time-delay systems: an overview of some recent advances and open problems," *Automatica*, vol. 39, pp. 1667–1694, 2003.

[54] O. J. M. Smith, "A controller to overcome dead time," *ISA Transactions*, vol. 6, pp. 28–33, 1959.

[55] Z. Artstein, "Linear systems with delayed controls: a reduction," *Automatic Control, IEEE Transactions on*, pp. 443–445, 1982.

[56] W. Kwon and A. E. Pearson, "Feedback Stabilization of Linear Systems with Delayed Control," *IEEE Transactions on Automatic Control*, vol. 25, pp. 266–269, 1980.

[57] A. Manitius and A. Olbrot, "Finite spectrum assignment problem for systems with delays," *Automatic Control, IEEE Transactions on*, pp. 541–553, 1979.

[58] Q. C. Zhong, "On Distributed Delay in Linear Control Laws-Part I: Discrete-Delay Implementations," *IEEE Transactions on Automatic Control*, vol. 49, pp. 2074–2080, 2004.

[59] M. Krstić, "On compensating long actuator delays in nonlinear control," *Automatic Control, IEEE Transactions on*, vol. 53, pp. 1684–1688, 2008.

[60] ——, "Input delay compensation for forward complete and strict-feedforward nonlinear systems," *Automatic Control, IEEE Transactions on*, pp. 287–303, 2010.

[61] ——, *Delay Compensation for Nonlinear, Adaptive, and PDE Systems*. Birkhauser, 2009.

[62] M. Jankovic, "Control of nonlinear systems with time delay," *Decision and Control, 2003. Proceedings. 42nd*, pp. 4545–4550, 2004.

[63] ——, "Control of cascade systems with time delay – the integral cross-term approach," *Proceedings of the 45th IEEE Conference on Decision and Control*, pp. 2547–2552, 2006.

[64] ——, "Cross-Term Forwarding for Systems With Time Delay," *IEEE Transactions on Automatic Control*, vol. 54, pp. 498–511, 2009.

[65] M. Nihtila, "Adaptive control of a continuous-time system with time-varying input delay*1," *Systems & Control Letters*, vol. 12, pp. 357–364, 1989.

[66] ——, "Finite pole assignment for systems with time-varying input delays," in *Decision and Control, 1991., Proceedings of the 30th IEEE Conference on*. IEEE, 1991, pp. 927–928.

[67] M. Krstić, "Lyapunov stability of linear predictor feedback for time-varying input delay," *Automatic Control, IEEE Transactions on*, pp. 1336–1341, 2010.

[68] N. Bekiaris-Liberis and M. Krstic, "Compensation of Time-Varying Input and State Delays for Nonlinear Systems," *Journal of Dynamic Systems, Measurement, and Control*, vol. 134, p. 011009, 2012.

[69] R. Su, "On the linear equivalents of nonlinear systems," *Systems & Control Letters*, vol. 2, pp. 48–52, 1982.

[70] L. Hunt, R. Su, and G. Meyer, "Global transformations of nonlinear systems," *Automatic Control, IEEE Transactions on*, pp. 24–31, 1983.

[71] A. Isidori and A. Ruberti, "On the synthesis of linear input-output responses for nonlinear systems," *Systems & Control Letters*, vol. 4, pp. 17–22, 1984.

[72] A. Isidori and A. Krener, "On feedback equivalence of nonlinear systems," *Systems & Control Letters*, vol. 2, pp. 118–121, 1982.

[73] A. J. Krener, A. Isidori, and W. Respondek, "Partial and robust linearization by feedback," in *Proceedings of the 22nd IEEE Conference on Decision and Control (CDC)*, 1983, pp. 2–6.

[74] T. Oguchi and A. Watanabe, "Input-output linearization of nonlinear systems with time delays in state variables," *International Journal of Systems Science*, pp. 573–578, 1998.

[75] A. Germani, C. Manes, and P. Pepe, "Linearization and decoupling of nonlinear delay systems," *American Control Conference, 1998*, pp. 1948–1952, 1998.

[76] S. Tøffner-Clausen, "System Identification and Robust Control : A Synergistic Approach," Ph.D. dissertation, Aalborg University, 1995.

[77] J. Doyle, K. Glover, P. Khargonegar, and B. Francis, "State space solutions to standard H2 and Hinf control problems," in *American Control Conference, 1988*, 1988, pp. 1691–1696.

[78] J. Doyle, K. Glover, and P. P. Khargonekar, "State-space Solutions to Standard H_2 and H_∞ Control Problems," *IEEE Transactions on Automatic Control*, vol. 34, 1989.

[79] R. Chiang and M. Safonov, "Design of H_∞ Controller for a Lightly Damped System using a Bilinear Pole Shifting Transform," in *American Control Conference (ACC), 1991*, vol. 4. IEEE, 1991, pp. 1927–1928.

[80] R. Chiang and M. G. Safonov, "H^∞ Synthesis Using a Bilinear Pole Shifting Transform," *Journal of guidance, control, and dynamics*, vol. 15, pp. 1111–1117, 1992.

[81] S. Skogestad and I. Postlethwaite, *Multivariable feedback control : analysis and design*. New York : Wiley, 1996.

[82] K. Zhou, J. C. Doyle, and K. Glover, *Robust and optimal control*. Upper Saddle River, N.J. : Prentice Hall, 1996.

[83] K. Zhou and J. C. Doyle, *Essentials of robust control*. Upper Saddle River, N.J. : Prentice Hall, 1998.

[84] J. Hauser, S. Sastry, and P. Kokotovic, "Nonlinear control via approximate input-output linearization: The ball and beam example," *IEEE Transactions on Automatic Control*, vol. 31, 1992.

[85] B. Chang, H. Kwtany, and S.-S. Hu, "An Application of Robust Feedback Linearization to a Ball and Beam Control Problem," in *Proceedings of the 1998 IEEE International Conference on Control Applications.*, vol. 1. IEEE, 1998, pp. 694–698.

[86] R. Fales and A. Kelkar, "Robust control design for a wheel loader using mixed sensitivity h-infinity and feedback linearization based methods," *Proceedings of the 2005, American Control Conference.*, vol. 1, pp. 4381–4386, 2005.

[87] T. Yu, K. Chan, J. Tong, B. Zhou, and D. Li, "Coordinated robust nonlinear boiler-turbine-generator control systems via approximate dynamic feedback linearization," *Journal of Process Control*, vol. 20, pp. 365–374, 2010.

[88] E. Menon, *Liquid Pipeline Hydraulics*. CRC Press, 2004.

[89] A. E. Bryson and Y.-C. Ho, *Applied Optimal Control: Optimization, Estimation, and Control*. Blaisdell, 1969.

[90] M. Knudsen, "A sensitivity approach for estimation of physical parameters," in *Proceedings of the 10th IFAC Symposium on System Identification, Copenhagen July 1994*, 1994, pp. 231–236.

Part II

Papers

Paper A

Modeling of Nonlinear Marine Cooling Systems with Closed Circuit Flow

Michael Hansen
Jakob Stoustrup
Jan Dimon Bendtsen

The paper has been published in the
Proceedings of the 18th IFAC World Congress Vol. 18(1), pp. 5537–5542, 2011.

Abstract

We consider the problem of constructing a mathematical model for a specific type of marine cooling system. The system in question is used for cooling the main engine and auxiliary components, such as diesel generators, turbo chargers and main engine air coolers for certain classes of container ships. The purpose of the model is to describe the important dynamics of the system, such as nonlinearities, transport delays and closed circuit flow dynamics to enable the model to be used for control design and simulation. The control challenge is related to the highly non-standard type of step response, which requires more detailed modeling.

1 Introduction

Maritime transportation is today considered to be the most energy efficient means of transportation when considering fuel consumption per ton goods [1]. However, only in recent years have energy optimization of container ships and especially their subsystems gained the appropriate attention when building and modifying such ships. One of the subsystems that shows significant potential when it comes to energy optimization is the cooling system for the main engine and auxiliary components. Today, the cooling systems used onboard several classes of container ships are typically controlled manually with the assistance of a few simple controllers. This means that the pumps in this type of cooling system are used excessively, and that operating conditions for the consumers in the cooling system are not necessarily optimal. To deal with these shortcomings it is desired to introduce a control scheme that is not only optimal in terms of energy consumption, but also able to ensure optimal operating conditions for the consumers in the cooling system.

This paper concerns the construction of a model for the marine cooling system that can be used for controller design and simulation. Later work will deal with design and verification of controllers based on the models derived here.

Similar modeling have been carried out in [2] and [3], where design of control laws for a system with hydraulic resemblance to the system in this work, is considered. However, since the objective in [2] and [3] is to control the pressure at some end users, the constructed model and corresponding controller design only covers the hydraulic part of the system. In our context it is desired to include the thermodynamics of the system, as the temperature of the consumers in the cooling system is of great importance when it comes to set point optimization. Therefore the method from [2] is adopted to cover the hydraulics, while the main contribution of this paper is the derivation of a thermodynamic model for the cooling system.

The size and structure of the cooling system results in significant transport delays that are dependent on the flow rates in the system. The introduction of energy optimiz-

ing control is likely to decrease the overall flow rates in the system, which means that the transport delays will increase. Furthermore, because the coolant is recirculated, the cooling system is subject to closed circuit flow dynamics, i.e., the response to any action performed on the system will repeat itself in some form. The result is that a classic control design may prove insufficient when dealing with both delays and closed circuit flow dynamics; this is best illustrated through a simple example. Let us assume that the system can be modeled as a linear first order system with a time delay as illustrated in Fig. A.1. The closed circuit flow dynamics is modeled by the red positive feedback path in Fig. A.1. The open loop unit step response for the system in Fig. A.1 with

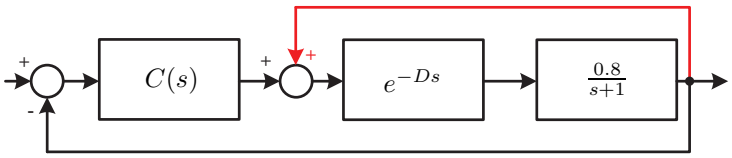

Fig. A.1: Example system with time delay D and closed circuit dynamics modeled with positive feedback.

$D = 20$ and $C(s) = 1$ is illustrated in the top plot of Fig. A.2. The system is stable

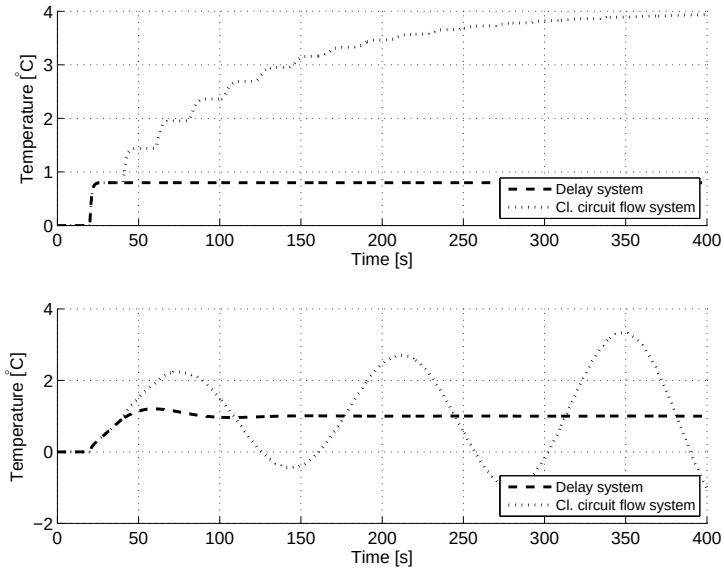

Fig. A.2: Top plot: Simulated open loop step response for first order delay system with and without closed circuit dynamics. Bottom plot: Simulated closed loop step response for PI compensated first order delay system with and without closed circuit dynamics.

both with and without the red positive feedback path in Fig. A.1, though the responses are very different. We now apply a regular PI controller on the form [4]:

$$C(s) = k_p + \frac{k_i}{s} , \tag{A.1}$$

where we set $k_p = 0.2$ and $k_i = \frac{1}{4}$. The resulting closed loop unit step response is illustrated in the bottom plot of Fig. A.2. The PI compensated system without the red feedback path from Fig. A.1 is clearly stable, while the system including the red feedback path is unstable. This example illustrates how it is possible to design a PI controller for a delay system such that the compensated system is stable, and how the same compensated system becomes unstable if it is subject to closed circuit flow dynamics. In future control design, which is not presented in this paper, theory from infinite dimensional systems will be applied for compensation of delays and of the closed circuit flow dynamics. The model derived in this paper is therefore structured to facilitate this control design approach.

In Section 2 the cooling system is outlined in order to provide an overview of its structure and function. Section 3 describes the derivation of the model, which is divided into a hydraulic and thermodynamic part. Section 4 provides verification of part of the derived model and a simulation example to illustrate the dynamics of the model. Finally, conclusions are given in Section 5.

2 System Description

The cooling system consists of three circuits; a sea water (SW) circuit, a low temperature fresh water (LT FW) circuit and a high temperature fresh water (HT FW) circuit. This is illustrated in Fig. A.3 where q_{LT} and q_{SW} are volumetric flows in the LT FW and SW circuits, while q_{HT} is the volumetric flow to the HT FW circuit.

As the name implies, the SW circuit pumps sea water through the cold side of the central coolers for lowering the temperature of the coolant in the LT FW and HT FW circuits. The LT FW circuit contains all the auxiliary components that need cooling, such as diesel generators and turbochargers, all coupled in parallel. The HT FW circuit is only responsible for cooling the main engine of the ship, and since the cooling demand for the main engine is very strict there is little room for energy optimization in this part of the system. The main concern is therefore the LT FW circuit and the SW circuit.

Models are constructed based on the assumptions that all flows are turbulent, and there are no laminar flow effects. There is also no heat loss to surroundings, i.e., heat exchange only takes place in the consumers or in the central coolers. There is no phase change of the coolant, and density as well as specific heat of the coolant is assumed to be constant in the temperature range of interest. Finally, the coolant in the system is assumed to be incompressible.

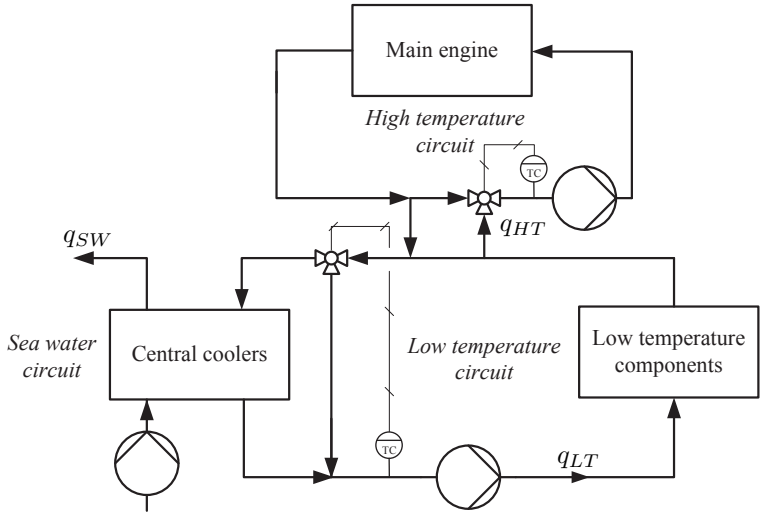

Fig. A.3: Simplified system layout.

Each consumer in the LT FW system consists of a control valve in series with a heat exchanger and two pipe sections, as illustrated in Fig. A.4. From a control point of

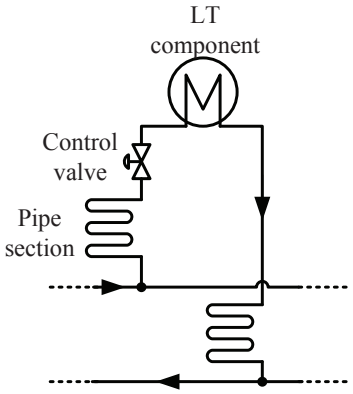

Fig. A.4: Structure of the components in the LT circuit.

view it is desired to adjust the temperature of the components in the LT FW circuit to an operational and energy-wise optimal set point. This should be achieved by the most energy efficient control inputs which are generated by the pumps and control valves. The model should therefore express how the control input and disturbances affect the

temperature of the components as illustrated in Fig. A.5.

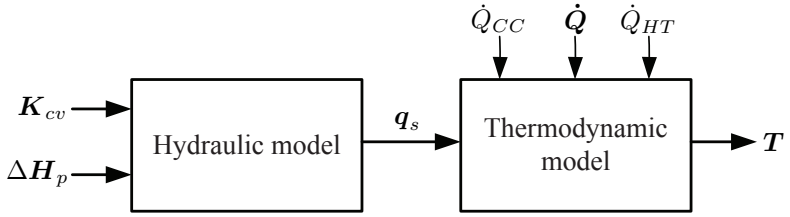

Fig. A.5: Block diagram of the model structure.

In Fig. A.5, $\boldsymbol{K}_{cv}$, $\Delta \boldsymbol{H}_p$, and $\boldsymbol{q}_s$ denotes the position of the control valves, delivered pump head, and volumetric flows, while $\dot{Q}_{CC}, \dot{\boldsymbol{Q}}$ and $\dot{Q}_{HT}$ are heat transfer from Central FW Coolers, consumers, and the HT FW circuit, respectively.

3 Modeling

The modeling is divided into two parts; a hydraulic part and a thermodynamic part. The reason for this division is that the thermodynamics in the system is assumed not to influence the hydraulics and it is therefore possible to consider the overall system as a thermodynamic part in cascade with a hydraulic part. In addition, there is a separation of time scales since the time constants of the heat dynamics are much slower than the hydraulic dynamics. The purpose of the hydraulic model is to describe the flow through the components in the three circuits as a function of the pump speeds and the position of the control valves. These flows are inputs to the thermodynamic model, which describes the temperature of the components in the system as a function of the sea water temperature, the heat generated by the components and of course the flows in the system.

3.1 Hydraulic model

The hydraulic model is separated into two parts; the SW circuit hydraulics and the LT FW circuit hydraulics, respectively. Due to the small number of components and the simple structure of the SW circuit, equations governing the flow for this system are derived directly using basic hydraulic laws. In the LT FW circuit however, the individual consumers are placed in parallel and are modeled as illustrated in Fig. A.4. This structure yields strong similarities with the system presented and modeled in [2] and the model for the LT FW circuit hydraulics is therefore constructed by following the same method and notation. This means that valves are described by the relation:

$$p_i - p_j = K_v |q_v| q_v \ , \tag{A.2}$$

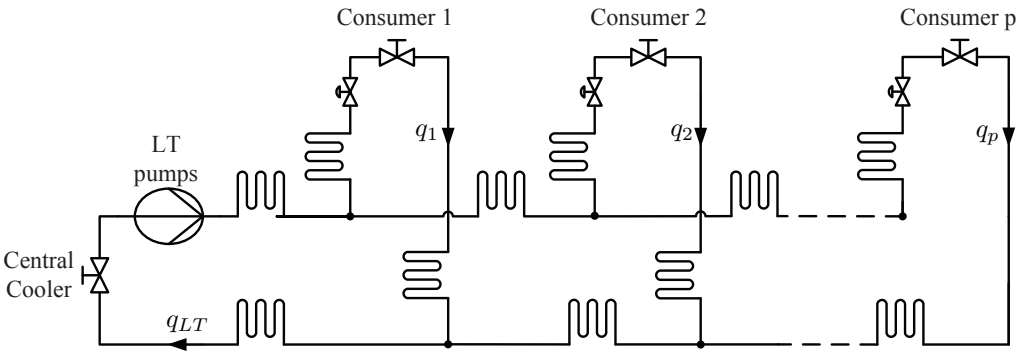

Fig. A.6: Simplified hydraulic structure of the LT FW circuit where valves model the pressure losses in the heat exchangers.

where $(p_i - p_j)$ is the pressure drop across the valve, K_v is a variable describing the valve position, i.e. the change in hydraulic resistance of the valve, and q_v is the volumetric flow through the valve. In a similar manner, pipe sections are modeled as:

$$J\frac{dq_p}{dt} = (p_i - p_j) - K_p|q_p|q_p \ , \tag{A.3}$$

where J and K_p are constant parameters for the pipe section, $(p_i - p_j)$ is the pressure drop along the pipe and q_p is the flow through the pipe. Finally, pumps are simply modeled as a pressure difference:

$$p_i - p_j = -\Delta H_p \ , \tag{A.4}$$

where $(p_i - p_j)$ is the pressure across the pump and ΔH_p is the delivered pump head.

The SW circuit consists of two pumps in parallel, two pipe sections and a heat exchanger which is modeled as a valve from a hydraulic point of view [5]. Since the circuit is not closed there should also be included a pressure drop due to the difference in height between the sea water circuit inlet and outlet. Since the sum of pressure drops in a closed loop must equal zero, the models given in (A.2), (A.3) and (A.4) can be combined to yield the following result:

$$\begin{aligned}\Delta H_{p,SW} =&(J_{p1} + J_{p2})\dot{q}_{SW} \\ &+ (K_{p1} + K_{cc} + K_{p2})|q_{SW}|q_{SW} + \Delta p_{io} \ ,\end{aligned} \tag{A.5}$$

where $\Delta H_{p,SW}$ is the delivered pump head, J_{p1}, J_{p2}, K_{p1} and K_{p2} are pipe section parameters, K_{cc} describes the hydraulic resistance in the central cooler and Δp_{io} is the pressure difference due to difference in height between SW inlet and outlet. Rearranging and combining constants such that $J_{SW} = J_{p1} + J_{p2}$ and $K_{SW} = K_{p1} + K_{cc} + K_{p2}$ yields:

$$J_{SW}\dot{q}_{SW} = -K_{SW}|q_{SW}|q_{SW} - \Delta p_{io} + \Delta H_{p,SW} \ . \tag{A.6}$$

The hydraulics of the LT FW circuit is assumed to have the structure shown in Fig. A.6. Compared to the simplified diagram from Fig. A.3 it is seen that the shunt at the central cooler is not included in the hydraulic structure. This is justified by the observation that in the final control scheme it is desired to control the inlet water temperature in the LT FW circuit using the pumps in the SW circuit, such that the shunt valve is closed at all times, and thereby does not influence the hydraulics of the LT FW system. Using the notation from [2] the hydraulic model for the LT FW system can be constructed as:

$$\boldsymbol{B}\boldsymbol{J}\boldsymbol{B}^T\dot{\boldsymbol{q}} = -\boldsymbol{B}\boldsymbol{\lambda}(\boldsymbol{K}_p, \boldsymbol{B}^T\boldsymbol{q}) - \boldsymbol{B}\boldsymbol{\mu}(\boldsymbol{K}_v, \boldsymbol{B}^T\boldsymbol{q}) - \boldsymbol{B}\boldsymbol{\mu}_{cv}(\boldsymbol{\varphi}_{cv}, \boldsymbol{B}^T\boldsymbol{q}) + \boldsymbol{B}\Delta\boldsymbol{H}_p \tag{A.7}$$

where B is the fundamental loop matrix, see [2] for details. Furthermore, we have that:

$$\begin{aligned}
\Delta\boldsymbol{H}_p &= [\Delta H_{p,1}, \ldots, \Delta H_{p,m}]^T \ , \\
\boldsymbol{J} &= diag\{J_1, \ldots, J_k\} \ , \\
\boldsymbol{\lambda}(\boldsymbol{K}_p, \boldsymbol{q}_c) &= [\lambda_1(K_{p,1}, q_{c,1}), \ldots, \lambda_m(K_{p,m}, q_{c,m})]^T \ , \\
\boldsymbol{\mu}(\boldsymbol{K}_v, \boldsymbol{q}_c) &= [\mu_1(K_{v,1}, q_{c,1}), \ldots, \mu_m(K_{v,m}, q_{c,m})]^T \ , \\
\boldsymbol{\mu}_c(\boldsymbol{K}_{cv}, \boldsymbol{q}_c) &= [\mu_{c,1}(K_{cv,1}, q_{c,1}), \ldots, \mu_{c,m}(K_{cv,m}, q_{c,m})]^T \ ,
\end{aligned} \tag{A.8}$$

where m is the number of components in the hydraulic network. The index $\{cv\}$ in (A.7) indicates contributions from controllable valves, as these generates inputs to the hydraulic system and should be distinguished from other valve types.

3.2 Thermodynamic model

The thermodynamic model is derived using basic thermodynamic laws, and consists of three parts; one part describing the temperature change in the components and two parts describing the transport phenomenon between the central coolers and the components in the LT FW circuit. All consumers are modeled as heat exchangers, so by use of the first law of thermodynamics and Reynolds Transport Theorem [6] it is possible to derive the following equation:

$$\begin{aligned}
\sum \dot{Q} - \sum \dot{W} = &\frac{d}{dt}\int_\Omega e\rho \ dV \\
&+ \sum e_{out}\rho_{out}A_{out}v_{out} \\
&- \sum e_{in}\rho_{in}A_{in}v_{in} \ ,
\end{aligned} \tag{A.9}$$

where $\dot{Q}$ is heat transfer rate in or out of the system, $\dot{W}$ is the rate of work transfer in or out of the system, e is the specific energy of the system and ρ is the density of the fluid elements in the system. Also, Ω is the control volume, v is the average velocity

of the flow at in- or outlet, and A is the control volume cross section area at the in- or outlet.

In this case, the rate of the work transfer term can be described as the pressure forces acting on the inlet and outlet of the control volume, which can be written as

$$\sum \dot{W} = \dot{W}_{pf} = p_{in} A_{in} v_{in} - p_{out} A_{out} v_{out} \ . \tag{A.10}$$

Since there is only a single flow from inlet to outlet it is possible to write:

$$\dot{m} = \rho_{in} A_{in} v_{in} = \rho_{out} A_{out} v_{out} \ . \tag{A.11}$$

It is assumed that the change in potential and kinetic energy in the control volume can be neglected such that $e = u$ with u being the internal energy per mass unit. Also, $\sum \dot{Q} = \dot{Q}_{con}(t)$ which leads to the following result:

$$\frac{d}{dt} \int_{\Omega} e(t)\rho \ dV = \dot{m} \left(h_{in}(t) - h_{out}(t) \right) + \dot{Q}_{con}(t) \tag{A.12}$$

where we also have exploited the fact that enthalpy is defined as $h = u + \frac{p}{\rho}$. Since there is no change of phase of the coolant in and out of the control volume, the enthalpy terms can be approximated by [7]:

$$\Delta h \approx c_p \Delta T \ , \tag{A.13}$$

where c_p is the specific heat for the coolant and T is the temperature of the coolant. It is desired to have the model express the change in temperature rather than the change in stored energy. Preferably, the equation should express the change of energy in the control volume as a function of the outlet temperature. In order to keep the expression simple it is chosen to use the crude approximation:

$$\frac{d}{dt} \int_{\Omega} e(t)\rho \ dV \approx \rho c_p V_{CV} \frac{d \, T_{out}(t)}{dt} \ , \tag{A.14}$$

where V_{CV} is the volumetric size of the control volume. This yields the result:

$$\rho c_p V_{CV} \frac{d \, T_{out}(t)}{dt} = \dot{m}(t) c_p (T_{in}(t) - T_{out}(t)) + \dot{Q}_{con}(t) \ . \tag{A.15}$$

This means that in general for consumer $i = 1, \ldots, p$ we can write

$$\frac{d \, T_i(t)}{dt} = \frac{1}{\rho c_p V_i} \left(\dot{m}_i(t) c_p (T_{in,i}(t) - T_i(t)) + \dot{Q}_i(t) \right) \ , \tag{A.16}$$

where $\dot{m}_i$ is the mass flow rate through the consumer, V_i is the internal volume of the consumer, $\dot{Q}_i$ is the energy transfer from the consumer, while $T_{in,i}$ and T_i are the temperatures of the coolant at the inlet and outlet, respectively, of the consumer.

Because of the distance from the central cooler to the consumers there is a transport delay in the temperature of the coolant at the outlet of the central cooler, to the inlet of the individual consumer. This delay is different for each consumer due to their spacing relative to the central cooler. To derive an expression for the inlet temperature for each consumer as a function of the central cooler outlet temperature and the corresponding transport delay, the structure in Fig. A.7 is considered.

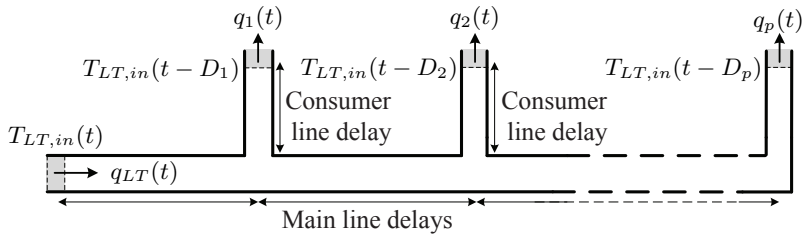

Fig. A.7: The distribution of coolant from the central coolers to the consumers in the LT FW circuit.

The relation between the flow rate and the corresponding transport delay in the temperature of the water at the inlet of consumer i can be written as:

$$T_{in,i}(t) = T_{LT,in}(t - D_i) \ , \tag{A.17}$$

with the flow dependent delay D_i given by:

$$D_i = \underbrace{\sum_{j=1}^{i} \left(a_{m,j} \sum_{k=j}^{n} q_k^{-1} \right)}_{\text{Main line delays}} + \underbrace{a_{c,i} q_i^{-1}}_{\text{Consumer line delay}} \ , \tag{A.18}$$

where $a_{m,i}$ and $a_{c,i}$ are system specific constants, and q_i is the flow to the i'th consumer.

For calculating the temperature of the coolant in the return path, i.e. the temperature of the coolant to the HT FW circuit, the structure in Fig. A.8 is considered.

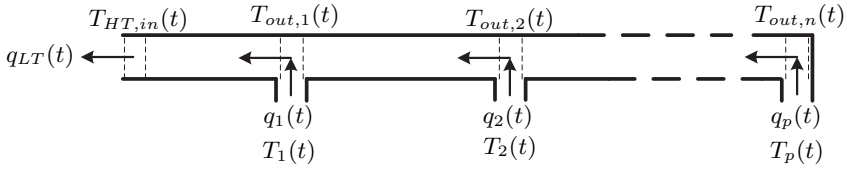

Fig. A.8: The combination of coolant flows from the consumers in the LT FW circuit to the HT FW circuit inlet.

According to Fig. A.8 the temperature at the inlet to the HT FW circuit can be written as:

$$T_{HT,in}(t) = T_{out,1}(t - D_{out,1}), \tag{A.19}$$

with the delay $D_{out,i}$ given by:

$$D_{out,i} = b_{m,i}\left(\sum_{j=i}^{n} q_j\right)^{-1} , \tag{A.20}$$

where $b_{m,i}$ is a system specific constant, and q_j is the flow from the j'th consumer. The temperature $T_{out,1}$ can be calculated in a recursive manner by solving the following equation iteratively for $j = n, n-1, \ldots, 1$:

$$\begin{aligned} T_{out,i}(t) =& T_i(t - D_{con,i})\frac{q_i(t)}{\sum_{j=i}^{n} q_j(t)} \\ &+ T_{out,n-1}(t - D_{out,n-1})\frac{\sum_{j=i+1}^{n} q_j(t))}{\sum_{j=i}^{n} q_j(t)} , \end{aligned} \tag{A.21}$$

where the delay $D_{con,i}$ is given by:

$$D_{con,i} = b_{c,i}q_i^{-1} . \tag{A.22}$$

Equation (A.21) builds on the assumption that the temperature of the coolant at consumer outlet no. i can be described by the temperature of the coolant from consumer i plus the temperature of the coolant at consumer outlet $i+1$ delayed by the time it takes the coolant to travel from consumer $i+1$ to i.

Since it is not desired to modify the control of the HT FW system, the HT FW circuit's impact on the temperature in the LT FW circuit is added to the model as a measured disturbance. It is assumed that the flow to the HT FW circuit equals the flow from the HT FW circuit. Denoting this flow by q_{HT} and the temperature of the water from the HT FW circuit by $T_{HT,out}$ the inlet temperature to the central coolers can be written as:

$$\begin{aligned} T_{LT,out} =& T_{HT,in}(t - D_{HT,out} - D_{HT,in}) \cdot \frac{(q_{LT} - q_{HT})}{q_{LT}} \\ &+ T_{HT,out}(t - D_{HT,out})\frac{q_{HT}}{q_{LT}} , \end{aligned} \tag{A.23}$$

where

$$D_{HT,out} = b_{HT,out}q_{LT}^{-1} \tag{A.24}$$

$$D_{HT,in} = b_{HT,in}(q_{LT} - q_{HT})^{-1} . \tag{A.25}$$

To close the circuit all we need is to describe the relation between the temperature into the central cooler, $T_{LT,out}$ and the temperature out of the central cooler, which has previously been defined as the inlet temperature $T_{LT,in}$. This relation is modeled using Equation (A.16) where the heat transfer to the SW circuit is considered to be steady state, which yields the result:

$$\begin{aligned}\frac{d\,T_{LT,in}(t)}{dt} =& \frac{1}{\rho c_p V_{CC}} \left[\dot{m}_{in}(t) c_p (T_{LT,out}(t) - T_{LT,in}(t)) \right. \\ &\left. + \dot{m}_{SW}(t) c_{p,SW} (T_{SW,in}(t) - T_{SW,out}(t))\right] \ .\end{aligned} \tag{A.26}$$

where $c_{p,SW}$ is the specific heat of the sea water.

To sum up the model, the dynamics of the hydraulic part is given by (A.7), while the dynamics of the thermodynamic part is governed by equations (A.16) and (A.26). The inlet temperatures for the LT FW system, the HT FW system, and the central coolers are described by relations (A.17), (A.19), (A.21) and (A.23) with delays given by (A.18), (A.20), (A.22), (A.24) and (A.25). Descriptively we can state the combined hydraulic and thermodynamic model as:

$$\begin{aligned}\dot{\boldsymbol{x}} &= f(\boldsymbol{x}, \boldsymbol{y}, \boldsymbol{u}, \boldsymbol{w}) \\ \boldsymbol{y} &= g(\boldsymbol{x}, \boldsymbol{y}, \boldsymbol{D}) \\ \boldsymbol{D} &= h(\boldsymbol{x})\end{aligned} \tag{A.27}$$

where:

$$\begin{aligned}\boldsymbol{x} =& [q_{SW}, q_{LT}, q_1, \ldots, q_n, T_{LT,in}, T_1, \ldots, T_p] \in \mathbb{R}^{2p+3} \\ \boldsymbol{y} =& [T_{LT,out}, T_{HT,in}, T_{in,1}, \ldots, T_{in,p}, \\ & T_{out,1}, \ldots, T_{out,p}] \in \mathbb{R}^{2p+2} \\ \boldsymbol{u} =& [H_{p,SW}, H_{p,LT}, K_{cv,1}, \ldots, K_{cv,p}] \in \mathbb{R}^{p+2} \\ \boldsymbol{w} =& [T_{SW,in}, T_{SW,out}, T_{HT,out}, q_{HT}, \dot{Q}_1, \ldots, \dot{Q}_p] \in \mathbb{R}^{p+4} \\ \boldsymbol{D} =& [D_{HT,in}, D_{HT,out}, D_1, \ldots, D_p, \\ & D_{out,1}, \ldots, D_{out,p}, D_{con,1}, \ldots, D_{con,p}] \in \mathbb{R}^{3p+2} \ .\end{aligned}$$

4 Model Verification

Measurement data from the M-class vessel “Margrethe Maersk” have been obtained and is used for model verification. Since the implemented control on “Margrethe Maersk” only requires a small number of measurements, the available data for model verification are very sparse. The sampling time of the data is 5 minutes, and the data only covers a few key temperatures as well as the main engine (ME) load and the speed of the pumps.

The consequence is that it is not possible to verify the hydraulic model as only the flow through the pumps can be estimated from the measurements and not the flow through each individual branch in the LT FW system. Also, the low sampling rate means that it is not possible to observe any transport phenomena in the measured temperature due to aliasing. However, it is possible to verify the model for the largest consumer in the LT FW circuit, namely the main engine scavenge air coolers, as both the inlet and outlet temperatures for this consumer are measured, and the flow through it can be reasonably estimated. Furthermore, the heat generated by the ME scavenge air coolers is a function of the ME load and can be approximated as well.

The measurement data covers a period of 68 days, and because model parameters for the ME scavenge air coolers are unknown, part of the measurement data is used for parameter estimation, while another part is used for model verification. The simulated and measured temperature responses for one of the three ME scavenge air coolers aboard "Margrethe Maersk" are illustrated in Fig. A.9(a) for a period of 6 days. The data used for parameter estimation are from a time period 34 days earlier, also covering a period of 6 days. Fig. A.9(a) shows how the dynamics of the simulated response matches well with measured response. The top plot of Fig. A.9(b) illustrates the LT FW inlet temperature while the bottom plot shows the ME load during the test period.

To illustrate the models ability to represent the closed circuit flow dynamics, we construct an example where the model is applied to a system with two identical consumers that are subject to different flows, and have different spacing relative to the central coolers. Due to the limited space it is not possible to state the model parameters for the example here, but it is possible to choose a set of parameters such that the model generates the dynamics shown in this example. The model is subjected to a positive step in the ME load, which increases the heat generated by the consumers. This step occurs after 5000 s and the top plot of Fig. A.10 shows how the closed circuit flow dynamics influences the outlet temperature responses for the two consumers. The effect of the delays is best observed from the shift in the inlet temperatures in the bottom plot of Fig. A.10.

5 Conclusions

We have presented a model of a marine cooling system with application to control design and simulation. The small number of available measurements restricted the verification of the model to only include part of the thermodynamics. The verification showed that when applying the thermodynamic consumer model to the ME scavenge air coolers in the LT circuit, the model response was very close to the measured response. An example showed that the model includes the dynamics necessary for adequately representing the behavior of the system. Future work includes verifying the remaining model and using the model for control design; first for developing a base line control for performance comparison, and later for designing energy and set point optimizing control laws.

References

[1] J.-P. Rodrigue, C. Comtois, and B. Slack, *The Geography of Transport Systems*. Routledge, 2006.

[2] C. De Persis and C. S. Kallesøe, "Pressure regulation in nonlinear hydraulic networks by positive controls," in *European Control Conference*, 2009.

[3] ——, "Proportional and proportional-integral controllers for a nonlinear hydraulic network," in *Proceedings of the 17th IFAC World Congress*, 2008.

[4] G. J. Silva, A. Datta, and S. P. Bhattacharyya, "Pi stabilization of first-order systems with time delay," *Automatica*, vol. 37, pp. 2025–2031, 2001.

[5] C. De Persis and C. S. Kallesøe, "Quantized controllers distributed over a network: An industrial case study," in *Mediterranean Conference on Control and Automation*, 2009.

[6] D. F. Young, B. R. Munson, T. H. Okiishi, and W. W. Huebsch, *A Brief Introduction to Fluid Mechanics*. John Wiley & Sons Ltd, 2007.

[7] M. Massoud, *Engineering Thermofluids: Thermodynamics, Fluid Mechanics, and Heat Transfer*. Springer, 2005.

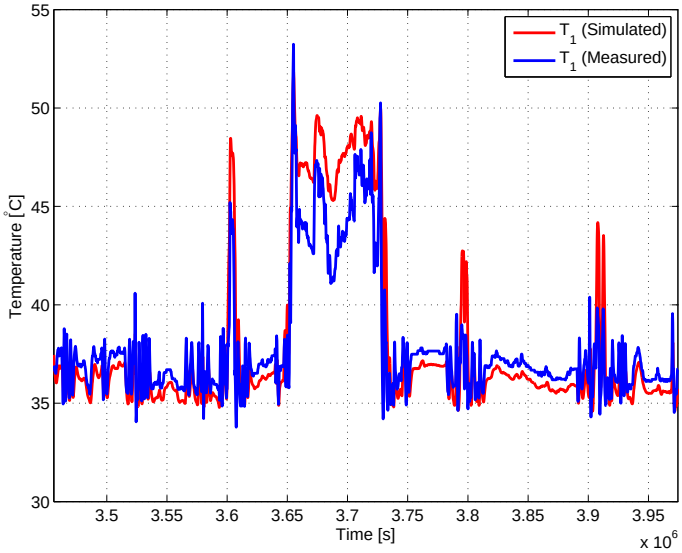

(a) Simulated and measured outlet temperature of ME scavenge air cooler 1

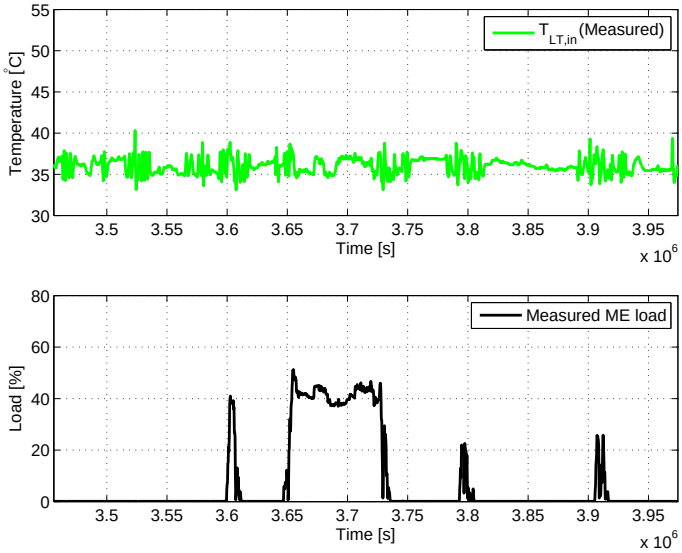

(b) Top plot: Inlet temperature for ME scavenge air cooler 1. Bottom plot: ME load percentage.

Fig. A.9: Simulation results for ME scavenge air cooler 1.

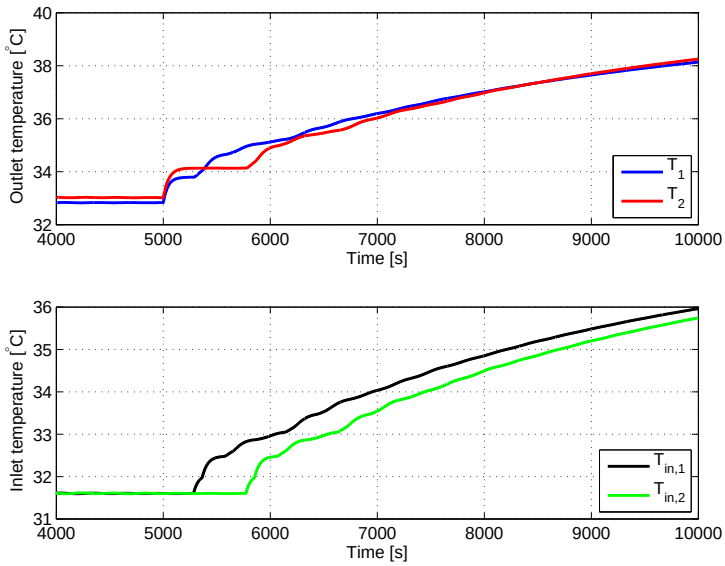

Fig. A.10: Top plot: Simulated outlet temperature responses for the two consumers in the example. Bottom plot: Simulated inlet temperature for the two consumers.

Paper B

Control of Non-linear Marine Cooling System

Michael Hansen
Jakob Stoustrup
Jan Dimon Bendtsen

The paper has been published in the
Proceedings of the IEEE International Conference on Control Applications, pp. 88–93,
2011.

The layout has been revised. This version of the paper has been modified from its original published version to include minor corrections.

Abstract

We consider the problem of designing control laws for a marine cooling system used for cooling the main engine and auxiliary components aboard several classes of container vessels. We focus on achieving simple set point control for the system and do not consider compensation of the non-linearities, closed circuit flow dynamics or transport delays that are present in the system. Control laws are therefore designed using classical control theory and the performance of the design is illustrated through a simulation example where it is compared to a reference control design.

1 Introduction

In recent years the attention to energy efficiency in the shipping industry has increased as a consequence of fluctuating oil prices [1] and a growing focus on CO_2, NO_x and SO_x emissions from maritime transportation [2]. This has led to several initiatives within the shipping industry to bring down the energy consumption in ocean-going vessels, ranging from waste heat recovery systems to energy optimization of subsystems [3].

In this paper we consider design of control laws for a cooling system found aboard several classes of ocean-going container vessels. The system in question is used for cooling the main engine and auxiliary components and currently makes use of a very simple control method. In the current control, the pumps in the cooling system are operated in three steps based on the temperature of the sea water and the load on the main engine [4]. The result is that the pumps in this type of cooling system are used excessively, and that operating conditions are unlikely to be optimal in particular for the main engine auxiliary components. This leaves a significant potential for energy savings by improving the existing controls, not only by lowering the power consumption of the pumps, but also by ensuring optimal operating conditions for the main engine auxiliary components and thereby improving their energy efficiency. The focus in this paper is on the latter, which means that the control design aims at achieving the desired set point temperatures for main engine auxiliary components, rather than achieving optimal energy efficiency for the pumps.

A model for the cooling system was derived in [5] and is adopted here for the control design and for simulating the compensated system. The control laws derived in this paper serves the purpose of improving the performance of the cooling system compared to the current control method.

The remainder of the paper is structured as follows: In Section 2 we give a short description of the system and present the model. In Section 3 we present the control strategy and derive control laws for the system. Section 4 presents simulation results for the control design and conclusions are given in Section 5.

2 Model

The cooling system consists of three circuits; a sea water (SW) circuit, a low temperature fresh water (LT FW) circuit and a high temperature fresh water (HT FW) circuit. This is illustrated in Fig. B.1 where q_{LT} and q_{SW} are volumetric flows in the LT FW and SW circuits, while q_{HT} is the volumetric flow to the HT FW circuit.

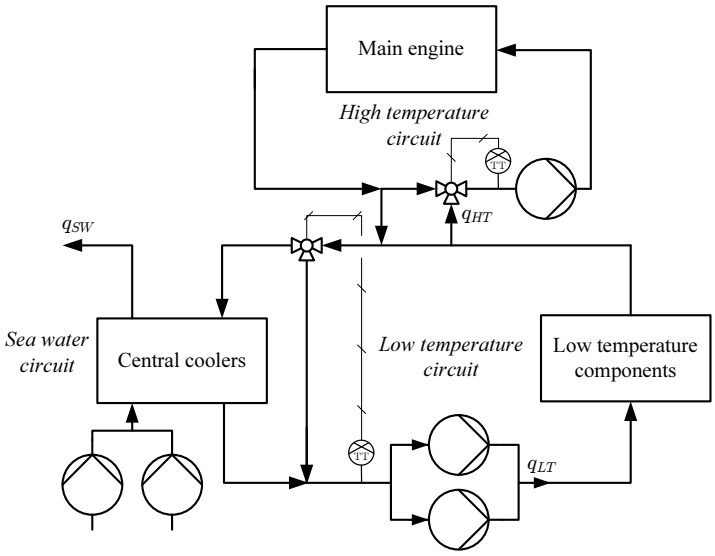

Fig. B.1: Simplified system layout.

The SW circuit pumps sea water through the cold side of the central coolers for lowering the temperature of the coolant in the LT FW and HT FW circuits. The HT FW circuit only contains the main engine of the ship, while the LT FW circuit contains all the main engine auxiliary components in a parallel configuration. In the current control scheme, the SW circuit pumps are operated in three steps depending on the temperature of the sea water and the operating mode of the vessel. This setup is designed such that the SW circuit provides sufficient cooling, even when the sea water temperature is high, which means that under most operating conditions the SW circuit generates excess cooling. Similar to the SW pumps the LT FW pumps are also controlled in three steps, depending on the sea water temperature, the operating mode of the vessel, and the main engine load percentage. There is a requirement for the temperature of the coolant to be at least 36°C at the inlet of some consumers, which is ensured by a temperature controller that adjusts the amount of coolant that is flowing through the shunt, past the central coolers.

We employ a model for the cooling system constructed in [5], and essential parts are repeated here for convenience. The model consists of two parts; one describing the hydraulics and one describing the thermodynamics.

2.1 Hydraulics

The hydraulic model describes the flow in the SW circuit and LT FW circuit respectively. The equation governing the flow in the SW circuit is given by:

$$J_{SW}\dot{q}_{SW} = -K_{SW}|q_{SW}|q_{SW} - \Delta p_{io} + \Delta H_{p,SW} \ , \tag{B.1}$$

where J_{SW} and K_{SW} are pipe section parameters, q_{SW} is the volumetric flow, Δp_{io} is the pressure drop due to difference in height from the sea water intake and outlet, and $\Delta H_{p,SW}$ is the delivered pump head.

The hydraulic model for the LT FW circuit was originally adopted from [6] and we use the same notation and definitions here. This means that we model valves as:

$$p_i - p_j = K_v|q_v|q_v \ , \tag{B.2}$$

where $(p_i - p_j)$ is the pressure drop across the valve, K_v is a variable describing the hydraulic resistance of the valve, and q_v is the volumetric flow through the valve. As a remark we introduce the index $\{cv\}$ for controllable valves to distinguish them from non-controllable valves, which we denote by index $\{v\}$. For simplicity, we also leave out valve characteristics and assume that the hydraulic resistance of a valve can be controlled directly, i.e., we do not take the non-linear relationship between valve opening degree and hydraulic resistance into account. Pipes are modeled as:

$$J\frac{dq_p}{dt} = (p_i - p_j) - K_p|q_p|q_p \ , \tag{B.3}$$

where J and K_p are constant parameters for the pipe section, $(p_i - p_j)$ is the pressure drop along the pipe and q_p is the flow through the pipe. Finally, pumps are modeled by:

$$p_i - p_j = -\Delta H_p \ , \tag{B.4}$$

where $(p_i - p_j)$ is the pressure across the pump and ΔH_p is the delivered pump head.

In the design presented in this paper we assume that the LT FW circuit contains only two consumers, resulting in a hydraulic structure as illustrated in Fig. B.2.

The model for the circuit illustrated in Fig. B.2 is derived using network theory and by applying the analogy between electrical and hydraulic circuits where voltage and currents corresponds to pressure and flows. Since we will only sketch the modeling approach here, the interested reader can refer to [6] and [7] for a more general and

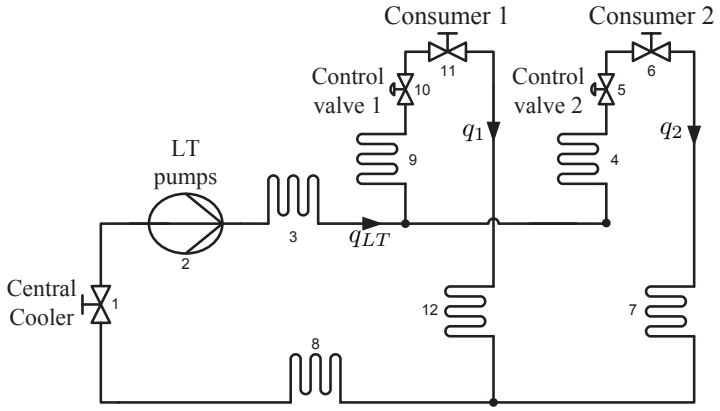

Fig. B.2: Assumed hydraulic structure for the LT FW circuit in this design example.

detailed description. By inspection, it is possible to identify two independent flows in Fig. B.2, namely q_1 and q_2. Using the electrical circuit analogy we can exploit Kirchhoff's voltage law for the two fundamental loops that includes q_1 and q_2, by which we achieve:

$$\begin{aligned} 0 = &- \Delta p_1 + \Delta p_2 - \Delta p_3 - \Delta p_4 - \Delta p_5 - \Delta p_6 \\ &- \Delta p_7 - \Delta p_8 \ , \end{aligned} \tag{B.5}$$

$$\begin{aligned} 0 = &- \Delta p_1 + \Delta p_2 - \Delta p_3 - \Delta p_9 - \Delta p_{10} - \Delta p_{11} \\ &- \Delta p_{12} - \Delta p_8 \ , \end{aligned} \tag{B.6}$$

where Δp_i is the pressure across component i in Fig. B.2. Each pressure term in (B.5) and (B.6) is replaced by its corresponding model from (B.2)-(B.4). Realizing that the individual component flows can be written as a linear combination of the independent flows q_1 and q_2 and assuming that flows are always positive, i.e., $q_1 \geq 0$ and $q_2 \geq 0$, we get that:

$$\begin{aligned} 0 = &- (K_{v1} + K_{p3} + K_{p8})(q_1 + q_2)^2 - (J_3 + J_8)\frac{d(q_1 + q_2)}{dt} \\ &- (J_4 + J_7)\frac{dq_2}{dt} - (K_{p4} + K_{cv5} + K_{v6} + K_{p7})q_2^2 + \Delta H_p \\ 0 = &- (K_{v1} + K_{p3} + K_{p8})(q_1 + q_2)^2 - (J_3 + J_8)\frac{d(q_1 + q_2)}{dt} \\ &- (J_9 + J_{12})\frac{dq_1}{dt} - (K_{p9} + K_{cv10} + K_{v11} + K_{p12})q_1^2 + \Delta H_p \ . \end{aligned}$$

Through some tedious but straightforward calculations it is possible obtain the following

expressions for the dynamics of the flows q_1 and q_2:

$$\begin{aligned}\dot{q}_1 =& - K_{11}q_1^2 - K_{12}q_1^2\varphi_{cv,1} + K_{13}q_2^2\varphi_{cv,2} + K_{14}\Delta H_{p,LT} - K_{15}(q_1+q_2)^2 \\ &+ K_{16}q_2^2 \ ,\end{aligned} \tag{B.7}$$

$$\begin{aligned}\dot{q}_2 =& - K_{21}q_2^2 - K_{22}q_2^2\varphi_{cv,2} + K_{23}q_1^2\varphi_{cv,1} + K_{24}\Delta H_{p,LT} - K_{25}(q_1+q_2)^2 \\ &+ K_{26}q_1^2 \ ,\end{aligned} \tag{B.8}$$

where $K_{11}, K_{12}, K_{13}, K_{14}, K_{21}, K_{22}, K_{23}$ and K_{24} are all positive circuit specific parameters, while $\varphi_{cv1} = K_{cv10}$ and $\varphi_{cv2} = K_{cv5}$ denotes the hydraulic resistances of control valve 1 and 2, respectively.

2.2 Thermodynamics

The thermodynamic model derived in [5] includes flow dependent delays and also models how the coolant is recirculated in the system. Though a possible approach would be to linearize the delays and include them in the control design presented here, it is chosen not to as the purpose here is to design simple baseline control laws, while later work will consider compensation of delays and closed circuit flow behavior. The thermodynamic model applied for control design in this paper therefore consists of two equations; one governing the dynamics of the central cooler, and one governing the dynamics of the consumers in the LT FW circuit. For consumer $i = 1, \ldots, p$ in the LT FW circuit we have that:

$$\frac{d\,T_i(t)}{dt} = \frac{1}{\rho c_p V_i}\left(q_i(t)\rho c_p(T_{LT,in}(t) - T_i(t)) + \dot{Q}_i(t)\right) \ , \tag{B.9}$$

where q_i is the volumetric flow rate through the consumer, V_i is the internal volume of the consumer, T_i is the outlet temperature of the consumer, $T_{LT,in}$ is the outlet temperature of the central cooler (into the LT FW circuit), $\dot{Q}_i$ is the heat transfer from the consumer, ρ is the density of the coolant and c_p is the specific heat of the coolant.

For the central cooler we have that:

$$\begin{aligned}\frac{d\,T_{LT,in}(t)}{dt} =& \frac{1}{\rho c_p V_{CC}}\left[q_{LT}(t)\rho c_p(T_{LT,out}(t) - T_{LT,in}(t))\right. \\ &\left. + \ q_{SW}(t)\rho_{SW}c_{p,SW}(T_{SW,in}(t) - T_{SW,out}(t)\right] \ ,\end{aligned} \tag{B.10}$$

where $T_{LT,out}$ is the inlet temperature of the central cooler on the LT FW side, $T_{SW,in}$ is the inlet temperature of the central cooler on the SW side and $T_{SW,out}$ is the outlet temperature of the central cooler on the SW side. Also, q_{LT} is the volumetric flow rate through the LT FW side of the central cooler, q_{SW} is the volumetric flow rate through the SW side of the central cooler, V_{CC} is the internal volume of the central cooler, ρ_{SW}

is the density of the sea water and $c_{p,SW}$ is the specific heat of the sea water.

Equations (B.1) and (B.8)-(2.1) constitutes the hydraulic model for the SW and LT FW circuit respectively, while equations (B.9) and (B.10) make up the thermodynamic model.

3 Control Design

The control design is divided into two parts; control laws for the SW circuit and control laws for the LT FW circuit. Furthermore, since both the SW and LT FW circuit can be considered as a hydraulic part cascaded with a thermodynamic part we use a cascaded control design for both circuits as illustrated in Fig. B.3.

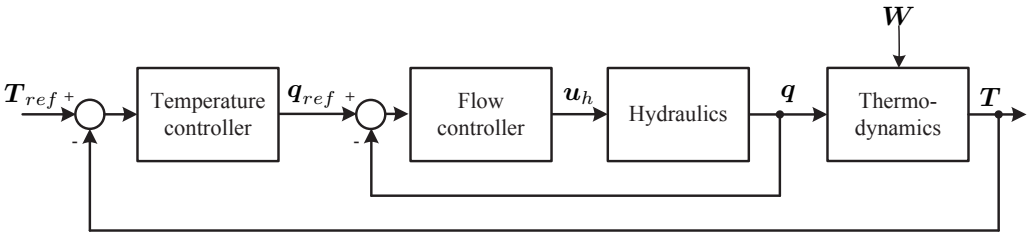

Fig. B.3: Block diagram for the cascaded control setup. u_h denotes the hydraulic inputs, i.e. φ_{cv1}, φ_{cv2}, $H_{p,SW}$ and $H_{p,LT}$. $W(t)$ denotes the disturbances to the thermodynamics of the system, such as $\dot{Q}_1$, $\dot{Q}_2$ and $T_{SW,in}$.

3.1 Design of Flow Controllers

The purpose of the flow controllers is to assure that the flows in the system track the references given by the temperature controllers. We start by designing the controller for the flow in the SW circuit, q_{SW}, using the model given by (B.1). We again assume that the flow is only going in one direction, i.e. $q_{SW} \geq 0$. We can now rewrite (B.1) and obtain:

$$\dot{q}_{SW} = \frac{1}{J_{SW}} \left(-K_{SW} q_{SW}^2 - \Delta p_{io} + \Delta H_{p,SW} \right) \ . \tag{B.11}$$

A linearized small perturbation model is obtained using a first order Taylor expansion:

$$\frac{d\,\hat{q}_{SW}}{dt} = \frac{1}{J_{SW}} \left(-2K_{SW} \bar{q}_{SW} \hat{q}_{SW} + \Delta \hat{H}_{p,SW} \right) \ , \tag{B.12}$$

where we use $\bar{q}_{SW}$ to denote the steady state value of q_{SW} and $\hat{q}_{SW}$ to denote a small perturbation from the steady state value of q_{SW}. The same notation applies for $\Delta H_{p,SW}$.

The transfer function from delivered pump head, $\Delta H_{p,SW}$ to the SW flow rate, q_{SW} is according to Equation (B.12) given by:

$$G_{SW}(s) = \frac{\hat{q}_{SW}(s)}{\Delta \hat{H}_{p,SW}(s)} = \frac{\frac{1}{2K_{SW}\bar{q}_{SW}}}{s\frac{J_{SW}}{2K_{SW}\bar{q}_{SW}} + 1} \ . \tag{B.13}$$

In this design example we use $K_{SW} = 10$, $\bar{q}_{SW} = 0.183$ and $J_{SW} = 1$. We pursue a standard PI controller design, given in the form of:

$$D(s) = K_{PI}\left(1 + \frac{1}{sT_{PI}}\right) \ . \tag{B.14}$$

As design parameters for all flow controllers we use phase margin and crossover frequency and make the choice of $PM = 70°$ at $\omega_0 = 0.4$ rad/s. From the requirements for phase margin and crossover frequency we can determine K_{PI} and T_{PI} from [8]:

$$|D(s)G(s)|_{s=j\omega_0} = 1 \ , \tag{B.15}$$

$$\tan^{-1}\left(\frac{\mathrm{Im}(D(s)G(s))}{\mathrm{Re}(D(s)G(s))}\right)\Bigg|_{s=j\omega_0} = PM - 180° \ . \tag{B.16}$$

By inserting (B.13) and (B.14) into (B.15) and (B.16) we can solve for K_{PI} and T_{PI}, which for the SW flow controller yields:

$$D_{SW}(s) = -0.88\left(1 - \frac{1}{0.61s}\right) \ . \tag{B.17}$$

For the LT FW circuit flow we have the linearized small perturbation versions of (B.8) and (2.1) given by:

$$\begin{aligned}
\frac{d\,\hat{q}_1}{dt} &= \hat{q}_1 2(-K_{11}\bar{q}_1 - K_{12}\bar{q}_1\bar{\varphi}_{cv,1} - K_{15}\bar{q}_1 - K_{15}\bar{q}_2) \\
&\quad + \hat{q}_2 2(K_{13}\bar{q}_2\bar{\varphi}_{cv,2} - K_{15}\bar{q}_2 - K_{15}\bar{q}_1 + K_{16}\bar{q}_2) \\
&\quad - \hat{\varphi}_{cv1}(K_{12}\bar{q}_1^2) + \hat{\varphi}_{cv2}(K_{13}\bar{q}_2^2) + K_{14}\Delta\hat{H}_{p,LT}, \qquad \text{(B.18)} \\
\frac{d\,\hat{q}_2}{dt} &= \hat{q}_1 2(K_{23}\bar{q}_1\bar{\varphi}_{cv,1} - K_{25}\bar{q}_1 - K_{25}\bar{q}_2 + K_{26}\bar{q}_1) \\
&\quad + \hat{q}_2 2(-K_{21}\bar{q}_2 - K_{22}\bar{q}_2\bar{\varphi}_{cv,2} - K_{25}\bar{q}_2 - K_{25}\bar{q}_1) \\
&\quad - \hat{\varphi}_{cv2}(K_{22}\bar{q}_2^2) + \hat{\varphi}_{cv1}(K_{23}\bar{q}_1^2) + K_{24}\Delta\hat{H}_{p,LT}. \qquad \text{(B.19)}
\end{aligned}$$

Assuming that we use φ_{cv1} to control q_1 and φ_{cv2} to control q_2 we leave out cross-coupling terms in (B.18)-(B.19) and by the Laplace transform we achieve the following

transfer functions:

$$G_{q1}(s) = \frac{\hat{q}_1(s)}{\hat{\varphi}_{cv1}(s)} = \frac{-K_{12}\bar{q}_1^2}{s + 2(K_{11}\bar{q}_1 + K_{12}\bar{q}_1\bar{\varphi}_{cv,1} + K_{15}\bar{q}_1 + K_{15}\bar{q}_2)}, \tag{B.20}$$

$$G_{q2}(s) = \frac{\hat{q}_2(s)}{\hat{\varphi}_{cv2}(s)} = \frac{-K_{22}\bar{q}_2^2}{s + 2(K_{21}\bar{q}_2 + K_{22}\bar{q}_2\bar{\varphi}_{cv,2} + K_{25}\bar{q}_2 + K_{25}\bar{q}_1)}. \tag{B.21}$$

For this design example we use the hydraulic parameters presented in Table B.1.

Table B.1: Hydraulic parameters for LT FW circuit.

K_{11}	K_{12}	K_{15}	$\bar{q}_1$	$\bar{\varphi}_{cv1}$
15	$\frac{1}{3}$	$\frac{1}{6}$	0.050	3820
K_{21}	K_{22}	K_{25}	$\bar{q}_2$	$\bar{\varphi}_{cv2}$
15	$\frac{1}{3}$	$\frac{1}{6}$	0.042	5013

Just as for the SW flow controller design we pursue a PI compensator as given by (B.14) using the same design parameters. As before we determine K_{PI} and T_{PI} for the LT FW flow controllers from (B.15) and (B.16) using the transfer functions given by (B.20) and (B.21). With the parameters in Table B.1 this yields:

$$D_{q1}(s) = 2.77 \times 10^3 \left(1 - \frac{1}{0.77s}\right), \tag{B.22}$$

$$D_{q2}(s) = 3.53 \times 10^3 \left(1 - \frac{1}{0.76s}\right). \tag{B.23}$$

This completes the design for the flow controllers.

3.2 Design of Temperature Controllers

The temperature controllers serve the purpose of keeping the LT FW circuit inlet temperature, $T_{LT,in}(t)$, and the outlet temperature of the consumers, $T_1(t), \ldots, T_p(t)$, at a specified reference. Since the system operates in steady state mode for extended periods at a time, it is important to achieve zero steady state error for the temperatures in the system. Therefore we use a regular PI controller design for each control loop to remove steady state errors. We again use phase margin and crossover frequency as design parameters for the PI compensator and we choose $PM = 70°$ and $\omega_0 = 0.002$ rad/s in the design of the consumer outlet temperature controllers. For the LT FW inlet temperature controller we choose $PM = 70°$ and $\omega_0 = 0.01$ rad/s such that the dynamics of the LT FW inlet temperature is faster than the consumer outlet temperature but still significantly slower than the dynamics of the hydraulics.

Starting with the control design for the consumer outlet temperature, we make a first order Taylor expansion of Equation (B.9) to achieve the linearized small perturbation model given by:

$$\frac{d\,\hat{T}_i}{dt} = \frac{1}{V_i}\left(\hat{q}_i(\bar{T}_{LT,in} - \bar{T}_i) + \bar{q}_i(\hat{T}_{LT,in} - \hat{T}_i) + \frac{\hat{\dot{Q}}_i}{\rho c_p}\right) . \tag{B.24}$$

The transfer functions from the flows to the consumer outlet temperatures are given by:

$$G_{T1}(s) = \frac{\hat{T}_1(s)}{\hat{q}_1(s)} = \frac{\frac{1}{\bar{q}_1}(\bar{T}_{LT,in} - \bar{T}_1)}{s\frac{V_1}{\bar{q}_1} + 1} , \tag{B.25}$$

$$G_{T2}(s) = \frac{\hat{T}_2(s)}{\hat{q}_2(s)} = \frac{\frac{1}{\bar{q}_2}(\bar{T}_{LT,in} - \bar{T}_2)}{s\frac{V_2}{\bar{q}_2} + 1} . \tag{B.26}$$

We use a regular PI design as given by Equation (B.14) and apply the same design procedure as for the flow controllers. Thermodynamic parameters used for this design example are illustrated in Table B.2.

Table B.2: Thermodynamic parameters for cooling system.

c_p [J/(kg· K)]	$\dot{Q}_1$ [W]	ρ [kg/m^3]	$\bar{T}_{SW,in}$ [°C]	V_{cc} [m^3]	V_1 [m^3]	$\bar{T}_1$ [°C]	$\bar{q}_{LT}$ [m^3/s]
4181	6×10^6	1000	24	20	13.5	65	0.09
$c_{p,SW}$ [J/(kg· K)]	$\dot{Q}_2$ [W]	ρ_{SW} [kg/m^3]	$\bar{T}_{SW,out}$ [°C]	$\bar{T}_{LT,in}$ [°C]	V_2 [m^3]	$\bar{T}_2$ [°C]	$\bar{T}_{cc,in}$ [°C]
3993	6×10^6	1025	40	36	13.5	70	67.8

The temperature controllers for the consumer outlet temperature are then given by:

$$D_{T1}(s) = -2.91 \times 10^{-4}\left(1 + \frac{1}{75.78s}\right) , \tag{B.27}$$

$$D_{T2}(s) = -6.81 \times 10^{-4}\left(1 + \frac{1}{111.83s}\right) . \tag{B.28}$$

For the control of the LT FW inlet temperature we linearize the model given by (B.10), by which we obtain:

$$\begin{aligned}\frac{d\,\hat{T}_{LT,in}}{dt} = \frac{1}{\rho c_p V_{cc}}\Big[&\hat{q}_{LT}c_p\rho(\bar{T}_{LT,out} - \bar{T}_{LT,in}) + \hat{T}_{LT,out}c_p\rho\bar{q}_{LT} \\ &- \hat{T}_{LT,in}c_p\rho\bar{q}_{LT} + \hat{q}_{SW}c_{p,SW}\rho_{SW}(\bar{T}_{SW,in} - \bar{T}_{SW,out}) \\ &+ \hat{T}_{SW,in}c_{p,SW}\rho_{SW}\bar{q}_{SW} - \hat{T}_{SW,out}c_{p,SW}\rho_{SW}\bar{q}_{SW}\Big] .\end{aligned} \tag{B.29}$$

The transfer function from the SW flow rate to the LT FW inlet temperature is given by:

$$G_{Tin}(s) = \frac{\hat{T}_{LT,in}(s)}{\hat{q}_{SW}(s)} = \frac{\frac{c_{p,SW}\rho_{SW}(\bar{T}_{SW,in}-\bar{T}_{SW,out})}{\rho c_p \bar{q}_{LT}}}{\left(s\frac{V_{cc}}{\bar{q}_{LT}}+1\right)} \ . \tag{B.30}$$

Using the parameters given by Table B.2 and applying the the same design procedure as for the LT FW consumer outlet temperature, we achieve the following compensator design:

$$D_{Tin}(s) = -0.01\left(1+\frac{1}{101.30s}\right) \ . \tag{B.31}$$

This completes the design for the temperature controllers.

4 Simulation Results

The controllers designed in Section 3 are assessed through a simulation study using the non-linear model derived in [5]. For comparison, we also simulate a control design that is similar to what is currently implemented on the cooling system. Both control designs are subject to the same conditions and disturbances, and the idea is to show how the design derived in this paper compares to a design that is close to the current implementation. The comparison control operates the LT FW pumps in a stepwise manner based on the main engine load percentage, $\text{ME}_{load}(t)$, and the sea water temperature, $T_{SW,in}(t)$. This is similar to the control implemented on the cooling system today, but instead of controlling the LT FW inlet temperature using the three-way valve as described in Section 2, we use the corresponding control derived in this paper.

In the simulation scenario constructed here, the comparison control has two modes of operation for the LT FW pumps: one pump running or two pumps running in parallel. The mode of operation depends on the relation:

$$\begin{aligned} \text{1 pump running if:} \quad & \text{ME}_{load}(t) < -2T_{SW,in}(t) + 134 \\ \text{2 pumps running if:} \quad & \text{ME}_{load}(t) \geq -2T_{SW,in}(t) + 134 \end{aligned}$$

The relation between the main engine load percentage and the total power dissipated in both consumers is linearly approximated in the interval that is of interest in this context by:

$$\dot{Q}_{total} = \text{ME}_{load}\frac{2}{5} \times 10^6 - 16 \times 10^6 \text{ W} \quad \text{for} \ \ \text{ME}_{load} \in [50; 90] \ .$$

In the simulations, the two control designs undergoes the same steps in the main engine load percentage; first from 70% to 90% at time $t = 2000$ s and then from 70% to 60% at

time $t = 12000$ s. It is assumed that the heat is dissipated equally in the two consumers, which means that the load percentage of 70% corresponds to the operating point chosen for the consumer outlet temperature controller design. Additional simulation parameters are illustrated in Table B.3.

Table B.3: Parameters for simulation examples. Parameters marked with * denotes system specific delay parameters for the non-linear model, see [5] for details.

$T_{1,ref}$ [°C]	$T_{2,ref}$ [°C]	$T_{LT,in,ref}$ [°C]	$T_{SW,in}$ [°C]	$T_{SW,out}$ [°C]
65	70	36	24	40
$a_{m,1}$* [m^3]	$a_{m,2}$* [m^3]	$a_{c,1}$* [m^3]	$a_{c,2}$* [m^3]	
8	8	4	4	

The consumer outlet temperature responses for the comparison control are illustrated in the top plot of Fig. B.4 while the consumer inlet temperatures are shown in the bottom plot of the same figure. For making comparison between the responses for the two control designs easier, the consumer temperature references are included in Fig. B.4, even though they are not used by the comparison control design. The top plot of Fig. B.5 shows the flow rates for the comparison control during the simulation, while the bottom plot illustrates the corresponding main engine load percentage.

It is clear from the temperature responses for the comparison control in Fig. B.4 that the lack of feedback control means the temperatures cannot be controlled to some predefined set points, unless the set points and main engine load percentage are exactly what the comparison control was designed for. The consequence is that the individual consumers do not necessarily operate at optimal conditions as was pointed out in Section 1. Temperature responses for the control designed in this paper are illustrated in Fig. B.6, while Fig. B.7 shows the corresponding flow rates and main engine load percentage.

From the temperature responses in Fig. B.6 it is seen that the control design presented in this paper is able to bring the consumer outlet temperatures to the defined set points, even when the main engine load percentage does not correspond to the operating point used in the control design. Fig. B.6 also illustrates how the nonlinearities causes the compensated system to have a longer settling time during a negative step in the main engine load percentage, compared to a positive step. Compensation for this uneven performance of the control design could possibly be achieved through a nonlinear control design, which however, is outside the scope of this paper.

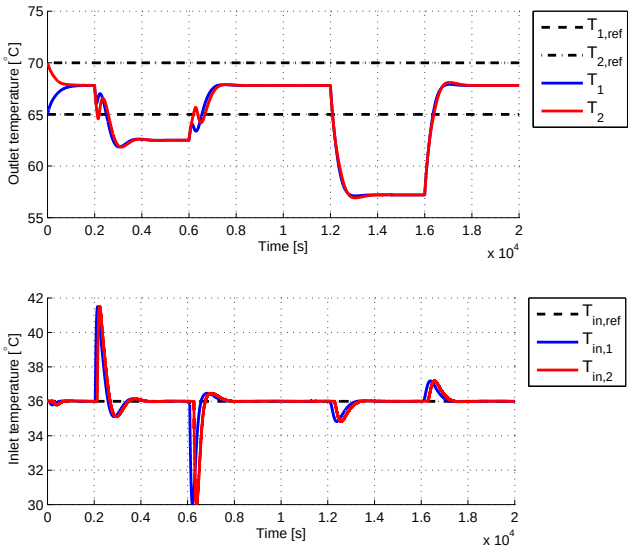

Fig. B.4: Top plot illustrates the temperature of the coolant out of the two consumers during the simulation using the comparison control, i.e. with no temperature control. Bottom plot shows the corresponding consumer inlet temperatures which are displaced in time due to transport delays.

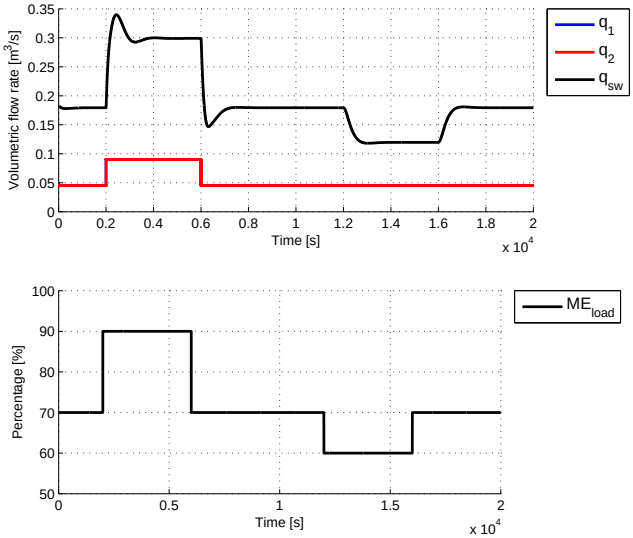

Fig. B.5: Top plot illustrates the flow rate through the two consumers and the corresponding SW circuit flow during the simulation using the comparison control. Bottom plot shows the main engine load percentage during the simulation.

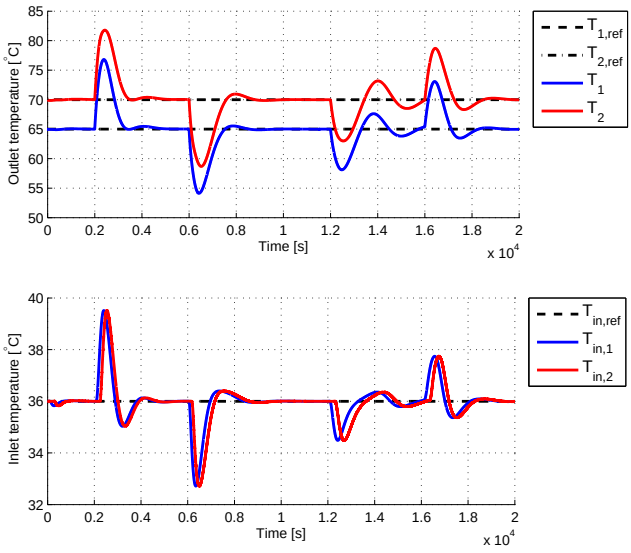

Fig. B.6: Top plot illustrates the temperature of the coolant out of the two consumers during the simulation with the control design presented in this paper. Bottom plot shows the corresponding consumer inlet temperatures which are identical but displaced in time due to transport delays.

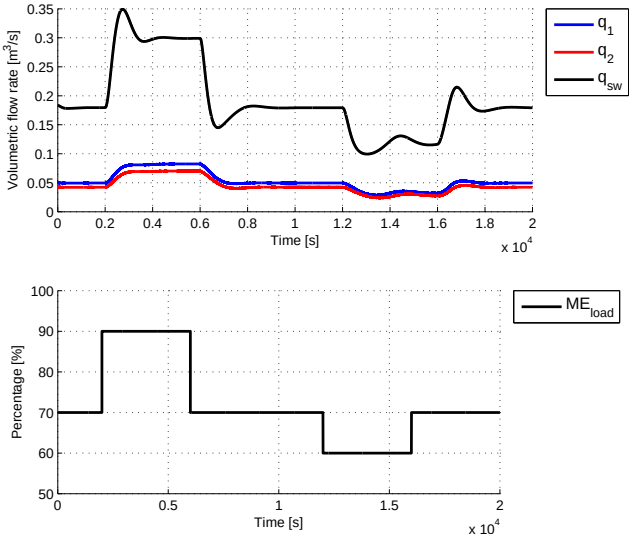

Fig. B.7: Top plot illustrates the flow rate through the two consumers and the corresponding SW circuit flow during the simulation using the non-linear model. Bottom plot shows the main engine load percentage during the simulation.

5 Conclusions and Future Works

We have presented a simple control design for a non-linear marine cooling system. Control laws were derived using model based control design from the model presented in [5]. The non-linear models were linearized and classical control theory was applied to obtain a cascaded PI controller design.

Through a simulation example the controllers designed in this paper were compared to a control design that is similar in operation to what is currently implemented on the cooling system. The simulation example indicated that the design presented in this paper achieves its purpose of controlling the temperatures in the cooling system to predefined set points, even when disturbances deviates from the chosen operating point. This is an improvement over the comparison control since this is unable to control the system according to set points and reject constant disturbances. Possible improvements for the control design presented here includes ensuring consistent performance in the entire range of operation, i.e. for all possible main engine load percentages and sea water temperatures.

In future work we will look at compensation of the non-linearities, closed circuit flow dynamics and transport delays. Optimization of pump power consumption is another subject that will also be dealt with in future work. The control design derived in this paper will then serve as a performance benchmark for investigating dynamic performance and power consumption.

References

[1] C. Beverelli, H. Benamara, and R. Asariotis, "Oil Prices and Maritime Freight Rates: An Empirical Investigation," *United Nations Conference on Trade and Development*, 2010.

[2] J. Faber, A. Markowska, D. Nelissen, M. Davidson, I. C. Eyring, Veronika, P. Roche, E. Humpries, N. Rose, J. Graichen, and M. Cames, "Technical support for european action to reducing greenhouse gas emissions from international maritime transport," *Commissioned by: European Commission*, 2009.

[3] Green Ship of the Future, "Green ship magazine," *www.greenship.org*, 2009.

[4] T. L. Andersen, D. F. Lauritzen, and J. T. Madsen, "Optimized control for energy optimization of shipboard cooling system," *Master thesis, Aalborg University, Section for Automation and Control*, 2009.

[5] M. Hansen, J. Stoustrup, and J. D. Bendtsen, "Modeling of nonlinear marine cooling system with closed circuit flow," in *Proceedings of the 18th IFAC World Congress*, 2011, pp. 5537–5542.

[6] C. De Persis and C. S. Kallesøe, "Pressure regulation in nonlinear hydraulic networks by positive controls," in *European Control Conference*, 2009.

[7] ——, "Proportional and proportional-integral controllers for a nonlinear hydraulic network," in *Proceedings of the 17th IFAC World Congress*, 2008.

[8] G. F. Franklin, J. D. Powell, and A. Emami-Naeini, *Feedback Control of Dynamical Systems*. Prentice Hall, 2006.

Paper C

An LPV Model for a Marine Cooling System with Transport Delays

Michael Hansen
Jakob Stoustrup
Jan Dimon Bendtsen

The paper has been published in the
Proceedings of the 14th International Conference on Harbor, Maritime & Multimodal Logistics Modelling and Simulation, pp. 119–124, 2011.

The layout has been revised. This version of the paper has been modified from its original published version to include minor corrections.

Abstract

We address the problem of constructing a linear parameter varying (LPV) model for a nonlinear marine cooling system with flow dependent delays. We focus on the choice of scheduling variables for the LPV model to represent important nonlinear dynamics, and to preserve the flow dependency of the transport delays in the system. To this end, we redefine one of the system inputs to obtain a scheduling parameter that describes the time-varying operating point for this input, and also make some simple, but justifiable approximations in order to keep the number of scheduling variables low. A simulation example is provided to illustrate the performance of the LPV model compared to the original nonlinear model.

1 Introduction

In this paper we consider the nonlinear marine cooling system with flow dependent delays that was first introduced in [1]. The cooling system is used aboard container vessels for cooling the main engine and auxiliary components such as main engine scavenge air coolers, turbo chargers, diesel generators, etc. The motivation for considering this system is the potential energy savings that can be obtained by improving the currently implemented control, which is very energy inefficient due to an excessive use of the pumps in the cooling system. However, because of the structure of the system, the dynamic behavior includes transport delays and nonlinearities, which complicates the design of more advanced control laws. This entails that the models used for control design must describe the important dynamics of the system sufficiently accurate, but also has a form that fits the control design method.

One approach for dealing with the problem of control design for nonlinear systems is by use of linear parameter varying (LPV) control theory [2]. LPV systems are characterized by being dependent on an unknown, but measurable time-varying parameter that describes the variations in the plant dynamics. When designing control for the LPV system, the time-varying parameter is used for scheduling the control laws according to how the system dynamics changes. This makes LPV control applicable to a wide range of systems, including a large class of nonlinear systems that can be converted to an LPV form. With the combination of theory from optimal and robust control it is possible to guarantee stability, optimal performance and robustness of an LPV model in the entire field of operation. This is contrary to former gain scheduling approaches where a global nonlinear control design is obtained from interpolating local linear controllers, and where guarantees of performance and robustness cannot be made in general [3], [4]. Some results on the use of LPV control theory for systems with time-varying delays have been presented in [5], [6], [7] and is part of the motivation for this work. However, the use of LPV control theory requires that the system model has an LPV representation

which can be difficult to obtain [8].

The objective in this paper is to rewrite the nonlinear model from [1] into the form of an LPV model that includes the flow dependent transport delays, and represents important dynamics sufficiently accurate. We only consider the thermodynamic part of the model, while appropriate control is assumed to be designed for the hydraulics such that the flows in the system can be considered as free input variables.

Related work is presented in [8] where a third order nonlinear model of the airpath of a turbocharged diesel engine is converted to an LPV model. However, delays are not a part of the nonlinear model considered [8], and the resulting LPV model is of the quasi-LPV type i.e, where scheduling variables depends on the system dynamics, which is somewhat different from what we seek here. The main contribution of this paper lies in the inclusion of transport delays when converting the nonlinear model to an LPV representation, and in the corresponding choice of scheduling parameters for adequately describing the transport delays as well as the nonlinear dynamics in the resulting LPV model.

The remaining paper is structured as follows: In Section 2 we make a brief presentation of the nonlinear model considered in this paper. In Section 3 we bring the model into an LPV form and in Section 4 we compare the performance of the LPV model with the original nonlinear model. Finally, concluding remarks are presented in Section 5.

We make use of the following fairly standard notation: $\mathbb{R}$ denotes the set of real numbers while $\mathbb{R}_+$ denotes the set of non-negative real numbers. $\mathbb{R}^{n\times m}$ is the set of real $n \times m$ matrices and $C^1(\mathcal{M},\mathcal{N})$ is the set of continuous functions mapping from $\mathcal{M}$ to $\mathcal{N}$ with first order continuous derivatives.

2 Nonlinear Model

The cooling system consists of three circuits; a sea water (SW) circuit, a low temperature fresh water (LT FW) circuit and a high temperature fresh water (HT FW) circuit. In this work the HT FW circuit is not of interest, and is therefore left out in the following. A simplified layout of the system considered in this work is illustrated in Fig. C.1.

The SW circuit pumps sea water through the cold side of the heat exchanger for lowering the temperature of the coolant in the LT FW circuit. The LT FW circuit contains all the main engine auxiliary components in a parallel configuration, and the supplied cooling is controlled through the flow rates in the system, $q_{SW}(t)$ and $q_{LT}(t)$. The nonlinear thermodynamic model consists of two parts; one to describe the temperature change in the coolant out of each consumer in the LT FW circuit, and one to describe temperature change of the coolant out of the LT FW side of the heat exchanger.

The dynamics for the consumers $i = 1,\dots,p$, with $\boldsymbol{q} = [q_1,\ q_2,\dots,\ q_p]^T$ is described

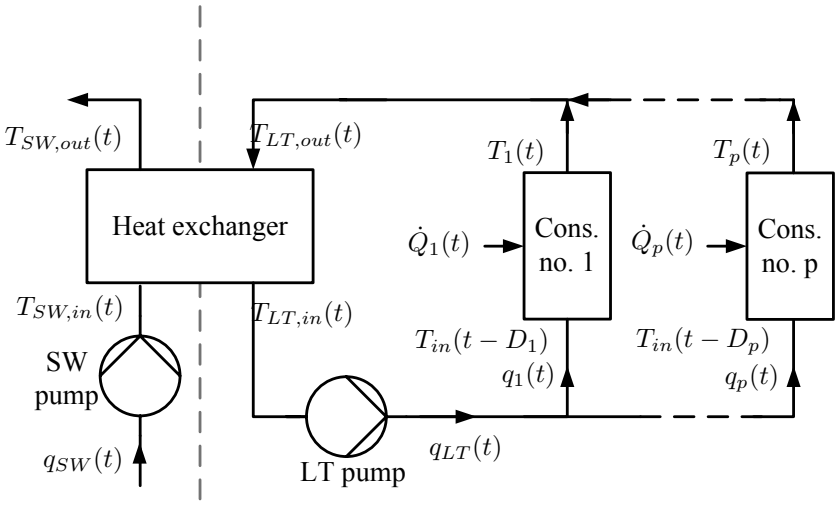

Fig. C.1: Simplified layout of the cooling system considered. The sea water (SW) circuit is to the left, while the low temperature (LT FW) circuit containing all the consumers is to the right.

by:

$$\dot{T}_i(t) = \frac{1}{V_i}\left[q_i(t)(T_{LT,in}(t - D_i(q)) - T_i(t)) + \frac{\dot{Q}_i(t)}{\rho c_{p,FW}} \right] \tag{C.1}$$

where q_i is the volumetric flow rate through the consumer, V_i is the internal volume of the consumer, T_i is the outlet temperature of the consumer and $T_{LT,in}$ is the outlet temperature of the heat exchanger (into the LT FW circuit). Also, $\dot{Q}_i$ is the heat transfer from the consumer to the coolant, ρ is the density of the coolant and $c_{p,FW}$ is the specific heat of the coolant. We here consider the case where the flows $q_1(t), q_2(t), \ldots, q_p(t)$ satisfy the relation:

$$\begin{aligned} q_1(t) &= c_1 q_{LT}(t) \\ q_2(t) &= c_2 q_{LT}(t) \\ &\vdots \\ q_p(t) &= c_p q_{LT}(t) \ , \end{aligned}$$

where $\{c_i\}_{i=1}^{p}$ are positive constants, subject to:

$$\sum_{i=1}^{p} c_i = 1 \ .$$

For the dynamics of $T_{LT,in}(t)$ we have that:

$$\dot{T}_{LT,in}(t) = \frac{1}{V_{CC}} \left[q_{LT}(t)(T_{LT,out}(t) - T_{LT,in}(t)) + q_{SW}(t) \frac{\rho_{SW} c_{p,SW}}{\rho c_{p,FW}} (T_{SW,in}(t) - T_{SW,out}(t)) \right] , \tag{C.2}$$

where $c_{p,SW}$ is the specific heat of sea water, ρ_{SW} is the density of sea water, and $T_{LT,out}(t)$ is the temperature of the coolant into the LT FW side of the heat exchanger. Also, $T_{SW,in}(t)$ and $T_{SW,out}(t)$ are the temperatures of the sea water in and out of the SW side of the heat exchanger. The transport delays are described by the relation:

$$D_i(q) = \sum_{j=1}^{i} \left(a_{m,j} \sum_{k=j}^{p} \frac{1}{q_k} \right) + \frac{a_{c,i}}{q_i} , \tag{C.3}$$

where $a_{m,i}$ and $a_{c,i}$ are system specific positive constants. It is assumed that the temperatures $T_{LT,out}(t)$, $T_{SW,in}(t)$ and $T_{SW,out}(t)$ are measurable while the heat transfers $\dot{Q}_1(t), \ldots, \dot{Q}_p(t)$ are unknown but belonging to the set:

$$\mathcal{W} := \{ \dot{Q} \in C(\mathbb{R}, \mathbb{R}); 0 < \underline{Q} \leq \dot{Q}(t) \leq \overline{Q} < \infty \} , \tag{C.4}$$

i.e., the heat transfer from each consumer is continuous, positive and bounded from below by $\underline{Q}$ while bounded from above by $\overline{Q}$. Also, we assume that delays $D_1, \ldots, D_p$ belongs to the set:

$$\mathcal{D} := \{ D \in C(\mathbb{R}, \mathbb{R});\ 0 \leq D(q) \leq \overline{D} < \infty;\ \dot{D}(q) < 1\ \forall t \in \mathbb{R}_+ \} ,$$

which ensures that $t - D_i(q)$ is monotonically increasing for all D_i. The requirement that the first order derivative of the delays must be less than one is a necessary requirement, but obviously causes restrictions to how fast the input is allowed to change due to the relation between the inputs and the delays. In other words this means that the flow rates in the system cannot be allowed to decreased arbitrarily fast. Also, since it is required that the delays are positive and bounded from above by $\overline{D}$, the flow rates $q_1(t), \ldots, q_p(t)$ must be non-zero and positive, which is considered to be the case for all relevant operating conditions.

3 Construction of LPV Model

We seek a representation of the input-affine time delay system given by (C.1) and (C.2) on the LPV form of [7]:

$$\begin{aligned}\dot{\boldsymbol{x}}(t) =& \boldsymbol{A}(\boldsymbol{p}(t))\boldsymbol{x}(t) + \sum_{i=1}^{k} \boldsymbol{A}_{Di}(\boldsymbol{p}(t))\boldsymbol{x}(t - D_i(\boldsymbol{p}(t))) \\ &+ \boldsymbol{B}_1(\boldsymbol{p}(t))\boldsymbol{w}(t) + \boldsymbol{B}_2(\boldsymbol{p}(t))\boldsymbol{u}(t)\end{aligned} \tag{C.5}$$

where $\boldsymbol{x}(t) \in \mathbb{R}^{n_x}$ is the state vector, $\boldsymbol{w}(t) \in \mathbb{R}^{n_w}$, is the disturbance vector and $\boldsymbol{u}(t) \in \mathbb{R}^{n_u}$ is the input vector. The initial condition for the delay system in (C.5) is given by:

$$\boldsymbol{x}(\theta) = \phi(\theta) \ , \quad \theta \in \left[-\overline{D}, 0\right] \ . \tag{C.6}$$

The time-varying parameter $\boldsymbol{p}(t)$ belongs to the set of allowable parameter trajectories defined as:

$$\mathcal{P} := \{\boldsymbol{p} \in \mathcal{C}(\mathbb{R}, \mathbb{R}^m);\ p(t) \subset \mathbb{R}^m, |\dot{\rho}_j(t)| \leq v_j,\ j = 1, 2, \ldots, m,\ \forall t \in \mathbb{R}_+\} \ , \tag{C.7}$$

where $\{v\}_{j=1}^{m}$ are positive constants, which means that the parameters have bounded trajectories, and bounded variation rate. Choosing scheduling variables is not a trivial matter as there are several factors that come into play. It is obviously desired to describe the important dynamics of the system adequately by the choice of parameters. However, it is also essential to keep the number of parameters as low as possible, as a high number of parameters complicates the control design for the system [8].

In this particular case, a reasonable choice for a scheduling variable is the temperature difference $(T_{SW,in}(t) - T_{SW,out}(t))$ which is measurable and satisfy the requirements for bounded trajectories and bounded variation rates as given by (C.7). However, in order to describe the dynamics of $T_i(t)$ on the linear form (C.5), as well as to preserve the flow dependency of the delays, we need an additional parameter. We therefore write $q_{LT}(t)$ as:

$$q_{LT}(t) = \tilde{q}_{LT}(t) + \hat{q}_{LT}(t) \ , \tag{C.8}$$

where $\tilde{q}_{LT}(t)$ represents the time varying operating point of the flow, while $\hat{q}_{LT}(t)$ is a small perturbation from this operating point.

Choosing $\tilde{q}_{LT}(t)$ as a scheduling variable along with $(T_{SW,in}(t) - T_{SW,out}(t))$, we get that:

$$\boldsymbol{p}(t) = \begin{pmatrix} p_1(t) \\ p_2(t) \end{pmatrix} = \begin{pmatrix} \tilde{q}_{LT}(t) \\ (T_{SW,in}(t) - T_{SW,out}(t)) \end{pmatrix} \tag{C.9}$$

This brings (C.1) and (C.2) to the form:

$$\dot{T}_i(t) = \frac{1}{V_i}\Big[c_i p_1(t)(T_{LT,in}(t - D_i(p_1(t))) - T_i(t)) + c_i \hat{q}_{LT}(t)(T_{LT,in}(t - D_i(p_1(t))) - T_i(t)) + \frac{\dot{Q}_i(t)}{\rho c_{p,FW}}\Big] , \tag{C.10}$$

$$\dot{T}_{LT,in}(t) = \frac{1}{V_{CC}}\left[(p_1(t) + \hat{q}_{LT}(t))(T_{LT,out}(t) - T_{LT,in}(t)) + q_{SW}(t)\frac{\rho_{SW} c_{p,SW}}{\rho c_{p,FW}} p_2(t)\right] . \tag{C.11}$$

We define the state, disturbance and input vectors, $\boldsymbol{x}(t), \boldsymbol{w}(t), \boldsymbol{u}(t)$ from C.5 as:

$$\boldsymbol{x}(t) = \begin{pmatrix} T_1(t) \\ T_2(t) \\ \vdots \\ T_p(t) \\ T_{LT,in}(t) \end{pmatrix} \quad \boldsymbol{w}(t) = \begin{pmatrix} \dot{Q}_1(t) \\ \dot{Q}_2(t) \\ \vdots \\ \dot{Q}_p(t) \\ T_{LT,out}(t) \end{pmatrix} \quad \boldsymbol{u}(t) = \begin{pmatrix} \hat{q}_{LT}(t) \\ q_{SW}(t) \end{pmatrix} . \tag{C.12}$$

It is clear that (C.10) and (C.11) cannot be brought directly to the form of (C.5) without simplifications or introducing additional scheduling variables. Since it is desired to keep the number of scheduling variables low, we make the following approximation for (C.10):

$$\hat{q}_{LT}(t)(T_{LT,in}(t - D_i(p_1(t))) - T_i(t)) \approx \hat{q}_{LT}(t)(\bar{T}_{LT,in} - \bar{T}_i)$$

where are $\bar{T}_{LT,in}$ and $\bar{T}_i$ are constant set point values for $T_{LT,in}(t)$ and $T_i(t)$, respectively. This approximation can be justified by the fact that the purpose of designing control laws for the system is to keep the temperatures at or close to predefined set points. This means that with properly designed control laws, the temperatures $T_{LT,in}(t)$ and $T_i(t)$ should be close to $\bar{T}_{LT,in}$ and $\bar{T}_i$ at all times, making the approximation error small.

For (C.11) we make the approximation:

$$(p_1(t) + \hat{q}_{LT}(t)) \approx p_1(t) .$$

The argument here is that it is not desired to use $\hat{q}_{LT}(t)$ as an control input for $T_{LT,in}(t)$, and since it only constitutes a small perturbation from $p_1(t)$ it is reasonable to discard it in this context, as it otherwise appears multiplicative with the disturbance $T_{LT,out}(t)$.

This results in approximated models given by:

$$\dot{T}_i(t) \approx \frac{1}{V_i}\Big[c_i p_1(t)(T_{LT,in}(t - D_i(p_1(t))) - T_i(t)) + c_i \hat{q}_{LT}(t)(\bar{T}_{LT,in} - \bar{T}_i) + \frac{\dot{Q}_i(t)}{\rho c_{p,FW}}\Big] \tag{C.13}$$

$$\dot{T}_{LT,in}(t) \approx \frac{1}{V_{CC}}\left[p_1(t)(T_{LT,out}(t) - T_{LT,in}(t)) + q_{SW}(t)\frac{\rho_{SW} c_{p,SW}}{\rho c_{p,FW}} p_2(t)\right] . \tag{C.14}$$

The system given by (C.13) and (C.14) can now be written in the form of (C.5). With the choice of input, state and disturbance vectors as given by (C.12) we get that $\boldsymbol{A}(\boldsymbol{p}(t))$ can be written as:

$$\boldsymbol{A}(\boldsymbol{p}(t)) = \begin{bmatrix} \frac{-c_1}{V_1}p_1(t) & 0 & \cdots & 0 \\ 0 & \ddots & & \vdots \\ \vdots & & \frac{-c_p}{V_p}p_1(t) & 0 \\ 0 & \cdots & 0 & \frac{-1}{V_{CC}}p_1(t) \end{bmatrix}. \tag{C.15}$$

For matrices $\boldsymbol{A}_{Di}(\boldsymbol{p}(t))$ we have that:

$$\boldsymbol{A}_{Di}(\boldsymbol{p}(t)) = \begin{bmatrix} 0 & \cdots & 0 & \delta_{i,1}\frac{c_1}{V_1}p_1(t) \\ \vdots & \ddots & & \vdots \\ 0 & \cdots & 0 & \delta_{i,p}\frac{c_p}{V_p}p_1(t) \\ 0 & \cdots & & 0 \end{bmatrix}, \tag{C.16}$$

for $i = 1, \ldots, p$ and where δ is defined as:

$$\delta_{i,j} = \begin{cases} 1 & \text{for } i = j \\ 0 & \text{for } i \neq j \end{cases}$$

Furthermore, for $\boldsymbol{B}_1(\boldsymbol{p}(t))$ and $\boldsymbol{B}_2(\boldsymbol{p}(t))$ we have that:

$$\boldsymbol{B}_1(\boldsymbol{p}(t)) = \begin{bmatrix} \frac{1}{V_1 c_{p,FW}\rho} & 0 & \cdots & 0 \\ 0 & \ddots & & \vdots \\ \vdots & & \frac{1}{V_p c_{p,FW}\rho} & 0 \\ 0 & \cdots & 0 & \frac{1}{V_{CC}}p_1(t) \end{bmatrix} \tag{C.17}$$

$$\boldsymbol{B}_2(\boldsymbol{p}(t)) = \begin{bmatrix} \frac{c_1(\bar{T}_{LT,in} - \bar{T}_1)}{V_1} & 0 \\ \vdots & 0 \\ \frac{c_p(\bar{T}_{LT,in} - \bar{T}_n)}{V_p} & 0 \\ 0 & \frac{\rho_{SW}c_{p,SW}}{\rho c_{p,FW}}p_2(t) \end{bmatrix}. \tag{C.18}$$

Equations (C.15)-(C.18) constitutes the generic LPV model for the cooling system, and with the definitions of scheduling variables in (C.9) we have that delays are written as:

$$D_i(\boldsymbol{p}(t)) = \sum_{j=1}^{i} \left(a_{m,j} \sum_{k=j}^{p} \frac{1}{c_k p_1(t)} \right) + \frac{a_{c,i}}{c_i p_1(t)}. \tag{C.19}$$

To make the structure of the LPV model clear, as well as to illustrate how the LPV model compares to the original nonlinear model, we construct a fictitious simulation example in the following part.

4 Simulation Studies

We consider a simulation example for a system with two consumers i.e., where $n = 2$. According to (C.15)-(C.18) we have that:

$$\begin{aligned}\dot{\boldsymbol{x}}(t) = &\begin{bmatrix} \frac{-c_1}{V_1}p_1(t) & 0 & 0 \\ 0 & \frac{-c_2}{V_2}p_1(t) & 0 \\ 0 & 0 & \frac{-1}{V_{CC}}p_1(t) \end{bmatrix} x(t) \\ &+ \begin{bmatrix} 0 & 0 & \frac{c_1}{V_1}p_1(t) \\ 0 & 0 & 0 \\ 0 & 0 & 0 \end{bmatrix} \boldsymbol{x}(t - D_1(\boldsymbol{p}(t))) + \begin{bmatrix} 0 & 0 & 0 \\ 0 & 0 & \frac{c_2}{V_2}p_1(t) \\ 0 & 0 & 0 \end{bmatrix} \boldsymbol{x}(t - D_2(\boldsymbol{p}(t))) \\ &+ \begin{bmatrix} \frac{1}{V_1 c_{p,FW}\rho} & 0 & 0 \\ 0 & \frac{1}{V_2 c_{p,FW}\rho} & 0 \\ 0 & 0 & \frac{1}{V_{CC}}p_1(t) \end{bmatrix} \boldsymbol{w}(t) + \begin{bmatrix} \frac{c_1(\bar{T}_{LT,in} - \bar{T}_1)}{V_1} & 0 \\ \frac{c_2(\bar{T}_{LT,in} - \bar{T}_2)}{V_2} & 0 \\ 0 & \frac{\rho_{SW} c_{p,SW}}{\rho c_{p,FW}}p_2(t) \end{bmatrix} \boldsymbol{u}(t) \ . \end{aligned} \tag{C.20}$$

Accordingly, delays $D_1(\boldsymbol{p}(t))$ and $D_2(\boldsymbol{p}(t))$ are given by:

$$\begin{aligned} D_1(\boldsymbol{p}(t)) &= \frac{a_{m,1}}{p_1(t)} + \frac{a_{c,1}}{c_1 p_1(t)} \\ D_2(\boldsymbol{p}(t)) &= \frac{a_{m,1}}{p_1(t)} + \frac{a_{m,2}}{c_2 p_1(t)} + \frac{a_{c,2}}{c_2 p_1(t)} \end{aligned} \tag{C.21}$$

Thermodynamic parameters are shown in Table C.1 while system parameters are illustrated in Table C.2. Be aware that only the V_1 and V_2 parameters have been estimated from an actual cooling system, while other system specific parameters have been chosen for this example. The reason for not having more parameters for the actual system is simply the lack of available measurement data for parameter estimation.

Table C.1: Thermodynamic parameters.

$c_{p,FW}$ [J/(kg· K)]	$c_{p,SW}$ [J/(kg· K)]	ρ [kg/m^3]	ρ_{SW} [kg/m^3]
4181	3993	1000	1025

The LPV model represented by (C.20) and the corresponding nonlinear model, which we will not state here, are subjected to the same input and disturbances as well as changes in scheduling variables. The model outputs are then compared to illustrate

Table C.2: System parameters for simulation examples.

V_{CC} [m^3]	V_1 [m^3]	V_2 [m^3]	$a_{m,1}$ [m^3]	$a_{m,2}$ [m^3]
20	13.5	13.5	30	10
$a_{c,1}$ [m^3]	$a_{m,2}$ [m^3]	c_1 [-]	c_2 [-]	
10	10	0.51	0.49	

how well the LPV model approximates the nonlinear model. The simulation scenario is constructed such that the system is in steady state with the chosen initial conditions. The division of the input into a time varying set point and a perturbation from the set point as given by (C.8), is implemented using a simple first order discrete low pass filter with a cut off frequency of 0.002 rad/s. Initial conditions for the simulation are illustrated in Table C.3 and the responses for both the LPV and nonlinear model are shown in Fig. C.2. Fig. C.3 shows the input signals, $\hat{q}_{LT}(t)$, $q_{LT}(t)$ and $q_{SW}(t)$, while Fig. C.4 illustrates the disturbances in terms of $\dot{Q}_1(t)$, $\dot{Q}_2(t)$ and $T_{LT,out}(t)$. Finally, Fig. C.5 shows the scheduling variables, $p_1(t)$ and $p_2(t)$, where $p_1(t)$ is the low pass filtered input, $q_{LT}(t)$.

Table C.3: Initial conditions for simulation examples.

$T_{SW,in}(0)$ [°C]	$T_1(0)$ [°C]	$T_2(0)$ [°C]	$T_{LT,in}(0)$ [°C]	$\dot{Q}_1(0)$ [W]	$\dot{Q}_2(0)$ [W]
24	45	50	36	$4 \cdot 10^6$	$6 \cdot 10^6$
$T_{SW,out}(0)$ [°C]	$q_{LT}(0)$ [m^3/s]	$q_{SW}(0)$ [m^3/s]	$x(\theta)$ for $\theta \in [-\overline{D}, 0]$ [°C]		
40	0.21	0.59	$[45\ 50\ 36]^T$		

The purpose of the simulation example is not to illustrate a real world scenario, but rather to excite the models in a way that shows how well the LPV model approximates the original nonlinear model. It is expected that the model outputs will differ only when the approximated part of the LPV model is excited. As can be seen from Fig. C.2, deviations between the LPV model and the nonlinear model occurs in the transitions of the input $q_{LT}(t)$, which is expected since all approximation in the LPV model has to do with $q_{LT}(t)$. Despite the deviations, the LPV model captures all important dynamics and is considered to be sufficiently accurate for control design.

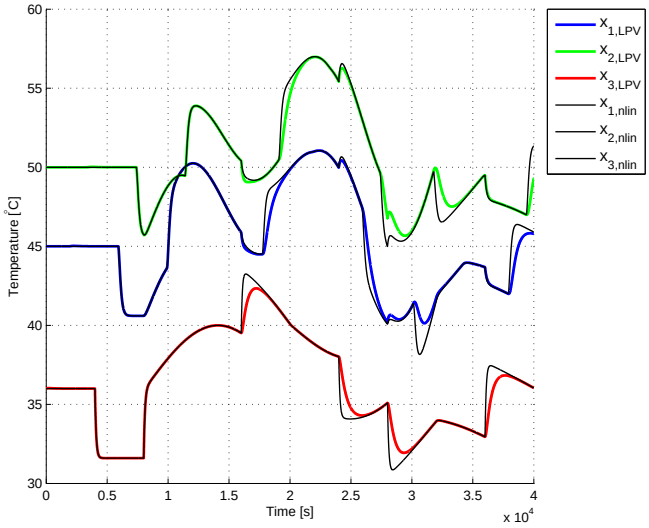

Fig. C.2: Comparison between LPV and nonlinear model outputs. Index 'LPV' denotes LPV model output, while 'nlin' denotes nonlinear model output.

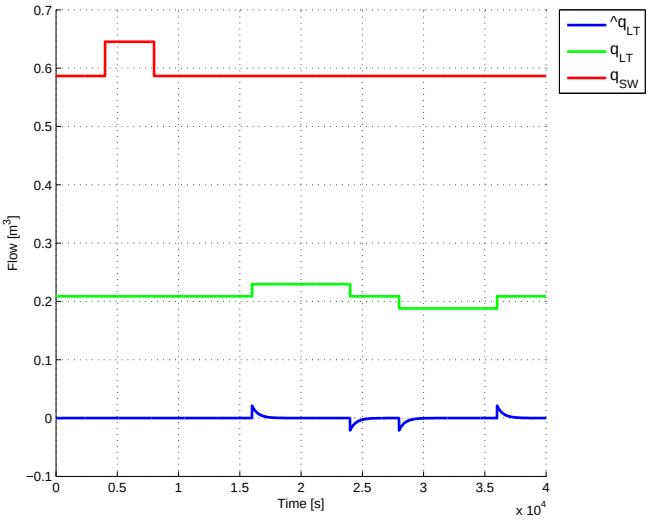

Fig. C.3: Plot of input signal $\hat{q}_{LT}(t)$ for the LPV model and $q_{LT}(t)$ for the nonlinear model. The input $q_{SW}(t)$ is the same for both models.

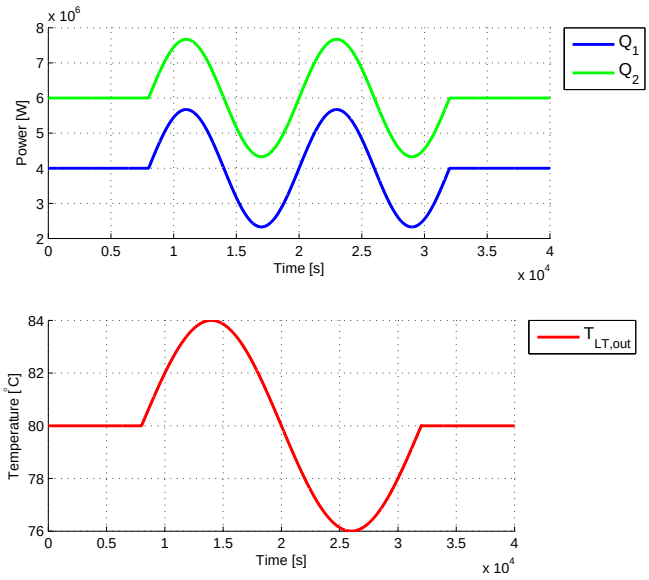

Fig. C.4: Top plot illustrates disturbances $\dot{Q}_1(t)$ and $\dot{Q}_2(t)$, while the bottom plot shows the disturbance $T_{LT,out}(t)$.

5 Concluding Remarks

We have presented the conversion of a nonlinear model to an LPV model for a marine cooling system with transport delays. The choice of scheduling variables for the LPV model was based on an attempt to keep the number of scheduling variables as low as possible, while still capturing the important nonlinear dynamics of the system and preserving the flow dependency of the delays. To illustrate the performance of the LPV model compared to the original nonlinear model, a simulation example was constructed. The simulation showed that the LPV model output only differed from the original nonlinear model when the input was excited, which was expected since all approximations in the LPV model was related to this input. The simulations indicate that the LPV model is sufficiently accurate for control design, and future work involves design of energy optimizing control laws that ensures robustness with the presence of disturbances and transport delays.

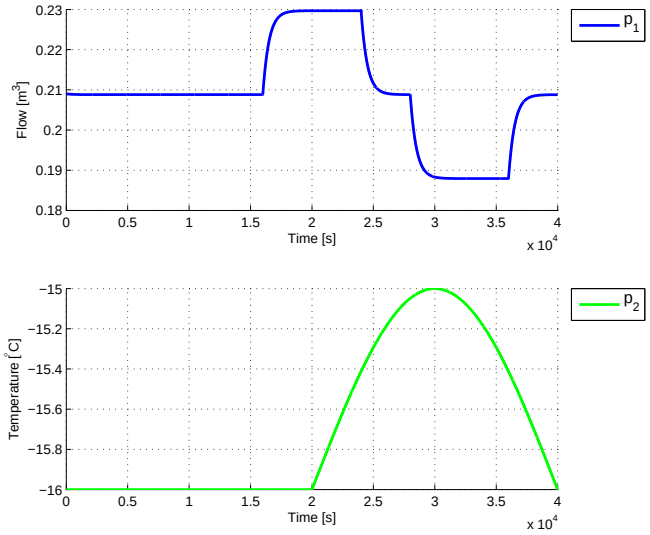

Fig. C.5: Top plot illustrates parameter $p_1(t)$ which is the low pass filtered input $q_{LT}(t)$, while the bottom plot shows the parameter $p_2(t)$ which is the temperature difference $(T_{SW,in}(t) - T_{SW,out}(t))$.

References

[1] M. Hansen, J. Stoustrup, and J. D. Bendtsen, "Modeling of nonlinear marine cooling system with closed circuit flow," in *Proceedings of the 18th IFAC World Congress*, 2011, pp. 5537–5542.

[2] R. Toth, *Modeling and Identification of Linear Parameter-Varying Systems*. Springer, 2010.

[3] J. S. Shamma and M. Athans, "Gain scheduling: Potential hazards and possible remedies," *IEEE Control Systems Magazine*, no. June, 1992.

[4] P. Apkarian and R. J. Adams, "Advanced gain-scheduling techniques for uncertain systems," *IEEE Transactions on Control Systems Technology*, vol. 6, pp. 21–32, 1998.

[5] R. Zope, J. Mohammadpour, K. Grigoriadis, and M. Franchek, "Robust fueling strategy for an SI engine modeled as an linear parameter varying time-delayed system," in *American Control Conference (ACC), 2010*. IEEE, 2010, pp. 4634–4639.

[6] K. Tan, K. M. Grigoriadis, and F. Wu, "H_∞ and L_2 - to - L_∞ gain control of linear parameter-varying systems with parameter-varying delays," in *IEEE Proceedings - Control Theory and Applications*, vol. 150, 2003, p. 509.

[7] F. Wu and K. M. Grigoriadis, "LPV Systems with parameter-varying time delays: analysis and control," *Automatica*, vol. 37, pp. 221–229, 2001.

[8] M. Jung and K. Glover, "Control-oriented linear parameter-varying modelling of a turbocharged diesel engine," in *Proceedings of 2003 IEEE Conference on Control Applications, 2003.*, 2003, pp. 155–160.

Paper D

Robust Nonlinear Control Design with Application to a Marine Cooling System

Michael Hansen
Jakob Stoustrup
Jan Dimon Bendtsen

The paper has been published in the
Proceedings of 7th IFAC Symposium on Robust Control Design, pp. 381–386, 2012.

Abstract

In this paper we consider design of control laws for a marine cooling system with flow dependent delays by use of principles from feedback linearization. To deal with model uncertainties and delay mismatches, a robust linear H_∞ controller is designed for the feedback linearized system. In this context, we apply a bilinear transformation to obtain a well-posed H_∞ problem. Robustness of performance for the resulting robust nonlinear control design is evaluated through a simulation example where a comparison is made to a linear control design.

1 Introduction

Control of nonlinear systems is often achieved by use of linear controllers designed for a linear approximation of the nonlinear system at some chosen operating point. A shortcoming of this approach is that validity of the linear approximation is very often limited to a small region around the chosen operating point. As a consequence the performance of the linear controller is likely to deteriorate as the system moves away from the operating point chosen in the design [1]. One way of dealing with this is by feedback linearization where the objective is to find a state feedback control law and possibly a change of variables to transform the nonlinear system into a linear equivalent [2]. However, to achieve successful cancellation of nonlinearities in the system, the plant model has to be exact. If the system is subject to uncertainties, which is the case for most real processes, the performance of the feedback linearization is degraded, sometimes even to the point where instability occurs.

In this paper we consider application of feedback linearization together with robust control design to a marine cooling system with flow dependent delays. This system was introduced in [3]. The use of linear robust control design in combination with feedback linearization has been investigated on several occasions, see for instance [1] and [4]. In this paper we take a heuristic approach to include time-varying state delays in the feedback linearization to achieve a linear and delay free equivalent system. However, as the marine cooling system is not exempt from neither uncertainties nor measurement noise, the cancellation of nonlinearities and delays through feedback linearization cannot be exact. Since the cooling system in question plays a vital role in the operation of a marine vessel, robustness of performance is an important aspect of the controlled cooling system. Hence, it should be ensured that inexact cancellation by the feedback linearization does not result in significant deterioration of the closed loop system performance, or even worse, causes instability. To this end, a linear H_∞ controller is designed for the feedback linearized system to deal with model uncertainties and delay estimation errors. Robustness of performance is illustrated through a simulation example, and is compared to a linear base-line control design from [5]. The results shows a clear improvement in

both performance and robustness of performance for the design approach applied in this paper, compared to the linear reference design.

The structure of the paper is as follows: In Section 2 we introduce the model of the marine cooling system considered in this paper. Section 3 deals with the transformation of the nonlinear system into a linear equivalent using feedback linearization. Section 4 describes robust control design for the feedback linearized system, and performance of the overall control design is evaluated through a simulation example in Section 5. Finally, concluding remarks are given in Section 6.

We make use of the following notation: $\mathbb{R}$ denotes the set of real numbers while $\mathbb{R}_+$ denotes the set of non-negative real numbers. $\mathbb{R}^{n\times m}$ is the set of real $n \times m$ matrices and $C(\mathcal{M},\mathcal{N})$ is the set of continuous functions mapping from $\mathcal{M}$ to $\mathcal{N}$. Vectors are written in bold, and I_n denotes the $n \times n$ identity matrix, while $\mathbf{0}_{n,m}$ denotes the $n \times m$ zero matrix.

2 Marine Cooling System Model

We consider the problem of designing robust nonlinear control laws for the marine cooling system introduced in [3]. A simplified diagram of the cooling system is illustrated in Fig. D.1. The circuit on the left is denoted seawater (SW) circuit and has the single purpose of pumping seawater through the primary (cold) side of the heat exchanger. The objective is to remove heat from the coolant circulating through the machinery in the low temperature (LT) circuit on the right, i.e., on the secondary (hot) side of the heat exchanger. The LT circuit contains various types of auxiliary machinery in a parallel configuration, i.e. the consumers in Fig. D.1 ranges from diesel generators to air condition condensers. As a consequence, the individual consumer provides very different heat loads to the cooling system and have various flow requirements. To keep the model complexity to a minimum, the same first order ODE model is applied to all consumers. It is assumed that heat exchange only takes place in the consumers of the cooling system, and in the heat exchanger.

Using notation from Fig. D.1 the dynamics of the system is governed by:

$$\dot{T}_i(t) = \frac{1}{V_i}\left[q_i(t)(T_{LT,in}(t - D_i(\boldsymbol{q})) - T_i(t)) + \frac{\dot{Q}_i(t)}{\rho c_p}\right] \tag{D.1}$$

$$\dot{T}_{LT,in}(t) = \frac{1}{V_{CC}}\left[\sum_{i=1}^{p} q_i(t)(T_{LT,out}(t) - T_{LT,in}(t)) + q_{SW}(t)\frac{\rho_{SW}c_{p,SW}}{\rho c_p}\Delta T_{SW}(t))\right], \tag{D.2}$$

for $i = 1, 2, \ldots, p$, where q denotes volumetric flow rate, V is internal volume, T is temperature and $\dot{Q}$ denotes heat transfer. Furthermore, ρ and c_p are respectively the density and specific heat of the coolant, $\Delta T_{SW} = T_{SW,in} - T_{SW,out}$ and $\boldsymbol{q} = [q_1, q_2, \ldots, q_p]^T$.

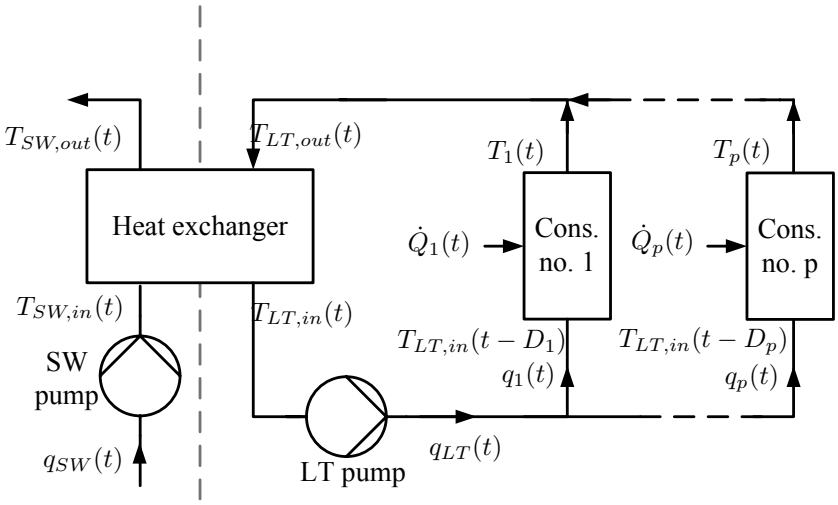

Fig. D.1: Simplified layout of the cooling system considered in this work.

Due to the size and layout of the cooling system, there is a transport delay in the coolant temperature from the heat exchanger to each of the consumers. Delays are modeled by:

$$D_i(\boldsymbol{q}) = \sum_{j=1}^{i} a_{m,j} \left(\sum_{k=j}^{p} q_k \right)^{-1} + \frac{a_{c,i}}{q_i} \ , \tag{D.3}$$

where $a_{m,j}$ and $a_{c,i}$ are positive, system specific constants.

In this setting, we define states, controllable inputs, and exogenous inputs as:

$$\boldsymbol{x} = \begin{bmatrix} T_1(t) \\ \vdots \\ T_p(t) \\ T_{LT,in}(t) \end{bmatrix} \quad \boldsymbol{u} = \begin{bmatrix} q_1(t) \\ \vdots \\ q_p(t) \\ q_{SW}(t) \end{bmatrix} \quad \boldsymbol{w}_1 = \begin{bmatrix} \dot{Q}_1(t) \\ \vdots \\ \dot{Q}_p(t) \end{bmatrix}. \tag{D.4}$$

With the definitions in (D.4) the state equations can be represented as:

$$\dot{\boldsymbol{x}}(t) = \sum_{i=1}^{m} f_i(\boldsymbol{x}(t), \boldsymbol{x}(t - D_i(\boldsymbol{u})))u_i(t) + B_w \boldsymbol{w}_1(t) \ , \tag{D.5}$$

where $\boldsymbol{x} \in \mathbb{R}^{n_x}$, $\boldsymbol{u} \in \mathbb{R}^{n_u}$, $\boldsymbol{w}_1 \in \mathbb{R}^{n_d}$, $B_w \in \mathbb{R}^{n_x \times n_d}$ and $f_i(\cdot)$ are smooth vector fields defined on a subset of $\mathbb{R}^{n_x}$.

We assume that the parameter varying delays are bounded, i.e. $D_i(\boldsymbol{q})$ for $i = 1, \ldots, n_u$ belongs to the set:

$$\mathcal{D} := \{D \in C(\mathbb{R}, \mathbb{R}); 0 \leq D \leq \overline{D} < \infty;\ \forall \boldsymbol{q} \in \mathbb{R}^p_+\}\ .$$

To ensured delays are bounded entails according to (D.3) that inputs must be strictly positive. In this context we only consider situations where there is a positive heat load and as a consequence the temperature difference of the coolant at the in- and outlet of a consumer is always positive, i.e. $0 < (T_i(t) - T_{LT,in}(t - D_i(\boldsymbol{q}))\ , \forall t \in \mathbb{R}_+$. The bilinear nature of the systems means that flow rates must be strictly positive for the system to be at an equilibrium, and it is not unreasonable to bound the flows, and thereby the inputs such that: $0 < \underline{\boldsymbol{U}} \leq \boldsymbol{u} \leq \overline{\boldsymbol{U}}$.

Similar, disturbances are assumed to be bounded but unknown, i.e. they belong to the set:

$$\mathcal{W} := \{\dot{Q} \in C(\mathbb{R}, \mathbb{R}); 0 < \underline{Q} \leq \dot{Q} \leq \overline{Q} < \infty;\ \forall t \in \mathbb{R}_+\}\ .$$

Initial conditions for the system in (D.5) are governed by:

$$\boldsymbol{x}(0) = \boldsymbol{x}_0\ , \tag{D.6}$$

$$\boldsymbol{x}(\theta) = \phi(\theta) \quad , \quad \theta \in \left[-\overline{D}, 0\right]\ , \tag{D.7}$$

and we define that:

$$\boldsymbol{x}_t(\theta) = x(t + \theta)\ . \tag{D.8}$$

It is assumed that $\boldsymbol{x}_t(\theta)$ is available to the controller.

3 Feedback Linearization Design

From general feedback linearization theory it is well known that the nonlinear state equations can be linearized through state feedback of the form:

$$\boldsymbol{u} = \alpha(\boldsymbol{x}) + \gamma^{-1}(\boldsymbol{x})\boldsymbol{v}\ , \tag{D.9}$$

if the state equations follows the structure of:

$$\dot{\boldsymbol{x}} = \boldsymbol{A}\boldsymbol{x} + \boldsymbol{B}\gamma(\boldsymbol{x})[\boldsymbol{u} - \alpha(\boldsymbol{x})]\ , \tag{D.10}$$

where $\boldsymbol{A} \in \mathbb{R}^{n_x \times n_x}$, $\boldsymbol{B} \in \mathbb{R}^{n_x \times n_u}$, $\alpha : \mathbb{R}^{n_x} \mapsto \mathbb{R}^{n_u}$, $\gamma : \mathbb{R}^{n_x} \mapsto \mathbb{R}^{n_u \times n_u}$, $\gamma(x)$ is nonsingular in the domain of interest, and the pair $(\boldsymbol{A}, \boldsymbol{B})$ is controllable [2].

By writing γ as a function of both states and delayed states using (D.3) to estimate the delays, i.e. $\gamma(\boldsymbol{x}, \boldsymbol{x}(t - \hat{D}_1), \ldots, \boldsymbol{x}(t - \hat{D}_n))$ the system in (D.5) is written as:

$$\dot{\boldsymbol{x}}(t) = \boldsymbol{B}_v\gamma(\cdot)\boldsymbol{u}(t) + \boldsymbol{B}_w\boldsymbol{w}_1(t)\ . \tag{D.11}$$

Under invertibility assumptions on γ the system is linearized through the feedback law:

$$\boldsymbol{u}(t) = \gamma(\cdot)^{-1}\boldsymbol{v}(t) \ , \tag{D.12}$$

where $\boldsymbol{v}(t)$ is a linear control input.

Since delays in the case of the marine cooling system depends on the input, a practical remark is in order. The use of an input dependent delay estimate in the feedback linearization has the immediate consequence that the control law will depend on the current input. To avoid this algebraic constraint, we approximate the delays by:

$$\hat{D}_i(\boldsymbol{q}) \approx \sum_{j=1}^{i} a_{m,j} \left(\sum_{k=j}^{p} q_k(t-\tau) \right)^{-1} + \frac{a_{c,i}}{q_i(t-\tau)} \ , \tag{D.13}$$

where τ is a small positive constant, i.e. we use previous input values to estimate the current delays.

To ease the notation in the following, we define:

$$\Lambda = \frac{\rho_{SW} c_{p,SW}}{\rho c_p} \Delta T_{SW}(t) \ , \tag{D.14}$$

$$\Phi = T_{LT,out}(t) - T_{LT,in}(t) \ , \tag{D.15}$$

$$\Psi_i = (T_{LT,in}(t - \hat{D}_i) - T_i(t)) \ . \tag{D.16}$$

Bringing (D.1) and (D.2) to the form of (D.10) results in:

$$\dot{\boldsymbol{x}} = \overbrace{\begin{bmatrix} \frac{1}{V_1} & 0 & \dots & 0 \\ 0 & \ddots & & \vdots \\ \vdots & & \frac{1}{V_p} & 0 \\ 0 & \dots & 0 & \frac{1}{V_{cc}} \end{bmatrix}}^{\boldsymbol{B}_v} \overbrace{\begin{bmatrix} \Psi_1 & 0 & \dots & 0 \\ 0 & \ddots & & \vdots \\ \vdots & & \Psi_p & 0 \\ \Phi & \dots & \Phi & \Lambda \end{bmatrix}}^{\gamma} \overbrace{\begin{bmatrix} q_1(t) \\ \vdots \\ q_p(t) \\ q_{SW}(t) \end{bmatrix}}^{\boldsymbol{u}} + \overbrace{\begin{bmatrix} \frac{1}{\rho c_p V_1} & 0 & \dots & 0 \\ 0 & \ddots & & \vdots \\ \vdots & & & \frac{1}{\rho c_p V_p} \\ 0 & \dots & \dots & 0 \end{bmatrix}}^{\boldsymbol{B}_w} \overbrace{\begin{bmatrix} \dot{Q}_1(t) \\ \vdots \\ \dot{Q}_p(t) \end{bmatrix}}^{\boldsymbol{w}_1} \tag{D.17}$$

We need to ensure that γ is non-singular, and in this case it is sufficient to look at the product of the diagonal and check if this is nonzero in the domain of interest:

$$\Lambda \prod_{i=1}^{p} \Psi_i \neq 0 \ , \quad \forall t \in \mathbb{R}_+ \ . \tag{D.18}$$

We have already argued that $\Psi_i < 0$, and a similar argument can be applied for Λ: Since we only consider the system during operation, the heat transfer from the LT side of the system will ensure that ΔT_{SW} will be strictly negative, and we have that $\Lambda < 0,\ \forall t \in \mathbb{R}_+$.

From the state feedback law (D.9), and the fact that $\alpha(x) = 0$, we get that:

$$\boldsymbol{u} = \gamma^{-1}(\cdot)\boldsymbol{v} = \begin{bmatrix} \frac{1}{\Psi_1} & 0 & \dots & 0 \\ 0 & \ddots & & \vdots \\ \vdots & & \frac{1}{\Psi_p} & 0 \\ \frac{\Phi}{\Psi_1 \Lambda} & \dots & \frac{\Phi}{\Psi_p \Lambda} & \frac{1}{\Lambda} \end{bmatrix} \boldsymbol{v} \ . \tag{D.19}$$

Because the feedback linearization relies on exact cancellation of nonlinear terms, any model uncertainties or mismatch between the estimated delay and actual delay will degrade the performance of the feedback linearization. This can be represented as:

$$\dot{\boldsymbol{x}} = \boldsymbol{B}_v \gamma \hat{\gamma}^{-1} \boldsymbol{v} + \boldsymbol{B}_w \boldsymbol{w}_1 \tag{D.20}$$

$$\Downarrow$$

$$\dot{\boldsymbol{x}} = \boldsymbol{B}_v (I + \Delta) \boldsymbol{v} + \boldsymbol{B}_w \boldsymbol{w}_1 \ , \tag{D.21}$$

where $\hat{\gamma}$ estimates the system nonlinearities and Δ represents the mismatch between the estimated and actual system nonlinearities due to uncertainties. However, rather than using the representation in (D.21) we accommodate for this uncertainty by adding an output disturbance term, $\boldsymbol{w}_2 \in \mathbb{R}^{n_x}$. This can be interpreted as a way of describing additive norm bounded modeling uncertainties for output feedback H_∞ control [6].

By this approach the feedback linearized system can be represented as the stabilizable system:

$$\begin{aligned} \dot{\boldsymbol{x}} &= \boldsymbol{B}_v \boldsymbol{v} + \boldsymbol{B}_w \boldsymbol{w}_1 \\ \boldsymbol{y} &= \boldsymbol{C}_0 \boldsymbol{x} + \boldsymbol{D}_0 \boldsymbol{w}_2 \ , \end{aligned} \tag{D.22}$$

where $\boldsymbol{C}_0, \boldsymbol{D}_0 \in \mathcal{R}^{n \times n}$ for this system are identity matrices.

This setup is illustrated in Fig. D.2 an forms the basis for the H_∞ control design in the following.

4 Robust Control Design

Design of the linear control input $\boldsymbol{v}(t)$ for the feedback linearized system in (D.22) is done by use of robust control theory. We use the standard 2×2 block formulation as illustrated in Fig. D.3. This means that:

$$G(s) = \boldsymbol{C}(sI - \boldsymbol{A})^{-1}\boldsymbol{B} + \boldsymbol{D} := \left[\begin{array}{c|c} \boldsymbol{A} & \boldsymbol{B} \\ \hline \boldsymbol{C} & \boldsymbol{D} \end{array}\right] \ , \tag{D.23}$$

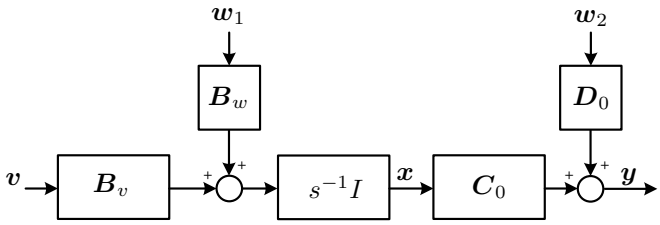

Fig. D.2: Linear equivalent of feedback linearized marine cooling system with an additive uncertainty term, $\boldsymbol{w}_2$.

for the system given by the state space representation $\boldsymbol{A}$, $\boldsymbol{B}$, $\boldsymbol{C}$ and $\boldsymbol{D}$. Combining exogenous inputs, $\boldsymbol{w}_1$ and $\boldsymbol{w}_2$, into a single vector and introducing an error vector, $\boldsymbol{z}$, penalizing the states and inputs, yields:

$$\boldsymbol{w} = \begin{bmatrix} \boldsymbol{w}_1 \\ \boldsymbol{w}_2 \end{bmatrix} \tag{D.24}$$

$$\boldsymbol{z} = \boldsymbol{x} + \rho_0 \boldsymbol{v} \tag{D.25}$$

where $\rho_0 > 0$ is a scaling factor for the control penalty.

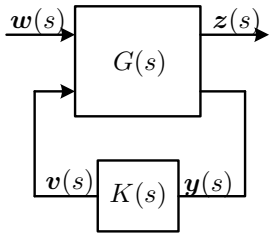

Fig. D.3: The H_∞ control problem in a 2×2 block formulation.

We apply the partitioning from [7] to (D.23) to achieve:

$$G(s) = \left[\begin{array}{c|cc} \boldsymbol{A} & \boldsymbol{B}_1 & \boldsymbol{B}_2 \\ \hline \boldsymbol{C}_1 & \boldsymbol{D}_{11} & \boldsymbol{D}_{12} \\ \boldsymbol{C}_2 & \boldsymbol{D}_{21} & \boldsymbol{D}_{22} \end{array}\right] \tag{D.26}$$

where $\boldsymbol{B}$, $\boldsymbol{C}$ and $\boldsymbol{D}$ have been partitioned according to $\boldsymbol{z}$, $\boldsymbol{y}$, $\boldsymbol{w}$ and $\boldsymbol{v}$, respectively.

With the definitions of $\dot{\boldsymbol{x}}$, $\boldsymbol{y}$, $\boldsymbol{w}$ and $\boldsymbol{z}$ for the marine cooling system in question, we can write the matrices in (D.26) as:

$$\boldsymbol{B}_1 = \begin{bmatrix} \boldsymbol{B}_w & \mathbf{0}_{n_x,n_x} \end{bmatrix} \quad \text{(D.27)} \qquad \boldsymbol{D}_{11} = \mathbf{0}_{n_x,(p+n_x)} \quad \text{(D.31)}$$

$$\boldsymbol{B}_2 = \boldsymbol{B}_v \quad \text{(D.28)} \qquad \boldsymbol{D}_{12} = \rho_0 I_{n_x} \quad \text{(D.32)}$$

$$\boldsymbol{C}_1 = I_{n_x} \quad \text{(D.29)} \qquad \boldsymbol{D}_{21} = [\mathbf{0}_{n_x,p} \;\; \boldsymbol{D}_0] \quad \text{(D.33)}$$

$$\boldsymbol{C}_2 = I_{n_x} \quad \text{(D.30)} \qquad \boldsymbol{D}_{22} = \mathbf{0}_{n_x,n_x} \quad \text{(D.34)}$$

We now have a 2×2 block formulation of the robust control problem. However, it is evident from Fig. D.2 and (D.22) that the system has poles on the imaginary axis. This means we are dealing with a nonstandard problem which cannot be solved with standard H_∞ theory directly. To this end we apply a bilinear transformation to shift the poles of the feedback linearized system from the origin and transform the system model into a close approximation which allows standard H_∞ control design. Once the controller is designed for the approximate model, the inverse bilinear transformation is applied to get the final controller for the original plant model [8].

We apply the $j\omega$-axis pole shifting transformation described in details in [9] given by:

$$s = \frac{\tilde{s} + p_1}{(\frac{\tilde{s}}{p_2}) + 1} \;, \tag{D.35}$$

where $p_1, p_2 < 0$ are the endpoints of a circle being mapped by (D.35) from the left s-plane into the $j\tilde{\omega}$-axis of the $\tilde{s}$-plane. Correspondingly, the inverse transformation is given by:

$$\tilde{s} = \frac{-s + p_1}{(\frac{s}{p_2}) - 1} \;. \tag{D.36}$$

An important aspect of the bilinear transformation in (D.35) is the choice of p_1 and p_2. A property of the weighted mixed sensitivity problem formulation is that any unstable plant pole within the specified control bandwidth is approximately shifted to its $j\omega$-axis mirror image once the loop is closed with an H_∞ controller. Since the bilinear transformation maps the poles from the $j\omega$-axis in the s-plane to a circle centered at $-(p_1 + p_2)/2$ in the $\tilde{s}$-plane, the parameter p_1 in (D.35) and (D.36) plays an essential role when placing dominant closed loop poles in the s-plane. Contrary to p_1, the choice of p_2 is of little importance to the design, and can be chosen such that: $p_2 \gg$ control bandwidth [8].

Having mapped the system to the $\tilde{s}$-plane using appropriate values for p_1 and p_2, we find a H_∞ optimal controller, $K(\tilde{s})$, by solving the two standard 2-Riccati equations from [7]. The final controller, $K(s)$, is then obtained by applying the inverse bilinear transformation from (D.36) to $K(\tilde{s})$.

5 Simulation Example

To clarify the design methodology in its entirety as well as to evaluate both performance and robustness of performance we consider a simulation example where $p = 2$, i.e. we have that:

$$\dot{T}_1(t) = \frac{1}{V_1}\left[q_1(t)(T_{LT,in}(t - D_1(\boldsymbol{q})) - T_1(t)) + \frac{\dot{Q}_1(t)}{\rho c_p}\right], \tag{D.37}$$

$$\dot{T}_2(t) = \frac{1}{V_2}\left[q_2(t)(T_{LT,in}(t - D_2(\boldsymbol{q})) - T_2(t)) + \frac{\dot{Q}_2(t)}{\rho c_p}\right], \tag{D.38}$$

$$\dot{T}_{LT,in}(t) = \frac{1}{V_{CC}}\left[\sum_{i=1}^{2} q_i(t)(T_{LT,out}(t) - T_{LT,in}(t)) + q_{SW}(t)\frac{\rho_{SW} c_{p,SW}}{\rho c_p}\Delta T_{SW}(t))\right], \tag{D.39}$$

where the thermodynamic parameters for the cooling system is illustrated in Table D.1.

Table D.1: Thermodynamic parameters for cooling system.

c_p [J/(kg· K)]	ρ [kg/m^3]	$c_{p,SW}$ [J/(kg· K)]	ρ_{SW} [kg/m^3]	V_{CC} [m^3]	V_1 [m^3]	V_2 [m^3]
4181	1000	3993	1025	20	13.5	13.5

The corresponding delays are given by:

$$D_1(\boldsymbol{q}) = \frac{a_{m,1}}{q_1 + q_2} + \frac{a_{c,1}}{q_1} \tag{D.40}$$

$$D_2(\boldsymbol{q}) = \frac{a_{m,1}}{q_1 + q_2} + \frac{a_{m,2} + a_{c,2}}{q_2} \tag{D.41}$$

From (D.19) we find γ^{-1} as:

$$\gamma^{-1} = \begin{bmatrix} \frac{1}{\Psi_1} & 0 & 0 \\ 0 & \frac{1}{\Psi_2} & 0 \\ \frac{\Phi}{\Psi_1 \Lambda} & \frac{\Phi}{\Psi_2 \Lambda} & \frac{1}{\Lambda} \end{bmatrix} \tag{D.42}$$

We then have that:

$$\dot{\boldsymbol{x}} = \begin{bmatrix} \frac{1}{V_1} & 0 & 0 \\ 0 & \frac{1}{V_2} & 0 \\ 0 & 0 & \frac{1}{V_{CC}} \end{bmatrix} \boldsymbol{v} + \begin{bmatrix} \frac{1}{\rho c_p V_1} & 0 \\ 0 & \frac{1}{\rho c_p V_2} \\ 0 & 0 \end{bmatrix} \boldsymbol{w}_1 \tag{D.43}$$

$$\boldsymbol{y} = I_3 \boldsymbol{x} + I_3 \boldsymbol{w}_2 \ . \tag{D.44}$$

We choose $\rho_0 = 1.2$ and partition the system matrices according to (D.27)-(D.34). For the bilinear transformation we choose $p_1 = -10 \times 10^{-3}$, $p_2 = -100$ and obtain a H_∞ controller using `hinfsyn()` in Matlab.

To evaluate performance we apply the proposed controller to a nonlinear simulation model of the marine cooling system and compare the response with the base-line (PI) control design presented in [5]. In the first simulation scenario we consider the nominal case, where the system is subjected to step-wise disturbances while at the operating point used in the design for the base-line controller. To evaluate and compare robustness of performance for the two designs we also consider parameter perturbations of $\pm$ 50% for V_1, V_2, V_{CC}, $a_{m,1}$ and $a_{m,2}$ resulting in 32 combinations of extreme values. These combinations are all tested, and responses are plotted along the response for the nominal system for both controller design. Parameters for the first simulation scenario are presented in Table D.2 and disturbances are plotted in Fig. D.4.

Table D.2: Parameters for 1st simulation run.

$T_{1,ref}$ [°C]	$T_{2,ref}$ [°C]	$T_{LT,in,ref}$ [°C]	$T_{SW,in}$ [°C]	$T_{SW,out}$ [°C]	V_1 [m^3]
65	70	36	24	40	13.5±50%
$a_{m,1}$ [m^3]	$a_{m,2}$ [m^3]	$a_{c,1}$ [m^3]	$a_{c,2}$ [m^3]	V_{CC} [m^3]	V_2 [m^3]
30±50%	40±50%	20	10	20±50%	13.5±50%

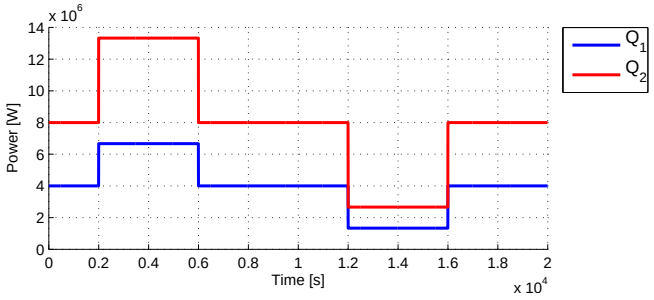

Fig. D.4: Disturbances $Q_1(t)$ and $Q_2(t)$.

Responses for the base line control is shown in Fig. D.5 while the response for the control design presented in this paper is illustrated in Fig. D.6.

Comparing Fig. D.5 and Fig. D.6 it is evident that the control design presented in this paper does not suffer from the same transient peaks during disturbance steps as the base-line control. However, due to the lack of integral action in the H_∞ controller, the temperature response for this control design is subject to a small steady state error.

This could be avoided by introducing an integrator to the H_∞ controller as in [6], which however, is outside the scope of this paper. The results also shows that even under considerable variations of system parameters the closed-loop system controlled by the control design proposed in this paper performs almost identical to the nominal one. For the case of the base-line control, the parameter variations does influence the closed-loop response, but never to the point where instability occurs.

Next, we consider a scenario where the temperature references are changed, such that the base-line control is no longer at the operating point used in the design. We then subject the system to the same disturbances as in the previous case. Parameters for the second simulation run are shown in Table D.3.

Table D.3: Parameters for 2nd simulation run.

$T_{1,ref}$ [°C]	$T_{2,ref}$ [°C]	$T_{LT,in,ref}$ [°C]	$T_{SW,in}$ [°C]	$T_{SW,out}$ [°C]	V_1 [m^3]
55	60	40	24	40	13.5±50%
$a_{m,1}$ [m^3]	$a_{m,2}$ [m^3]	$a_{c,1}$ [m^3]	$a_{c,2}$ [m^3]	V_{CC} [m^3]	V_2 [m^3]
30±50%	40±50%	20	10	20±50%	13.5±50%

Responses for the base-line control are plotted in Fig. D.7 while the responses for the proposed design are plotted in Fig D.8.

As before, parameter variations does influence the closed loop response for the base-line design, while they are barely visible in the closed loop response for the control design presented in this paper. The change in operating conditions affects the disturbance rejection performance of the base-line control resulting in increased transient peaks when the disturbances are stepped. Contrary, the change in operating conditions causes no visible change in disturbance attenuation performance for the proposed control design.

6 Concluding Remarks

We have presented a heuristic but systematic approach to design a robust nonlinear controller for a marine cooling system with flow dependent delays. The design methodology was comprised by principles from feedback linearization to deal with delays and nonlinearities, while a H_∞ control design was used to ensure robustness towards model uncertainties and disturbances. Robustness of performance for the composite control design was illustrated through a simulation example. Results from the simulation showed that robustness towards both parameter variations and changes in operating conditions for the proposed design was significantly improved compared to a base-line PI control design. From this it is concluded that the design approach proposed in this paper yields a simple, yet effective way of compensating delays and nonlinearities while maintaining

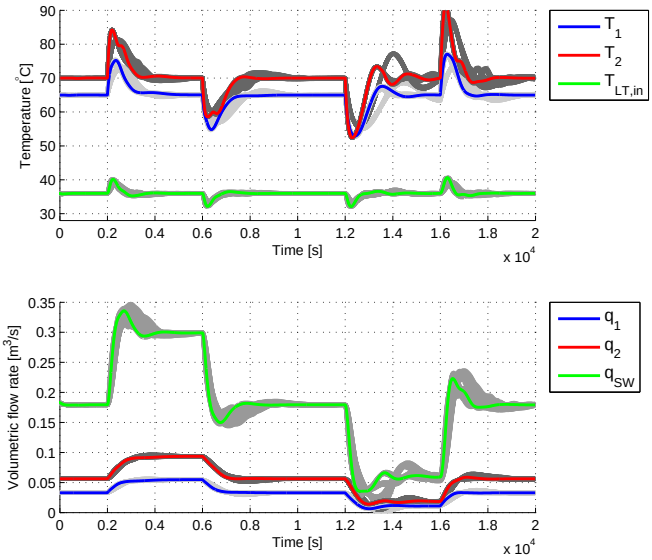

Fig. D.5: Temperature response and corresponding input signals for base-line controller

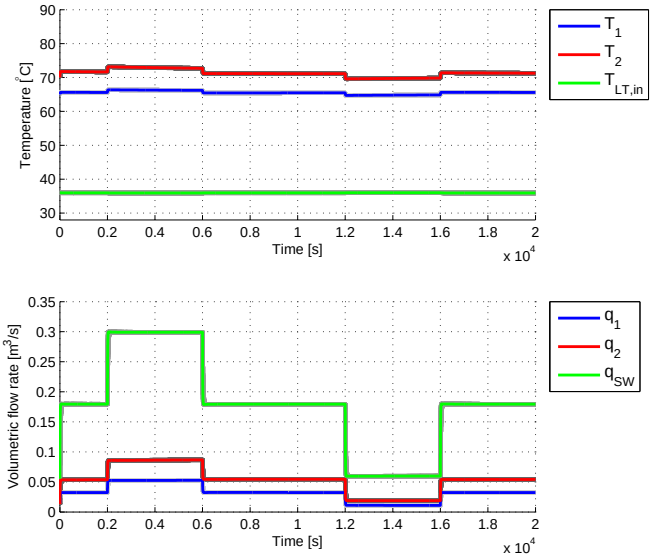

Fig. D.6: Temperature response and corresponding input signals for H_∞ controller applied to feedback linearized system.

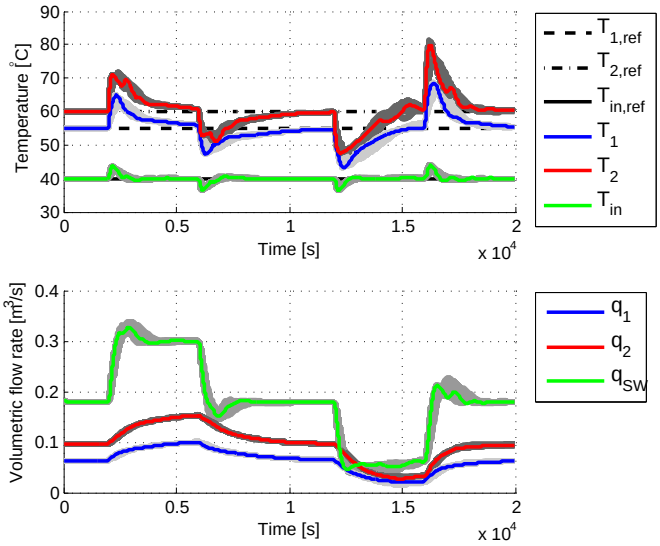

Fig. D.7: Temperature response and corresponding input signals for base-line controller

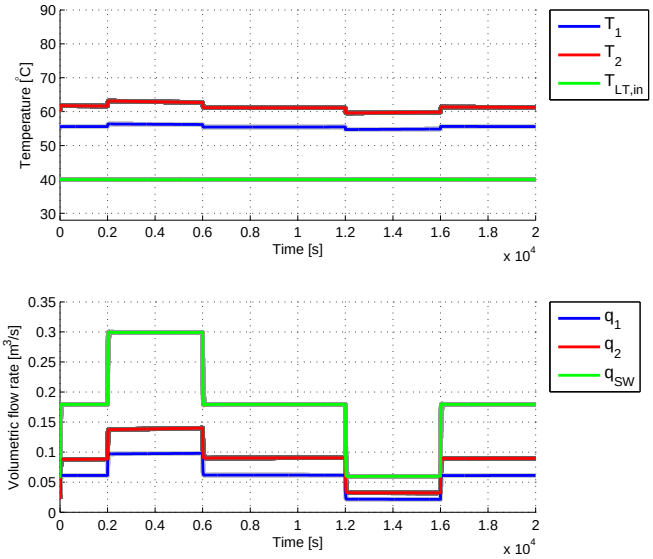

Fig. D.8: Temperature response and corresponding input signals for H_∞ controller applied to feedback linearized system.

robustness of performance. However, the control does require some storage of data as the control law relies on previous values of one of the states. Also, lack of integral action in the proposed design resulted in a small steady state error, which will be addressed in future works. Future works also includes verification of the proposed design through implementation on a full scale cooling system aboard a container vessel in service.

References

[1] A. L. D. Franco, H. Bourlès, E. R. D. Pieri, and H. Guillard, "Robust Nonlinear Control Associating Robust Feedback Linearization and H_∞ Control," *IEEE Transactions on Automatic Control*, vol. 51, pp. 1232–1236, 2006.

[2] H. K. Khalil, *Nonlinear Systems*. Prentice Hall, 2001.

[3] M. Hansen, J. Stoustrup, and J. D. Bendtsen, "Modeling of nonlinear marine cooling system with closed circuit flow," in *Proceedings of the 18th IFAC World Congress*, 2011, pp. 5537–5542.

[4] B. Chang, H. Kwtany, and S.-S. Hu, "An Application of Robust Feedback Linearization to a Ball and Beam Control Problem," in *Proceedings of the 1998 IEEE International Conference on Control Applications.*, vol. 1. IEEE, 1998, pp. 694–698.

[5] M. Hansen, J. Stoustrup, and J. D. Bendtsen, "Control of Non-linear Marine Cooling System," in *Proceedings of the 2011 IEEE Multi-Conference on Systems and Control (MSC)*, 2011, pp. 88–93.

[6] S. W. Su, B. D. Anderson, and T. S. Brinsmead, "Use of Integrator in Nonlinear H_∞ Design for Disturbance Rejection," *Automatica*, vol. 38, pp. 1951–1957, 2002.

[7] J. Doyle, K. Glover, and P. P. Khargonekar, "State-space Solutions to Standard H_2 and H_∞ Control Problems," *IEEE Transactions on Automatic Control*, vol. 34, 1989.

[8] R. Chiang and M. Safonov, "Design of H_∞ Controller for a Lightly Damped System using a Bilinear Pole Shifting Transform," in *American Control Conference (ACC), 1991*, vol. 4. IEEE, 1991, pp. 1927–1928.

[9] R. Chiang and M. G. Safonov, "H^∞ Synthesis Using a Bilinear Pole Shifting Transform," *Journal of guidance, control, and dynamics*, vol. 15, pp. 1111–1117, 1992.

Paper E

Modeling and Control of a Single-Phase Marine Cooling System

Michael Hansen
Jakob Stoustrup
Jan Dimon Bendtsen

The paper has been accepted for publication in Control Engineering Practice, 2013

Abstract

This paper presents two model-based control design approaches for a single-phase marine cooling system. Models are derived from first principles and aim at describing significant system dynamics including nonlinearities and transport delays, while keeping the model complexity low. The two approaches investigated are: A baseline design for performance comparison, and a nonlinear robust control design. Performance and robustness of performance for the two control designs are evaluated through a simulation example. Both designs show good robustness towards parameter variations, while the nonlinear robust design performs better in terms of disturbance rejection.

1 Introduction

To this day, maritime transportation remains the most energy efficient means of transportation when considering fuel consumption per ton freighted goods [1]. However, there still exist a significant potential for energy optimization when it comes to container vessels, especially when considering ship subsystems and their interconnections. With a growing attention to reduction of CO_2, SO_x and NO_x emissions from maritime transportation [2], combined with fluctuating oil prices in recent years [3], there are now strong incentives to improve the energy efficiency of ocean-going vessels.

This paper presents a number of results on modeling and control of a cooling system that can be found aboard several classes of container vessels in operation today. The overall aim is to lower the energy consumption of this cooling system, while ensuring both sufficient cooling and stability in the presence of disturbances such as main engine load conditions and seawater temperature.

Improving control of this particular system has two significant impacts on the overall energy efficiency of the vessel: The first and most direct impact is through reduction of pump power consumption by lowering flow rates in the system such that only necessary cooling is generated. From the affinity laws it is known that there is a cubic relationship between pump flow rate and pump power consumption, which in other terms means that a flow rate reduction of e.g. 10 % results in a reduction of pump power consumption by about 27 %.

The second impact concerns machinery connected to the cooling system, i.e., the consumers of the system. Since the energy efficiency of each consumer often depends on the operating conditions provided by the cooling system, there is a potential for lowering the energy consumption by ensuring that these operating conditions are optimal. An example of this could be cooling of the scavenge air for the main engine (typically a two-stroke diesel engine) of the ship, where the temperature of the scavenge air influences the specific fuel oil consumption (SFOC) of the main engine. From an energy efficiency point of view, the scavenge air temperature should be kept as low as possible as this

decreases the SFOC [4]. However, the temperature cannot be arbitrary low as this increases condensation and the risk of water carry-over to the cylinders which can cause severe wear on the cylinder liner [5]. By controlling the temperature of the scavenge air to a predefined optimal set point it is possible to lower the SFOC of the main engine, while avoiding too much condensation with resulting water carry-over to the cylinders.

Related work can be found in [6] which considers the derivation of a numerical model for the same type of marine cooling system as considered here, but with focus on simulation and transient analysis when designing the cooling system layout. Derivation of models for the marine cooling system aimed specifically at control design in terms of structure and complexity was considered previously by the authors in [7]. Based on these models, design of simple control laws for baseline comparison was dealt with in [8]. In [9] a heuristic nonlinear robust control design method was presented and applied to the cooling system to compensate for nonlinearities and transport delays. This paper summarizes, expands and compares results from these papers to give a full overview of the status as of today.

The structure of the paper is as follows: Section 2 briefly outlines the structure and mode of operation for the cooling system considered in this work. This is followed by first principle models for the hydraulics and thermodynamics of the cooling system. In Section 3 control laws for the cooling system hydraulics are initially designed. This is followed by a baseline control design for the thermodynamic part of the cooling system, using classical control theory. The final part of Section 3 presents a heuristic but structured approach to a nonlinear robust control design for the thermodynamic part of the cooling system. Performance of the nonlinear robust control is compared to the baseline control in Section 4 through a simulation example and concluding remarks are presented in Section 5.

The following notation is used: $\mathbb{R}$ denotes the set of real numbers while $\mathbb{R}_+$ denotes the set of non-negative real numbers. $\mathbb{R}^{n\times m}$ is the set of real $n \times m$ matrices, and $C^k(\mathcal{M},\mathcal{N})$ is the set of continuous functions mapping from vector space $\mathcal{M}$ to vector space $\mathcal{N}$ with continuous derivatives up to order k. $\boldsymbol{I}_n$ denotes the $n\times n$ identity matrix, while $\mathbf{0}_{n,m}$ denotes the $n \times m$ zero matrix.

2 Modeling

The cooling system consists of three circuits; a seawater (SW) circuit, a low temperature, fresh water (LT FW) circuit and a high temperature, fresh water (HT FW) circuit. This setup is illustrated in Figure E.1, where q_{LT} and q_{SW} are volumetric flows in the LT FW and SW circuits, while q_{HT} is the volumetric flow to the HT FW circuit.

The SW circuit pumps water from the sea through the cold side of the central coolers for lowering the temperature of the coolant in the LT FW and HT FW circuits. The LT

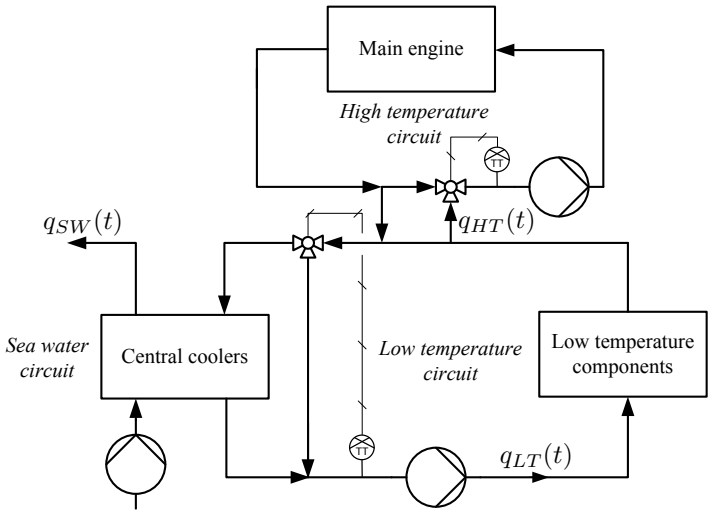

Fig. E.1: Simplified layout of the single-phase marine cooling system.

FW circuit contains auxiliary machinery such as diesel generators, air condition units, and turbochargers, all placed in a parallel configuration. The HT FW circuit contains the main engine (ME) of the ship, and since the cooling demand for this component is very strict there is little room for energy optimization in this part of the system from a cooling point of view. As a result, the main focus in this work is therefore the LT FW and SW circuits.

In the current mode of operation, all pumps in the system are controlled in open loop; that is, pumps are running at one of two speeds depending on the temperature of the seawater and the ME load. Coolant temperature is controlled in two places by the three-way valves illustrated in Figure E.1. This is done by either shunting coolant past the central coolers, or adjusting the amount of coolant that is recirculated in the HT FW circuit. The layout of the system is designed such that sufficient cooling can be provided for the machinery even under worst-case conditions, i.e. at high seawater temperature and maximum ME load. However, this is at the expense of excess cooling being generated when the ship is not operating under worst case conditions, which is most of the time.

In the following it is assumed that all flows are turbulent and there are no laminar flow effects. There is also no heat loss to surroundings, i.e. heat exchange only takes place in the consumers or in the central coolers. The coolant does not undergo phase changes and its density as well as specific heat is assumed to be constant in the temperature range of interest. Finally, the coolant in the system is assumed to be incompressible.

A model-based approach to control design is taken in this work, which entails deriving dynamic models for the marine cooling system. The model is divided into two parts, configured in series: A hydraulic part and a thermodynamic part. Time is denoted as $t \in \mathbb{R}_+$ while pump head, $\Delta \boldsymbol{H}_p(t) \in \mathbb{R}_+^2$, and hydraulic resistance of control valves, $\boldsymbol{\varphi}_{cv}(t) \in \mathbb{R}_+^p$, are the manipulated inputs for the hydraulic model. Similar, the system flow rates, $\boldsymbol{q}_s(t) \in \mathbb{R}^{(p+1)}$, are outputs of the hydraulic model and act as manipulated inputs for the thermodynamic model. The coolant temperature at the outlet of the central coolers and consumers, $\boldsymbol{T}(t) \in \mathbb{R}_+^{(p+1)\times 1}$, are thermodynamic model outputs, while disturbances acting on the thermodynamic model, $\boldsymbol{W}(t) \in \mathbb{R}_+^{(p+1)\times 1}$, cover heat transfer from the consumers and the SW temperature. This setup is illustrated in Figure E.2.

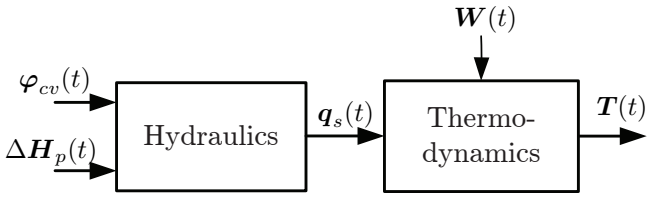

Fig. E.2: Model overview and configuration.

Hydraulic Model

It is assumed that the hydraulic layout of the SW and LT FW circuits conforms to the structure depicted in Figure E.3. It should be noted that the 3-way valve and central cooler bypass from Figure E.2 is not included in Figure E.3. The argument is that a main objective with improving control of the cooling system is to make the 3-way valve redundant such that no coolant flows through the bypass.

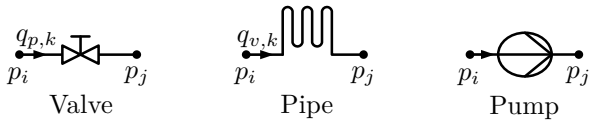

In this work the general framework from [10] and [11] is adopted for modeling the hydraulic network. The method is based on network theory and the well known analogy between electrical and hydraulic circuits, where voltage and current corresponds to pressure and flow, respectively. The following models for the hydraulic components in the cooling system are used:

Valve model:

$$p_i - p_j = \mu(K_{v,k}, q_{v,k}) \ , \tag{E.1}$$

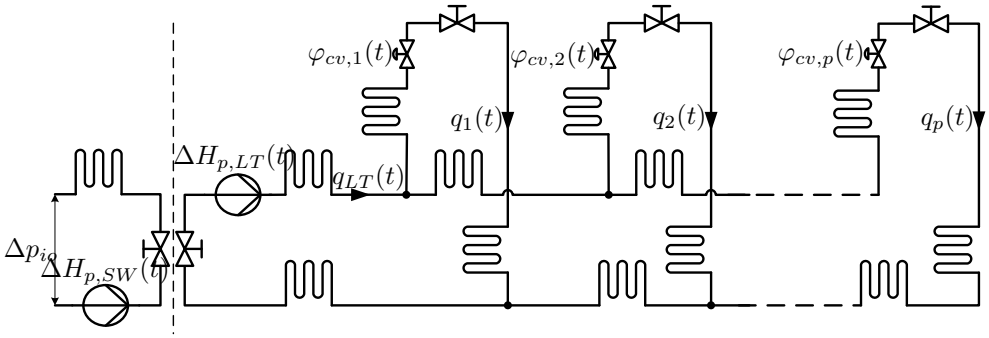

Fig. E.3: Hydraulic structure of the SW and LT FW circuits.

where $(p_i - p_j)$ is the pressure drop between points i and j, i.e., across the valve, $K_{v,k}$ is a parameter describing the hydraulic resistance of the k'th valve and $q_{v,k}$ is the volumetric flow through the k'th valve. Also, $\mu \in C^\infty(\mathbb{R}_+ \times \mathbb{R}, \mathbb{R})$ is a strictly monotonically increasing function of both its arguments. Controllable valves are denoted with index $\{cv\}$ and φ is used for the hydraulic resistance of a controllable valve to distinguish them from non-controllable valves.

Pipe model:

$$J_k \frac{dq_{p,k}}{dt} = (p_i - p_j) - \lambda(K_{p,k}, q_{p,k}) \ , \tag{E.2}$$

where J_k is the inertance for the k'th pipe section while $K_{p,k}$ is the hydraulic resistance for the k'th pipe section. Also, $(p_i - p_j)$ is the pressure drop along the pipe, $q_{p,k}$ is the flow through the k'th pipe and $\lambda \in C^\infty(\mathbb{R}_+ \times \mathbb{R}, \mathbb{R})$ is a strictly monotonically increasing function of both its arguments.

Pump model:

$$p_i - p_j = -\Delta H_{p,k} \ , \tag{E.3}$$

where $\Delta H_{p,k}$ is the delivered pressure by the k'th pump. In this scope, a quasi-static pump response is assumed such that the pump moves from one steady state operating point to another. This means that pump dynamics is neglected, which is justified by the fact that the rate of change for this application is much less than one tenth of the rotational frequency of the shaft [12]. Also, it is assumed for simplicity that pumps are able to deliver the required pressure regardless of the flow through the pump.

By applying Kirchoff's loop law to each fundamental loop in the hydraulic network it is possible to set up equations for the relationship between pressure and flow for the

loop. To this end, the fundamental loop matrix $\boldsymbol{B} \in \mathbb{R}^{p \times m}$ is introduced:

$$B_{ij} = \begin{cases} 1 & \text{if component } j \text{ is in loop } i \text{ and directions agree} \\ -1 & \text{if component } j \text{ is in loop } i \text{ and directions do not agree} \\ 0 & \text{if component } j \text{ is not in loop } i \end{cases} \tag{E.4}$$

where $i = 1, 2, \ldots, m$ and m is the total number of components in the hydraulic network, while $j = 1, 2, \ldots, p$ and p is the number of loops in the associated graph equivalent to the number of consumers. Agreement of direction in this context relates to the reference direction defined for the component and loop, respectively. In this work, the choice of reference directions is defined such that signs in $\boldsymbol{B}$ are positive. The aim is a model of the form:

$$\dot{\boldsymbol{q}} = f(\boldsymbol{q}, \boldsymbol{\varphi}_{cv}, \Delta \boldsymbol{H}_p) \ , \tag{E.5}$$

where $\boldsymbol{q} = [q_1, q_2, \ldots, q_p]^T$ is a vector of free flows, i.e. the flows through each loop in the network; see Figure E.3. By combining the individual component models it is possible to characterize the differential pressure for each component with:

$$\begin{aligned} \Delta p_i = J_i \dot{q}_{c,i} + \lambda_i(K_{p,i}, q_{c,i}) + \mu_i(K_{v,i}, q_{c,i}) \\ + \mu_{cv,i}(\varphi_{cv,i}, q_{c,i}) - \Delta H_{p,i}, \end{aligned} \tag{E.6}$$

It applies that: $J_i = \lambda_i = \mu_i = \mu_{cv,i} = 0$ if the i'th components is a pump, $\mu_i = \mu_{cv,i} = \Delta H_{p,i} = 0$ if the i'th component is a pipe, $J_i = \lambda_i = \Delta H_{p,i} = \mu_{cv,i} = 0$ if the i'th component is a valve, and $J_i = \lambda_i = \Delta H_{p,i} = \mu_i = 0$ if the i'th component is a control valve. $\Delta \boldsymbol{h}$ and $\boldsymbol{q}_c$ are defined as vectors where the elements are the pressure drops of and flows through each component in the network, respectively. Then, from Kirchhoff's loop law and the definitions of $\boldsymbol{q}$, $\boldsymbol{q}_c$, $\Delta \boldsymbol{h}$ and $\boldsymbol{B}$, it is implied that: $\boldsymbol{0} = \boldsymbol{B}^T \Delta \boldsymbol{h}$ and $\boldsymbol{q}_c = \boldsymbol{B}^T \boldsymbol{q}$. To simplify notation, the following definitions are introduced:

$$\begin{aligned} \Delta \boldsymbol{H}_p &= [\Delta H_{p,1}, \ldots, \Delta H_{p,m}]^T \ , \\ \boldsymbol{J} &= diag\{J_1, \ldots, J_k\} \ , \\ \boldsymbol{\lambda}(\boldsymbol{K}_p, \boldsymbol{q}_c) &= [\lambda_1(K_{p,1}, q_{c,1}), \ldots, \lambda_m(K_{p,m}, q_{c,m})]^T \ , \\ \boldsymbol{\mu}(\boldsymbol{K}_v, \boldsymbol{q}_c) &= [\mu_1(K_{v,1}, q_{c,1}), \ldots, \mu_m(K_{v,m}, q_{c,m})]^T \ , \\ \boldsymbol{\mu}_c(\boldsymbol{\varphi}_{cv}, \boldsymbol{q}_c) &= [\mu_{c,1}(\varphi_{cv,1}, q_{c,1}), \ldots, \mu_{c,m}(\varphi_{cv,m}, q_{c,m})]^T \ . \end{aligned} \tag{E.7}$$

From this the resulting model can be written as:

$$\begin{aligned} \boldsymbol{B}\boldsymbol{J}\boldsymbol{B}^T \dot{\boldsymbol{q}} = &- \boldsymbol{B}\boldsymbol{\lambda}(\boldsymbol{K}_p, \boldsymbol{B}^T \boldsymbol{q}) - \boldsymbol{B}\boldsymbol{\mu}(\boldsymbol{K}_v, \boldsymbol{B}^T \boldsymbol{q}) \\ &- \boldsymbol{B}\boldsymbol{\mu}_{cv}(\boldsymbol{\varphi}_{cv}, \boldsymbol{B}^T \boldsymbol{q}) + \boldsymbol{B}\Delta \boldsymbol{H}_p \ . \end{aligned} \tag{E.8}$$

In this context, an expression relating to the Darcy-Weisbach equation [13] is used for λ_i, μ_i and $\mu_{c,i}$, i.e. for the i'th component it applies that:

$$\mu_i(K_{v,i}, q_{c,i}) = K_{v,i} q_{c,i}^2 \tag{E.9}$$

$$\mu_{c,i}(\varphi_{cv,i}, q_{c,i}) = \varphi_{cv,i} q_{c,i}^2 \tag{E.10}$$

$$\lambda_i(K_{p,i}, q_{c,i}) = K_{p,i} q_{c,i}^2 \ . \tag{E.11}$$

It is clear that (E.9)-(E.11) are not strictly monotonically increasing for negative argument values, but it is argued that for this application it is only relevant to consider unidirectional flow rates, i.e., $q_i \in \mathbb{R}_+$ for $i = 1, 2, \ldots, m$. The same methodology can be applied to the SW circuit:

$$J_{SW} \dot{q}_{SW} = -K_{SW} q_{SW}^2 - \Delta p_{io} + \Delta H_{p,SW} \ , \tag{E.12}$$

where J_{SW} and K_{SW} are constant parameters for the SW circuit, and Δp_{io} is the pressure drop due to height difference between seawater intake and outlet, i.e. it is a constant pressure loss term. Equations (E.8) and (E.12) make up the hydraulics models for the LT FW and SW circuits, respectively.

Thermodynamic Model

The thermodynamics covers the heat exchange between consumers and the coolant, as well as the heat exchange between the SW and LT FW circuit through the central coolers. It is assumed that consumers can be regarded as a volume where heat is transferred to the coolant flowing through.

From the first law of thermodynamics and Reynolds's Transport Theorem [14], it is possible to write for each consumer:

$$\begin{aligned} \sum \dot{Q}_s - \sum \dot{W}_s = & \frac{d}{dt} \int_\Omega e\rho \, dV \\ & + \sum e_{out} \rho_{out} A_{out} v_{out} \\ & - \sum e_{in} \rho_{in} A_{in} v_{in} \ , \end{aligned} \tag{E.13}$$

where $\sum \dot{Q}_s$ is the total heat transfer rate in or out of the system, $\sum \dot{W}_s$ is the total rate of work transfer in or out of the system, e denotes specific energy and ρ is the density of the fluid elements in the system. Also, Ω is the control volume, v is the average velocity of the flow at in- or outlet, and A is the control volume cross section area at the in- or outlet. As there is only a single flow in and out of the volume, it is apparent that:

$$\dot{m} = \rho_{in} A_{in} v_{in} = \rho_{out} A_{out} v_{out} \ , \tag{E.14}$$

where $\dot{m}$ is the mass flow through the volume. The rate of work transfer can be described as the sum of pressure forces acting on the inlet and outlet of the control volume:

$$\sum \dot{W}_s = \dot{W}_{pf} = p_{in} A_{in} v_{in} - p_{out} A_{out} v_{out} \ . \tag{E.15}$$

The changes in potential and kinetic energy in the control volume is neglected, implying that $e = u$ where u is the internal energy per mass unit. Furthermore, heat transfer to the system is denoted by $\sum \dot{Q}_s = \dot{Q}(t)$. From the definition of specific enthalpy, $H = u + \frac{p}{\rho}$, the expression becomes:

$$\frac{d}{dt} \int_\Omega e\rho \ dV = \dot{m} \left(h_{in} - h_{out} \right) + \dot{Q} \ . \tag{E.16}$$

As there is no phase change of the coolant, it is possible to approximate the specific enthalpy by $\Delta H \approx c_p \Delta T_c$, where c_p is the specific heat for the coolant and T_c is the temperature of the coolant [15]. Preferably, the model should express the change of energy in the volume as a function of the outlet temperature. To achieve this it is approximated that:

$$\frac{d}{dt} \int_\Omega e(t)\rho \ dV \approx \rho c_p V_{CV} \frac{d \, T_{out}(t)}{dt} \ , \tag{E.17}$$

where V_{CV} is the volumetric size of the control volume. Thereby, the resulting consumer model becomes:

$$\dot{T}_{out}(t) = \frac{1}{\rho c_p V_{CV}} \left[\dot{m}(t) c_p (T_{in}(t) - T_{out}(t)) + \dot{Q}(t) \right] \ . \tag{E.18}$$

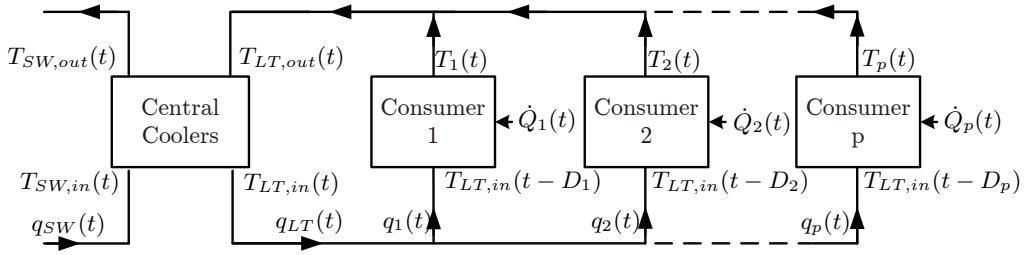

Fig. E.4: Structure and notation for cooling system thermodynamics.

Delays $D_1, \ldots, D_p$ arise from transport of coolant from the central coolers to the respective consumers in the cooling system. This means that the delays depend on the

layout of the system as well as the flow rates to the individual consumers. Based on the structure in Figure E.4 it is assumed that the delays can be described by:

$$D_i = \underbrace{\sum_{j=1}^{i} \left(a_{m,j} \sum_{k=j}^{p} q_k^{-1} \right)}_{\text{Main line delays}} + \underbrace{a_{c,i} q_i^{-1}}_{\text{Consumer line delay}} , \tag{E.19}$$

where q_i is the volumetric flow to the i'th consumer, while $a_{m,i}$ and $a_{c,i}$ correspond to inner volumes of the main line pipe section i, and consumer line pipe section i, respectively. It is assumed that this model is applicable to all consumers in the cooling system and by use of the notation from Figure E.4 it is given that for $i = 1, \ldots, p$:

$$\begin{aligned} \dot{T}_i(t) = & \frac{1}{\rho c_p V_i} \big[q_i(t) \rho c_p (T_{LT,in}(t - D_i) - T_i(t)) \\ & + \dot{Q}_i(t) \big] . \end{aligned} \tag{E.20}$$

For the central coolers the same model is applied as for the consumers, except that the heat transfer between the LT FW and SW circuit is written as a function of temperatures and mass flow rates. Assuming steady state heat transfer from the LT FW circuit to the SW circuit the model is given by:

$$\begin{aligned} \dot{T}_{LT,in}(t) = & \frac{1}{V_{CC}} \big[q_{LT}(t) (T_{LT,out}(t) - T_{LT,in}(t)) \\ & + q_{SW}(t) \frac{\rho_{SW} c_{p,SW}}{\rho c_p} (T_{SW,in}(t) - T_{SW,out}(t)) \big] . \end{aligned} \tag{E.21}$$

where ρ_{SW} and $c_{p,SW}$ are the density and specific heat of seawater, respectively.

3 Control Structure and Design

With the model structure presented in Section 2 a cascaded control configuration as illustrated in Figure E.5 is pursued. This partitioning is justified by the assumption that the thermodynamics in the system does not influence the hydraulics and there is a separation of time scales since the time constants of the heat dynamics are significantly slower than those of the hydraulics. State-feedback is considered for the flow controller in the inner loop of Figure E.5. Two designs are considered for the temperature control in the outer loop: A baseline design based on PI control and a nonlinear robust design based on feedback linearization and H_∞ control. This structure is chosen to help compensate for the nonlinear dynamics in the hydraulic model, and while state-feedback is considered in this work for the inner loop controller, other linear design techniques could have been employed, such as the one presented in [8].

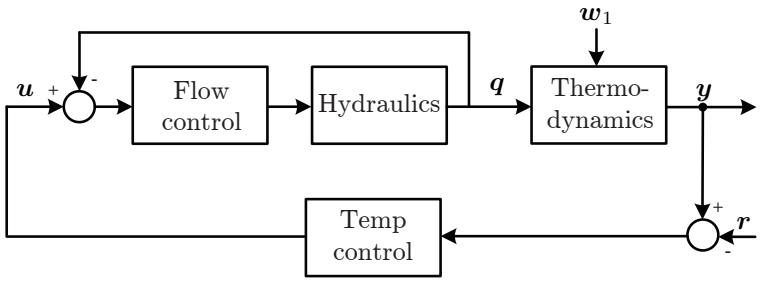

Fig. E.5: Block diagram for the cascaded control setup.

3.1 Flow Control

Design of control for the inner loop in Figure E.5, is based on the model derived in Section 2. For notational simplicity and without loss of generality it is assumed that the number of consumers in the cooling system is $p = 2$. From (E.8) it is possible to write the independent flows through consumer 1 and 2 as:

$$\begin{aligned}\dot{q}_1 =& -K_{11}q_1^2 - K_{12}q_1^2\varphi_{cv,1} + K_{13}q_2^2\varphi_{cv,2} \\ &+ K_{14}\Delta H_{p,LT} - K_{15}(q_1+q_2)^2 + K_{16}q_2^2 \end{aligned} \tag{E.22}$$

$$\begin{aligned}\dot{q}_2 =& -K_{21}q_2^2 - K_{22}q_2^2\varphi_{cv,2} + K_{23}q_1^2\varphi_{cv,1} \\ &+ K_{24}\Delta H_{p,LT} - K_{25}(q_1+q_2)^2 + K_{26}q_1^2 \end{aligned} \tag{E.23}$$

where K_{ij} are positive system specific parameters, while $\varphi_{cv,1}$ and $\varphi_{cv,2}$ denotes the hydraulic resistances of control valve 1 and 2, respectively. It is assumed that the LT FW pump delivers a constant pressure, $\Delta\bar{H}_{p,LT}$. By linearizing (E.22) and (E.23) using a first order Taylor approximation at the operating point $(\bar{q}_1, \bar{q}_2, \bar{q}_{SW}, \bar{\varphi}_1, \bar{\varphi}_2)$, it is possible to obtain the state equations:

$$\begin{aligned}\begin{bmatrix} \dot{\hat{q}}_1 \\ \dot{\hat{q}}_2 \\ \dot{\hat{q}}_{SW} \end{bmatrix} =& \begin{bmatrix} a_{11} & a_{12} & 0 \\ a_{21} & a_{22} & 0 \\ 0 & 0 & a_{33} \end{bmatrix} \begin{bmatrix} \hat{q}_1 \\ \hat{q}_2 \\ \hat{q}_{SW} \end{bmatrix} \\ &+ \begin{bmatrix} b_{11} & b_{12} & 0 \\ b_{21} & b_{22} & 0 \\ 0 & 0 & b_{33} \end{bmatrix} \begin{bmatrix} \hat{\varphi}_{cv1} \\ \hat{\varphi}_{cv2} \\ \Delta\hat{H}_{p,SW} \end{bmatrix}, \end{aligned} \tag{E.24}$$

or:

$$\dot{\hat{\boldsymbol{q}}}_s = \boldsymbol{M}\hat{\boldsymbol{q}}_s + \boldsymbol{N}\hat{\boldsymbol{\psi}}\ , \tag{E.25}$$

where:

$$
\begin{aligned}
a_{11} &= 2(-K_{11}\bar{q}_1 - K_{12}\bar{q}_1\bar{\varphi}_{cv,1} - K_{15}\bar{q}_1 - K_{15}\bar{q}_2) \\
a_{12} &= 2(K_{13}\bar{q}_2\bar{\varphi}_{cv,2} - K_{15}\bar{q}_2 - K_{15}\bar{q}_1 + K_{16}\bar{q}_2) \\
a_{21} &= 2(K_{23}\bar{q}_1\bar{\varphi}_{cv,1} - K_{25}\bar{q}_1 - K_{25}\bar{q}_2 + K_{26}\bar{q}_1) \\
a_{22} &= 2(-K_{21}\bar{q}_2 - K_{22}\bar{q}_2\bar{\varphi}_{cv,2} - K_{25}\bar{q}_2 - K_{25}\bar{q}_1) \\
a_{33} &= (-2K_{SW}\bar{q}_{SW})J_{SW}^{-1}
\end{aligned}
$$

$$
\begin{aligned}
b_{11} &= K_{12}\bar{q}_1^2 \qquad & b_{12} &= K_{13}\bar{q}_2^2 \qquad & b_{21} &= K_{23}\bar{q}_1^2 \\
b_{22} &= K_{22}\bar{q}_2^2 \qquad & b_{33} &= J_{SW}^{-1}
\end{aligned}
$$

A control law of the form: $\hat{\boldsymbol{\psi}} = -\boldsymbol{F}\hat{\boldsymbol{q}}_s$ is pursued, where $\boldsymbol{F}$ is chosen such that $\boldsymbol{M} - \boldsymbol{N}\boldsymbol{F}$ is Hurwitz. This could for instance be done by solving an LQR problem using the cost function:

$$
J = \int_0^\infty (\hat{\boldsymbol{q}}_s^T \boldsymbol{Q}\hat{\boldsymbol{q}}_s + \hat{\boldsymbol{\psi}}^T \boldsymbol{R}\hat{\boldsymbol{\psi}})dt \ , \tag{E.26}
$$

where the matrices $\boldsymbol{Q}$ and $\boldsymbol{R}$ for example may be determined using Bryson's rule [16]. Finding the feedback matrix $\boldsymbol{F}$ is then a matter of solving the algebraic Ricatti equation, which can be done using standard software. In the following, the controlled hydraulic subsystem is considered as a simple finite gain due to the difference in timescale compared to the thermodynamics of the system.

3.2 Baseline Temperature Control Design

Two temperature control designs are considered in the following: A baseline design based on classical control theory, and a nonlinear robust control design to compensate for nonlinearities and delays. The baseline design is dealt with in this section, while the nonlinear robust design is described in Section 3.3. As the name implies, the baseline control serves the purpose of providing a base of comparison for more advanced control strategies. This also means that delay compensation is not considered in the baseline control design and standard PI controllers are employed.

First, the linearized small perturbation model is determined at the operating point $(\bar{T}_i, \bar{q}_i, \bar{T}_{LT,in})$, and subsequently the transfer function from $\hat{q}_i(s)$ to $\hat{T}_i(s)$ is found:

$$
G_i(s) = \frac{\hat{T}_i(s)}{\hat{q}_i(s)} = \frac{\frac{1}{\bar{q}_i}(\bar{T}_{LT,in} - \bar{T}_i)}{s\frac{V_i}{\bar{q}_i} + 1} \ . \tag{E.27}
$$

Similar, for the central coolers:

$$G_{LT_{in}}(s) = \frac{\hat{T}_{LT,in}(s)}{\hat{q}_{SW}(s)} = \frac{\frac{c_{p,SW}\rho_{SW}}{c_p\rho\bar{q}_{LT}}(\bar{T}_{SW,in} - \bar{T}_{SW,out})}{\left(s\frac{V_{CC}}{\bar{q}_{LT}} + 1\right)} \ . \tag{E.28}$$

Using phase margin, PM, and crossover frequency, ω_0, as design parameters and choosing PI controllers of the form:

$$D(s) = K_{PI}\left(1 + \frac{1}{sT_{PI}}\right) \ , \tag{E.29}$$

the parameters K_{PI} and T_{PI} can be determined from:

$$|D(s)G(s)|_{s=j\omega_0} = 1 \ , \tag{E.30}$$

$$\tan^{-1}\left(\frac{\mathrm{Im}(D(s)G(s))}{\mathrm{Re}(D(s)G(s))}\right)\Bigg|_{s=j\omega_0} = PM - 180^\circ \ . \tag{E.31}$$

3.3 Nonlinear Robust Temperature Control Design

A robust nonlinear design approach is now considered to deal with both the nonlinearities of the system and the transport delays described in Section 2. Initially, states, control inputs and disturbances are defined as:

$$\boldsymbol{x} = \begin{bmatrix} T_1(t) \\ \vdots \\ T_p(t) \\ T_{LT,in}(t) \end{bmatrix} \quad \boldsymbol{u} = \begin{bmatrix} q_1(t) \\ \vdots \\ q_p(t) \\ q_{SW}(t) \end{bmatrix} \quad \boldsymbol{w}_1 = \begin{bmatrix} \dot{Q}_1(t) \\ \vdots \\ \dot{Q}_p(t) \end{bmatrix} \tag{E.32}$$

With the definitions in (E.32) the state equations can be represented as:

$$\dot{\boldsymbol{x}}(t) = \sum_{i=1}^{n_u} f_i(\boldsymbol{x}(t), \boldsymbol{x}(t - D_i(\boldsymbol{u})))u_i(t) + \boldsymbol{B}_w\boldsymbol{w}_1(t) \ , \tag{E.33}$$

where $\boldsymbol{x} \in \mathbb{R}^{n_x}$, $\boldsymbol{u} \in \mathbb{R}^{n_u}$, $\boldsymbol{w}_1 \in \mathbb{R}^{n_d}$, $\boldsymbol{B}_w \in \mathbb{R}^{n_x \times n_d}$ and $f_i(\cdot)$ are smooth vector fields defined on a relevant subset of $\mathbb{R}^{n_x}$.

It is assumed that the parameter varying delays are bounded, i.e., all $D_i(\boldsymbol{u})$, $i = 1, \ldots, n_u$, belong to the set:

$$\mathcal{D} := \{D \in C(\mathbb{R}^p, \mathbb{R}); 0 \leq D(\boldsymbol{u}) \leq \overline{D} < \infty \quad \forall \boldsymbol{u} \in \mathbb{R}_+^{n_u}\} \ . \tag{E.34}$$

Ensuring delays are bounded requires that flow rates in the LT FW circuit are strictly positive. In this context it is only relevant to consider situations where all consumers provide a positive heat load to the system and as a consequence the temperature difference of the coolant at the in- and outlet of each consumer is always positive, i.e. $0 < (T_i(t) - T_{LT,in}(t - D_i(\boldsymbol{u}))\ , \forall t \in \mathbb{R}_+$. The bilinear nature of the system means that flow rates must be strictly positive for the system to be at an equilibrium, and it is thus reasonable to constrain the flows, and thereby the inputs such that: $0 < \underline{U} \leq u_i \leq \overline{U}$ for $i = 1, 2, \ldots, n_u$.

Similar, disturbances are assumed to be bounded but unknown, i.e. they belong to the set:

$$\begin{aligned} \mathcal{W} :=& \{Q \in C(\mathbb{R}, \mathbb{R}); 0 < \underline{Q} \leq Q(t) \leq \overline{Q} < \infty \\ & \forall t \in \mathbb{R}_+\} \ . \end{aligned} \tag{E.35}$$

Initial conditions for the system in (E.33) are governed by:

$$\boldsymbol{x}(0) = \boldsymbol{x}_0 \ , \tag{E.36}$$

$$\boldsymbol{x}(\theta) = \boldsymbol{\phi}(\theta) \quad , \quad \theta \in \left[-\overline{D}, 0\right] \ , \tag{E.37}$$

and the state history for $t \in \mathbb{R}_+$ is defined as:

$$\boldsymbol{x}_t(\theta) = \boldsymbol{x}(t + \theta) \quad , \quad \theta \in \left[-\overline{D}, 0\right] \ . \tag{E.38}$$

It is assumed that $\boldsymbol{x}_t(\theta)$ is available to the controller.

To ease notation in the following it is defined that:

$$\begin{aligned} \Lambda &= \frac{\rho_{SW} c_{p,SW}}{\rho c_p}(T_{SW,in}(t) - T_{SW,out}(t)) \ , \\ \Phi &= T_{LT,out}(t) - T_{LT,in}(t) \ , \\ \Psi_i &= (T_{LT,in}(t - D_i) - T_i(t)) \ . \end{aligned} \tag{E.39}$$

From the definitions in (E.32) and (E.39) it is possible to write the nonlinear thermodynamic model as:

$$\dot{\boldsymbol{x}}(t) = \boldsymbol{B}\boldsymbol{\gamma}(\cdot)\boldsymbol{u}(t) + \boldsymbol{B}_w \boldsymbol{w}_1(t) \ , \tag{E.40}$$

where

$$\boldsymbol{B} = \begin{bmatrix} \frac{1}{V_1} & 0 & \dots & 0 \\ 0 & \ddots & & \vdots \\ \vdots & & \frac{1}{V_p} & 0 \\ 0 & \dots & 0 & \frac{1}{V_{cc}} \end{bmatrix} , \tag{E.41}$$

$$\boldsymbol{\gamma}(\cdot) = \begin{bmatrix} \Psi_1(\cdot) & 0 & \dots & 0 \\ 0 & \ddots & & \vdots \\ \vdots & & \Psi_p(\cdot) & 0 \\ \Phi(\cdot) & \dots & \Phi(\cdot) & \Lambda(\cdot) \end{bmatrix} , \tag{E.42}$$

$$\boldsymbol{B}_w = \begin{bmatrix} \frac{1}{\rho c_p V_1} & 0 & \dots & 0 \\ 0 & \ddots & & \vdots \\ \vdots & & & \frac{1}{\rho c_p V_p} \\ 0 & \dots & \dots & 0 \end{bmatrix} . \tag{E.43}$$

Under the assumption that the flow rates are known, the delays can be estimated using (E.19). Also, if $\boldsymbol{\gamma}(\cdot)$ is nonsingular in the domain of interest, one can obtain an equivalent delay free and linear system through feedback linearization by use of the control law:

$$\boldsymbol{u}(t) = \boldsymbol{\gamma}^{-1}(\cdot)\boldsymbol{v}(t) , \tag{E.44}$$

where $\boldsymbol{v}(t)$ is a linear control input [17]. For $\boldsymbol{\gamma}$ to be nonsingular in the domain of interest it is sufficient to ensure that the product of the diagonal elements is nonzero, i.e.:

$$\Lambda \prod_{i=1}^{p} \Psi_i \neq 0 , \quad \forall t \in \mathbb{R}_+ . \tag{E.45}$$

In the specific case of the marine cooling system it applies that Λ is strictly negative as the domain of interest is when the system is in operation. This means there is a positive heat transfer from the LT FW circuit to the SW circuit such that $T_{SW,in}(t) < T_{SW,out}(t) \ \ , \forall t$. A similar argument holds for Ψ_i as the consumers provide a positive heat load on the cooling system, such that $T_{LT,in}(t-D_i) < T_i(t) \ \ , \forall t$. As a consequence Ψ_i is strictly negative for $i = 1, \dots, p$.

As feedback linearization relies on exact cancellation of nonlinear terms, model uncertainties and measurement noise may introduce inaccuracies in the feedback linearization. In this sense it is possible to write:

$$\begin{aligned} \dot{\boldsymbol{x}} &= \boldsymbol{B}\boldsymbol{\gamma}\hat{\boldsymbol{\gamma}}^{-1}v + \boldsymbol{B}_w\boldsymbol{w}_1 \\ \boldsymbol{y} &= \boldsymbol{x} + \boldsymbol{n} , \end{aligned} \tag{E.46}$$

where $\hat{\boldsymbol{\gamma}}$ is the estimate of system nonlinearities and $\boldsymbol{n} \in \mathbb{R}^{n_x}$ is measurement noise. This may be represented as:

$$\begin{aligned} \dot{\boldsymbol{x}} &= \boldsymbol{B}(\boldsymbol{I}_{n_u} + \Delta)\boldsymbol{v} + \boldsymbol{B}_w \boldsymbol{w}_1 \ , \\ &= \boldsymbol{B}\boldsymbol{v} + \boldsymbol{B}\boldsymbol{w}_2 + \boldsymbol{B}_w \boldsymbol{w}_1 \\ \boldsymbol{y} &= \boldsymbol{x} + \boldsymbol{n} \ , \end{aligned} \tag{E.47}$$

where Δ represents the mismatch due to uncertainties and $\boldsymbol{w}_2 \in \mathbb{R}^{n_u}$ is a disturbances term included to account for these uncertainties in the design. It is assumed that:

$$\frac{1}{\rho_0}||\Delta||_\infty = \frac{1}{\rho_0} \sup_\omega \sigma_{\max}(\Delta(j\omega)) \leq 1 \ , \tag{E.48}$$

where $\rho_0 \in \mathbb{R}_+$ can be considered as the maximum percentage error between the nominal input, $\boldsymbol{v}$, and the actual input. Furthermore, $\boldsymbol{B}_w$ is scaled to normalize $\boldsymbol{w}_1$ such that $||\tilde{\boldsymbol{w}}_1||_\infty \leq 1$. Hence:

$$\tilde{\boldsymbol{B}}_w = \begin{bmatrix} \frac{\overline{Q}_1}{\rho c_p V_1} & 0 & \dots & 0 \\ 0 & \ddots & & \vdots \\ \vdots & & & \frac{\overline{Q}_p}{\rho c_p V_p} \\ 0 & \dots & \dots & 0 \end{bmatrix} \ , \tag{E.49}$$

where $\overline{Q}_1, \overline{Q}_2, \dots, \overline{Q}_p$ are upper bounds for the disturbances in $\boldsymbol{w}_1$. The problem can then be formulated as in Figure E.6. To reject constant disturbances the linearized

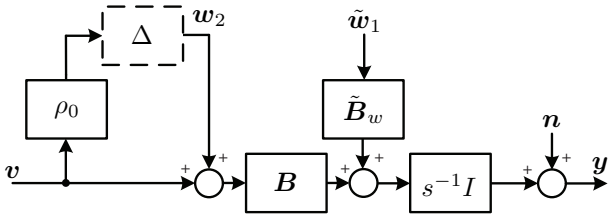

Fig. E.6: Linear equivalent of feedback linearized marine cooling system with uncertainties and disturbances.

model is augmented to include integral error states such that the feedback linearized

system is represented as:

$$\begin{aligned}\begin{bmatrix} \dot{\boldsymbol{x}} \\ \dot{\boldsymbol{e}} \end{bmatrix} &= \begin{bmatrix} \mathbf{0}_{n_x} & \mathbf{0}_{n_x} \\ \boldsymbol{I}_{n_x} & \mathbf{0}_{n_x} \end{bmatrix} \begin{bmatrix} \boldsymbol{x} \\ \boldsymbol{e} \end{bmatrix} + \begin{bmatrix} \boldsymbol{B} \\ \mathbf{0}_{n_x,n_u} \end{bmatrix} \boldsymbol{v} \\ &+ \begin{bmatrix} \tilde{\boldsymbol{B}}_w \\ \mathbf{0}_{n_x,n_d} \end{bmatrix} \tilde{\boldsymbol{w}}_1 + \begin{bmatrix} \boldsymbol{B} \\ \mathbf{0}_{n_x,n_u} \end{bmatrix} \boldsymbol{w}_2 \\ &+ \begin{bmatrix} \mathbf{0}_{n_x} \\ \boldsymbol{I}_{n_x} \end{bmatrix} \boldsymbol{n} \end{aligned} \tag{E.50}$$

$$\begin{bmatrix} \boldsymbol{y} \\ \boldsymbol{y}_e \end{bmatrix} = \begin{bmatrix} \boldsymbol{x} \\ \boldsymbol{e} \end{bmatrix} + \begin{bmatrix} \boldsymbol{I}_{n_x} \\ \mathbf{0}_{n_x} \end{bmatrix} \boldsymbol{n} \ , \tag{E.51}$$

where $\boldsymbol{e} \in \mathbb{R}^{n_x}$ are the integral error states. To deal with the system uncertainties and disturbances, the linear control input $\boldsymbol{v}$ is designed using robust control theory. To formulate a standard H_∞ problem [18] the exogenous inputs, $\tilde{\boldsymbol{w}}_1$, $\boldsymbol{w}_2$ and $\boldsymbol{n}$, are combined into a single vector. Also, an error vector, $\boldsymbol{z}$, penalizing states and control inputs is introduced. This yield:

$$\boldsymbol{w} = \begin{bmatrix} \tilde{\boldsymbol{w}}_1 \\ \boldsymbol{w}_2 \\ \boldsymbol{n} \end{bmatrix} \qquad \boldsymbol{z} = \begin{bmatrix} \boldsymbol{x} \\ \rho_0 \boldsymbol{v} \end{bmatrix} \ . \tag{E.52}$$

The partitioning from [18] is applied such that:

$$\boldsymbol{G}(s) = \left[\begin{array}{c|cc} \boldsymbol{A} & \boldsymbol{B}_1 & \boldsymbol{B}_2 \\ \hline \boldsymbol{C}_1 & \boldsymbol{D}_{11} & \boldsymbol{D}_{12} \\ \boldsymbol{C}_2 & \boldsymbol{D}_{21} & \boldsymbol{D}_{22} \end{array}\right] \ , \tag{E.53}$$

where system matrices have been partitioned according to $\boldsymbol{z}$, $\boldsymbol{y}$, $\boldsymbol{w}$ and $\boldsymbol{v}$, respectively.

As a consequence of all poles being placed on the imaginary axis the problem is non-standard and it cannot be solved with standard H_∞ theory directly. To overcome this problem a bilinear transformation is applied to shift the poles of the feedback linearized system from the origin and transform the system model into a close approximation which allows for standard H_∞ control design. Once the controller is designed for the approximate model, the inverse bilinear transformation is applied to get the final controller for the original plant model [19]. In this paper, the $j\omega$-axis pole shifting transformation is applied, which is described in details in [20]. This is given by:

$$s = \frac{\tilde{s} + p_1}{(\frac{\tilde{s}}{p_2}) + 1} \ , \tag{E.54}$$

where $p_1, p_2 < 0$ are the endpoints of the diameter of a circle being mapped by (E.54) from the left s-plane into the $j\tilde{\omega}$-axis of the $\tilde{s}$-plane. The parameters p_2 and especially

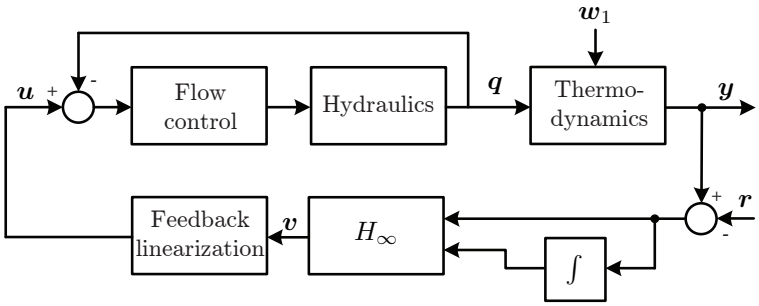

Fig. E.7: Structure of flow controller in configuration with the nonlinear robust temperature controller.

p_1 in (E.54) plays essential roles when placing dominant closed loop poles in the s-plane and thus becomes important design parameters for the H_∞ control design along with the weighting factor, ρ_0.

4 Simulation Example

To evaluate performance and robustness of performance for the control designs proposed in this paper a simulation scenario is considered, where the number of consumers is two, i.e. $p = 2$.

The simulation model is implemented in MATLAB Simulink using the ODE45 solver, and consists of the nonlinear models from Section 2 i.e., equations (E.8), (E.12) and (E.19)-(E.21). Saturation of pump pressure has also been included in the simulation model, and so has heat exchanger characteristics based on the logarithmic mean temperature difference (LMTD) approach. By neglecting potential and kinetic energy as well as assuming constant specific heat and that no phase change occur, the heat transfer through the heat exchanger can be expressed by [15]:

$$\dot{Q}_{HE} = \frac{(T_{LT,out} - T_{SW,in})(\beta - 1)}{(\frac{\beta}{q_{LT} c_p \rho}) - (\frac{1}{q_{SW} c_{p,SW} \rho_{SW}})} , \tag{E.55}$$

with

$$\beta = e^{U_{HE} A_{HE} \left[\frac{1}{q_{LT} c_p \rho} - \frac{1}{q_{SW} c_{p,SW} \rho_{SW}} \right]} , \tag{E.56}$$

where U_{HE} is the overall heat transfer coefficient for the heat exchanger and A_{HE} is the heat exchanger surface area. From (E.55) the steady state heat transfer between the LT FW and SW circuit is calculated, which is used for modeling the seawater outlet temperature as a function of seawater inlet temperature and flow rates.

Responses for the baseline temperature control design are compared with those for the nonlinear robust control design using the same flow controller as the inner control loop in both cases. The design of flow controller, baseline temperature controller and nonlinear robust temperature controller for this simulation example follows the methodology presented in Section 3. Design parameters for the baseline design are illustrated in Table E.1, where $\omega_{0,i}$ is the crossover frequency for the consumer temperature controllers, and $\omega_{0,LT}$ is the crossover frequency for the LT FW inlet temperature controller.

The design parameter, ρ_0, is estimated numerically from noise bounds on the measurements included in $\boldsymbol{\gamma}$, and uncertainty bounds on the parameters in the delay estimation. Delay estimation errors are included in ρ_0 by bounding the derivative of the time delayed variable and evaluating the temperature deviation for the worst case delay estimation error. In this case, it is assumed that delay model parameters are subject to $\pm 30\%$ uncertainty and that the noise is bounded by $\pm 3\sigma_n$, where σ_n is the standard deviation of the signal noise. The standard deviation for noise on temperature measurements is denoted with sub index T, and with sub index q for flow measurements. The resulting ρ_0 is listed in Table E.1 along with the noise standard deviations and other parameters used for controller design. Model parameters are shown in Table E.2 and E.3 for respectively the hydraulic and thermodynamic model.

Table E.1: Design parameters.

PM	$\omega_{0,i}$	$\omega_{0,LT}$	ρ_0
60°	0.01	0.05	0.78
$\sigma_{n,T}$	$\sigma_{n,q}$	p_1	p_2
0.2	0.004	-0.003	-100

Table E.2: Parameters for linearized hydraulic model.

a_{11}	a_{12}	a_{21}	a_{22}	a_{33}
-15.94	5.47	5.92	-15.03	-8.80
b_{11}	b_{12}	b_{13}	b_{21}	b_{22}
-0.0029	0.0016	0.0015	-0.0033	1

MATLABS's `hinfsyn` is employed for the H_∞ control design in this context. `hinfsyn` uses the two-Riccati formula from [21] [18] and computes a controller with an order equivalent to that of the augmented system, which in this case is 6th order. Plotting the multiplicative-error singular values for the H_∞ controller as shown in Figure E.8 reveals the possibility of reducing the controller to 3 states with little change in performance. This is achieved through application of the Balanced Stochastic Truncation technique from [22], and only the response for the reduced order H_∞ controller is presented in the following.

Table E.3: Parameters for thermodynamic model.

Q_1 [W]	$a_{c,1}$ [m^3]	$a_{m,1}$ [m^3]	V_1 [m^3]	V_{CC} [m^3]
4.8×10^6	20±30%	30±30%	13.5	20
Q_2 [W]	$a_{c,2}$ [m^3]	$a_{m,2}$ [m^3]	V_2 [m^3]	
7.2×10^6	10±30%	40±30%	13.5	

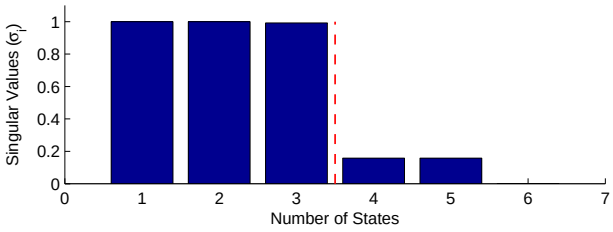

Fig. E.8: Multiplicative-error singular values of H_∞ controller.

In the first simulation scenario the system is subjected to step-wise disturbances while at the operating point used in the design of the baseline controller. This is reasonable because the heat load for several consumers directly depends on the main engine load and it is not uncommon for this to change in relative large steps during maneuvering.

To evaluate and compare robustness of performance for the two designs, parameter perturbations of ± 30% for $a_{c,1}$, $a_{c,2}$, $a_{m,1}$ and $a_{m,2}$, resulting in 16 combinations of extreme values, are also considered. These combinations are all tested, and responses are plotted along the response for the nominal system for both controller design. Disturbances are plotted in Figure E.9 and responses are plotted in Figure E.10 and E.11.

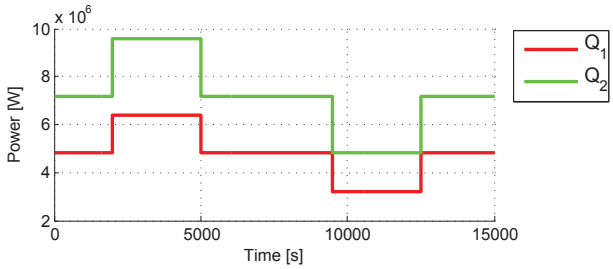

Fig. E.9: Disturbances $\dot{Q}_1(t)$ and $\dot{Q}_2(t)$.

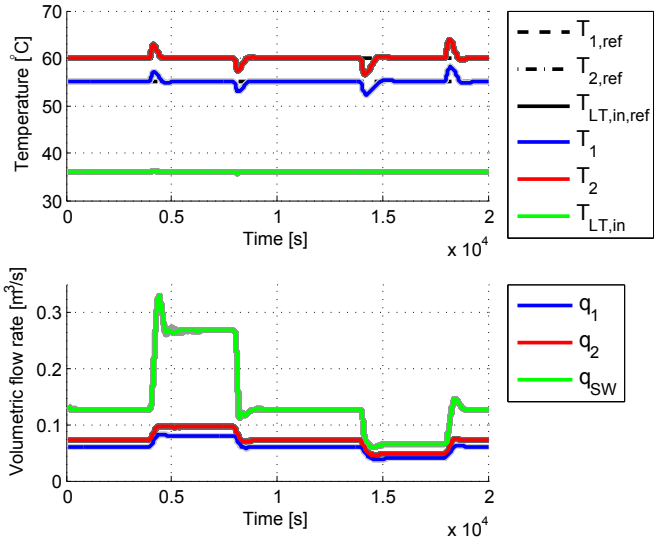

Fig. E.10: 1st run: Temperature and flow rate responses for baseline control configuration. Responses for nominal parameters are plotted in color, while responses for parameter perturbations are in gray.

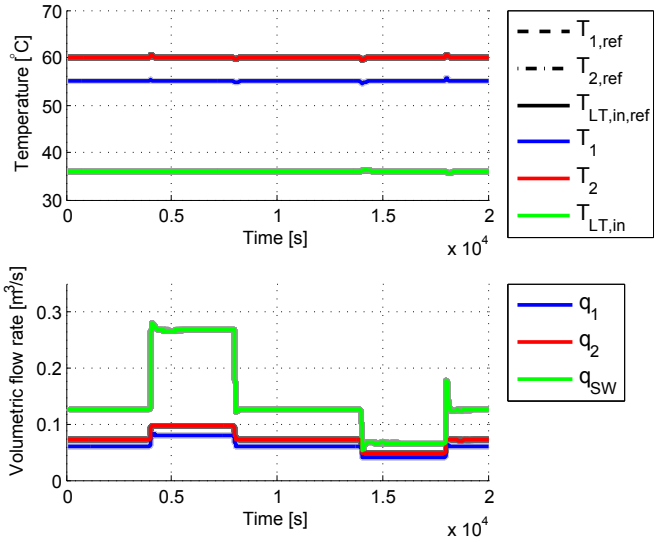

Fig. E.11: 1st run: Temperature and flow rate responses for nonlinear robust control configuration with reduced (3rd) order H_∞ controller. Responses for nominal parameters are plotted in color, while responses for parameter perturbations are in gray.

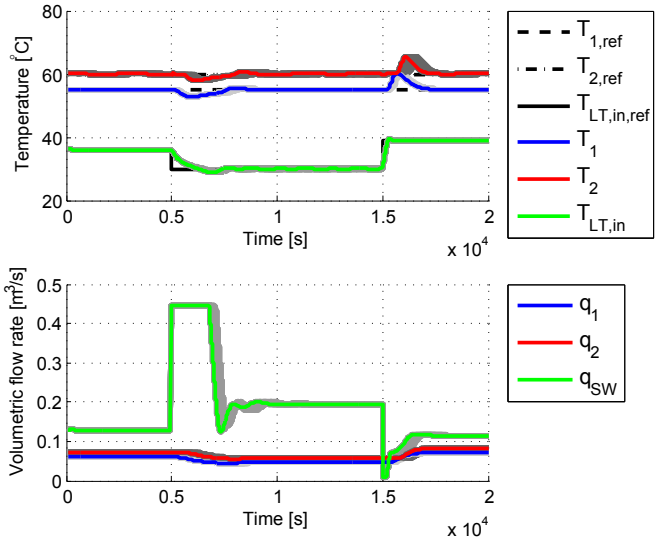

Fig. E.12: 2nd run: Temperature and flow rate responses for baseline control configuration. Responses for nominal parameters are plotted in color, while responses for parameter perturbations are in gray.

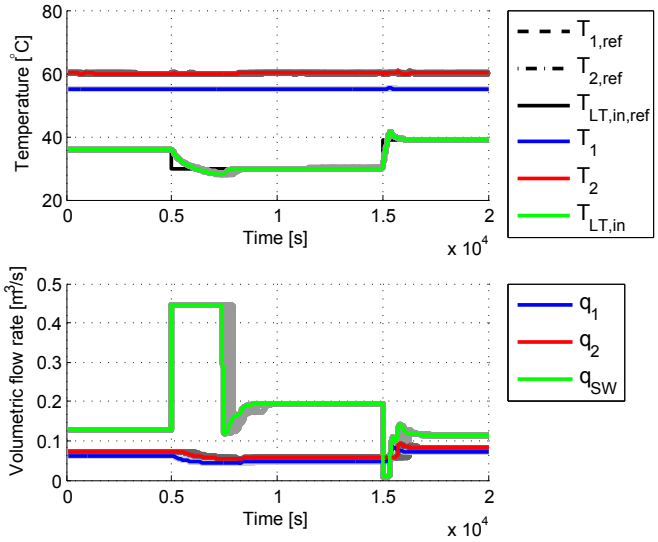

Fig. E.13: 2nd run: Temperature and flow rate responses for nonlinear robust control configuration with reduced (3rd) order H_∞ controller. Responses for nominal parameters are plotted in color, while responses for parameter perturbations are in gray.

Comparing responses for $T_1(t)$ and $T_2(t)$ in Figure E.10 and E.11 shows that the robust nonlinear design is superior to the baseline design in terms of disturbance rejection while the temperature response for the LT FW inlet temperature, $T_{LT,in}$, is very similar for both design.

In the second simulation scenario the system is subjected to step-wise changes in the reference for $T_{LT,in}(t)$ while at the operating point used in the design of the baseline controller. Also, the same parameter perturbations are evaluated, and responses are plotted along the response for the nominal system in Figure E.12 and E.13. The step-like response of the flow rates in Figure E.12 and E.13 when the temperature reference is changed from 36 °C to 30 °C is due to saturation of pump pressure. Comparing responses for the 2nd simulation example in Figure E.12 and E.13 shows similar robustness of performance and reference tracking performance of $T_{LT,in}(t)$. However, the robust nonlinear design again shows an improvement over the baseline design in terms of disturbance rejection for $T_1(t)$ and $T_2(t)$.

5 Conclusion

This paper presents two model-based approaches to design of controllers for a single-phase marine cooling system. Derivation of models for both control design and simulation is based on first-principles methods and aims at obtaining models of low complexity while still encompassing important system dynamics. This includes nonlinear flow characteristics in the hydraulic model, input affine behavior in the thermodynamic model and transport delays. The first control design is based on classical control theory and constitutes a baseline design mainly for performance comparison. The second design applies principles from feedback linearization to deal with delays and nonlinearities, while a H_∞ control design is used to ensure robustness towards model uncertainties and disturbances. Robustness of performance for the two control designs is illustrated through a simulation example that includes unmodeled dynamics and considers both parameter variations as well as changes in operating conditions. Both control designs show good robustness towards parameter variations, while the nonlinear robust design performs better in terms of disturbance rejection for consumer temperatures.

While energy optimization has not been addressed explicitly in the control designs, the relationship between pump flow rate and pump power consumption as given by the Affinity Laws, means that a reduction in pump power is achieved whenever the SW and LT circuit flow rates are reduced from the nominal system design. In this respect, the baseline and nonlinear robust design do not differ significantly since pump power is mainly determined by operating conditions and set points, which can be optimized separately from the feedback control design. Good disturbance rejection capabilities is a strong complementary benefit to set point optimization, however, since it allows the system to operate consistently close to the optimal conditions.

Future work involves verification of the proposed design through implementation on a full scale cooling system aboard a container vessel in operation.

References

[1] J.-P. Rodrigue, C. Comtois, and B. Slack, *The Geography of Transport Systems*. Routledge, 2006.

[2] J. Faber, A. Markowska, D. Nelissen, M. Davidson, I. C. Eyring, Veronika, P. Roche, E. Humpries, N. Rose, J. Graichen, and M. Cames, "Technical support for european action to reducing greenhouse gas emissions from international maritime transport," *Commissioned by: European Commission*, 2009.

[3] C. Beverelli, H. Benamara, and R. Asariotis, "Oil Prices and Maritime Freight Rates: An Empirical Investigation," *United Nations Conference on Trade and Development*, 2010.

[4] MAN Diesel and Turbo, *Influence of Ambient Temperature Conditions - Main engine operation of MAN B&W two-stroke engines*. MAN, 2010.

[5] K. Aeberli, "Sulzer RT-flex96C into Containership Service," in *Motor Ship Marine Propulsion Conference, Bilbao*, no. January 2005, 2005, pp. 1–11.

[6] T. Mrakovcic, V. Medica, and N. Skific, "Numerical Modelling of an Engine-Cooling System," *Journal of Mechanical Engineering*, no. 50, pp. 104–114, 2004.

[7] M. Hansen, J. Stoustrup, and J. D. Bendtsen, "Modeling of nonlinear marine cooling system with closed circuit flow," in *Proceedings of the 18th IFAC World Congress*, 2011, pp. 5537–5542.

[8] ——, "Control of Non-linear Marine Cooling System," in *Proceedings of the 2011 IEEE Multi-Conference on Systems and Control (MSC)*, 2011, pp. 88–93.

[9] M. Hansen, J. Stoustrup, and J. Bendtsen, "Robust Nonlinear Control Design with Application to a Marine Cooling System," in *Proceedings of the 7th IFAC Symposium on Robust Control Design (ROCOND)*, 2012, pp. 381–386.

[10] C. De Persis and C. S. Kallesøe, "Pressure regulation in nonlinear hydraulic networks by positive and quantized controls," *IEEE Transactions on Control Systems Technology*, vol. 19, pp. 1371–1383, 2011.

[11] ——, "Proportional and proportional-integral controllers for a nonlinear hydraulic network," in *Proceedings of the 17th IFAC World Congress*, 2008.

[12] C. E. Brennen, *Hydrodynamics of Pumps*. Concepts ETI, Inc and Oxford University Press, 1994.

[13] E. Menon, *Liquid Pipeline Hydraulics*. CRC Press, 2004.

[14] D. F. Young, B. R. Munson, T. H. Okiishi, and W. W. Huebsch, *A Brief Introduction to Fluid Mechanics*. John Wiley & Sons Ltd, 2007.

[15] M. Massoud, *Engineering Thermofluids: Thermodynamics, Fluid Mechanics, and Heat Transfer*. Springer, 2005.

[16] A. E. Bryson and Y.-C. Ho, *Applied Optimal Control: Optimization, Estimation, and Control*. Blaisdell, 1969.

[17] H. K. Khalil, *Nonlinear Systems*. Prentice Hall, 1996.

[18] J. Doyle, K. Glover, and P. P. Khargonekar, "State-space Solutions to Standard H_2 and H_∞ Control Problems," *IEEE Transactions on Automatic Control*, vol. 34, 1989.

[19] R. Chiang and M. Safonov, "Design of H_∞ Controller for a Lightly Damped System using a Bilinear Pole Shifting Transform," in *American Control Conference (ACC), 1991*, vol. 4. IEEE, 1991, pp. 1927–1928.

[20] R. Chiang and M. G. Safonov, "H^∞ Synthesis Using a Bilinear Pole Shifting Transform," *Journal of guidance, control, and dynamics*, vol. 15, pp. 1111–1117, 1992.

[21] J. Doyle, K. Glover, P. Khargonegar, and B. Francis, "State space solutions to standard H2 and Hinf control problems," in *American Control Conference, 1988*, 1988, pp. 1691–1696.

[22] M. G. Safonov and R. Y. Chiang, "Model reduction for robust control: A Schur relative error method," *International Journal of Adaptive Control and Signal Processing*, pp. 259–272, 1988.

Paper F

Experimental Validation of a Single-phase Marine Cooling System Model

Michael Hansen
Jakob Stoustrup
Jan Dimon Bendtsen

The paper has been submitted for publication, 2013

2013
The layout has been revised.

Abstract

This paper presents parameter estimation and experimental validation of a single-phase marine cooling system model previously proposed by the authors. Data for both parameter estimation and model validation is obtained from an experimental setup installed on the container vessel, "Maersk Senang". Though the complexity of the model is relatively low, results show that it captures important dynamics very well. The validated models are subsequently used for evaluating disturbance rejection capabilities and robustness of performance for a robust nonlinear control design in [1] and [2].

1 Introduction

Increased focus in recent years on CO_2 emissions from the shipping industry [3] combined with fluctuating oil prices [4] have spawned a series of retrofit projects that intends to increase the energy efficiency of ocean going vessels [5]. The primary source of CO_2 emissions from shipping is exhaust gases [6], which mainly originate from vessel propulsion and power production. This means that reductions in CO2 emissions and fuel oil consumption can be achieved by reducing power consumption of the individual subsystems of the vessel. A subsystem with significant potential in terms of energy optimization is the main engine

A subsystem with significant potential in terms of energy optimization is the main engine (ME) cooling system, which is responsible for cooling the main engine and auxiliary machinery as shown in Figure F.2. A model for this type of main engine cooling system was presented by the authors in [7] and used for model-based control design in [8], [1] and [2]. The overall aim is to lower the energy consumption of this cooling system, while ensuring both sufficient cooling and stability in the presence of disturbances such as main engine load conditions and seawater temperature.

Reducing the power consumption of the cooling system is first and foremost achieved by retrofitting variable frequency drives (VFDs) to the pumps in the cooling system. This makes it possible to lower the flow rates in the system in an energy-efficient manner, such that only necessary cooling is generated. From the Affinity Laws [9], it is known that there is a cubic relationship between pump flow rate and pump power consumption, which in simplified terms means that a flow rate reduction of e.g. 10 % results in a reduction of pump power consumption of about 27 %.

This paper presents results on the experimental validation of a model of this marine cooling system, and subsequently considers application of the control design from [1] and [2] to the validated model. Data for parameter estimation and model validation is compiled from a pilot installation on board a 6500 TEU container vessel currently operating in the Indian Ocean and South Chinese Sea (see Figure F.1).

The structure of the paper is as follows: Section 2 briefly outlines the model and

Fig. F.1: The cooling system SW pumps (a.) and LT FW pumps (b.) onboard the 6500 TEU container vessel "Maersk Senang" (c.), from which the experimental data is obtained.

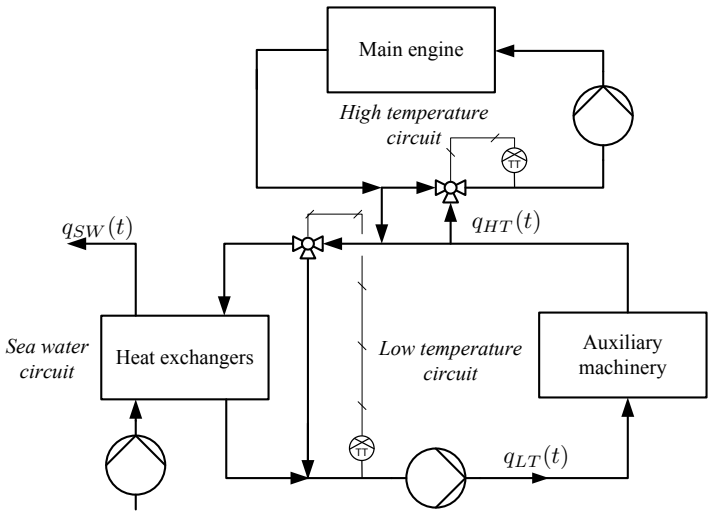

Fig. F.2: Simplified layout of the single-phase marine cooling system.

model structure for the cooling system in question. Section 3 details the experimental setup that is used in this work to obtain data for parameter estimation and model validation. The parameter estimation is presented in Section 4 while experimental validation of the model is considered in Section 5. Section 6 considers application of the control design method presented in [1] and [2] to the validated models. Finally, concluding remarks are presented in 7.

The following notation is used in this paper: $\mathbb{R}$ denotes the set of real numbers while $\mathbb{R}_+$ denotes the set of non-negative real numbers. $\mathbb{R}^{n\times m}$ is the set of real $n \times m$ matrices and $C^k(\mathcal{M},\mathcal{N})$ is the set of continuous functions mapping from vector space $\mathcal{M}$ to vector space $\mathcal{N}$ with continuous k'th order derivatives.

2 Marine Cooling System Model

A detailed description of the mathematical modeling for the single-phase marine cooling system is presented in [7]; a brief overview of the main model components is presented here for convenience. The structure of the model is illustrated in Figure F.3 and consists of two parts: a hydraulic part and a thermodynamic part.

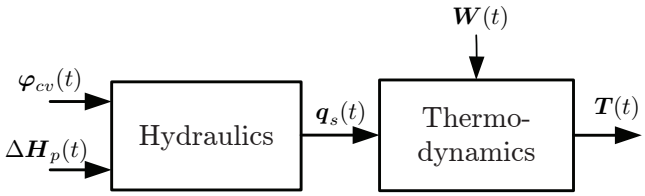

Fig. F.3: Model overview and configuration.

Hydraulics

The main engine cooling system hydraulics consists of a network of pipes, valves, control valves and pumps. The part of the model relating to the cooling system hydraulics is derived using the well known analogy between hydraulic and electric networks where pressure and flow correspond to voltage and current, respectively. For component $i = 1,\ldots,m$ where m is the total number of hydraulic components, the pressure drops can be characterized by:

$$\begin{aligned}\Delta p_i = J_i\dot{q}_{c,i} + \lambda_i(K_{p,i}, q_{c,i}) + \mu_i(K_{v,i}, q_{c,i}) \\ + \mu_{cv,i}(\varphi_{cv,i}, q_{c,i}) - \Delta H_{p,i},\end{aligned} \tag{F.1}$$

where Δp_i is the pressure across the component, J_i is the inertance of the component, $q_{c,i}$ is the flow through the component, while $K_{p,i}$, $K_{v,i}$, $\varphi_{cv,i}$ are hydraulic resistances.

Also, $\Delta H_{p,i}$ is the pump head delivered by the component and $\mu, \mu_{cv}, \lambda \in C^{\infty}(\mathbb{R}_{+} \times \mathbb{R}, \mathbb{R})$ are strictly monotonically increasing functions of both their arguments. In (F.1) we have $\mu_i = \mu_{cv,i} = \Delta H_{p,i} = 0$ if the i'th component is a pipe, $J_i = \lambda_i = \Delta H_{p,i} = \mu_{cv,i} = 0$ if the i'th component is a valve, $J_i = \lambda_i = \Delta H_{p,i} = \mu_i = 0$ if the i'th component is a control valve and $J_i = \lambda_i = \mu_i = \mu_{cv,i} = 0$ if the i'th components is a pump.

To shorten the notation, the following definitions are introduced:

$$\begin{aligned}
\Delta \boldsymbol{H}_p =& [\Delta H_{p,1}, \ldots, \Delta H_{p,m}]^T \ , \\
\boldsymbol{J} =& diag\{J_1, \ldots, J_k\} \ , \\
\boldsymbol{\lambda}(\boldsymbol{K}_p, \boldsymbol{q}_c) =& [\lambda_1(K_{p,1}, q_{c,1}), \ldots, \lambda_m(K_{p,m}, q_{c,m})]^T \ , \\
\boldsymbol{\mu}(\boldsymbol{K}_v, \boldsymbol{q}_c) =& [\mu_1(K_{v,1}, q_{c,1}), \ldots, \mu_m(K_{v,m}, q_{c,m})]^T \ , \\
\boldsymbol{\mu}_{cv}(\boldsymbol{\varphi}_{cv}, \boldsymbol{q}_c) =& [\mu_{cv,1}(\varphi_{cv,1}, q_{c,1}), \ldots \\
& \ldots, \mu_{cv,m}(\varphi_{cv,m}, q_{c,m})]^T \ .
\end{aligned} \tag{F.2}$$

As a result, the model can be written as:

$$\begin{aligned}
\boldsymbol{B}\boldsymbol{J}\boldsymbol{B}^T\dot{\boldsymbol{q}} =& -\boldsymbol{B}\boldsymbol{\lambda}(\boldsymbol{K}_p, \boldsymbol{B}^T\boldsymbol{q}) - \boldsymbol{B}\boldsymbol{\mu}(\boldsymbol{K}_v, \boldsymbol{B}^T\boldsymbol{q}) \\
& - \boldsymbol{B}\boldsymbol{\mu}_{cv}(\boldsymbol{\varphi}_{cv}, \boldsymbol{B}^T\boldsymbol{q}) + \boldsymbol{B}\Delta\boldsymbol{H}_p \ ,
\end{aligned} \tag{F.3}$$

where $\boldsymbol{B} \in \mathbb{R}^{p \times m}$ is the fundamental loop matrix, and $\boldsymbol{q} = [q_1, q_2, \ldots, q_p]^T$ is a vector of consumer flow rates. Here, expressions relating to the Darcy-Weisbach equation [10] are used for λ_i, μ_i and $\mu_{c,i}$:

$$\mu_i(K_{v,i}, q_{c,i}) = K_{v,i} q_{c,i}^2 \tag{F.4}$$

$$\mu_{cv,i}(\varphi_{cv,i}, q_{c,i}) = \varphi_{cv,i} q_{c,i}^2 \tag{F.5}$$

$$\lambda_i(K_{p,i}, q_{c,i}) = K_{p,i} q_{c,i}^2 \ . \tag{F.6}$$

Thermodynamics

The thermodynamics cover heat transfer between seawater, coolant and the consumers in the cooling system. For simplicity, it is assumed that heat transfer only takes place in heat exchangers and consumers. Consequently, one model type covers the thermodynamics of the consumers, while another (but similar) model cover the thermodynamics of the heat exchangers, which are denoted Central Fresh Water (FW) coolers in the following. The consumer model govern the coolant temperature at the consumer outlet as a function of coolant flow rate, coolant inlet temperature, and dissipated heat. It is assumed that this model is applicable to all consumers in the cooling system and by use

of the notation from Figure F.5 it is given that for $i = 1, \ldots, p$:

$$\begin{aligned}\dot{T}_i(t) =& \frac{1}{\rho c_p V_i}\big[q_i(t)\rho c_p(T_{LT,in}(t - D_i(\boldsymbol{q})) - T_i(t)) \\ &+ \dot{Q}_i(t)\big] \ ,\end{aligned} \tag{F.7}$$

where T_i is temperature of the coolant at the outlet of the consumer, V_i is a consumer specific parameter relating to the inner volume of the consumer, $\dot{Q}_i$ is the heat load on the consumer, while ρ and c_p are the density and specific heat of the coolant, respectively. Delays $D_1, \ldots, D_p$ arise from transport of coolant from the Central FW coolers to the respective consumers in the cooling system. This means that the delays depend on the layout of the system as well as the flow rates to the individual consumers. Based on the structure in Figure F.5 it is assumed that the delays can be described by:

$$D_i = \underbrace{\sum_{j=1}^{i}\left(a_{m,j}\sum_{k=j}^{n} q_k^{-1}\right)}_{\text{Main line delays}} + \underbrace{a_{c,i}q_i^{-1}}_{\text{Consumer line delay}} \ , \tag{F.8}$$

where $a_{m,i}$ and $a_{c,i}$ are system specific constants relating to the volume of the piping, and q_i is the volumetric flow to the i'th consumer.

For the Central FW coolers the same model is applied, except that the heat transfer between the LT and SW circuit is written as a function of temperatures and mass flow rates. Assuming steady state heat transfer from the LT circuit to the SW circuit the model is given by:

$$\begin{aligned}\dot{T}_{LT,in}(t) =& \frac{1}{V_{CC}}\big[q_{LT}(t)(T_{LT,out}(t) - T_{LT,in}(t)) \\ &+ q_{SW}(t)\frac{\rho_{sw}c_{p,sw}}{\rho c_p}T_{SW,in}(t) \\ &- q_{SW}(t)\frac{\rho_{sw}c_{p,sw}}{\rho c_p}T_{SW,out}(t)\big] \ ,\end{aligned} \tag{F.9}$$

where ρ_{sw} and $c_{p,sw}$ are the density and specific heat of seawater, respectively.

3 Experimental Setup

The instrumentation of the experimental setup is illustrated in Figure F.4 and Figure F.5. Sensor types are detailed in Table F.1.

The valves denoted CV_1 and CV_2 are modulating valves retrofitted to the coolant inlet of ME Lube Oil Cooler (LOC) 1 and 2. The valve denoted SOV is a shut-off valve

Table F.1: Sensor types for experimental setup.

Measurement	Type	Reference	Description
$T_{SW,in}$	PT100	Kjærulf Petersen RT-B	SW inlet temperature
$T_{SW,out}$	PT100	Kjærulf Petersen RT-B	SW outlet temperature
$T_{CC,out}$	PT100	Kjærulf Petersen RT-B	Central FW coolers FW outlet temp.
$T_{CC,in}$	PT100	Kjærulf Petersen RT-B	Central FW coolers FW inlet temp.
T_1	PT100	Kjærulf Petersen RT-B	ME LOC 1 FW outlet temperature
T_2	PT100	Kjærulf Petersen RT-B	ME LOC 2 FW outlet temperature
$T_{LO,1}$	PT100	Kjærulf Petersen RT-B	ME LOC 1 LO outlet temperature
$T_{LO,2}$	PT100	Kjærulf Petersen RT-B	ME LOC 2 LO outlet temperature
$T_{LT,in}$	PT100	Kjærulf Petersen RT-B	3-way valve mixing temperature
ΔH_{SW2}	0-4 bar	Rosemount 2051	SW pump 2 differential pressure
ΔH_{SW3}	0-4 bar	Rosemount 2051	SW pump 3 differential pressure
ΔH_{LT1}	0-4 bar	Rosemount 2051	LT pump 1 differential pressure
ΔH_{LT2}	0-4 bar	Rosemount 2051	LT pump 2 differential pressure
Δp_1	0-1 bar	Rosemount 2051	ME LOC 1 differential pressure
Δp_2	0-1 bar	Rosemount 2051	ME LOC 2 differential pressure
Δp_3	0-1 bar	Rosemount 2051	ME TC LOC differential pressure

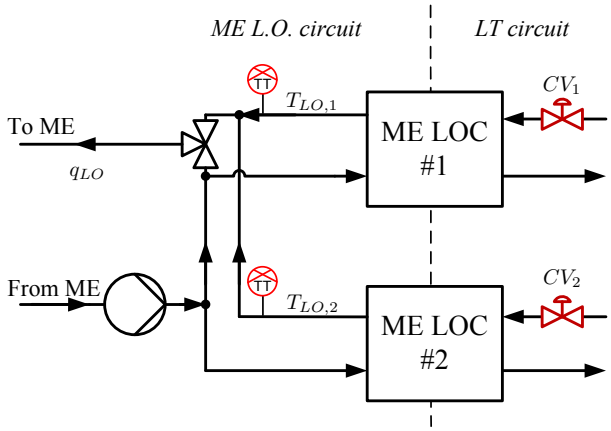

Fig. F.4: New instrumentation of ME Lube Oil Coolers (ME LOCs).

retrofitted to the coolant supply of one of the ME Scavenge Air Coolers (SACs), and is controlled externally, i.e. it is not considered a controllable input in this context. However, it can safely be assumed that *SOV* does not change position during normal operation, and for the remainder of this paper it is considered to be closed. There are two parallel variable speed pumps in both the SW and LT circuit. The parallel pumps are matched with respect to characteristics, and have a common speed reference such

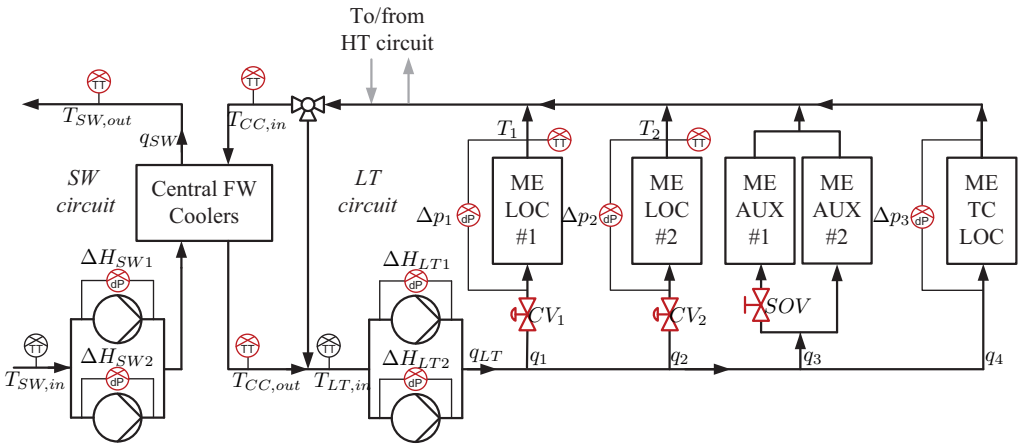

Fig. F.5: New instrumentation of LT FW cooling system. ME TC LOC is short for Main Engine Turbocharger Lube Oil Cooler.

that both pumps always run at the same speed.

4 Parameter Estimation

The data available from the technical drawings and specifications of the main engine cooling system is insufficient to calculate all the necessary dynamical model parameters. To solve this issue, the experimental setup and cooling system model are excited by the same input signals and model parameters are fitted to achieve the best possible correlation between the simulated and measured response. The parameter estimation is divided according to the two model parts: Hydraulics and thermodynamics.

Hydraulics

Assuming the LT circuit hydraulics conforms to the structure in Figure F.5, it is possible to apply the model from (F.3) and through some manipulation, one can achieve:

$$\begin{aligned}\dot{q}_i =& K_{i,1}q_1^2 + K_{i,2}q_2^2 + K_{i,3}q_3^2 + K_{i,4}q_4^2 \\ &+ K_{i,5}(q_1+q_2)^2 + K_{i,6}(q_1+q_2+q_3)^2 \\ &+ K_{i,7}(q_1+q_2+q_3+q_4)^2 + K_{i,8}q_1^2\varphi_1 \\ &+ K_{i,9}q_2^2\varphi_2 + K_{i,10}\Delta H_{p,LT}\ ,\end{aligned} \tag{F.10}$$

where $K_{i,j}$ are circuit specific parameters for $i = 1,\ldots,4$ and $j = 1,\ldots,10$. With the limited number of measurements relating to the hydraulic model it is difficult to obtain

reasonable estimates of all unknown parameters in (F.10). However, when designing controllers for the hydraulic part of the system, only parameters for a linearized model are necessary. By using a first order Taylor approximation at a chosen operating point it is possible to obtain a linearized state space representation of the model in (F.10).

It should be noted that the opening percentage of the control valves is used as input to the hydraulic model rather than the hydraulic resistance of the control valves. The same applies for the pumps, where the percentage of maximum pump speed is used as input. The argument is, that since the hydraulic model is intended for control design it is most reasonable to use the actual interfacing signals as model input when estimating parameters for the linearized hydraulic model. Consequently, in the following, the valve input represented by the opening percentage is denoted by ς_{cv1} and ς_{cv2}, while pump speed percentage is denoted by $\omega_{p,LT}$.

Coolant flow rates through the ME LOCs and ME TC LOC are not measured in the experimental setup, but are calculated from the differential pressure measurements, $\Delta p_1, \Delta p_2, \Delta p_3$, using data from the manufacturer and equation (F.4). Similar, the flow rates through the SW and LT FW pumps are calculated from the differential pressure measurements, $\Delta H_{SW1}, \Delta H_{SW2}, \Delta H_{LT1}, \Delta H_{LT2}$, by means of the pump performance curve. This is approximated by the polynomial [11]:

$$\Delta H(q) = a_{h0}\omega_{ns}^2 + a_{h1} q \omega_{ns} + a_{h2} q^2, \tag{F.11}$$

where ω_{ns} is the normalized rotational shaft speed while a_{h0}, a_{h1} and a_{h2} are pump specific coefficients estimated from the pump performance curve supplied by the pump manufacturer.

Table F.2: Operating point for estimation of parameters for the linearized hydraulic model.

$\bar{q}_1$ [m^3/s]	$\bar{q}_2$ [m^3/s]	$\bar{q}_3$ [m^3/s]	$\bar{q}_4$ [m^3/s]
0.0712	0.0707	0.0591	0.0131
$\bar{\varsigma}_{cv1}$ [% open]	$\bar{\varsigma}_{cv2}$ [% open]	$\bar{\omega}_{p,LT}$ [% of nom. RPM]	
61.10	70.75	59.55	

The operating point for the linearization and parameter estimation is listed in Table F.2, and the estimation is done using `ssest` in MATLAB [12]. The resulting state space representation of the linearized hydraulics is given by (F.12) and (F.13).

$$A = \begin{bmatrix} -1.866 & -0.086 & 0.837 & 7.420 \\ 0.770 & -0.660 & 1.320 & 0.034 \\ -0.527 & -1.860 & -2.562 & -18.527 \\ 0.062 & -0.016 & 0.074 & -0.776 \end{bmatrix} \tag{F.12}$$

$$B = \begin{bmatrix} 4.470 & 0.389 & -1.362 \\ -0.542 & 1.353 & -2.244 \\ -3.423 & -0.407 & 10.265 \\ -0.104 & 0.009 & 0.018 \end{bmatrix} \times 10^{-3} \tag{F.13}$$

Validation of the linearized hydraulic model as given by (F.12)-(F.13) is considered in Section 5.

Thermodynamics

For the experimental setup depicted in Figure F.5 it is relevant to consider the thermodynamics of the Central FW Coolers, modeled by (F.9), and the two ME LO Coolers, both modeled by (F.7). As the two ME LO Coolers are placed right next to each other and very close to the main line it is assumed that the delay in $T_{LT,in}(t)$ is the same for both ME LO Coolers, and can be simplified to:

$$D_1 = D_2 = \frac{a_m}{q_{LT}} \ . \tag{F.14}$$

In this sense, four parameters are to be estimated for the thermodynamic model, namely: V_1, V_2 V_{CC} and a_m.

The flow rate through pumps are again calculated from the measured pump head and pump speed, while consumer flow rates are calculated from the measured differential pressure. However, since data is collected while the system is in operation, the 3-way valve bypass is not closed, and thus the coolant flow through the Central FW coolers cannot be assumed to equal the flow through the pumps. To remedy this, the flow through the Central FW coolers is calculated by means of an energy balance for the 3-way valve, using the temperature measurements from each of its terminals, and the flow rate through the pumps. The same methodology is applied to calculate the ME LO flow rate through the ME LO coolers as this is used to estimate the heat load on these consumers. More specifically, the heat load on the ME LO coolers is calculated by:

$$\dot{Q}_{LOC}(t) = q_{LOC}(t)\rho_{LO}c_{p,LO}\Delta T_{LO}(t) \ , \tag{F.15}$$

where $q_{LOC}(t)$ is the LO flow rate through the ME LO Cooler, ρ_{LO} is the density of lube oil, $c_{p,LO}$ is the specific heat of lube oil, while $\Delta T_{LO}(t)$ is the temperature difference of the lube oil between the in- and outlet of the ME LO Cooler.

Model parameters for the thermodynamic model are estimated using the approach from [13]. In brief, given a vector of physical parameters, θ, the output of the model, $y_m(k)$, for an input sequence ϕ can for this application be determined by:

$$y_m(k) = \theta^T F(\phi(k)) \ , \tag{F.16}$$

where:

$$y_m(k) = [T_1(k), T_2(k), T_{LT,in}(k)]^T \tag{F.17}$$

$$\phi(k) = [T_1(k-1), T_2(k-1), T_{LT,in}(k-1) \ldots \ldots, q_1(k-1), q_2(k-1), q_{SW}(k-1)]^T \ . \tag{F.18}$$

In (F.16) $F()$ is a vector of possible nonlinear functions, i.e. the model is linear in the parameters. In this context, the model output error $\epsilon(k)$ and performance function $V(\theta)$ are given as:

$$\epsilon(k) = y(k) - y_m(k, \theta) \tag{F.19}$$

$$V(\theta) = \frac{1}{N} \sum_{k-1}^{N} \epsilon^2(k, \theta) \ . \tag{F.20}$$

Determining the parameter estimate θ_N from the input-output data, ϕ_N and y_N, with N number of samples, is then achieved by minimizing the performance function $V(\theta)$:

$$\theta_N = \arg\min_{\theta} V(\phi_N, y_N, \theta) \ , \tag{F.21}$$

which is done using a Gauss-Newton algorithm.

The parameter a_m is estimated from the cross covariance of measurements $\mathrm{T}_{LT,in}(t)$ and $\mathrm{T}_1(t)$ when the system is operated in steady state. First, the time delay for a given flow rate, $D_1(\bar{q}_{LT})$, is estimated by finding the time shift between the two measured signals which maximizes the cross covariance:

$$D_1 = \arg\max_{l} |\phi(l)| \ , \tag{F.22}$$

where ϕ is the cross covariance between measurements $\mathrm{T}_{LT,in}(t)$ and $\mathrm{T}_1(t)$. This is done for three different steady state flow rates, and the parameter a_m is fitted using least squares. The resulting estimated parameters are listed in Table F.3.

5 Experimental Validation

For experimental validation, the models presented in Section 2 are subjected to measured input data that has not been used for the parameter estimation in Section 4. The

Table F.3: Estimated parameters for thermodynamic model.

a_m [m^3]	V_1 [m^3]	V_2 [m^3]	V_{CC} [m^3]
12.74	9.11	9.39	13.6

model response is compared to the measured system response to evaluate if the model is accurate enough for both control design and simulation. Data for validation of both the hydraulic and thermodynamic part of the model is obtained over the same period of time.

Validation of hydraulic model

The simulated responses for the hydraulic model and the corresponding measured responses from the cooling system is plotted alongside in figures F.6-F.8. While there are cross couplings from all inputs to all flows, it is intended to use ς_{cv1} to control q_1, ς_{cv2} to control q_2 and $\omega_{p,LT}$ to control q_4. Consequently, these pairs of inputs and outputs are plotted together.

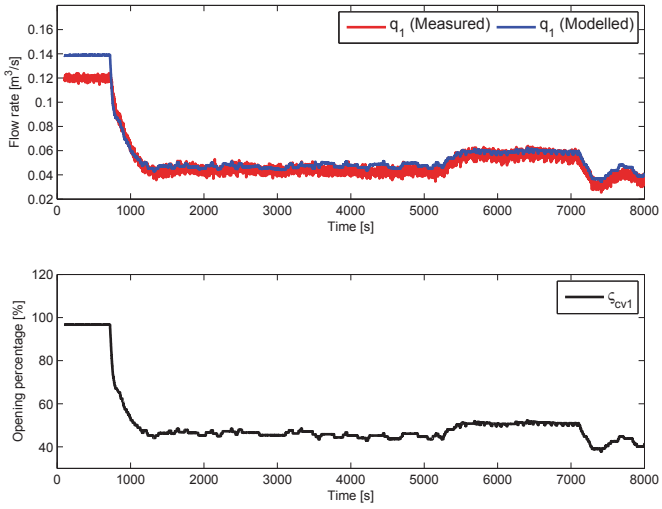

Fig. F.6: Comparison of measured and modeled response for q_1 of the linearized hydraulic model.

Comparing the simulated and measured response, it is evident that the dynamics matches fairly well, and the most significant deviations are due to offsets between the two responses, especially when the system is far from the operating point of the linearized model. However, in terms of control this is of little concern as steady state offsets can

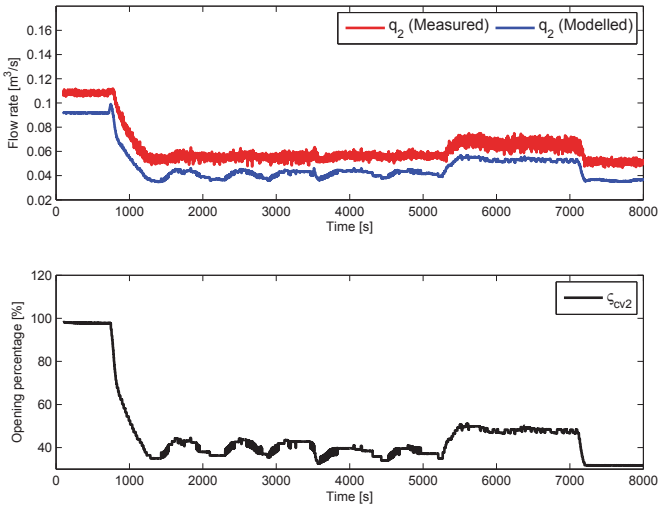

Fig. F.7: Comparison of measured and modeled response for q_2 of the linearized hydraulic model.

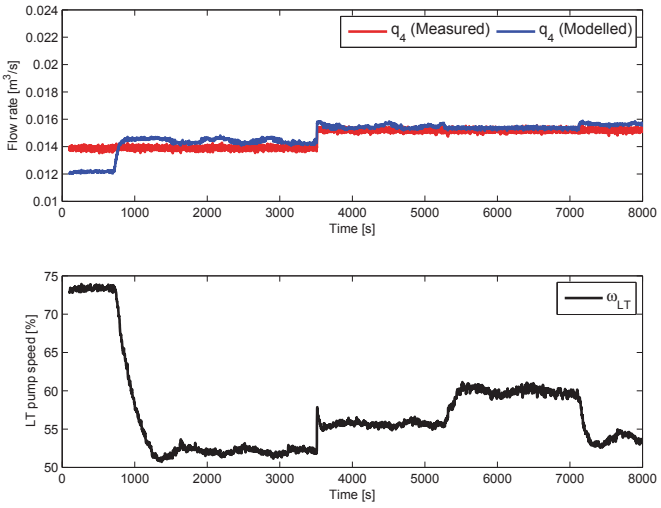

Fig. F.8: Comparison of measured and modeled response for q_4 of the linearized hydraulic model. The deviation for $t < 800s$ is a result of the linearization of the hydraulic model, and the fact that the system is far from the operating point used for the linearization.

be handled with integral action, and the hydraulic model is considered to be accurate enough in this context for both control design and simulation.

Validation of thermodynamic model

The simulated and measured temperature responses for the Central FW coolers and the two ME LO coolers are plotted in figures F.9-F.11.

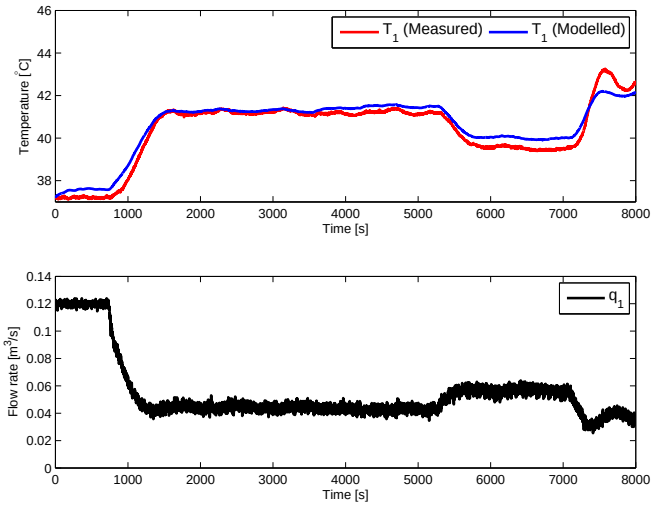

Fig. F.9: Comparison of measured and modeled response for the nonlinear thermodynamic model of the ME LOC 1.

As in the parameter estimation, the coolant flow through the Central FW coolers, and the lube oil flow through the two ME LO coolers is calculated from a heat balance on the corresponding 3-way valve. While this inevitably is a source of uncertainty for the simulation, comparing the three temperature responses reveals a good match for all three models when it comes to the dynamics. There are relatively small steady state offsets on the temperature responses for the two ME LO coolers, but this is of minor concern in the context of this work.

6 Application of control

The model validated in Section 5 is intended for use in both model-based control design and for preliminary verification of controllers through simulation. The control design considered in the context of this work follows the cascade structure illustrated in Figure F.12.

The control design is split according to the two feedback loops in Figure F.12. Design of the inner control loop follows the principles from the baseline design presented in [8] while the outer loop makes use of the robust nonlinear design considered in [1] and [2].

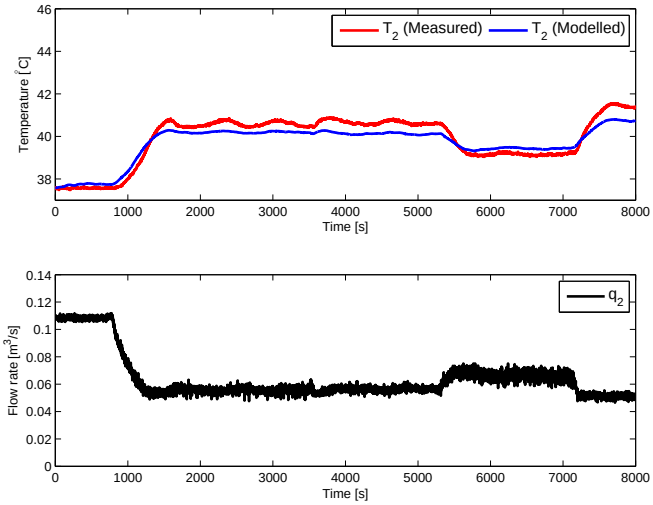

Fig. F.10: Comparison of measured and modeled response for the nonlinear thermodynamic model of the ME LOC 2.

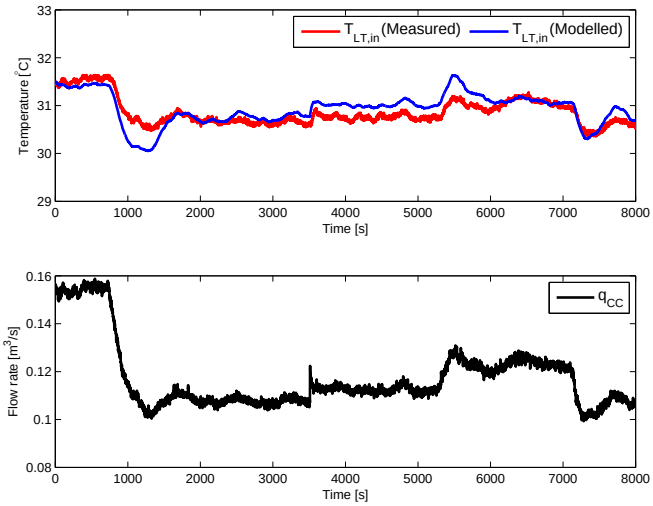

Fig. F.11: Comparison of measured and modeled response for the nonlinear thermodynamic model of the Central FW coolers.

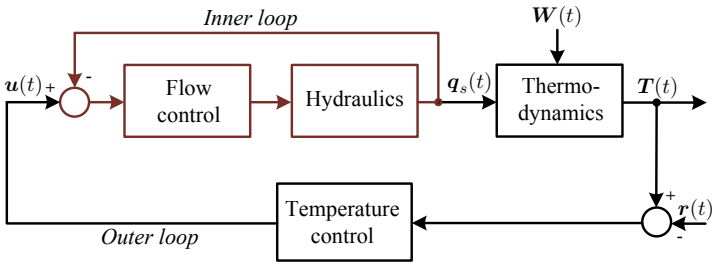

Fig. F.12: Block diagram for the cascade control setup.

6.1 Inner loop control design

For the inner loop controller it is chosen to ignore the cross-couplings in the linearized hydraulic model and pursue a control design consisting of three SISO controllers, each following a standard PI structure. In this context, the valve inputs ς_{cv1} and ς_{cv2} are used for controlling the flows q_1 and q_2, while the LT FW pump speed $\omega_{p,LT}$ is used for controlling the flow q_4. As a result, the inner control loop involves the three transfer functions:

$$G_{q1}(s) = \frac{\hat{q}_1(s)}{\hat{\varsigma}_{cv1}(s)} \ , \ G_{q2}(s) = \frac{\hat{q}_2(s)}{\hat{\varsigma}_{cv2}(s)} \ ,$$
$$G_{q4}(s) = \frac{\hat{q}_4(s)}{\hat{\omega}_{p,LT}(s)} \ , \tag{F.23}$$

which are derived from the model in (F.12)-(F.13).

It is chosen to design the controllers to satisfy the following phase margin and cross-over frequency requirements:

$$PM = 70^\circ \qquad \omega_c = 0.2 \text{ rad/s}$$

The closed loop response for the inner loop control is evaluated using the linearized hydraulic model from (F.12)-(F.13) and is shown in Figure F.13.

6.2 Outer loop control design

The design of the outer loop control uses a combination of feedback linearization and robust control theory, which was first considered for this type of marine cooling system in [1] and [2]. First, the thermodynamic model represented by (F.9)-(F.7) is brought to the form of:

$$\dot{\boldsymbol{x}} = B\gamma(\boldsymbol{x})[\boldsymbol{u} - \alpha(\boldsymbol{x})] + B_w \boldsymbol{w}_1 \ , \tag{F.24}$$

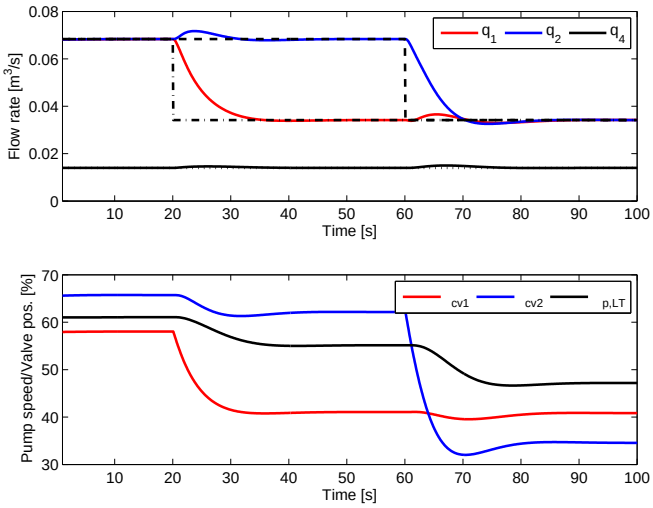

Fig. F.13: Simulated closed loop response for q_1, q_2 and q_4 when subjected to reference step. References are plotted as dotted black lines, and the reference for q_4 is held constant during the simulation. Lower plot shows associated control inputs.

by defining $\boldsymbol{x}, \boldsymbol{u}$ and $\boldsymbol{w}_1$ as:

$$\boldsymbol{x} = \begin{bmatrix} T_1 \\ T_2 \\ T_{LT,in} \end{bmatrix} \quad \boldsymbol{u} = \begin{bmatrix} q_1 \\ q_2 \\ q_{SW} \end{bmatrix} \quad \boldsymbol{w}_1 = \begin{bmatrix} \dot{Q}_1 \\ \dot{Q}_2 \end{bmatrix} .$$

For notational compactness, we introduce the symbols:

$$\Lambda = \frac{\rho_{sw} c_{p,sw}}{\rho c_p} \Delta T_{SW}(t) , \tag{F.25}$$

$$\Phi = T_{LT,out}(t) - T_{LT,in}(t) , \tag{F.26}$$

$$\Psi_i = T_{LT,in}(t - D_i(q_{LT})) - T_i(t) , \tag{F.27}$$

for $i = 1, 2$. The thermodynamic model is then described by:

$$\dot{\boldsymbol{x}} = \overbrace{\begin{bmatrix} \frac{1}{V_1} & 0 & 0 \\ 0 & \frac{1}{V_p} & 0 \\ 0 & 0 & \frac{1}{V_{cc}} \end{bmatrix}}^{B} \overbrace{\begin{bmatrix} \Psi_1 & 0 & 0 \\ 0 & \Psi_2 & 0 \\ 0 & 0 & \Lambda \end{bmatrix}}^{\gamma} \times \overbrace{\begin{bmatrix} q_1(t) & - & 0 \\ q_2(t) & - & 0 \\ q_{SW}(t) & - & \left(\frac{-q_{LT}(t)\Phi}{\Lambda}\right) \end{bmatrix}}^{[\boldsymbol{u}-\alpha(\boldsymbol{x})]} + \overbrace{\begin{bmatrix} \frac{1}{\rho c_p V_1} & 0 \\ 0 & \frac{1}{\rho c_p V_2} \\ 0 & 0 \end{bmatrix}}^{B_w} \overbrace{\begin{bmatrix} \dot{Q}_1(t) \\ \dot{Q}_2(t) \end{bmatrix}}^{\boldsymbol{w}_1} . \tag{F.28}$$

By estimating the delays, D_1, D_2, from (F.14), and under invertibility assumptions on γ, the nominal system in (F.28) can be linearized by the state feedback law:

$$\boldsymbol{u} = \alpha(\boldsymbol{x}) + \gamma^{-1}(\boldsymbol{x})\boldsymbol{v} \ . \tag{F.29}$$

The resulting feedback linearized system then takes the form of:

$$\dot{\boldsymbol{x}} = \boldsymbol{B}\boldsymbol{\gamma}[(\hat{\boldsymbol{\alpha}}(\boldsymbol{x}) + \hat{\boldsymbol{\gamma}}^{-1}\boldsymbol{v}) - \boldsymbol{\alpha}(\boldsymbol{x})] + \boldsymbol{B}_w\boldsymbol{w}_1 \ , \tag{F.30}$$

where $\hat{\boldsymbol{\gamma}}$ and $\hat{\boldsymbol{\alpha}}$ are estimates of $\boldsymbol{\gamma}$ and $\boldsymbol{\alpha}$. The linearizing feedback law in (F.29) relies on exact cancellation of nonlinear terms, which means that model uncertainties and measurement noise may introduce inaccuracies in the feedback linearization. Consequently, the linear control input $\boldsymbol{v}$ is designed using robust control theory to compensate for disturbances and model uncertainties. Thus, the system to be controlled is formulated as:

$$\dot{\boldsymbol{x}} = \boldsymbol{B}(I_3 + \Delta_\gamma)\boldsymbol{v} + \Delta_\alpha + \boldsymbol{B}_w\boldsymbol{w}_1 \tag{F.31}$$

$$= \boldsymbol{B}\boldsymbol{v} + \boldsymbol{B}\boldsymbol{w}_2 + \tilde{\boldsymbol{B}}_w\tilde{\boldsymbol{w}}_1 \tag{F.32}$$

$$\boldsymbol{y} = \boldsymbol{x} + \boldsymbol{n} \ , \tag{F.33}$$

where $\boldsymbol{w}_2 \in \mathbb{R}^3$ is a disturbances term included to account for the uncertainties in the design and $\boldsymbol{n} \in \mathbb{R}^3$ is measurement noise. In this context, it is assumed for Δ_γ and Δ_α that:

$$\frac{1}{\rho_\alpha}||\Delta_\alpha||_\infty = \frac{1}{\rho_\alpha}\sup_\omega \sigma_{\max}(\Delta_\alpha(j\omega)) \leq 1 \tag{F.34}$$

$$\frac{1}{\rho_\gamma}||\Delta_\gamma||_\infty = \frac{1}{\rho_\gamma}\sup_\omega \sigma_{\max}(\Delta_\gamma(j\omega)) \leq 1 \ , \tag{F.35}$$

where $\rho_\alpha \in \mathbb{R}_+$ and $\rho_\gamma \in \mathbb{R}_+$.

Going from (F.31) to (F.32), $\tilde{\boldsymbol{B}}_w \in \mathbb{R}^{3\times 3}$ and $\tilde{\boldsymbol{w}}_1 \in \mathbb{R}^3$ are introduced to account for both uncertainties and scaled such that $||\tilde{\boldsymbol{w}}_1||_\infty \leq 1$:

$$\tilde{\boldsymbol{B}} = \begin{bmatrix} \frac{\overline{\dot{Q}}_1}{\rho c_p V_1} & 0 & 0 \\ 0 & \frac{\overline{\dot{Q}}_2}{\rho c_p V_2} & 0 \\ 0 & 0 & \rho_\alpha \end{bmatrix}, \tag{F.36}$$

where $\overline{\dot{Q}}_1$ and $\overline{\dot{Q}}_2$ are upper bounds for $\dot{Q}_1$ and $\dot{Q}_2$, respectively.

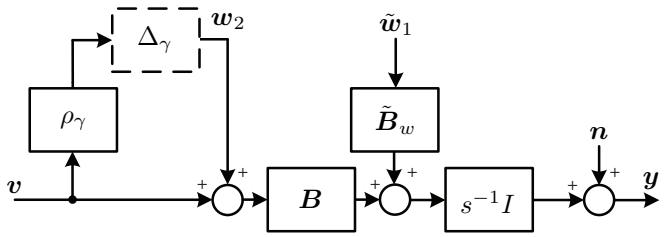

Fig. F.14: Linear equivalent of feedback linearized marine cooling system with uncertainties and disturbances.

The equivalent system is shown in Figure F.14. To include integral action in the outer control loop, the feedback linearized system is augmented with integral error states:

$$\begin{aligned} \begin{bmatrix} \dot{\boldsymbol{x}} \\ \dot{\boldsymbol{e}} \end{bmatrix} &= \begin{bmatrix} \boldsymbol{0}_{3\times 3} & \boldsymbol{0}_{3\times 3} \\ \boldsymbol{I}_3 & \boldsymbol{0}_{3\times 3} \end{bmatrix} \begin{bmatrix} \boldsymbol{x} \\ \boldsymbol{e} \end{bmatrix} + \begin{bmatrix} \boldsymbol{B} \\ \boldsymbol{0}_{3\times 3} \end{bmatrix} v \\ &\quad + \begin{bmatrix} \tilde{\boldsymbol{B}}_w \\ \boldsymbol{0}_{3\times 3} \end{bmatrix} \tilde{\boldsymbol{w}}_1 + \begin{bmatrix} \boldsymbol{B} \\ \boldsymbol{0}_{3\times 3} \end{bmatrix} \boldsymbol{w}_2 \\ &\quad + \begin{bmatrix} \boldsymbol{0}_{3\times 3} \\ \boldsymbol{I}_3 \end{bmatrix} \boldsymbol{n} \end{aligned} \tag{F.37}$$

$$\begin{bmatrix} \boldsymbol{y} \\ \boldsymbol{y}_e \end{bmatrix} = \begin{bmatrix} \boldsymbol{x} \\ \boldsymbol{e} \end{bmatrix} + \begin{bmatrix} \boldsymbol{I}_3 \\ \boldsymbol{0}_{3\times 3} \end{bmatrix} \boldsymbol{n}\,, \tag{F.38}$$

The outer control loop thereby follows the structure illustrated in Figure F.15.

A standard H_∞ problem [14] is then formulated by combining the exogenous inputs, $\tilde{\boldsymbol{w}}_1$, $\boldsymbol{w}_2$ and $\boldsymbol{n}$, into a single vector. Furthermore, an error vector, $\boldsymbol{z}$, is introduced to penalize states and control inputs:

$$\boldsymbol{w} = \begin{bmatrix} \tilde{\boldsymbol{w}}_1 \\ \boldsymbol{w}_2 \\ \boldsymbol{n} \end{bmatrix} \qquad \boldsymbol{z} = \begin{bmatrix} \boldsymbol{x} \\ \rho_\gamma \boldsymbol{v} \end{bmatrix}. \tag{F.39}$$

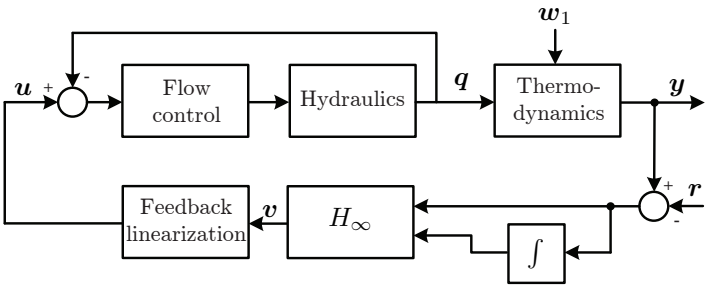

Fig. F.15: Structure of flow controller in configuration with the nonlinear robust temperature controller.

Partitioning the system matrices according to $\boldsymbol{z}$, $\boldsymbol{y}$, $\boldsymbol{w}$ and $\boldsymbol{v}$ yields the standard formulation:

$$\boldsymbol{G}(s) = \left[\begin{array}{c|cc} \boldsymbol{A} & \boldsymbol{B}_1 & \boldsymbol{B}_2 \\ \hline \boldsymbol{C}_1 & \boldsymbol{D}_{11} & \boldsymbol{D}_{12} \\ \boldsymbol{C}_2 & \boldsymbol{D}_{21} & \boldsymbol{D}_{22} \end{array}\right] . \tag{F.40}$$

Due to the feedback linearization, all poles are placed on the imaginary axis and the problem cannot be solved with standard H_∞ theory directly. This technicality is solved by applying the $j\omega$-axis pole shifting transformation to the feedback linearized system [15]:

$$s = \frac{\tilde{s} + p_1}{(\frac{\tilde{s}}{p_2}) + 1} , \tag{F.41}$$

where $p_1, p_2 < 0$ are the endpoints of the diameter of a circle being mapped by (F.41) from the left s-plane into the $j\tilde{\omega}$-axis of the $\tilde{s}$-plane. The H_∞-controller is designed for the approximate model obtained through (F.41), and the inverse bilinear transformation is subsequently applied to get the final controller for the original plant model [16]. The parameters p_2 and especially p_1 in (F.41) plays essential roles when placing dominant closed loop poles in the s-plane and are therefore important design parameters for the H_∞ control design along with the weighting factor, ρ_γ.

Design parameters for the H_∞ control design considered in this work are shown in Table F.4.

The values of ρ_γ and ρ_α are based on a numerical estimate from noise bounds on the measurements included in $\boldsymbol{\gamma}$ and $\boldsymbol{\alpha}$, as well as uncertainty bounds on the parameters in the delay estimation. Delay estimation errors are included in ρ_γ by bounding the derivative of the time delayed variable and evaluating the temperature deviation for the worst case delay estimation error.

Table F.4: Design parameters.

p_1	p_2	ρ_γ	ρ_α
-0.003	-100	1.9	0.009

6.3 Simulation

To evaluate robustness of performance for the design, parameter perturbations of $\pm$ 30% for a_m, V_1, V_2 and V_{CC}, resulting in 16 combinations of extreme values, are considered. These combinations are all tested, and the responses for the system with perturbed parameters are plotted in shades of gray while the response for the nominal system are colored. In the simulation scenario considered here, the system is subjected to step-wise changes in the heat load for the ME LO coolers. Since the heat dissipated in the lube oil is correlated with the ME load, this can be interpreted as rapid changes in the ME load which can be encountered during maneuvering. The heat load from the lube oil is assumed to be distributed equally between the two coolers, and is plotted in Figure F.16.

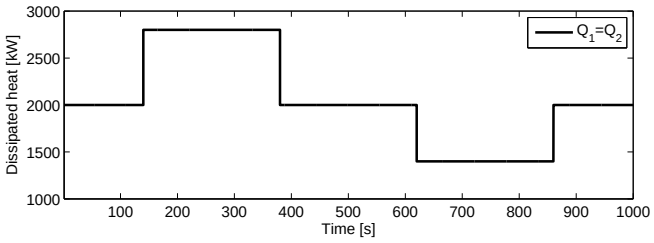

Fig. F.16: Step-wise changes in the heat dissipated in the ME LO Coolers.

The resulting temperature responses are shown in Figure F.17 for the consumer temperatures, $T_1(t)$ and $T_2(t)$, while the response for $T_{LT,in}$ is shown in Figure F.18. Temperature references are shown as dotted black lines.

Evaluating the responses in Figure F.18 and Figure F.17 shows that the control design performs well in terms of both disturbance rejection and robustness of performance.

7 Conclusion

This paper has presented parameter estimation and validation of a nonlinear model for a single-phase marine cooling system. Data for both parameter estimation and model validation was compiled from a pilot installation on board the container vessel ”Maersk Senang”. The model validation showed that despite the relative low model complexity

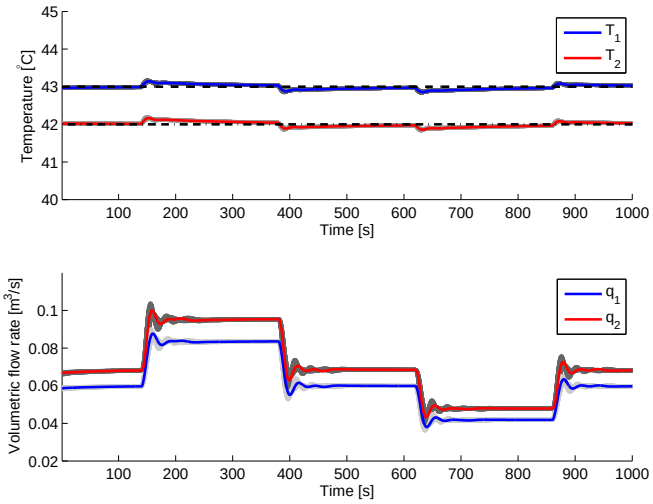

Fig. F.17: Closed loop response for T_1 and T_2 when subjected to disturbance steps. References are plotted as dotted black lines while responses for parameter perturbations are in shades of gray. Lower plot shows associated control inputs.

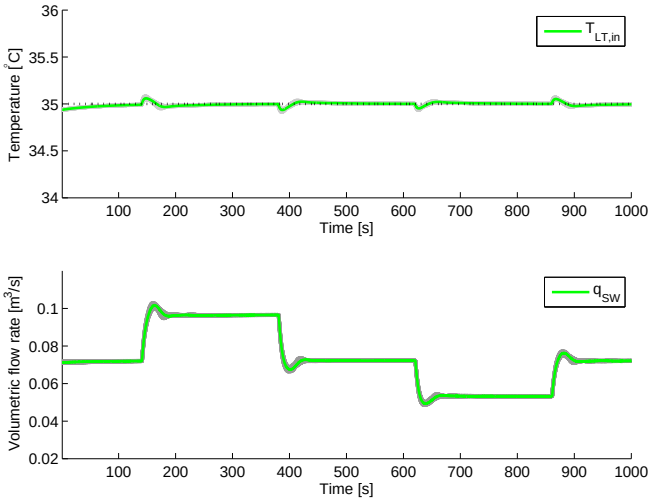

Fig. F.18: Closed loop response for $T_{LT,in}$ when subjected to disturbance steps. The reference is plotted as a dotted black line while responses for parameter perturbations are in shades of gray. Lower plot shows associated control input.

the simulated response was dynamically very close to the measured response, with relatively small steady state errors being the main source of deviation between model output and measurements. The robust nonlinear control design method previously proposed by the authors for this type of cooling system was subsequently applied to the validated model. The control design was evaluated through a simulation example using the validated models and showed excellent disturbance rejection capabilities and robustness of performance.

References

[1] M. Hansen, J. Stoustrup, and J. Bendtsen, "Robust Nonlinear Control Design with Application to a Marine Cooling System," in *Proceedings of the 7th IFAC Symposium on Robust Control Design (ROCOND)*, 2012, pp. 381–386.

[2] ——, "Modeling and Control of a Single-Phase Marine Cooling System," *Submitted for publication*, 2013. [Online]. Available: http://www.control.aau.dk/~jakob/selPubl/papers2013/cep2013_1.pdf

[3] Z. Bazari and T. Longva, "Assessment of IMO Mandated Energy Efficiency Measures for International Shipping," *International Maritime Organization (IMO)*, no. October, 2011.

[4] C. Beverelli, H. Benamara, and R. Asariotis, "Oil Prices and Maritime Freight Rates: An Empirical Investigation," *United Nations Conference on Trade and Development*, 2010.

[5] Green Ship of the Future, "Green ship magazine," *www.greenship.org*, 2009.

[6] O. Buhaug, J. J. Corbett, O. Endresen, and V. Eyring, "Second IMO GHG study 2009," *International Maritime Organization (IMO)*, 2009.

[7] M. Hansen, J. Stoustrup, and J. D. Bendtsen, "Modeling of nonlinear marine cooling system with closed circuit flow," in *Proceedings of the 18th IFAC World Congress*, 2011, pp. 5537–5542.

[8] ——, "Control of Non-linear Marine Cooling System," in *Proceedings of the 2011 IEEE Multi-Conference on Systems and Control (MSC)*, 2011, pp. 88–93.

[9] C. E. Brennen, *Hydrodynamics of Pumps*. Concepts ETI, Inc and Oxford University Press, 1994.

[10] E. Menon, *Liquid Pipeline Hydraulics*. CRC Press, 2004.

[11] B. Ulanicki, J. Kahler, and B. Coulbeck, "Modeling the Efficiency and Power Characteristics of a Pump Group," *Journal of Water Resources Planning and Management*, vol. 134, 2008.

[12] L. Ljung, *System Identification Toolbox User's Guide*. The Mathworks, Inc, 2012.

[13] M. Knudsen, "A sensitivity approach for estimation of physical parameters," in *Proceedings of the 10th IFAC Symposium on System Identification, Copenhagen July 1994*, 1994, pp. 231–236.

[14] J. Doyle, K. Glover, and P. P. Khargonekar, "State-space Solutions to Standard H_2 and H_∞ Control Problems," *IEEE Transactions on Automatic Control*, vol. 34, 1989.

[15] R. Chiang and M. G. Safonov, "H^∞ Synthesis Using a Bilinear Pole Shifting Transform," *Journal of guidance, control, and dynamics*, vol. 15, pp. 1111–1117, 1992.

[16] R. Chiang and M. Safonov, "Design of H_∞ Controller for a Lightly Damped System using a Bilinear Pole Shifting Transform," in *American Control Conference (ACC), 1991*, vol. 4. IEEE, 1991, pp. 1927–1928.

Appendix G

Technical report on instrumentation of a full scale test platform

Michael Hansen

This technical report has not been published.
2013

Abstract

This technical report outlines some of the considerations and highlights relating to the revised instrumentation of the marine cooling system used throughout this PhD project. It also describes the new instrumentation, as well as the structure and operation of the new control. Finally, based on measurements from the revised cooling system and assumptions on operation of the new control implementation, the yearly power consumption of the LT FW pumps is calculated along with the associated savings and payback time.

1 Introduction

The purpose of this technical report is to provide a detailed overview of the marine cooling system used in this PhD project for experimental validation of models, control strategies and power savings. This includes a description of the revised cooling system instrumentation, as well as some of the considerations that have been made in the process of designing this new setup.

Fig. G.1: 6500 TEU container vessel subject for installation of the test platform.

The new instrumentation is done on a container vessel with a capacity of 6500 twenty-foot equivalent units (TEU) currently (Q4, 2012) operating in the Indian Ocean and South Chinese Sea. The vessel measures 319×40 m and is powered by a 85.000 bhp two-stroke diesel engine with a cooling system designed for a heat load of approximately 45.000 kW. Beside the main engine, the vessel also features four auxiliary engines for power production, each rated to a power output of approximately 2.1 MW. The vessel do not have a WHR system or a shaft generator, and all power is therefore produced by the auxiliary engines.

2 Current instrumentation and operation

The work in this PhD project only considers control of the SW and LT FW circuits since the cooling requirements for the main engine restricts the possibility to modify the instrumentation in this circuit. Consequently, the HT circuit is not detailed in the following. A simplified layout of the unmodified cooling system is shown in Figure G.2. Since the cooling system contains about 30 consumers, only groups of key consumers are shown in Figure G.2.

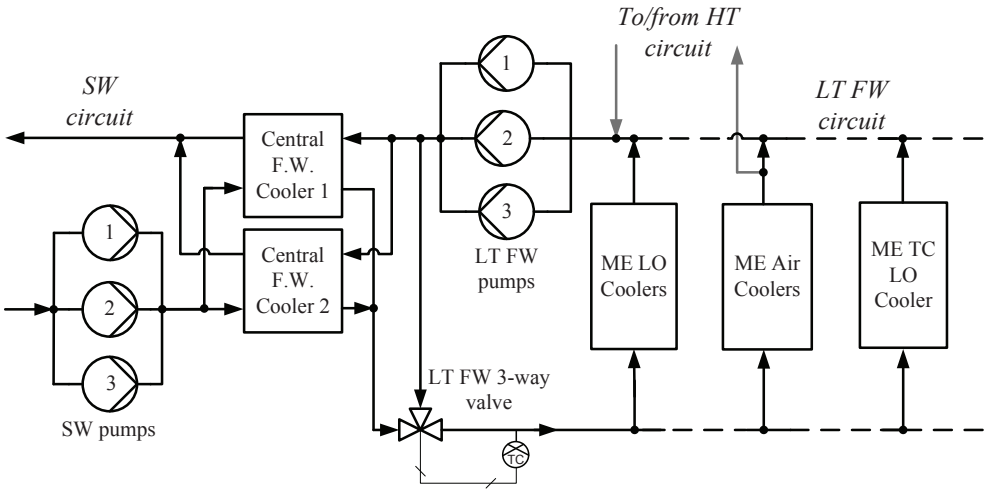

Fig. G.2: Simplified layout of the marine cooling system illustrating configuration of pumps and key consumers.

The current instrumentation features three single speed pumps in a parallel configuration in both the SW and LT FW circuit. Each pump have a capacity of 50% of the maximum flow rate, which means that only two pumps are operated at the same time, while the third is stand-by. The 3-way valve in the LT FW circuit controls the amount of coolant that bypasses the LT FW coolers to maintain a constant coolant temperature at the consumer inlets. This ensures that temperatures stays within design limits during fluctuations in the seawater temperature and ME load. The temperature control is implemented by means of a local PID controller using the coolant temperature at the 3-way valve outlet as feedback.

The heat load and required coolant flow rate varies significantly for different consumers. Table G.1 provides an overview of the 5 groups of consumers which according to the design specification sets the highest requirement for flow rate. With the current instrumentation the only possibility the crew has for reducing power consumption of the cooling system is by switching of one of the pumps in either the SW of LT FW

Table G.1: Percentage of total heat load and flow rate requirement for the 5 most significant consumer groups.

Consumer	Heat load (% of total)	Design flow rate (% of total)
ME Scavenge Air Coolers (SAC) (1-3)	48 %	34 %
ME lube oil (LO) Coolers 1 & 2	14 %	28 %
Auxiliary engines (1-4)	10 %	12 %
Alternators (1-4)	1 %	7 %
Air Condition (AC) condenser 1 & 2	<1 %	6 %

circuit. Whether and when it is possible to turn of a pump is entirely a crew assessment and there are currently no established guidelines as this may depend on the individual vessel. Consequently, the cooling systems onboard two sister ships that are more or less identical, may be operated differently due to differences in crew preferences and assessments. This may seem insignificant, but does in fact play an important role when estimating the possible power reduction by the introduction of a new control strategy.

3 Estimated power reduction

The reduction of pump power mainly comes down to reducing the flow rate through the pumps. This is achieved by reducing the coolant flow rate through the individual consumers of the cooling system to match the actual heat dissipation. This entails installation of variable frequency drives (VFDs) for both the SW and LT FW pumps as well as control valves for relevant consumers. The overview in Table G.1 shows how a small number of consumers account for a major part of the heat dissipation and required coolant flow rate. It therefore makes little sense to retrofit valves to consumers that account for only a small percentage of the total flow requirement, as the potential saving by throttling the flow to these consumers do not justify the installation cost of a valve. To be able to evaluate what would be a sensible compromise between installation cost and obtainable savings, the power reductions for various instrumentation levels are calculated. In this context, four instrumentation levels are considered as illustrated in Table G.2.

The auxiliary engines from Table G.1 are not included in the instrumentation as they have an integrated valve which shuts off the supply of coolant when the auxiliary engine is not running. Though the three ME SACs accounts for the largest portion of both heat load and coolant flow, it is chosen not to throttle the flow to the ME SACs. This is mainly due to the recommendations from the manufacturer not to do so, as well as to avoid the possible influence it would have on the temperature control in the HT circuit. However, this particular vessel is equipped with a turbocharger cut-out system, that is,

Table G.2: Instrumentation levels considered in the estimation of power reductions.

Equipment	Instrumentation			
	level 1	level 2	level 3	level 4
VFDs for SW pumps	X	X	X	X
VFDs for LT FW pumps	X	X	X	X
Valves for ME LO cooler	X	X	X	X
Valve for ME SAC #2		X	X	X
Valves for AC condenser			X	X
Valves for Alternators				X

a system that enables shut down of one of the three ME turbochargers when the vessel is slow steaming. This improves the SFOC of the main engine at low speeds, but it also means that there is no air flow through the ME SAC #2 when this system is active. As a result, instrumentation levels 2-4 considers an automatic shut-off valve for the coolant supply to the ME SAC #2 which is operated in parallel with the turbocharger cut-out system.

To calculate the potential saving for each configuration, the heat load on the cooling system at various ME loads is estimated based on data supplied by the main engine manufacturer. Consumers for which the heat load is not correlated with the ME load are assumed to provide maximum heat load at all times. Assuming steady state operation, the required coolant flow rates in the LT FW and SW circuits are calculated for different combinations of ME loads, seawater temperatures and instrumentation levels. By means of the Affinity Laws and pump data provided by the pump manufacturer, a power consumption profile is calculated for each of the four instrumentation levels. The power consumption profile for the instrumentation levels considered in this work are illustrated in Figure G.3.

The power consumption profiles in Fig. G.3 assumes that two auxiliary engines are running at all time, and are calculated using the rated pump motor power rather than the power at nominated pump speed. They also assume only a 91 % efficiency of the VFDs at all load conditions and should generally be seen as worst-case scenarios.

The sudden change in power consumption at 50% ME load in Figure G.3 for instrumentation levels 2-4 is caused by the shut-off valve on the ME SAC #2 as this is where the turbocharger cut-out system is engaged. The flatness of the power consumption profiles at low ME load is mainly due to a minimum speed limit for the SW pumps which needs to be sustained to ensure proper cooling of the pump.

The power consumption profile for each configuration is weighted with the operational profile of the vessel, see Fig. G.4, and compared to the current power consumption of the cooling system. The current power consumption is estimated based on assumptions of best practice in the manual operation of the pumps, that is, the crew always turns of a SW pump when sailing at low seawater temperature, and also turns of a LT

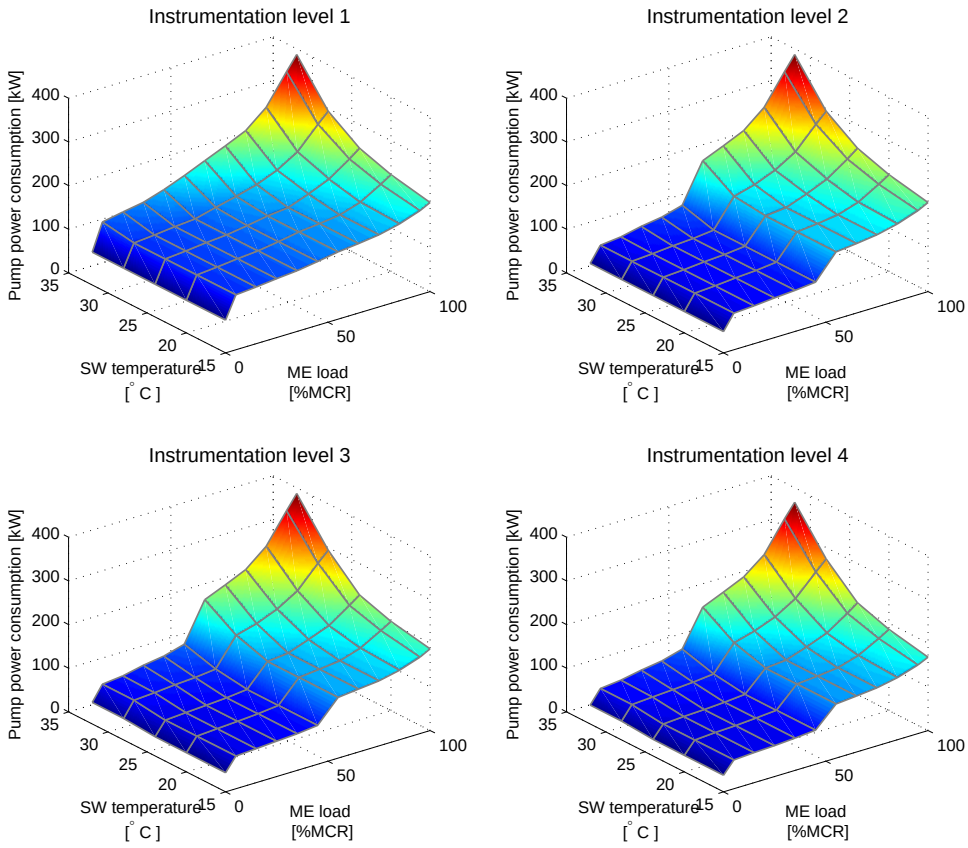

Fig. G.3: Power consumption profile for all instrumentation levels considered in this scope.

FW pump when in port. The resulting estimated power saving for this vessel series is illustrated in Table G.3. The payback time in Table G.3 is calculated with a 7% discount rate for the payback and only considers the cost of the hardware installation, thus it does not include expenses relating to development of control software, licenses or man hours for project management.

Instrumentation level 2 is chosen for implementation in this project not only because it has the shortest payback time, but it is also assessed to be the most reasonable compromise between investment cost, practical feasibility, and power saving potential. The split between the savings for the LT FW circuit and SW circuit is listed in Table G.4 for instrumentation level 2.

The split in Table G.4 is of interest since control of the SW pumps for technical reasons is implemented in the ships AMS, and is thereby separated from the control

Table G.3: Comparison of estimated savings and payback time for the four instrumentation levels for the vessel class considered in this context.

Instrumentation	Energy consumption [kWh/year]	Savings [kWh/year]	Savings [%]	Payback time [months]
None	2.317.753	-	-	-
Level 1:	1.182.246	1.135.507	49	14
Level 2:	847.264	1.470.489	63	11
Level 3:	810.059	1.507.694	65	12
Level 4:	717.692	1.600.061	69	12

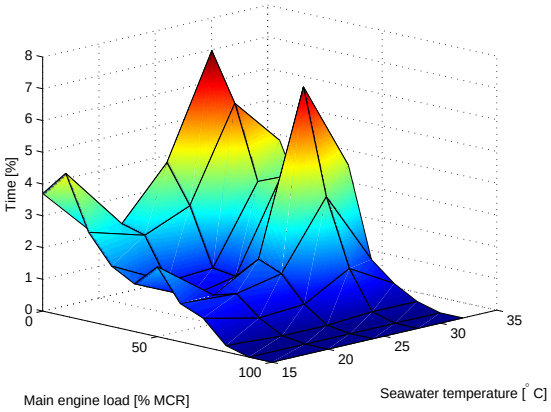

Fig. G.4: Average operational profile of 6500 TEU class container vessel series.

implementation considered in this PhD project. Consequently, it is not possible in the context of this project to verify the estimated savings for the SW circuit, and only savings for the LT FW circuit are considered in the following. Despite this, the revised instrumentation of the SW circuit is still detailed in the following sections as measurements from this part of the cooling system is used to validate models in this PhD project.

4 Revised instrumentation

The revised instrumentation requires modification to the SW circuit, the LT FW circuit and the ME LO circuit. This includes installation of new temperature transmitters, differential pressure transmitters, VFDs and new PLC hardware. It is intended to let the test installation be separate add-on to the existing system, such that crew is able

Table G.4: Savings split between LT FW circuit and SW circuit for instrumentation level 2.

	Energy consumption [kWh/year]	Savings [kWh/year]	Savings [%]	Payback time [months]
LT FW circuit	656.742	749.358	53	15
SW circuit	190.522	718.009	79	8

to default back to the original mode of operation in case of malfunction. The exact hardware modifications to the SW, LT FW and ME LO circuits are detailed in the following sections.

SW circuit modifications

The hardware modifications to the SW circuit are illustrated in Figure G.5 where new components are colored in red. The reason for equipping SW pump 2 and 3 with VFDs rather than e.g. 1 and 2 is purely practical, and is not important in the context of the work presented here.

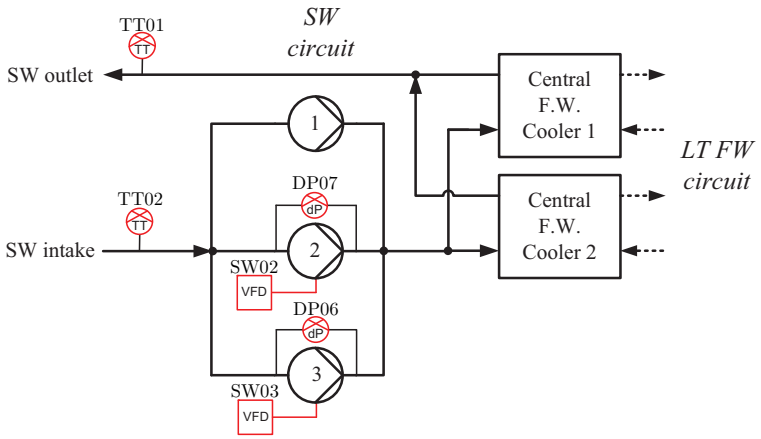

Fig. G.5: Revised instrumentation of SW circuit. New components are colored in red.

An overview of the retrofitted equipment for the SW circuit is presented in Table G.5. The addition of VFDs for SW pump 2 and 3 allows the speed of these pumps to be controlled from 42–100 % of nominal speed. The minimum speed of 42 % for the VFDs ensures proper cooling of the pump motors as well as sufficient lubrication of bearings as these both depends on the speed of the pump motor.

Table G.5: New components for SW circuit modifications.

Tag no.	Measurement	Range	Reference	Description
TT01	$T_{SW,out}$	-10–60°C	KP RT-B	SW outlet temperature
TT02	$T_{SW,in}$	-10–60°C	KP RT-B	SW inlet temperature
DP07	ΔH_{SW2}	0–4 bar	Rosemount 2051	SW pump 2 diff. pressure
DP06	ΔH_{SW3}	0–4 bar	Rosemount 2051	SW pump 3 diff. pressure
SW02	-	42–100 %	ABB ACS800	SW pump 2 VFD
SW03	-	42–100 %	ABB ACS800	SW pump 3 VFD

LT FW circuit modifications

The hardware modifications to the LT FW circuit are illustrated in Figure G.6 where new components are colored in red. An important note in relation to Figure G.6 is that

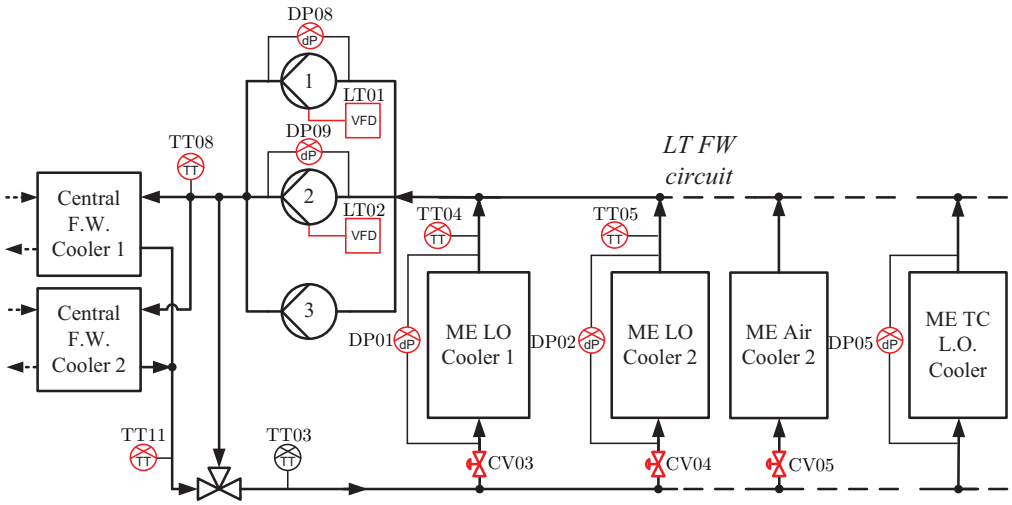

Fig. G.6: Revised instrumentation of LT FW circuit. New components are colored in red.

while CV03 and CV04 are controllable valves, CV05 is an externally controlled shut-off valve. Due to space limitations, all new valves are of the butterfly type, which has the advantage of a very compact design. Description of retrofitted components for the LT FW circuit are presented in Table G.6.

The differential pressure measurements over the two ME LOCs and the ME TC LOC makes it possible to calculate the coolant flow through each of these consumers. Similar to the pumps in the SW circuit, the flow rate through the LT FW pumps is calculated from the speed reference to the pumps and the measured pump head.

Table G.6: New components for LT FW circuit modifications.

Tag no.	Measurement	Range	Reference	Description
TT03	$T_{LT,3WV}$	0–60°C	KP RT-B	LT FW 3-way valve temperature
TT04	T_1	0–80°C	KP RT-B	ME LOC 1 FW temperature
TT05	T_2	0–80°C	KP RT-B	ME LOC 2 FW temperature
TT08	$T_{CC,in}$	0–80°C	KP RT-B	CFWC FW inlet temperature
TT011	$T_{CC,out}$	0–60°C	KP RT-B	CFWC FW outlet temperature
DP01	Δp_{LOC1}	0–1 bar	Rosemount 2051	ME LOC 1 FW diff. pressure
DP02	Δp_{LOC2}	0–1 bar	Rosemount 2051	ME LOC 2 FW diff. pressure
DP05	Δp_{TC}	0–1 bar	Rosemount 2051	ME TC LOC FW diff. pressure
DP08	ΔH_{LT1}	0–4 bar	Rosemount 2051	LT FW pump 1 diff. pressure
DP09	ΔH_{LT2}	0–4 bar	Rosemount 2051	LT FW pump 2 diff. pressure
CV03	-	0–100 %	ARI-ZESA	ME LOC 1 FW valve
CV04	-	0–100 %	ARI-ZESA	ME LOC 2 FW valve
CV05	-	Open/cl.	ARI-ZESA	ME air cooler 2 FW valve
LT01	-	42–100 %	ABB ACS800	LT FW pump 1 speed
LT02	-	42–100 %	ABB ACS800	LT FW pump 2 speed

ME LO circuit modifications

The hardware modifications to the ME LO circuit are illustrated in Figure G.7 where new components are colored in red.

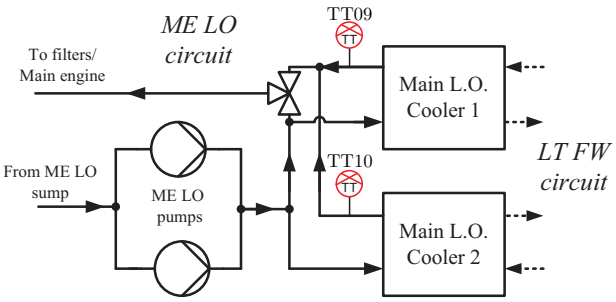

Fig. G.7: Revised instrumentation of ME LO circuit. New components are colored in red.

Description of retrofitted components for the ME LO circuit are presented in Table G.7.

Control hardware setup

To separate the new cooling system control from the existing alarm and monitoring system (AMS) on the ship, a new control hardware platform is installed. This setup

Table G.7: New components for ME LO circuit modifications.

Tag no.	Measurement	Range	Reference	Description
TT09	$T_{LO,1}$	0–80°C	KP RT-B	ME LOC 1 LO temperature
TT10	$T_{LO,2}$	0–80°C	KP RT-B	ME LOC 2 LO temperature

consists of a programmable automation controller (PAC) with a number of analog and digital in- and output modules. It also features a control panel that allows the crew to operate the control system, i.e. change set points and limits. New hardware components are listed in Table G.8, and the setup is outlined in Fig. G.8.

Table G.8: New PLC hardware for revised cooling system instrumentation.

Type	Pcs.	Signal(s)	Reference	Description
CPU	1	DVI-D, USB	Beckhoff CX5020	PLC CPU module
HMI	1	DVI-D, E-USB	Beckhoff CP6902	Control Panel
USB-C	1	USB, E-USB	Beckhoff CU8800	USB to Extended-USB converter
AI	3	4–20 mA	Beckhoff KL3458	Analog input card (8 channels)
AO	1	4–20 mA	Beckhoff KL4428	Analog output card (8 channels)
AO	1	4–20 mA	Beckhoff KL4424	Analog output card (4 channels)
DI	2	0/24 V	Beckhoff KL1408	Digital input card (8 channels)
DO	1	0/24 V	Beckhoff KL2408	Digital output card (8 channels)

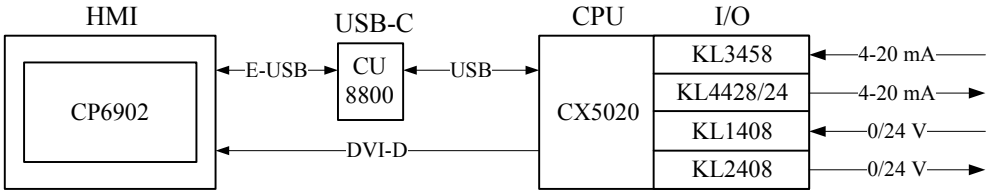

Fig. G.8: New control hardware setup.

The new control hardware setup for the revised cooling system control only interfaces with the existing control system of the vessel through a digital alarm channel, to notify the crew of any faults on the system. Beside measurements from the retrofitted temperature and differential pressure transmitters, the new control hardware setup also receives status of the pumps in both the SW and LT FW circuits. This is necessary, as starting and stopping of pumps remains under the control of the AMS, which means that relevant pumps must be started by the crew before engaging the new cooling system control. Once started, the speed of the pumps retrofitted with a VFD can be controlled by the new cooling system control.

Control software setup

To enable rapid prototyping, the control software for the test platform was implemented using Beckhoffs TwinCAT 3 automation software suite [1]. TwinCAT 3 supports execution of modules that are generated from models in the MATLAB/Simulink environment, which significantly shortens the process of implementing control laws designed in MATLAB/Simulink. The TwinCAT real-time kernel can directly execute these modules cyclical, or they can be called from other modules generated by other languages, for instance those under the IEC 61131-3 standard. The graphical user interface (GUI) is implemented via InduSoft Web Studio v7.1 for embedded platforms.

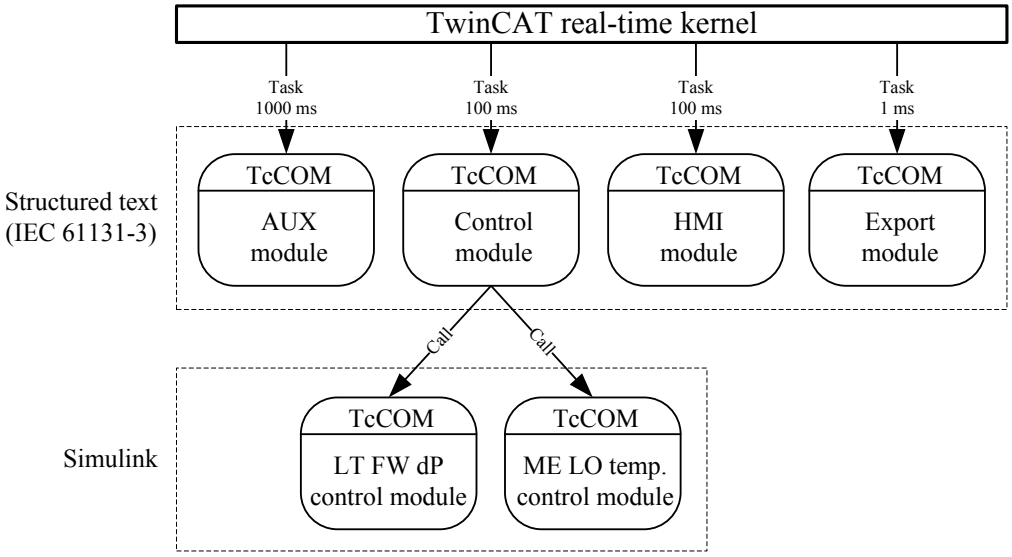

Fig. G.9: Outline of software setup for new cooling system control.

The structure of the software developed in the context of this PhD project is illustrated in Fig. G.9. It consists of four modules implemented in Structured Text (ST) where one of them calls two control modules implemented in MATLAB/Simulink. Briefly outlined, the four modules possess the following functionality:

Control module
The control module initially makes a diagnostics check on all I/O channels to ensure that sensor data is valid. In case of signal faults or if one or more measurements are outside allowed limits, the control module sends an alarm signal to the ships AMS. If control is enabled by the user, and relevant conditions are satisfied,

the control module calls the respective controllers that have been implemented through MATLAB/Simulink, and subsequently writes the controller output to the analog output card. This module is executed with the highest priority.

HMI module
The human machine interface (HMI) module implements a number of functions which handles inputs and outputs for the GUI. This includes handling of status messages and log entries, as well as loading and saving of settings. This module is executed with medium priority.

AUX module
The AUX module implements auxiliary functions, such as data logging and acquisition of system time. By default, data is logged for a period of 8 hours with a sampling time of 1 s. This module is executed with low priority.

Export module
The export module handles export of event log and data to a USB flash drive, and can be enabled by the user through the GUI. When exporting event log, all current log entries are written to the USB flash drive in a text format. When exporting data the module writes the last 8 hours of logged data to a .CSV file on the USB flash drive. This module is executed with low priority.

Graphical user interface

The GUI is implemented separately from the control software, and its main purpose is presentation of data from the control system, such as measurements and events. It also enables the crew to change set points for the controllers, and switch to manual control of pumps and valves. The GUI consists of three tabs: Control settings, Set points and Log. Screen shots of the three tabs are shown in figures G.10 - G.12.

Control settings
The control settings tab enables activation and deactivation of automatic control, as well as manual setting of LT FW pump speed and ME LO Coolers FW valves.

Set points
The Set point tab enables changing the controller set points as well as actuator and alarm limits.

Log
The Log tab visualizes the history of faults (including time stamp and transmitter tag no.) and enables export of log and data to a USB flash drive. It also enables saving and loading of set point values. By default the log shows the 7 latest entries, but it is possible to scroll up and see previous entries using the arrows on the right.

Common

The lower part of each tab is common for all tabs and shows a mimic of the cooling system with relevant measurements. It also displays system messages, such as signal faults and notification of measurements outside allowed limits.

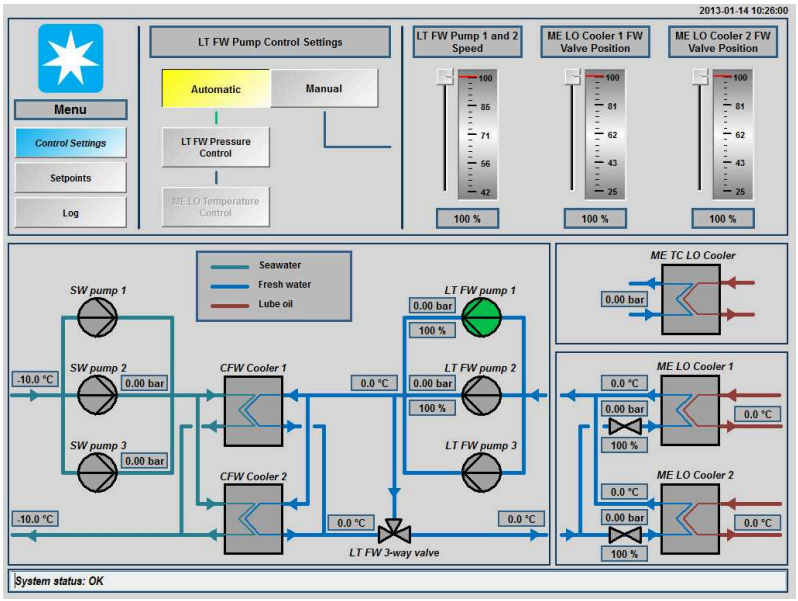

Fig. G.10: Screen shot of main control tab in the control software GUI.

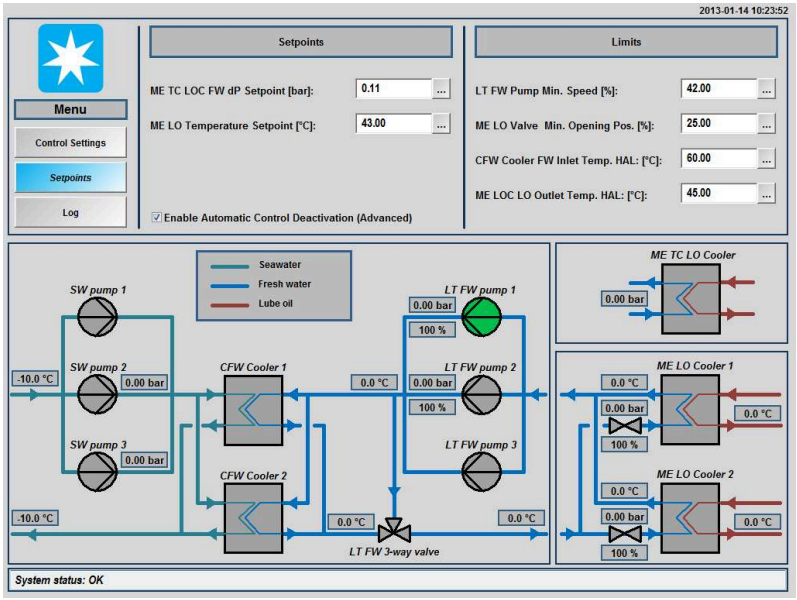

Fig. G.11: Screen shot of settings tab in the control software GUI.

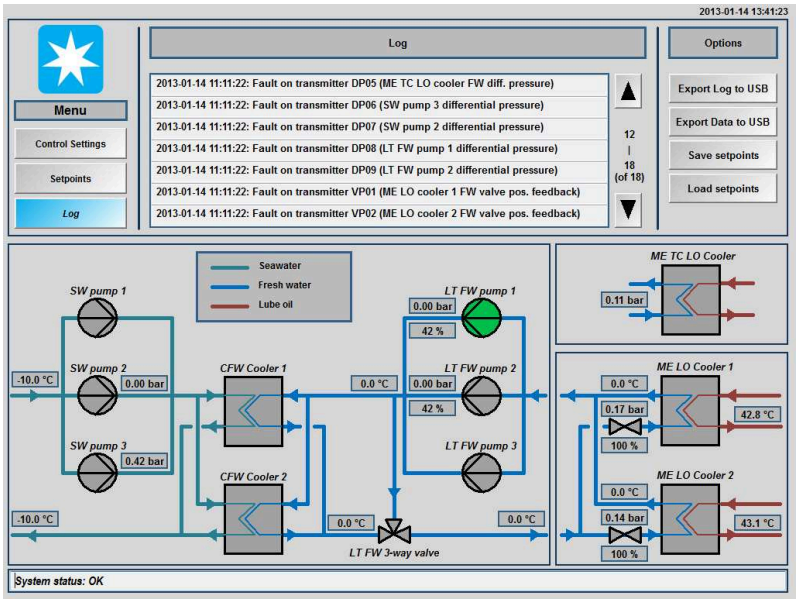

Fig. G.12: Screen shot of log tab in the control software GUI.

5 Implemented control

The control implemented on the test platform overall follows the baseline design presented in [2], but with two modifications. First, control of the SW pumps is for technical reasons implemented in the ships AMS, and is therefore not considered in the following. Secondly, to ensure sufficient cooling for consumers not retrofitted with a control valve, a controller is implemented to maintain a constant differential pressure over these consumer. This differential pressure is controlled using the speed of the LT FW pumps with the feedback signal measured across the ME TC LO Cooler by differential pressure transmitter, DP05. The design of this differential pressure controller, and all other controllers implemented on the test setup, is based on a standard PI controller and uses phase margin and cross-over frequency as design parameters. The control configuration is illustrated in Fig. G.13, and is denoted "LT FW Pressure Control" in the following.

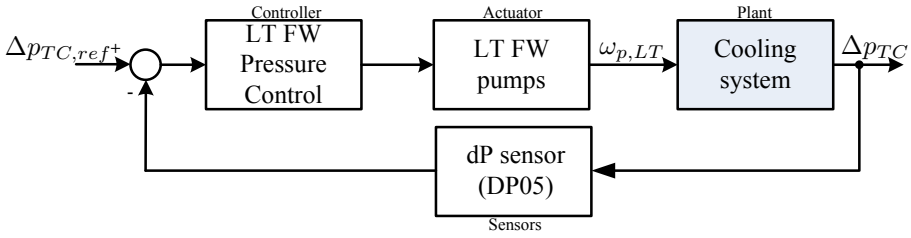

Fig. G.13: Block diagram for LT FW pressure control.

The temperature control implemented on the test platform follows the cascade control structure illustrated in Fig. G.14 and encompass control of the ME LO temperature. The inner loop from Fig. G.14 controls the coolant flow through the two ME LO coolers

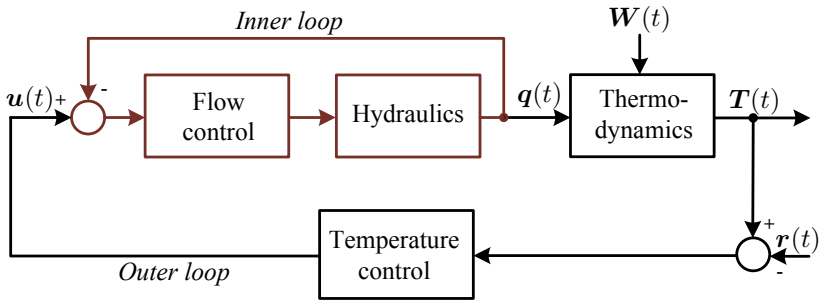

Fig. G.14: Block diagram for the cascade control setup.

using the retrofitted valves, CV03 and CV04. The feedback is provided by means of the two differential pressure transmitters DP01 and DP02, where the flow through the ME

LO coolers is calculated from:

$$q_i = K_{LOC,i}\sqrt{\Delta p_{LOC,i}} \quad \text{for} \quad i = 1, 2 \ , \tag{G.1}$$

where $K_{LOC,i}$ expresses the hydraulic resistance of ME LO Cooler i. The structure of the inner loop is illustrated in Fig. G.15. Since the flow dynamics are significantly faster than the temperature dynamics, the closed inner loop is considered to be a constant gain in the design of the outer loop.

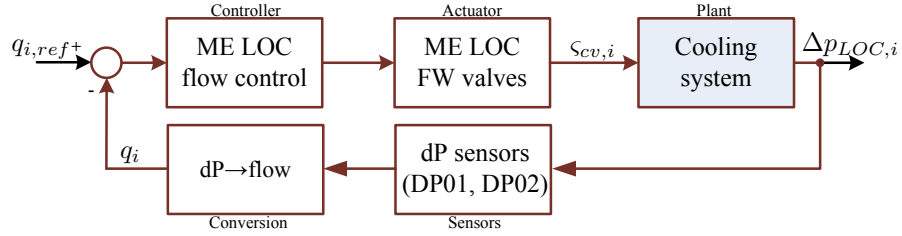

Fig. G.15: Block diagram for the flow control part (inner loop) of the ME LO temperature control.

While the temperature control design in [2] uses the coolant temperature at the consumer outlet as the controlled parameter, the temperature of the lube oil at the ME LO Cooler outlet is used in this implementation. The main reason for this is that this is a better measure for optimal operation of the ME LO Cooler, thus making it easier to define a sensible set point for the temperature control. Consequently, the outer loop follows the structure in Fig. G.16.

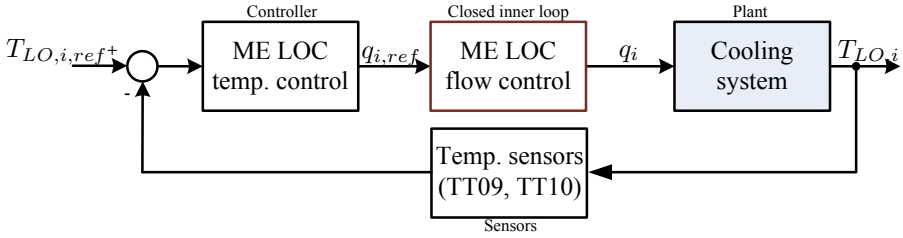

Fig. G.16: Block diagram for the temperature control part (outer loop) of the ME LO temperature control.

All controllers follow the standard PI structure:

$$C(s) = K_p\left(1 + \frac{1}{sT_i}\right) \ . \tag{G.2}$$

While the two ME LO coolers are identical in design and are placed next to each other, the flow and temperature dynamics differ slightly as shown in Paper F. However, for

this implementation, the same controller parameters are used for both coolers. Relevant parameters for the implemented controllers are listed in Table G.9, and responses for the controllers when subjected to a number of reference steps are illustrated in Fig. G.17-G.19.

Table G.9: Parameters for implemented

Controller	K_p	T_i	Phase margin	Cross-over frequency
LT FW Pressure Control	10.944	0.122	70 °	0.1 rad/s
ME LOC Flow Control	2.39	43.2	70 °	0.1 rad/s
ME LOC Temperature Control	-0.000933	15.735	70 °	0.0025 rad/s

The plots in Fig. G.17 shows the response for the LT FW Pressure Control along with the LT FW pump speed reference and measured LT FW pump head. Though the time scale and measurement noise makes it difficult to evaluate the controller performance, it does seem to follow the reference without any steady state errors or visible overshoot. Plots in Fig. G.18 and Fig. G.19 shows the temperature response, measured differential pressure and valve position for ME LO Cooler 1 and 2, respectively.

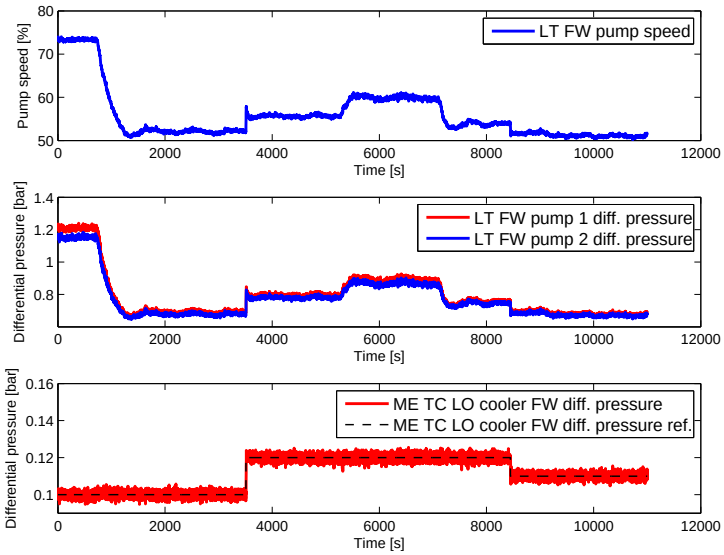

Fig. G.17

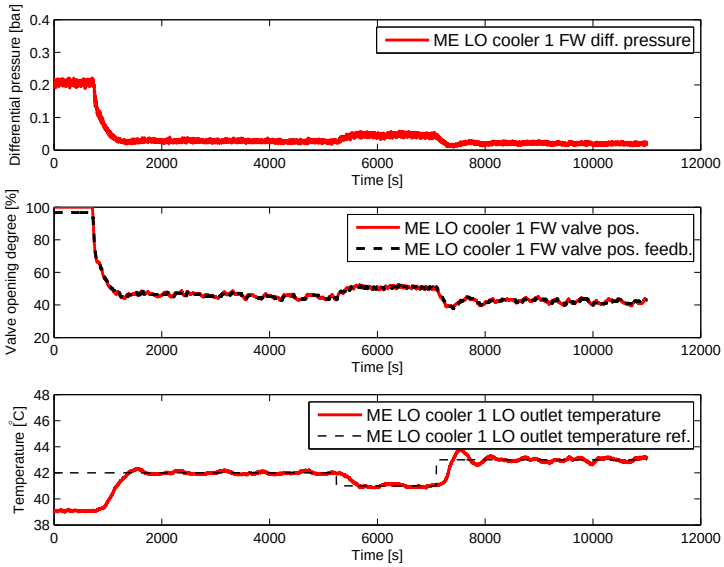

Fig. G.18

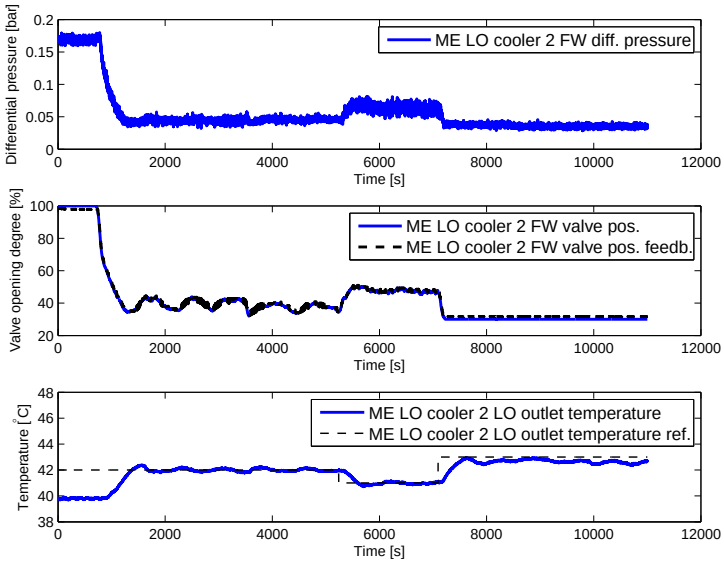

Fig. G.19

By comparing responses for the two ME LO coolers it is possible to see that the temperature response for ME LO Cooler 1 is faster than that for ME LO Cooler 2, which is a result of using the same controller parameters for both controller even though the dynamics of the coolers differ slightly. It is also possible to see that the controller for ME LO Cooler 2 is not able to reach the set point when this is raised to 43 °C, due to actuator saturation. The minimum limit for the valve opening degree is for the purpose of this test set to 30 % open, but can be adjusted to any value down to 0 %.

6 Achieved power reduction

The purpose of this section is to provide an overview of achievable power reductions for the LT FW pumps based on measurements from the new test platform. The intention is to establish a relationship between the ME load and the power consumption of the LT FW pumps when operated with the new cooling system control. This is ultimately paired with the operating profile of the vessel to give an indication of the potential saving over a period of time. Initially, the relationship between the ME load and the heat dissipated in the ME LO is extrapolated from data supplied by the engine manufacturer. Since data is only available for ME loads above 50 %, the fit below 50 % ME load does contain some uncertainty. Data points and the exponential trend line are illustrated in Fig. G.20.

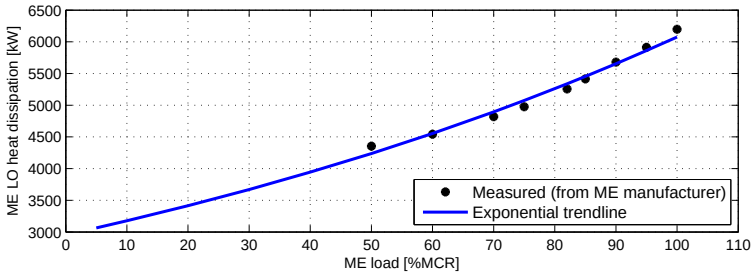

Fig. G.20: Heat dissipated in ME LO as function of ME load percentage.

The heat removed from each of the two ME LO coolers is for steady state operation given as:

$$\dot{Q}_{LO,i} = q_i c_p \rho (T_i - T_{LT,in}) \quad \text{for} \quad i = 1, 2 \ , \tag{G.3}$$

where q_i is the coolant flows through ME LO Cooler i, c_p is specific heat of the coolant, ρ is the density of the coolant, while $T_{LT,in}$ and T_i is the temperature of the coolant at the in- and outlet of ME LO Cooler i, respectively. It is assumed that the heat load is distributed equally between the two ME LO coolers, and that $T_i - T_{LT,in} = 8$ °C over

both ME LO coolers, which is partly ensured by the temperature control. The coolant flow rate through each of the ME LO coolers can be approximated by a function of the valve position and the differential pressure over the ME TC LO cooler:

$$q_i = f_i(\varsigma_{cv1}, \varsigma_{cv2}, \Delta p_{TC}) \quad \text{for } i = 1, 2 \, . \tag{G.4}$$

It is assumed that the LT FW Pressure Control from Fig. G.13 keeps the differential pressure over the ME TC LO Cooler constant at $\Delta p_{TC} = 0.1$ bar, and that the two ME LO Cooler valves are operated in parallel such that: $\varsigma_{cv1} = \varsigma_{cv2}$. The relationship governed by f_1 and f_2 is then estimated from experimental data, and the relationship between the heat dissipated in the lube oil, and the position of the ME LO cooler FW valves is subsequently determined as illustrated in Fig. G.21.

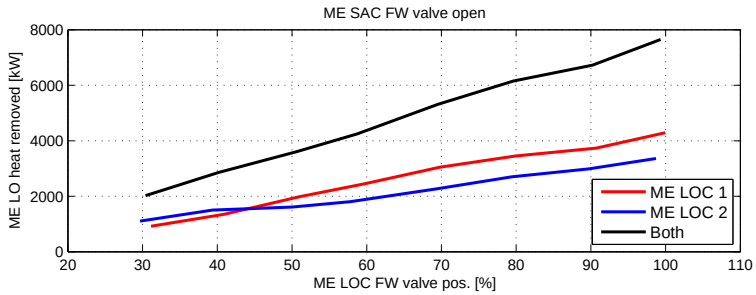

Fig. G.21: Heat removed from the two ME LOCs as function of the ME LOC FW valve positions. The coolant temperature difference over the two ME LO coolers is assumed to be constant at 8 °C, and the set point for ME TC LOC FW diff. pressure control is 0.1 bar.

The relationship between the position of the two ME LO Cooler valves and the power consumption of the LT FW pumps is determined experimentally, still using the assumption that $\Delta p_{TC} = 0.1$ bar, which is ensured by the LT FW Pressure Control. The resulting power consumption is plotted in Fig. G.22.

Through linear interpolation, the relationship between the ME load and LT FW pump power, given the assumptions above, is determined as illustrated in Fig. G.23. An important note here is that the relationship shown in G.23 is highly influenced by the set points of the implemented controllers. This means that increasing the set point for the LT FW Pressure Control will increase the LT FW pump power consumption, but will also increase the cooling of consumers where the temperature is not controlled. The set points used in the assumption above has been tested for ME loads up to 40 %, but may have to be adjusted for higher loads, which will increase the power consumption. Another important note is that the shut-off valve for the ME SAC #2 is operated in parallel with the TC cut-out system which is typically engaged at about 50 % ME load. This means that the actual power consumption will move from the red to the blue curve in Fig. G.22 when the TC cut-out system is disengaged, and vice-versa.

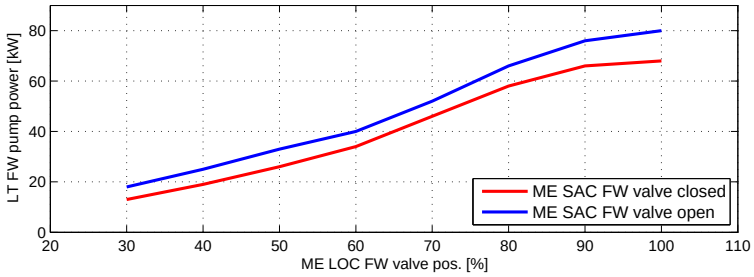

Fig. G.22: Measured power consumption for LT FW pumps as function of the ME LOC FW valve positions.

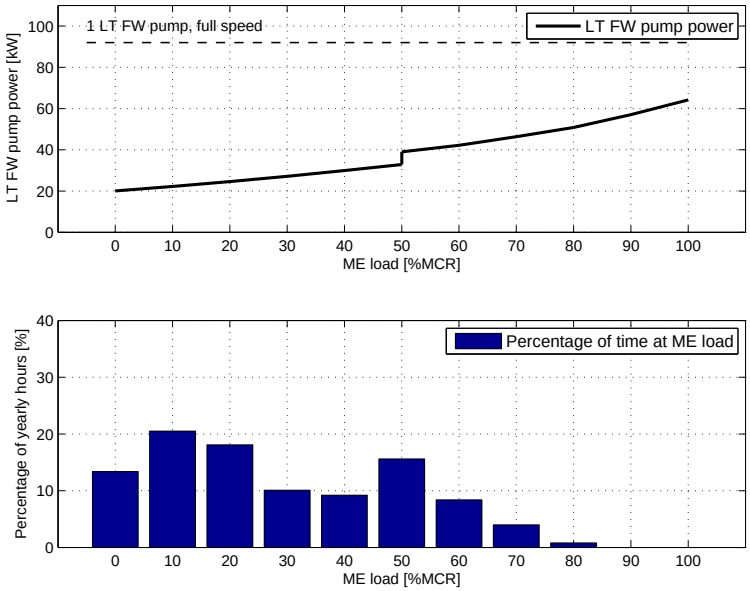

Fig. G.23: Upper plot: LT FW pump power consumption as function of ME load percentage. Lower plot: The percentage of yearly hours the vessels in this series operate at a given ME load.

The yearly power consumption for the test platform given the above assumption is obtained by weighting the power consumption profile from Fig. G.23 with the operational profile for the vessel series in Fig. G.4. The result is shown in Table G.10 and is considered to be a best-case estimate.

The saving for the LT FW circuit in Table G.10 is significantly lower than what is initially estimated in Section 3. This is explained by two main factors: First of all, the

Table G.10: Yearly power savings for the revised LT FW cooling system control based on measurements.

	Power consumption [kWh/year]	Savings [kWh/year]	Savings [%]	Payback time [months]
LT FW circuit	246.380	1.159.720	82	10

estimate in Section 3 is conservative in the sense that:

- The calculated pump power consumption is based on the nominal pump motor power (110 kW), which is higher than the actual power consumption at full speed (92 kW).
- The efficiency of the VFDs is assumed to be 91 % at all loads, while it is actually 97 % at nominal load for the drives used in this application [3].
- The coolant temperature is assumed to be 36 °C, but is 35 °C in the tests.
- Two auxiliary engines are assumed to be running at all times, but only one is running during the tests.

At the same time, the estimated power consumption in Table G.10 assumes that sufficient cooling is provided for consumers at a pressure set point of $\Delta p_{TC} = 0.1$ bar, which is based on cooling system documentation and input from crew. This effectively means that the flow through the consumers without temperature control is lower than design, which was the assumption in the estimate from Section 3. While this set point is tested at ME load of up to 40 % it may not be sufficent for higher loads and may need to be increased, which will also increase the LT FW pump power consumption. The actual yearly power consumption for the modified LT FW circuit is therefore expected to lie between the initial estimate in Table G.4 and the calculated consumption based on measurements in Table G.10. The associated power saving depends on the operational profile for the vessel, but just as much on the current operation of the cooling system by the crew. The crew on the vessel subject for this test installation reported that they where able to run with only one LT FW pump when at low ME load, while sister vessels where not able to do so due to problems with low pressure. The calculation in this technical report assumes that both LT FW pumps are running except when in port, so for vessels where the crew is able to run with only one pump, the actual saving for the revised cooling control system will be lower.

7 Concluding remarks

The purpose of the revised cooling system instrumentation documented in this technical report has mainly been to verify models, control strategy estimated power savings

for the LT FW circuit. The extend of the new instrumentation was chosen based on cost/benefit considerations for different instrumentation levels in Section 3. This included estimation of potential power savings for the revised cooling system, based on the operational profile of the vessel series, and assumptions on the current operation of the cooling system. The revised instrumentation for the cooling system, including new control hardware and software was considered in Section 4. This facilitated implementation of the control design considered in Section 5 which was evaluated by measuring the response to a series of steps in the controller references. The evaluation showed good performance in terms of transient response and reference tracking. Achievable savings based on measurements from the revised cooling system were considered in Section 6 and indicated significantly higher savings than the initial worst-case estimate in Section 3. The difference was explained by a conservative initial estimate of power savings, but also influenced by the assumptions on which the calculations of achievable savings in Section 6 where based on.

What remains to be established is how the new control implementation performs at higher ME loads, and how to tweak controller set points to obtain maximum power savings while ensuring sufficient cooling under all ME load conditions.

References

[1] Beckhoff, *TwinCAT 3 eXtended Automation (XA)*. Beckhoff Automation GmbH, 2012.

[2] M. Hansen, J. Stoustrup, and J. D. Bendtsen, "Control of Non-linear Marine Cooling System," in *Proceedings of the 2011 IEEE Multi-Conference on Systems and Control (MSC)*, 2011, pp. 88–93.

[3] ABB, *ACS800, single drives 0.55 to 5600 kW*. ABB industrial drives, 2012.